INFORMATION TO USERS

This manuscript has been reproduced from the microfilm master. UMI films the text directly from the original or copy submitted. Thus, some thesis and dissertation copies are in typewriter face, while others may be from any type of computer printer.

The quality of this reproduction is dependent upon the quality of the copy submitted. Broken or indistinct print, colored or poor quality illustrations and photographs, print bleedthrough, substandard margins, and improper alignment can adversely affect reproduction.

In the unlikely event that the author did not send UMI a complete manuscript and there are missing pages, these will be noted. Also, if unauthorized copyright material had to be removed, a note will indicate the deletion.

Oversize materials (e.g., maps, drawings, charts) are reproduced by sectioning the original, beginning at the upper left-hand corner and continuing from left to right in equal sections with small overlaps.

Photographs included in the original manuscript have been reproduced xerographically in this copy. Higher quality 6" x 9" black and white photographic prints are available for any photographs or illustrations appearing in this copy for an additional charge. Contact UMI directly to order.

Bell & Howell Information and Learning
300 North Zeeb Road, Ann Arbor, MI 48106-1346 USA
800-521-0600

UMI®

Université d'Ottawa · University of Ottawa

SEDIMENTOLOGY, STRATIGRAPHY, AND SHALLOW BURIAL ALTERATION OF THE UPPER JURASSIC SWIFT FORMATION, SOUTHEASTERN ALBERTA

By

Marianne Patricia Molgat

A thesis submitted to the School of Graduate Studies and Research
in partial fulfillment of the requirements
for the degree of M. Sc. in Earth Sciences

OTTAWA-CARLETON GEOSCIENCE CENTRE
AND
UNIVERSITY OF OTTAWA
OTTAWA, CANADA

National Library
of Canada

Acquisitions and
Bibliographic Services

395 Wellington Street
Ottawa ON K1A 0N4
Canada

Bibliothèque nationale
du Canada

Acquisitions et
services bibliographiques

395, rue Wellington
Ottawa ON K1A 0N4
Canada

Your file Votre référence

Our file Notre référence

0-612-57146-7

Canada

All truths are easy to understand once they are discovered; the point is to discover them.

-Galileo

Abstract

The Upper Jurassic (Oxfordian) Swift Formation in southeastern Alberta unconformably overlies Bathonian calcareous shales of the Rierdon Formation, and in turn is overlain by Lower Cretaceous sandstone, siltstone, and mudstone of the Basal Quartz Formation (Lower Mannville Group). The Swift comprises two unconformably bounded sequences: the shale member and ribbon sandstone. The shale member consists dominantly of shale with uncommon hummocky-cross-stratified siltstone. Comprising at least four parasequences that show a subtle upward-fining stacking pattern, it was deposited in an overall deepening, fully marine environment during the fourth Jurassic transgression across the Western Interior of North America. Deposition of Sequence 1 was terminated by a fall of relative sea level.

During the following lowstand, multiple, northeast-southwest trending meandering channels incised along the top of the subaerially exposed shale member. During a subsequent rise of relative sea level and transgression, lowstand deposits were thoroughly reworked by wave ravinement, which deposited a thin chert pebble lag. At the same time, lowstand channels were most probably widened. Associated also with transgression were significant changes in the physical and chemical conditions of the marine basin in the study area. These changes are most likely related to modifications in configuration of the basin and the development of a strait, which likely formed as a result of uplift along the Sweetgrass Arch, related to the onset of the Columbian-Nevadan Orogeny. Within this newly configured basin, brackish water conditions prevailed and bedload transport was principally by combined flows formed by variable speed low-energy microtidal currents and a weak oscillatory component related to storm waves. In addition, the basin during Sequence 2 was mud dominated and starved of bedload sediment, and consequently the ribbon sandstone consists predominantly of wavy to lenticular bedded strata. Thick, areally extensive, sand-rich deposits did not accumulate. Instead, differential deposition of bed-load sediment formed and temporarily maintained many small, irregularly shaped sand banks in the study area. The depositional history of individual sand banks was controlled by the relative contribution of the directionally

consistent, low-energy tidal (unidirectional) flow versus the wave (oscillatory) component, which varied more widely in both speed and direction. The net result of the spatial variability in sand deposition is the formation of a number of laterally discontinuous stratal patterns (upward-coarsening, -fining, -aggrading), even locally. These discrete stratal patterns stack vertically to form equally variable stratal assemblages that consist of aggrading, prograding or retrograding stacking patterns, again, even locally. The Swift stratal architecture, therefore, did not form in response to changes of relative sea level but instead to spatial and temporal variations in the patterns of deposition of sand-rich strata and to the local rates of lateral bank migration and bed aggradation.

The ribbon sandstone is further characterized by an areally extensive, 2-metre-thick radioactive marker horizon that occurs in the upper part of the sequence. The marker horizon coincides with an abrupt to gradual (decimetre-scale) upward change in colour from dark to light mudstone interlaminae. A change in iron-bearing accessory minerals, from glauconite and pyrite to only siderite coincides also with the colour change. These features are interpreted to be the result of pedogenic alteration and associated weak uranium mineralization. During the ~35 My hiatus following final withdrawal of the Oxfordian sea, a soil developed across the top of the Swift Formation. Upper portions of ribbon sandstone strata (present-day light ribbon sandstone) were altered in the Bt and C horizons of the ancient soil profile. Because of primary and secondary permeability heterogeneities within the soil layer, which controlled local groundwater flux and circulation, pedogenic alteration penetrated to variable stratigraphic depths throughout the study area. Also, atmospheric oxygen transported by percolating meteoric water, resulted in extensive decomposition of organic matter by in situ oxygen-respiring microbes, alteration of chemically unstable minerals such as feldspars and clay minerals, and oxidation of authigenic pyrite. At the same time, iron, derived in part from oxidized pyrite and altered glauconite, was reprecipitated as siderite in the altered ribbon sandstone because of high pCO_2 created by bacterial respiration and atmospheric input. During late pedogenesis, uranium was leached from unpreserved (Barremian?) volcanic ash deposits and subsequently mobilized by downward-migrating meteoric groundwater. Uranium was sorbed onto organic matter in unaltered mudstone interbeds at the interface

between the dark and light ribbon sandstone. The radioactive marker horizon between the light and dark ribbon sandstone, therefore, corresponds to a geochemical redox front that developed at variable depths in an ancient soil horizon. As such, this radioactive horizon, although readily recognizable and areally extensive, has no chronostratigraphic significance, and as a result would be a poor stratigraphic datum.

Résumé

Dans le sud-est de l'Alberta, la formation de Swift d'âge Jurassique supérieur (Oxfordien) superpose les argilites calcaire de la Formation Rierdon et est superposée par les grès, limonites et argilites continentaux de la Formation de Basal Quartz d'âge Crétacé inférieur (Groupe Mannville inférieur). Le Swift est constitué de deux séquences de dépôts : Le membre argileux et le grès rubané. Le membre argileux est composé principalement d'argilite interstratifiée avec de rares limonites comportant du litage oblique en mamelon, et comprend au moins quatre paraséquences qui forment une succession à caractère rétrogradationel subtil. Le membre argileux fut déposé dans un environnement marin marqué par des augmentations en profondeur durant la quatrième transgression marine jurassique dans l'intérieur de l'Ouest de l'Amérique de Nord. La déposition de la Séquence 1 pris fin lors d'une baisse du niveau marin relatif.

Durant la séquence de bas niveau qui suivit, plusieurs rivières à méandre, orientées généralement en direction nord-est - sud-ouest, se sont encaissées dans le membre argileux nouvellement exposé. Lors de la remontée subséquente du niveau marin, et de la transgression, les dépôts de bas niveau furent entièrement érodés par le remaniement des vagues qui déposa uniquement un mince résidu de graviers riche en silex. En même temps, les chenaux de bas niveau furent probablement élargis. Des changements importants quant aux conditions physiques et chimiques du bassin de déposition ont eu lieu suite à la nouvelle transgression marine dans la région d'étude. Ces changements sont liés à des modifications de la configuration du bassin Williston associées à un soulèvement tectonique probable le long de l'arc Sweetgrass, lequel fut causé par l'orogenèse du Colombien-Nevaden. Lors du soulèvement, un détroit franchissant l'arc de Sweetgrass s'est développé, à l'intérieur duquel des conditions d'eau saumâtre prédominaient. De plus, dans ce détroit, le transport des sédiments de charge de fond fut réalisé principalement par des courants combinés composés d'un faible courant de marée à vitesse variable et d'un faible courant oscillatoire relié à des conditions de tempêtes. Toutefois, durant la Séquence de dépôt 2, le bassin était dominé par de l'argile et généralement dépourvue de sédiments de charge de fond, et, par conséquent, le

grès rubané est formé principalement de lits lenticulaires et ondulés. D'épais dépôts riches en sable sont notamment absents. Cependant, plusieurs petits ($<25\ km^2$) bancs de sable de forme irrégulière se sont développés et temporairement maintenus suite à la déposition différentielle du sable. Chaque banc détient une histoire dépositionelle à lui propre qui fut contrôlée par la contribution relative des faibles courants de marée (unidirectionnels) versus les faibles courants oscillatoires. Le résultat final fut la formation synchrone et contiguë de successions à caractère progradationel, rétrogradationel et aggradationel, et ce, même localement. Ces successions individuelles s'empilent à leur tour pour former des assemblages stratigraphiques tout aussi variables comprenant un empilement aggradationel, rétrogradationel, et progradationel, une fois de plus, même localement. L'architecture stratigraphique de la Formation de Swift n'est pas reliée à des changements du niveau marin relatif, mais plutôt à des variations spatiale et temporelle dans les patrons de déposition du sable et des taux locaux d'aggradation et de migration latérale des lits individuels.

Le grès rubané est également marqué d'un horizon radioactif d'environ 2 mètres d'épaisseur qui se manifeste dans la partie supérieure de la séquence. Cet horizon marqueur coïncide avec un changement de couleur généralement abrupt des interlits d'argilites, d'où ces lits passent du gris foncé au gris pâle. Un changement dans le type de minéral de fer est également observé à travers cet horizon : La pyrite et la glauconite sont présentes dans le grès rubané foncé alors qu'uniquement la sidérite est discernable dans le grès rubané pâle. Toutes ces particularités sont interprétées d'être reliées à l'altération pédogénique du grès rubané et à une minéralisation en uranium. Au cours de l'hiatus ~ 35 millions d'années qui a suivi la régression marine marquant la fin de la Séquence 2, un sol s'est développé sur le dessus du grès rubané. Les strates de ce dernier ont été altérées en les horizons Bt et C d'un sol, aujourd'hui représentées par le grès rubané pâle. L'altération pédogénique atteignit différentes profondeurs dans la région d'étude selon les perméabilités primaires et secondaires locales des strates, lesquelles exerçaient un contrôle considérable sur le flux et la circulation des eaux souterraines. De plus, l'oxygénation substantielle dans le sol créa les conditions nécessaires à la décomposition quasi totale de la matière organique par les bactéries, l'altération des minéraux instables chimiquement tel que les feldspaths et les

minéraux argileux, et l'oxydation de la pyrite authigénique. Pendant ce temps, le fer, provenant en partie de l'altération de la pyrite et de la glauconite, fut, en présence du gaz carbonique produit par la respiration bactérienne et l'apport atmosphérique, reprécipité en sidérite. Tard durant la pédogénèse, de l'uranium lessivé à partir de minces lits non-préservés de cendres volcaniques (Barrémien ?), a été mobilisé vers le bas par l'eau météorique. Lorsque l'uranium en solution atteignit le front de réduction au contact du grès rubané pâle et foncé, il fut sorbé sur la matière organique présente dans les interlits d'argilite foncé. Par conséquent, l'horizon radioactif marqueur de la formation de Swift représente l'emplacement d'un front de réduction qui s'était développé à différentes profondeurs dans un ancien sol. Cet horizon radioactif, bien que facilement reconnaissable et répandu, ne comporte donc aucune signification chronostratigraphique, et par conséquent, ne devrait pas servir de surface stratigraphique pour fin de corrélations.

Acknowledgements

Funding for this research was provided by PanCanadian Petroleum Ltd and by NSERC operating and industrial-oriented research grants to R.W.C. Arnott, and are gratefully acknowledged. I would like to thank Dr. Bill Arnott for providing me with the opportunity to pursue graduate studies and work on this project. Your guidance and direction, continual support, and never-ending enthusiasm made this thesis an exciting, challenging, and successful endeavour. The ideas presented in this thesis profited greatly from discussions with numerous people, including Drs. Bill Arnott, Danielle Fortin, Ian Clark, Keiko Hattori, and Owen Dixon at the University of Ottawa, and Dan Potocki at PanCanadian Petroleum. Many thanks to the members if my thesis committee: Drs. Al Donaldson, Tony Fowler and Peter Johnson for their thorough and constructive criticism. To all in the G.G. Hatch Stable Isotope Laboratories at the University of Ottawa, in particular Wendy Abdi and Gilles St.-Jean: your competent technical knowledge, helpful and cheerful assistance, and friendship are sincerely appreciated. Thank you to Ron Hartree in the XRF lab for his invaluable assistance. I am indebted to Drs. André Lalonde, André Desrochers, and Tony Fowler for the use of their laboratory and lab equipment during the course of this thesis. I also would like to extend my sincere thanks to Hélène DeGouffe and Sylvie Thériault for providing daily smiles (and so much more); to Andrew Buttle for helping with drafting in my final blitz; and to Edward Hearn, for the daily freshly seeped afternoon tea and unique conversations. In essence, I extend my warmfelt thanks to the department of Earth Science at the University of Ottawa in its entirety for their selfless help.

To my friend Karen Bradshaw: you have been such a free-giving source of motivational energy to me over the course of my graduate studies and for that, if nothing else, I thank you. Heartfelt thanks to my good friends Craig Scott (a.k.a. SwaB or Mr. Volcano) and Natalie Ham (a.k.a. Gnat) for contributing to making my graduate years at the University of Ottawa, including the trip to the Caribbean, a most memorable experience. To my friend Clare O'Dowd: thank you for always being able to make me smile and giving me the means to release some stress when most needed.

Mom and Dad, thank you for continuously supporting me in my academic and personal endeavours et également pour les heures innombrables de service de gardiennage. Les mots peuvent difficilement exprimer toute ma gratitude. Merci à Claude et Lise de m'avoir donné la vie. Je me considère vraiment choyée de pouvoir entretenir une bonne relation avec vous et mes frères Pascal (futur géologue?) et Cédric.

Mein Liebling, ich danke Dir das Du Freude in mein Leben zurück gebracht hast. Deine Unterstützung und Ermutigung hat eine grosse Bedeutung für mich. Ich kann kaum erwarten mit Dir XC-zufliegen.

Finalement, un petit mot à mes enfants, Pascal, Caroline, et Martin. L'amour que je vous porte est plus grand que ne peuvent exprimer les mots. Les efforts que j'ai fournis au cours de ma formation universitaire sont, en partie, pour vous et nous en partagerons les fruits sous peu. J'ai, et aurai toujours, votre bonheur présent et futur à cœur. Gros bisous.

TABLE OF CONTENTS

Abstract/Résumé i

Acknowledgments vii

Table of Contents ix

List of Tables xi

List of Figures xiv

CHAPTER 1 INTRODUCTION

1.1 Introduction 1
1.2 Regional Geologic setting 1
  1.2.1 Origin of the Canadian Cordillera 1
  1.2.2 The Foreland Basin 8
1.3 Tectonic elements in proximity to the study area 17
1.4 Previous work on the Swift Formation 25
1.5 Sequence stratigraphy 31
1.6 Currents in shallow marine environments 32
  1.6.1 Oceanic currents 33
  1.6.2 Meteorological currents 34
  1.6.3 Tidal currents 35
1.7 Sedimentation in shallow marine environments 41
  1.7.1 Sedimentation in wave-dominated settings 41
  1.7.2 Sedimentation in tide-dominated settings 42
1.8 Paleosols 46

CHAPTER 2 Sedimentology and stratigraphy of the Swift Formation (Upper Jurassic) in southeastern Alberta: sedimentation on an open marine basin to a macrotidally-influenced intracontinental strait. 59

CHAPTER 3 Nature and origin of an areally-extensive marker horizon in the Swift Formation, southeastern Alberta. 130

CHAPTER 4 Conclusions 157

References 161

Appendices 174
- Appendix 1. Stratigraphic columns and miscellaneous lithological data 174
- Appendix 2. Petrographical analyses 240
- Appendix 3. Geochemical analyses 260
- Appendix 4. Wireline cross sections 264
- Appendix 5. Slice maps 270

LIST OF FIGURES

Figure 1.1. Simplified cross-section of the Western Canada Sedimentary Basin. 3

Figure 1.2. Allochthonous terranes and morphotectonic belts in the Canadian Cordillera. 6

Figure 1.3. Idealized cross-section across the Western Canada Foreland Basin. 11

Figure 1.4. Location of major tectonic and physiographic elements in the Western Canada Sedimentary Basin. 13

Figure 1.5. Depositional cycles during development of the Western Canada Foreland Basin. 15

Figure 1.6. Distribution of sub-components of the Sweetgrass Arch in southeastern Alberta and northern Montana. 19

Figure 1.7. Structure map of the top of the Rierdon Formation in southeastern Alberta. 22

Figure 1.8. Eagle Butte meteorite structure. 24

Figure 1.9. Map of tectonic domains that form the basement rocks in Alberta and northern Montana. 27

Figure 1.10. Stratigraphic nomenclature of Jurassic and Cretaceous strata in southeastern Alberta. 30

Figure 1.11. Orbital motion in wind-generated oceanic waves. 37

Figure 1.12. Origin of tides and tidal range 40

Figure 1.13. Tidal current speed and tidal rhythmites. 44

Figure 1.14. Streamwise variations in modern tidal-generated sedimentary structures. 48

Figure 1.15. Soil structures. 53

Figure 1.16. Common soil-forming regimes. 57

Figure 2.1. Location of study area and distribution of well control. 62

Figure 2.2. Paleogeography of North America during the Oxfordian (Late Jurassic). 65

Figure 2.3. Distribution of sub-components of the Sweetgrass Arch and tectonic domains that form the basement rocks in south-eastern Alberta and northern Montana. 67

Figure 2.4. Structure map of the top of the Rierdon Formation in southeastern Alberta. 69

Figure 2.5. Strata in the Eagle Butte meteorite impact structure (Twps. 8 and 9, Range 4w4). 71

Figure 2.6. Nomenclature of Jurassic and Cretaceous strata in southeastern Alberta. 74

Figure 2.7. Lithofacies of the shale member (Sequence 1). 80

Figure 2.8. Lithofacies 4. Interstratified mudstone, siltstone and sandstone. 84

Figure 2.9. Lithofacies 5. Small-scale cross-stratified fine sandstone. 90

Figure 2.10. High-energy deposits of the ribbon sandstone (Sequence 2). 93

Figure 2.11. Altered ribbon sandstone. 97

Figure 2.12. Well log showing the abrupt deflection of the gamma-ray curve at the dark and light ribbon sandstone contact. 100

Figure 2.13. Log character of the Swift Formation. 104

Figure 2.14. Rierdon/Mannville isopach and Precambrian structural elements 107

Figure 2.15. Isopach map of Rierdon 110

Figure 2.16. West to east and north-south cross-sections 112

Figure 2.17. Isopach map of the shale member 115

Figure 2.18. Present-day isopach map of the ribbon sandstone 118

Figure 2.19. Residual isopach map of the ribbon sandstone in which data points with thick Basal Quartz sandstone were disregarded. 120

Figure 2.20. Cross-sections across a ribbon sandstone sand bank and stacked five metre slice maps showing their spatial and temporal distribution. 124

Figure 3.1. Study area and location of samples for geochemical analysis 132

Figure 3.2. Stratigraphic nomenclature on Jurassic and Lower Cretaceous strata in southeastern Alberta. 135

Figure 3.3. Geological and geochemical attributes of the radioactive marker horizon. 139

Figure 3.4. Variation in depths of the radioactive marker horizon. 142

Figure 3.6 Analogue model (uranium roll-front deposits) for the emplacement of uranium and sphaerosiderite in the ribbon sandstone: 150

Figure 3.7 Two stage, early post-depositional history of the Swift Formation. 153

LIST OF TABLES

Table 1.1 Major horizons in paleosols, subordinate features and shorthand labels. 51

Table 2.1 Lithofacies descriptions and interpretations of the Swift Formation. 76

Chapter 1

1.1 Introduction

This thesis was prepared in a paper format, with the main body consisting of two journal articles. The introductory chapter, Chapter 1, covers background information relevant to this research project. Chapter 2 discusses the sedimentology and sequence stratigraphic framework of the Swift Formation, and Chapter 3 interprets the origin of a thin radioactive marker horizon near the top of the Swift Formation. The final chapter, Chapter 4, summarizes the principal conclusions of the thesis.

1.2 Regional Geological Setting

In western Canada, the Western Canada Sedimentary Basin comprises the full Phanerozoic sedimentary succession that overlies basement crystalline rocks. It forms a wedge that thickens westward from a zero edge on the Canadian Shield to less than 6 km in the Alberta Basin (Fig. 1.1) (Masters, 1984)). Its origin and evolution are inextricably linked to the origin and evolution of the Western Canada Cordillera that formed as a result of global plate tectonics. A brief discussion on the origin of the Canadian Cordillera, followed by an overview of the Western Canadian Foreland Basin and its deposits, are presented in the following sections.

1.2.1 Origin of the Canadian Cordillera

The Canadian Cordillera consists of a tectonic collage of allochtonous terranes. The geographical origin of the terranes and the magnitude and direction of their displacement prior to collision and accretion are still controversial. Some authors have suggested that terranes have been displaced by as much as 2000 km, whereas others proposed no displacement with respect to the position of the North American craton. Nonetheless, paleomagnetic (Irving and Yole, 1972; Irving *et al.*, 1980), paleontologic (Monger and Ross, 1971; Tipper, 1981) and structural data (Tempelman-Kluit, 1979; Gabrielse, 1985) suggest

Figure 1.1 Simplified cross-section of the Western Canada Sedimentary Basin. The sedimentary wedge trends northwesterly and thins eastward where it pinches out onto the craton.

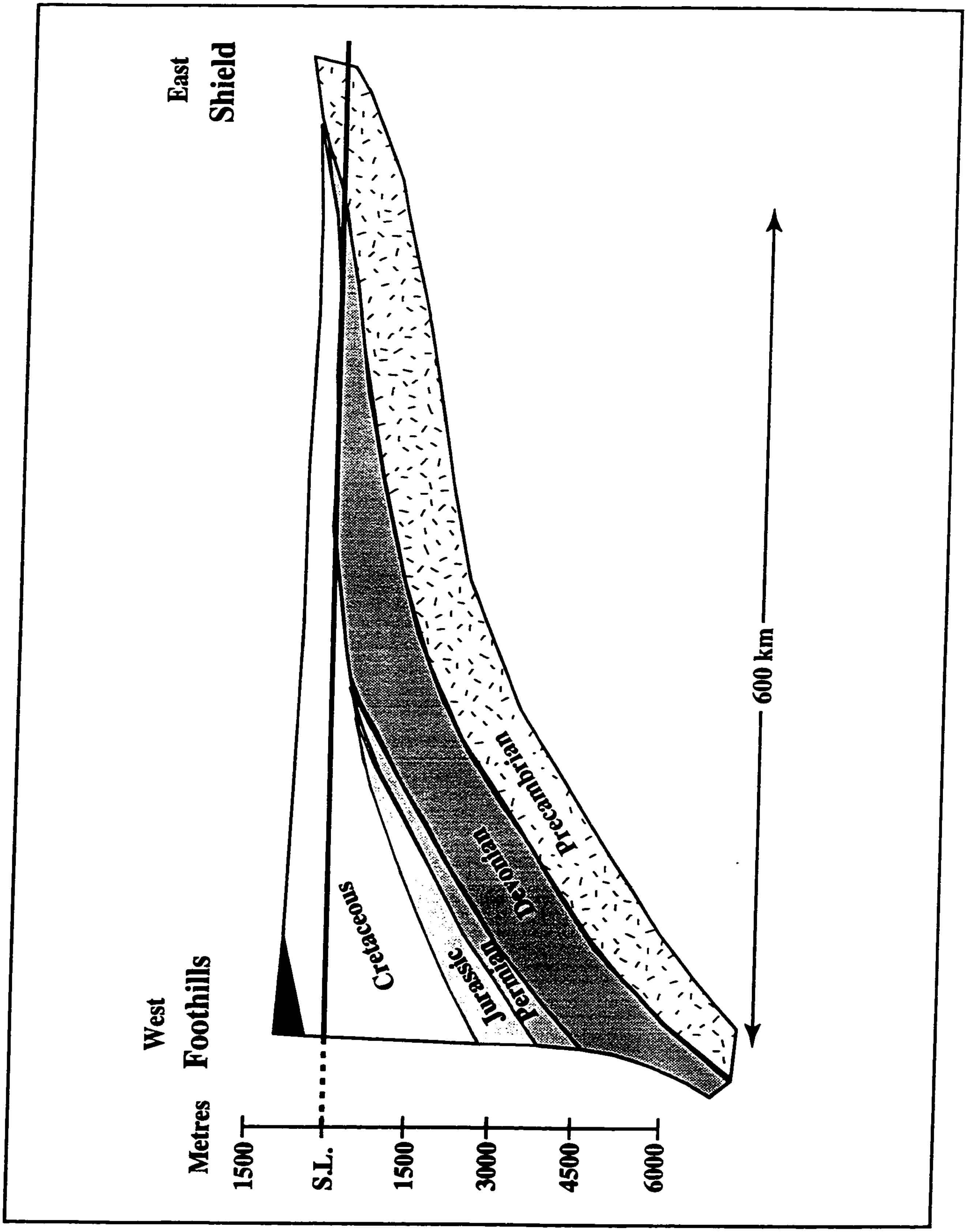
Metres
1500
S.L.
1500
3000
4500
6000
West
Foothills
East
Shield
Cretaceous
Jurassic
Permian
Devonian
Precambrian
600 km

that these terranes are allochtonous. Currently, over 200 terranes are recognized in the North American Cordillera (Coney *et al.*, 1980; Silbering *et al.*, 1987). The larger ones have similar tectonostratigraphic assemblages consisting oceanic volcanic arc rocks and include Quesnellia, Stikinia, Wrangellia and Alexander terranes (Figure 1.2a). Other terranes in the Canadian Cordillera are dominated by deep ocean basin sedimentary rocks, basaltic volcanic rocks and ultramafic rocks and form suture zones that essentially act as the glue that binds the terranes together. Larger ones include Slide Mountain, Cache Creek, Bridge River, Hozameen, Pacific Rim and Chugach terranes (Figure 1.2a). Terranes with similar physiographic, lithologic, metamorphic and structural elements are grouped into morphotectonic belts or tectonostratigraphic belts or zones. In the Canadian Cordillera, five belts are recognized. They are, from the east to west, the Foreland, Omenica, Intermontane, Coast and Insular belts (Fig. 1.2b).

The Foreland, Omenica and Intermontane belts developed during the Jura-Cretaceous Columbian Orogeny, caused by the collision of Intermontane allochtonous terranes along the western margin of the North American plate (Leckie and Smith, 1992). The Intermontane belt is composed dominantly of rocks of oceanic volcanic arc assemblage (Price *et al.*, 1985) and includes the Quesnellia, Stikinia and Cache Creek terranes. The suture zone between the Intermontane belt and the craton is characterized by amphibolite to greenshist-grade meta-sedimentary and –volcanic rocks of the Omenica belt (Monger, 1989). It comprises, among others, the Kootenay and Slide Mountain terranes and includes the Pelly and Selwin Mountains in the Yukon and the Cassiar, Omenica and Columbian Mountains in British Columbia. Its eastern limit is delineated by the Rocky Mountain trench, whereas its western limit is marked by a decrease in metamorphic grade to sub-greenshist (Monger, 1989). To the east, is the Foreland belt (or Rocky Mountain belt) consisting of Upper Proterozoic to Lower Tertiary supracrustal rocks that were scraped off the continental plate, and then horizontally compressed and stacked as west-verging thrust sheets (Leckie and Smith, 1992). Its eastern boundary is defined by the eastern limit of deformation.

The Coast and Insular belts formed during Upper Cretaceous Laramide Orogeny, related to the collision of two major terranes (Alexander and Wrangellia) with the North

Figure 1.2 Allochtonous terranes and morphotectonic belts in the Canadian Cordillera.

1.2a) Distribution of the major terranes in the Canadian Cordillera. YT: Yukon-Tanana terrane; CA: Cassiar terrane; SM: Slide Mountain terrane; KO: Kootenay terrane; MO: Monashee terrane; CC: Cache Creek terrane; ST: Stikinia terrane; CD: Cadwallader terrane; BR: Bridge River terrane; CN: Chilliwack-Noodsack terrane; QN: Quesnellia terrane; MT: Methow terrane; SH: Shuksan terrane; CG: Chugach terrane; AX: Alexander terrane; WR: Wrangellia terrane; CR: Crescent terrane. Adapted from Monger, 1989.

1.2b) Distribution of morphotectonic belts that formed as a result of accretionary tectonics. The highly metamorphosed Omenica and Coast Plutonic belts separate the comparatively unmetamorphosed Rocky Mountain, Intermontane, and Insular belts, and act as the glue that binds them together. From Monger, 1989.

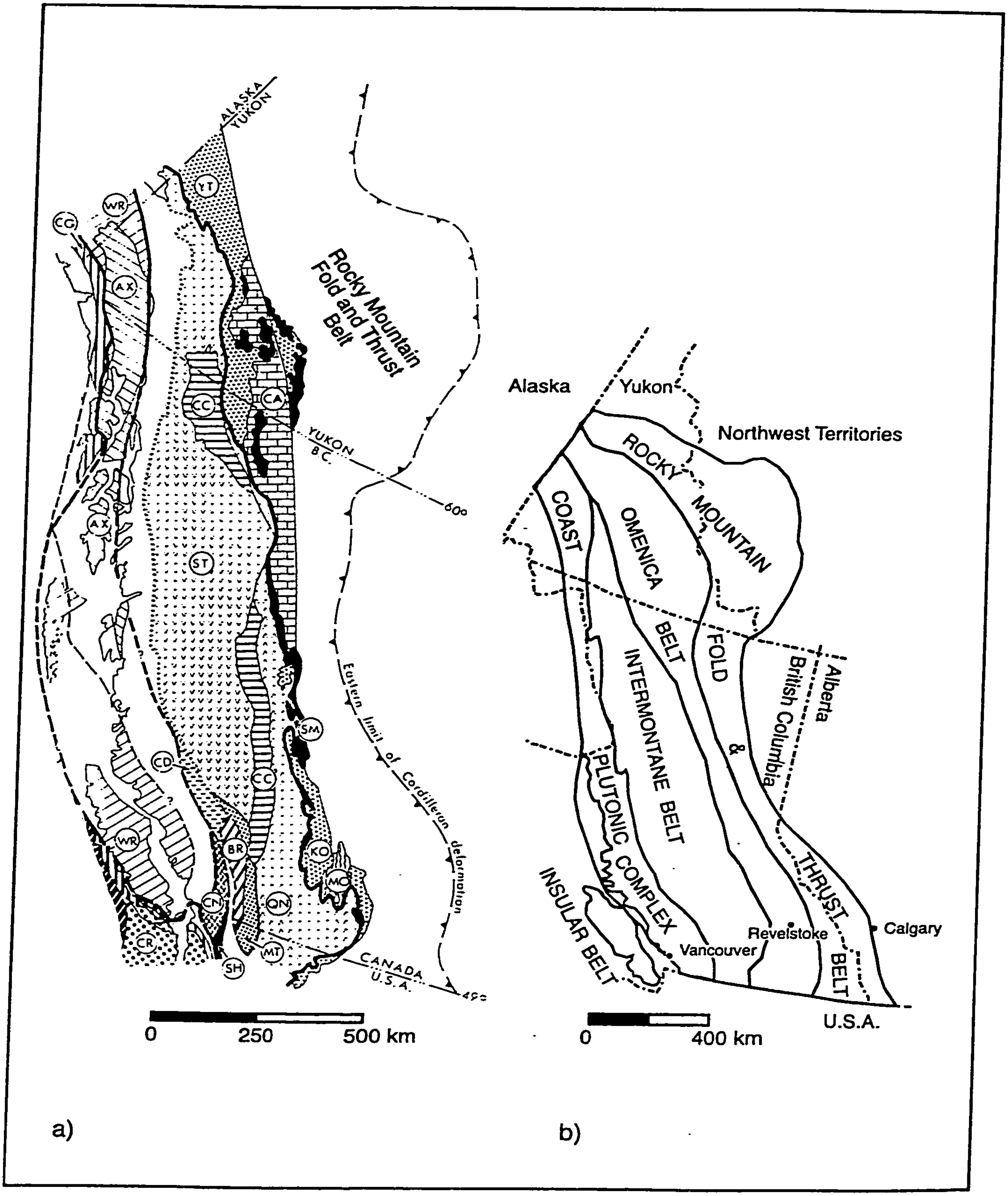
ALASKA
YUKON
YT
WR
CG
AX
Rocky Mountain Fold and Thrust Belt
CC
CA
YUKON
B.C.
60°
ST
SM
CD
CC
WR
BR
KO
MO
CN
QN
CR
SH
MT
Eastern limit of Cordilleran deformation
CANADA
U.S.A.
49°
0
250
500 km
a)
Alaska
Yukon
Northwest Territories
ROCKY MOUNTAIN FOLD & THRUST BELT
COAST PLUTONIC COMPLEX
OMENICA BELT
INTERMONTANE BELT
INSULAR BELT
Alberta
British Columbia
Revelstoke
Calgary
Vancouver
U.S.A.
0
400 km
b)

American craton and the previously accreted Intermontane terrane (Monger, 1989; Leckie and Smith, 1992). The Insular belt underlies the present continental shelf and slope off British Columbia, Vancouver Island, and the Saint Elias Range in northern British Columbia. It consists of volcanic and sedimentary strata and granitic rocks, and in addition to Alexander and Wrangellia, it comprises a number of smaller terranes. The suture zone between the Insular and Intermontane belts is delineated by the Coast belt, which consists of a high relief granitic complex dominated by relatively mafic plutonic rocks (quartz diorite, tonalite and diorite). This period of deformation is also characterized by renewed thrusting and stacking in the Foreland belt and significant additional crustal shortening of up to 200 km (Price, 1981).

The evolution of the Western Canada Cordillera and the Foreland Basin can be generally modelled as a three-stage process (Leckie and Smith, 1992). The first stage involved the development of a miogeocline and platform at the margin of the North American craton where rifting and rapid subsidence was common. This passive continental margin existed throughout the Paleozoic until the middle Jurassic, during which time sedimentation may have reached thicknesses in excess of 20 km (Price, 1981). The second stage occurred in Late Jurassic to Early Cretaceous time, and records the first collision between allochtonous terranes and the North America craton. In mid-Jurassic time, concurrent with the opening of the Atlantic Ocean, the Intermontane Superterrane collided obliquely with westward-subducting North America. The collision between these two plates, termed the Columbian Orogeny, resulted in the compression and translation of the outboard part of the North American platform and supracrustal platform rocks pushed onto the Lower Proterozoic crystalline craton in the form of thrust sheets. Tectonic thickening and related lithospheric flexure formed a narrow, northwest-southeast elongated foreland basin that was repeatedly inundated by southward-extending water from the northern Boreal sea and northward-extending warm marine water from the Gulfian sea. By Mid-Cretaceous time, convergence of the Intermontane terrane waned and a period of quiescence prevailed until Late Cretaceous, at which time subduction reversed to an easterly direction, presumably because of differences in buoyancies between the colliding plates.

Stage 3 marked renewed tectonic activity at the western margin of North America from Late Cretaceous to Early Paleocene time. Stage 3 is termed the Laramide Orogeny, related to the collision of a second allochtonous terrane, the easterly subducting Insular Superterrane, with the North American craton and accreted Intermontane Superterrane. Plutonic and volcanic activity was widespread at this time, and included, for example, the Coast Belt Granitic Complex, one of the largest Phanerozoic granitic complexes in the world (Roddick, 1983). In addition, eastward thrusting and stacking resumed, resulting in considerable crustal shorting and eastward expansion of the Foreland Basin (Price, 1981). Orogenic processes in western Canada ceased in the Paleocene when plate tectonics regimes changed from compression to basin and range-style crustal extension as the subduction zone moved seaward to its present location west of the Vancouver and Queen Charlotte Islands In all, since Early Jurassic time, a strip of oceanic lithosphere estimated at about 11 500 km wide has been subducted beneath the western edge of the North American craton, which has resulted in lateral growth of the craton by about 500 km.

1.2.2 The Foreland Basin

The Western Canadian Foreland Basin (WCFB) formed as a result of overthrusting of supracrustal rocks during Late Jurassic to Pliocene time. Because of loading, predominantly by the Rocky Mountain Belt (Foreland Belt), the lithosphere subsided and a foreland basin developed. The WCFB was repeatedly inundated by marine waters that extended north from the Gulfian sea and south from the Boreal sea, which at times formed a continuous body of water. The resulting Western Cretaceous Interior Seaway occupied different parts of the Foreland Basin from the Late Jurassic to the Tertiary, during which time up to 4800 metres of clastic sediment were deposited along its western margin. The WCFB, and foreland basins in general, can be divided into five paleophysiographic components (Kauffman, 1984). From west to east they are: 1) tectonically active highland (Rocky Mountain Belt), 2) zone of maximum subsidence caused by loading, 3) zone of high subsidence that corresponds to the deepest water portion of the basin (foredeep), 4) broad tectonic hinge zone (forebulge) that migrates in tandem with the Cordilleran deformation, and 5) a stable eastern platform characterized by low subsidence and sedimentation rates (Fig. 1.3).

Evolution of the WCFB is closely related to periods of tectonic activity that affected relative sea level, subsidence rates and sedimentation rates (Stockmal *et al.,* 1992). In addition, physiographic elements within the basin also influenced sedimentation style. Major tectonic elements include 1) the Rocky Mountain Belt that shed sediment into the basin, 2) the block-faulted Peace River Arch that has had recurrent movement since Cambrian time (Cant, 1988), 3) the Sweetgrass Arch that comprises several subarches, domes, and faulted folds (Prodruski, 1988), and has profoundly affected marine circulation and sedimentation patterns (Hayes, 1983), for example the deeply incised valleys in southwestern Saskatchewan during the Neocomian (Christopher, 1964), 4) the Punnichy Arch, which forms the northern margin of the Williston Basin, and 5) a series of northwest to southeast trending highs that formed in the Neocomian and consist of Jurassic, Mississippian, and Devonian strata (Rudkin, 1964) (Fig. 1.4). Additional structural elements such as the Williston Basin also influenced sedimentation patterns in the Western Canada Sedimentary Basin. The Williston Basin is a Late Cambrian to Early Tertiary intracratonic basin centered in North Dakota that has accumulated up to ~ 4.9 km of sediment (Wright *et al.*, 1994). During much of the Cordilleran Orogeny, the Williston and Alberta basins were connected, but because of uplift of the broad Bow Island Arch, they became periodically(?) separated during the Tertiary (Wright *et al.*, 1994).

Deposition in the Western Canada Foreland Basin can be divided into five discrete cycles that are bounded by major unconformities or discontinuities marked by changes in lithology (Leckie and Smith, 1992) (Fig. 1.5). The base of the first cycle consists of shale of the Jurassic (Oxfordian) Fernie Group. It lies unconformably above Paleozoic and Triassic sedimentary rocks of the former passive margin. The Fernie consists of marine shale that was deposited both on the passive margin and in the foreland basin, although the transition from one to the other remains unclear. The Fernie is conformably overlain by non-marine shale of the Kootenay Group that is then truncated by a basin-wide unconformity representing a hiatus of approximately 12 million years. During deposition of the Fernie-

Figure 1.3 Idealized cross-section across the Western Canada Foreland Basin indicating the location of its 5 major physiographic components, and relative amounts of subsidence and uplift (rebound) (modified from Kauffman, 1984).

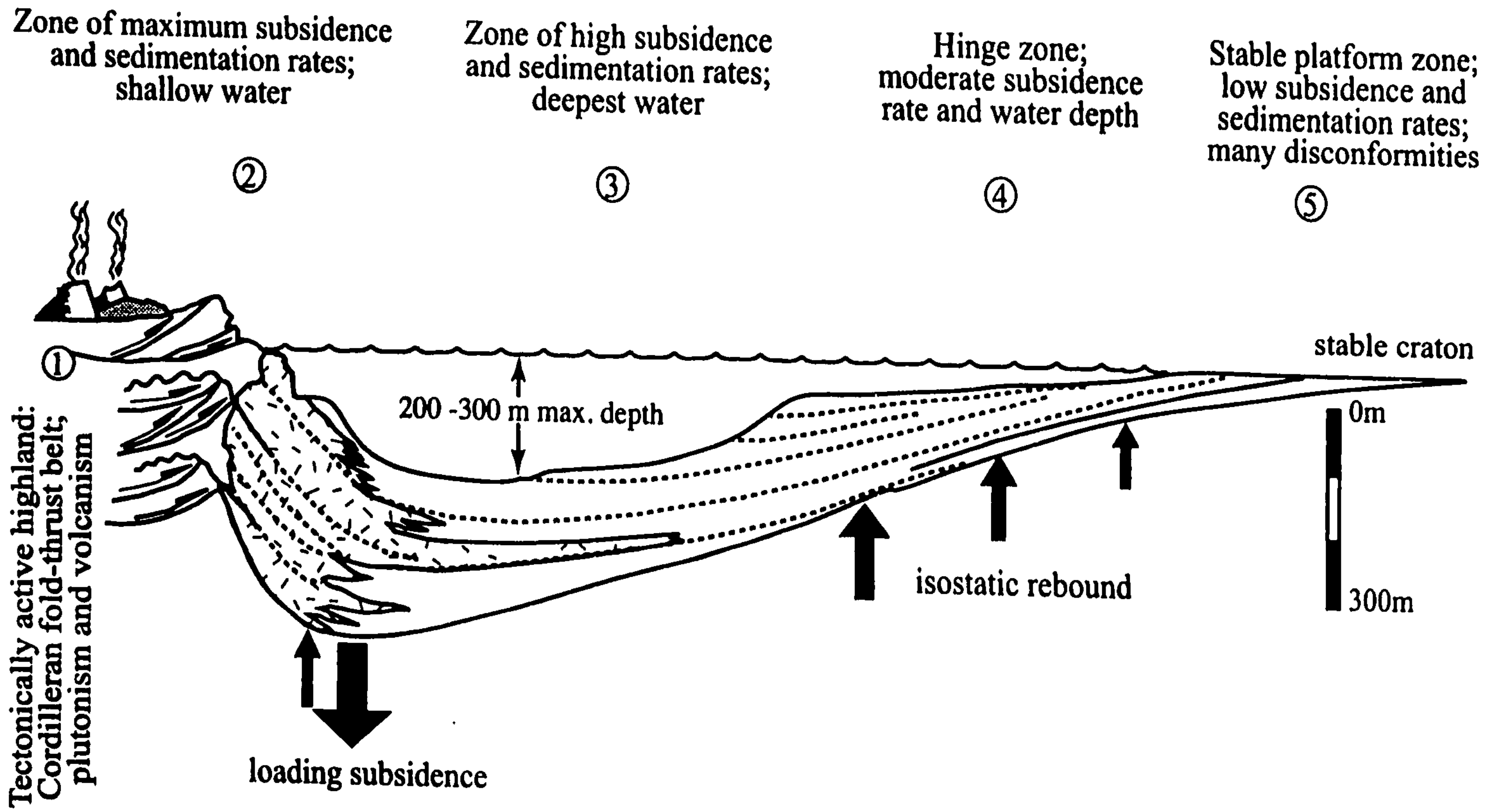Zone of maximum subsidence and sedimentation rates; shallow water
②
Zone of high subsidence and sedimentation rates; deepest water
③
Hinge zone; moderate subsidence rate and water depth
④
Stable platform zone; low subsidence and sedimentation rates; many disconformities
⑤
①
stable craton
200 -300 m max. depth
0m
300m
isostatic rebound
Tectonically active highland: Cordilleran fold-thrust belt; plutonism and volcanism
loading subsidence

Figure 1.4. Location of the major tectonic and physiographic elements that influenced depositional pattern sin the Western Canada Sedimentary Basin (modified from Leckie and Smith, 1992)

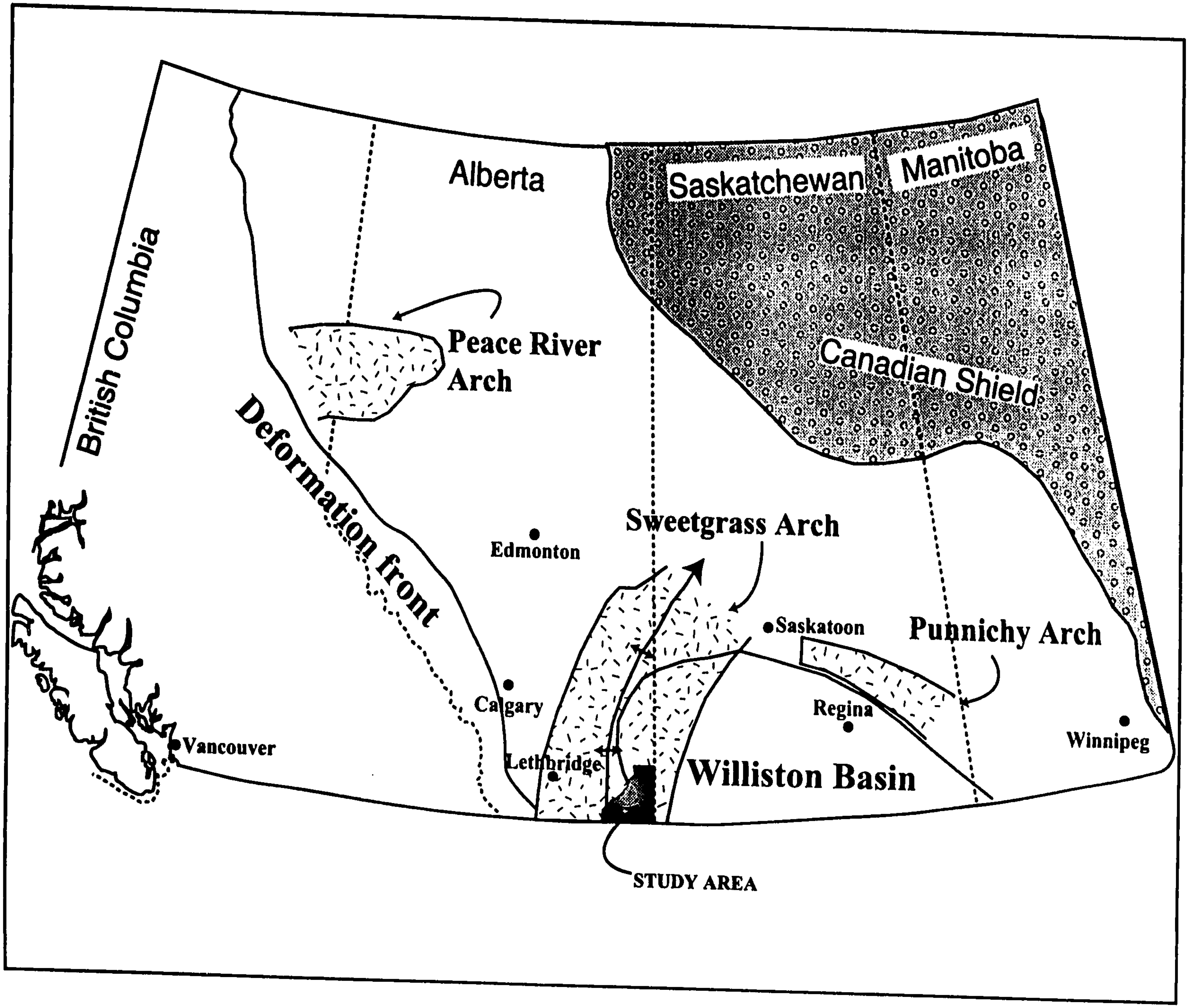
British Columbia
Alberta
Saskatchewan
Manitoba
Canadian Shield
Peace River Arch
Deformation front
Edmonton
Sweetgrass Arch
Saskatoon
Punnichy Arch
Calgary
Regina
Winnipeg
Vancouver
Lethbridge
Williston Basin
STUDY AREA

Figure 1.5. Stratigraphic column of the sediment deposited in the southern Alberta plains depicting the timing and duration of Leckie and Smith's five depositional cycles associated with the development of the Western Canada Foreland Basin (modified from Leckie and Smith, 1992).

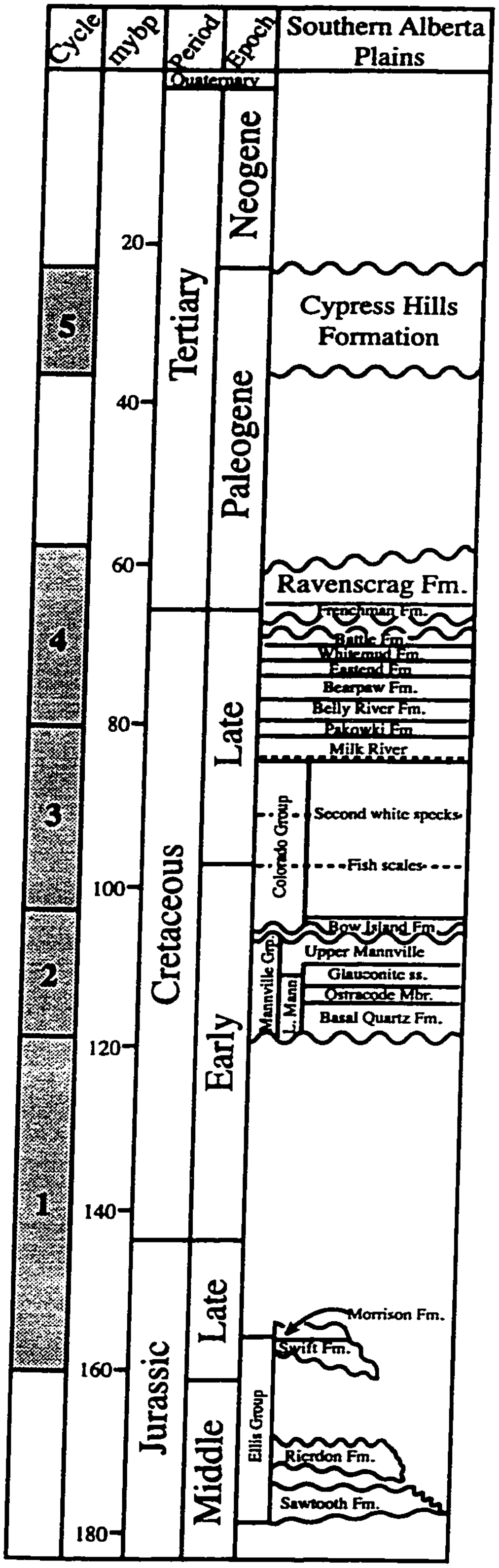
Cycle
mybp
Period
Epoch
Southern Alberta Plains
Quaternary
Neogene
Tertiary
Paleogene
Cretaceous
Late
Early
Jurassic
Late
Middle
5
4
3
2
1
20
40
60
80
100
120
140
160
180
Cypress Hills Formation
Ravenscrag Fm.
Frenchman Fm.
Battle Fm.
Whitemud Fm.
Eastend Fm.
Bearpaw Fm.
Belly River Fm.
Pakowki Fm.
Milk River
Colorado Group
Second white specks
Fish scales
Bow Island Fm.
Mannville Grp.
L. Mann
Upper Mannville
Glauconite ss.
Ostracode Mbr.
Basal Quartz Fm.
Ellis Group
Morrison Fm.
Swift Fm.
Rierdon Fm.
Sawtooth Fm.

Kootenay succession, the foreland basin was likely long and narrow with maximum subsidence in northeastern B.C., where the succession is up to about 2.7 km thick. Most of the preserved sediment occur in the Rocky Mountains and in the subsurface adjacent to the Foothills. Inition of the Fernie-Kootenay clastic wedge coincides loosely with the onset of the Columbian Orogeny. In the Williston Basin, lateral equivalents of the Fernie Group are shales and sandstones of the Swift Formation (Christopher, 1964; Hayes, 1983). The Swift comprises two members, the basal shale member and upper ribbon sandstone. Brenner and Davies (1974) and later, Hayes (1983), suggested that the shale member was deposited during regional transgression and the ribbon sandstone in shallow-marine conditions during a gradual regression.

The lower Cretaceous (Aptian to Middle Albian) Mannville and Blairmore groups make up the second cycle in the Western Canadian Foreland Basin. They include, in chronological order, 1) Cadomin, Ellerslie, Gething and Dina formations (alluvial fan, deltaic, estuarine and tidally influenced deposits), 2) Glauconite, Bluesky, Wabiskaw and Lloydminster stratal units (retrogradational shoreline, estuarine, and shallow shelf deposits), and 3) Upper Mannville and equivalent strata (stacked progradational shorelines and fluvial deposits). In general terms, this stratal succession suggests that during Cycle 2, the Boreal sea transgressed south, and then in Upper Mannville time withdrew because of northward progradation (Leckie and Smith, 1992). The Mannville wedge is bounded to the north by marine shales deposited on the Peace River Arch, which was a topographical low during Cycle 2 time (Stott, 1968, 1973; Leckie, 1986; Cant, 1988).

The third wedge corresponds to a long term period of global sea level rise (Haq *et al.*, 1987; Jervey, 1992) from Albian to Campanian time. Cycle 3 is characterized by three major marine inundations separated by two lowstand events. During this time more than 1100 metres of sediment was deposited (Leckie and Smith, 1992). Marine shales include the Joli Fou Formation and the Colorado and Upper Fort St. John groups, whereas lowstand deposits are represented by the Peace River-Viking and Cardium formations. At this time northward transgression of warm marine water from the Gulfian sea merged repeatedly with the Boreal sea. The end of Cycle 3 is marked by a regressive event and deposition of an areally extensive shoreface sandstone of the Milk River Formation across the southern plains (Leckie and Smith, 1992). Cycles 2 and 3 coincide with the accretion of North Cascades and Coast belts, and the Insular Superterrane (Stockmal *et al.*, 1992).

Cycle 4 comprises Campanian to Paleocene strata and includes the Belly River and Bearpaw formations, and the Edmonton Group to the top of the Paskapoo Formation. It is primarily characterized by non-marine deposition (with the notable exception of the marine Bearpaw Shale), that were deposited during an episode of high subsidence and thrusting, corresponding to the collision of the Coast and Insular Belt and the uplift of the Omenica belt (Leckie and Smith, 1992).

The final cycle constitutes Tertiary Conglomerates in the southern plains and include the Cypress Hills and Wood Mountain formations. Sedimentation during Cycle 5 post-dates compressional deformation in the foreland basin and its origin remains enigmatic. Leckie and Cheel (1989) proposed that the coarse boulders of the Cypress Hills conglomerates were remobilized because of uplift related to tertiary magmatic intrusions in the Sweetgrass Hills and Bearpaw Mountains of northern Montana.

1.3 Tectonic elements in proximity to the study area

Although few major structural features occur within or in proximity to southeastern Alberta, the few elements that are present have had a profound effect on depositional patterns. The major paleotectonic element is the Sweetgrass Arch. It forms the western and northwestern margins of the intracratonic Williston Basin and separates pre-Jurassic platform deposits in the west from post-Jurassic strata in the Alberta Basin to the east (Leckie and Smith, 1992; Poulton, 1984). The Sweetgrass Arch comprises several sub-components, each with different origins (Tovell, 1958; Herbaly, 1974). It includes the northwest-plunging South Arch and the northwest-striking Kevin-Sunburst Dome in north-central Montana (Hayes, 1983; Podruski, 1988; Arnott *et al.*, 1995) (Fig. 1.6). These discrete entities, which are separated along the Pendroy Fault Zone, underwent recurring tectonic movement during

Figure 1.6. Distribution of sub-components of the Sweetgrass Arch in southeastern Alberta and northern Montana, and location of various domal structures in proximity to the arch. Note the change in the trend of the arch near the international border from northwest to northeast-southwest (adapted from Podrusky, 1988; and Arnott *et al.*, 1995).

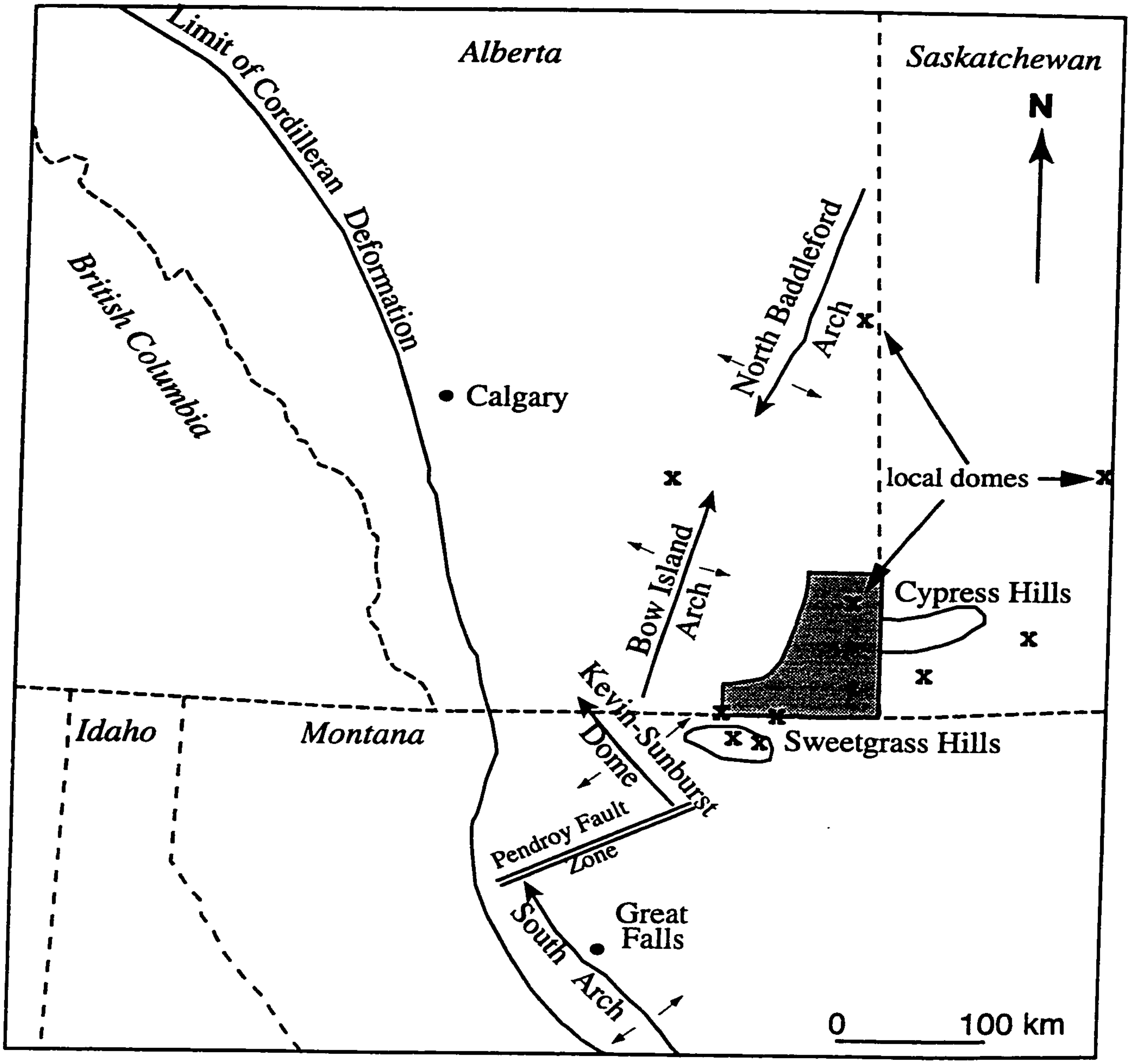
Alberta
Saskatchewan
N
Limit of Cordilleran Deformation
British Columbia
Calgary
North Baddleford Arch
local domes
Bow Island Arch
Cypress Hills
Kevin-Sunburst Dome
Sweetgrass Hills
Idaho
Montana
Pendroy Fault Zone
South Arch
Great Falls
0
100 km

the Cambrian, Jurassic, Cretaceous and Paleogene (Prodruski, 1988; Wright *et al.*, 1994; Arnott *et al.*, 1995). Facies patterns suggest that, during the Jurassic, the Sweetgrass Arch extended into southern Alberta as a broad, low amplitude, northeast-trending structure (Hayes, 1983; Podruski, 1988). Much later, during the Paleogene, a narrower but much higher north-east trending Bow Island Arch developed in proximity to the ancient Sweetgrass Arch as a result of compressional tectonics (Podruski, 1988). Despite its much younger age, the Bow Island Arch is commonly mistaken to be the northern extension of the Sweetgrass Arch. In any case, in the Late Jurassic, the Sweetgrass Arch was a major positive topographical feature in southeastern Alberta that significantly influenced marine circulation, sedimentation patterns, and erosional processes (Christopher, 1964; Brenner *et al.*, 1974; Hayes, 1983). The relative position of the Kevin-Sunburst Dome with respect to the northern portion of the Sweetgrass Arch in the Late Oxfordian likely resulted in the development of a strait between these structures. This strait effectively connected the Alberta Basin in the west to the ancestral Williston Basin in the east (Imlay, 1980, fig. 10). Within this strait, sediment transport mechanisms may have been significantly different from those in much of the rest of the Jurassic basin where sedimentation was dominated by suspension fallout.

Strata in southeastern Alberta are essentially undeformed, except for a consistent steep dip toward the northeast (Fig.1.7). This was caused by kilometre-scale uplift related to Eocene, alkalic igneous intrusion in the Sweetgrass Hills complex, which flanks the eastern side of the Kevin-Sunburst Dome in north-central Montana. Although these domal structures are concentrated in north-central Montana, they are not restricted to that area, and isolated intrusions also occur in southeastern Alberta and southwestern Saskatchewan (Podruski, 1988) (Fig. 1.6). However, some domal structures that occur in proximity to the Sweetgrass Arch have different origins, including salt dissolution and meteorite impact structures (Podruski, 1988). For example, in townships 8 and 9, range 4w4, Mississippian and Jurassic strata occur consistently higher than adjacent strata (Fig. 1.8). This anomalous feature represents the uplifted central core of a relatively small crater (~ 15 km in diametre) that was formed by a Late Cretaceous to Early Tertiary meteorite impact (Sawatsky, 1976; Ezeji-Okoye, 1985; Grieve *et al.*, 1998).

Figure 1.7. Structure map of the top of the Rierdon Formation in southeastern Alberta depicting steep northeast dipping strata. The anomalous dip direction and dip angle are related to Tertiary alkaline igneous intrusion in the Sweetgrass Hills of northern Montana.

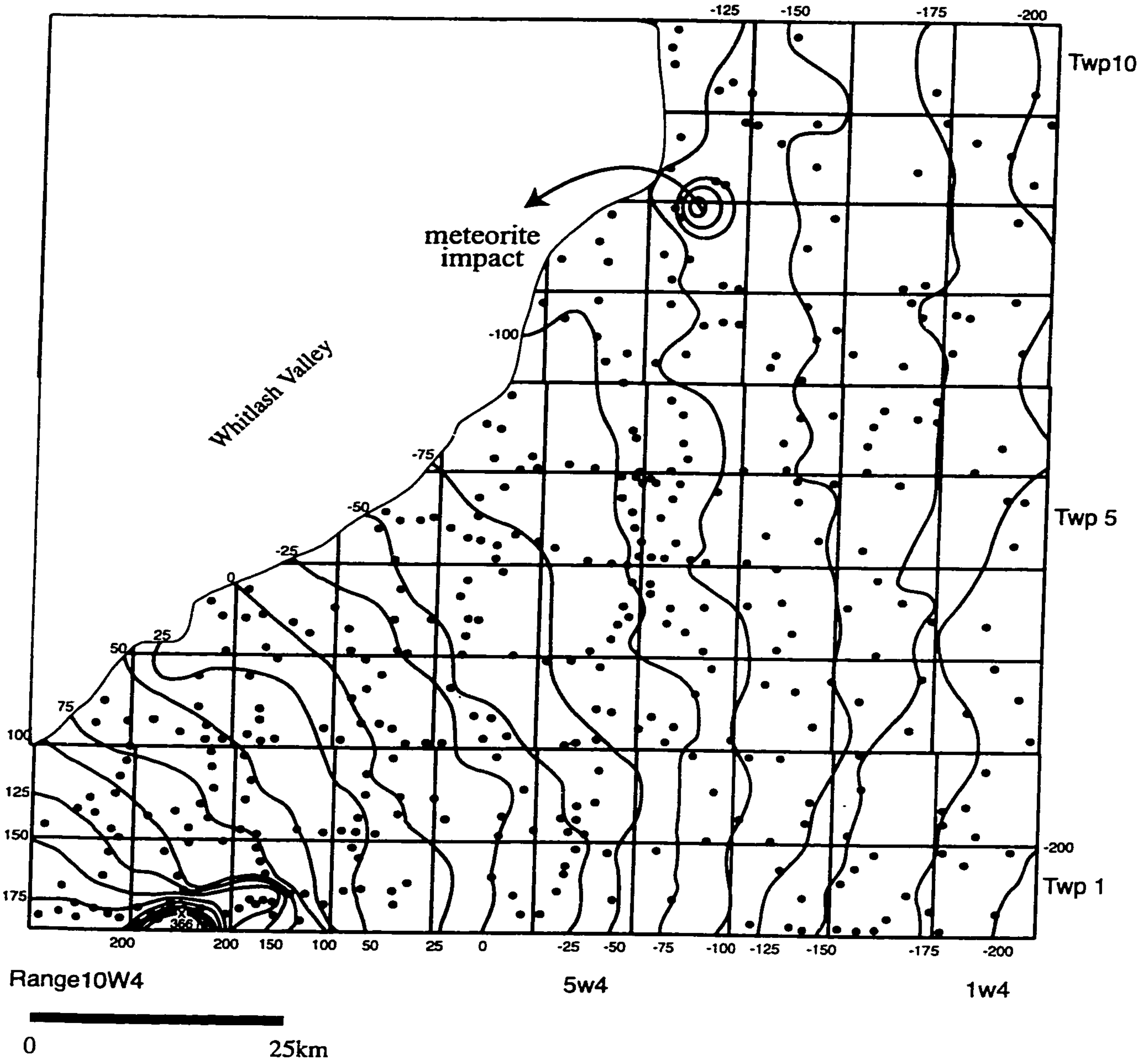
-125
-150
-175
-200
Twp10
meteorite impact
-100
Whitlash Valley
-75
-50
-25
0
25
50
75
100
125
150
175
366
Twp 5
-200
Twp 1
200
200
150
100
50
25
0
-25
-50
-75
-100
-125
-150
-175
-200
Range10W4
5w4
1w4
0
25km

Figure 1.8. Wireline cross section illustrating the vertical displacement of strata in the Eagle Butte meteorite impact structure (twps 8 and 9, range 4w4) and approximate location of wells with respect to a generalized complex crater structure. Significant displacement is evident in the central uplift portion of the crater (modified from Grieve *et al.*, 1995).

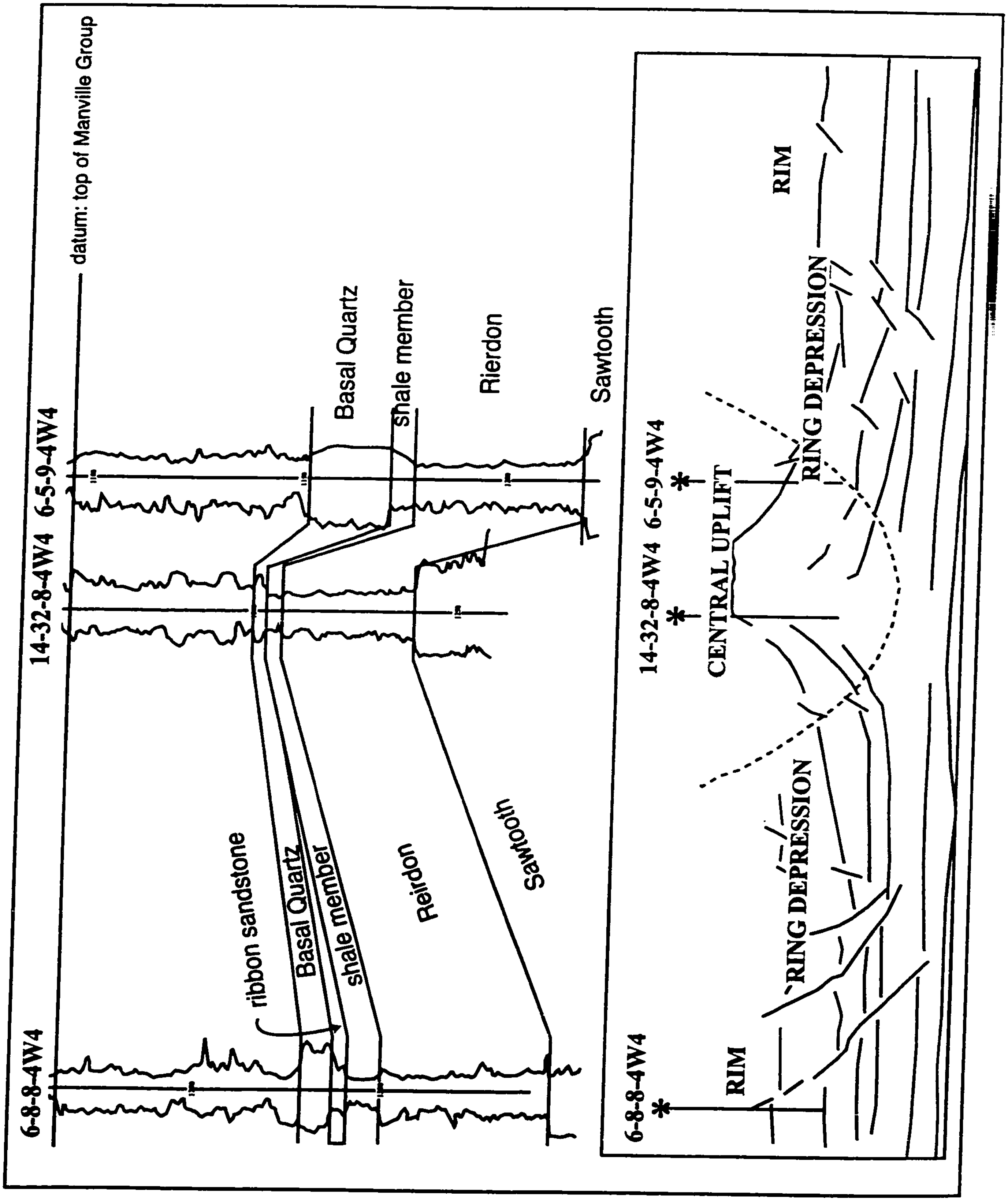
6-8-8-4W4
14-32-8-4W4
6-5-9-4W4
datum: top of Manville Group
ribbon sandstone
Basal Quartz
shale member
Reirdon
Sawtooth
Basal Quartz
shale member
Rierdon
Sawtooth
6-8-8-4W4
14-32-8-4W4
6-5-9-4W4
RIM
RING DEPRESSION
CENTRAL UPLIFT
RING DEPRESSION
RIM

In addition, the study area occurs on the Archean Medicine Hat Block. This Precambrian terrane is bounded to the north and west by the Vulcan Low, which represents an ancestral collisional suture zone (Hoffman, 1988), and, to the south is separated from the Wyoming Craton of the northern United States by a Proterozoic shear zone termed the Great Falls Tectonic Zone (O'Neill and Lopez, 1985) (Fig. 1.9). The Medicine Hat Block is characterized by a north-northwest-trending fabric of narrow positive and negative aeromagnetic anomalies of moderate intensity (Ross *et al.*, 1989). Based on drill core samples the terrane is interpreted to be composed largely of metaplutonic gneisses that are 2.65 – 3.27 Ga old (O'Neill *et al.*, 1988). Previously, there has been no suggestions of recurring tectonic movement during the Phanerozoic along the suture zones between the Precambrian terranes.

1.4 Previous work on the Swift Formation

Little has been published in the geological literature on the Oxfordian Swift Formation. Middle to Upper Jurassic marine shale and limestone were first recognized in Montana by Fisher (1909), who named them the Ellis Formation. Later, Cobban (1945) elevated the Ellis Formation to group status and subdivided it into the Sawtooth, Rierdon and Swift formation. He defined the Swift Formation from several exposures in Montana and recognized two informal members: a lower shale member and an upper sandstone member. At the type section on the Swift reservoir, Pondera County, Montana, the Swift Formation unconformably overlies calcareous shales of the Rierdon Formation. Its basal contact is characterized by glauconite-rich shale containing black chert pebbles and rounded belemnites fragments. The lower member is 16.6 metres thick and consists of dark grey, non-calcareous, finely micaceous shale with minor siltstone laminae, pyrite and large calcareous concretions. It, in turn, is overlain by the upper sandstone member, which comprises a thin (< 18 cm) basal glauconitic chert-pebble conglomerate and fine grain, small scale cross-stratified sandstone with abundant shale drapes, common coalified wood fragments and accessory glauconite. Coarse and medium sandstone are uncommon but do occur in the basal portion of the upper sandstone member. The Swift Formation is conformably overlain by continental

Figure 1.9. Map of tectonic domains that form the basement rocks in Alberta and northern Montana. The study area overlies part of the Archean Medicine Hat Block. The Vulcan Low and Great Falls Tectonic Zone, bound the Medicine Hat Block and represents ancient suture zones along which movement may have been reinitiated during the Columbian-Nevadan Orogeny. Wy: Wyoming Craton; GTZ: Great Fall Tectonic Zone; MHB: Medicine Hat Block; VL: Vulcan Low; LoB: Loverna Block; L: Lacombe Block; R: Rimbey High; T: Thornsby Low; Wa: Wabamun Domain; Rae: Rae Province; Ta: Taltson Arc; B: Buffalo Head Domain; C: Chinchaga Low; K: Ksituan High; Kw: Kiskatinaw; No: Nova Domain; H: Hottah Terrane; G: Great Bear Domain; F: Fort Simpson High; N: Nahani Terrane; STZ: Snowbird Tectonic Zone; HRF: Hay River Fault (modified from Ross *et al.*, 1991).

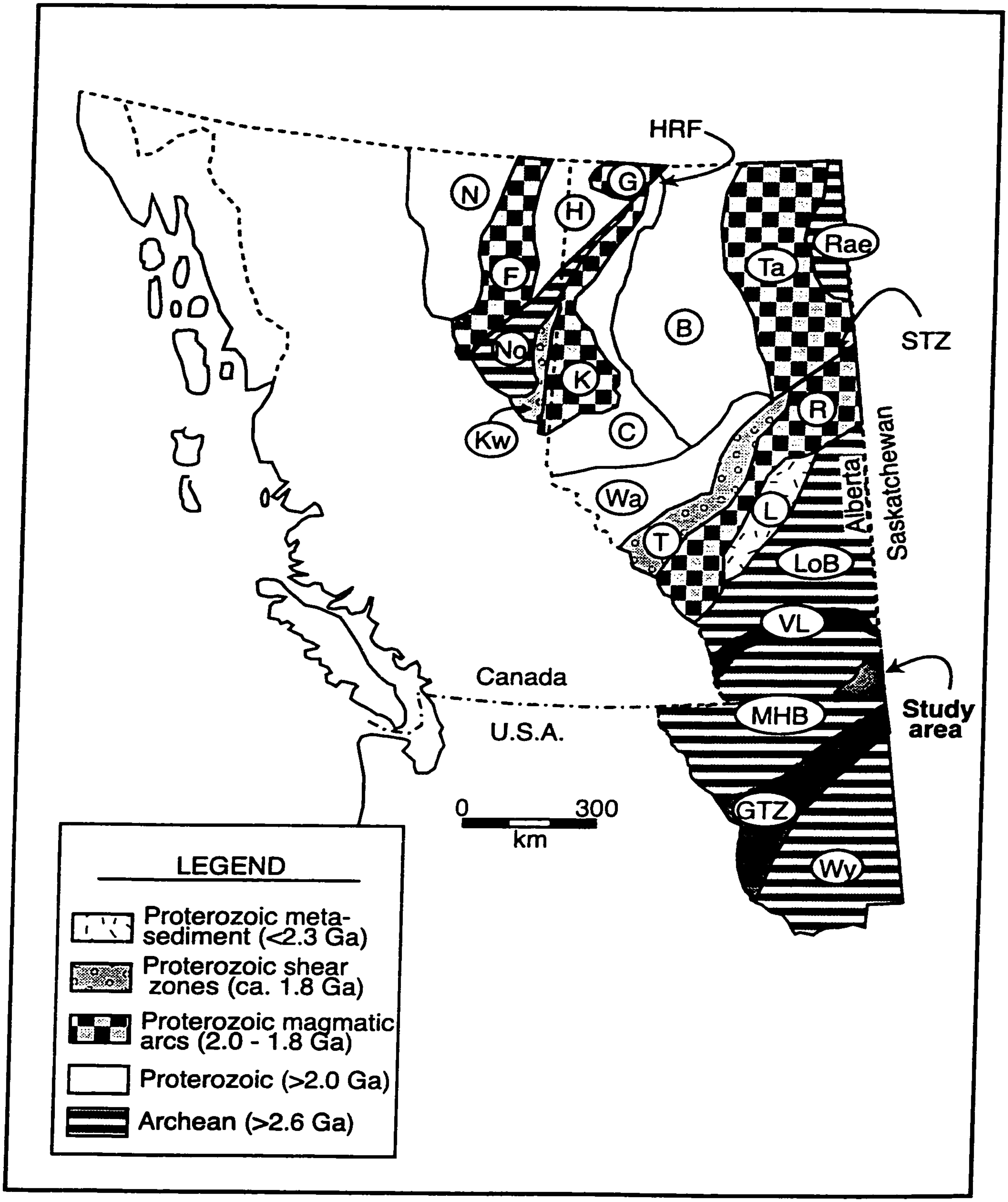
HRF
N
G
H
F
B
Rae
Ta
STZ
No
K
R
Kw
C
Wa
L
Alberta
Saskatchewan
T
LoB
VL
Canada
U.S.A.
Study area
MHB
0
300
km
GTZ
Wy
LEGEND
Proterozoic meta-sediment (<2.3 Ga)
Proterozoic shear zones (ca. 1.8 Ga)
Proterozoic magmatic arcs (2.0 - 1.8 Ga)
Proterozoic (>2.0 Ga)
Archean (>2.6 Ga)

deposits of the Morrison Formation or unconformably by Lower Cretaceious Cutbank and Sunburst fluvial sandstosne (Basal Quartz) (Fig. 1.10).

Weir (1949) subsequently extended Cobban's nomenclature to the subsurface in southern Alberta. Much later, Brenner and Davies (1974) proposed a two-stage depositional model for the Swift Formation in the northwestern states. The members in their study differ somewhat from those at type section in Montana. The lower member comprises two facies: mudstone in the basin, and sandstone along the western edge of the basin near the Belt Island trend highlands in southern Montana. The nearshore sandstone facies encompasses a range of lithologies and includes an upward-coarsening succession interpreted to reflect deposition in a prograding delta-like environment, and upward-fining channelized sandstone, interpreted to represent distributary channels fills. The lower member was interpreted to have been deposited during an overall transgression. This was then interpreted to be followed by a basin-wide regression and the deposition of two facies associations: 1) a nearshore sheet-like sandstone in western Montana and farther basinward, in central Montana, southern Alberta, and most of Wyoming, a marine sand bar facies (offshore bars). These "bars" consist of upward-coarsening successions that are up to 21 metres thick and several kilometres long, and are capped by medium-scale cross-stratified sandstone. Locally they occur as stacked successions. The interbar areas consist of flaser bedded strata. Locally, coquinoid sandstone bodies with erosive basal contact were incised into the bars and pinch-out into the interbar areas. Brenner and Davies (1974) interpreted these to be the high-energy storm deposits.

Hayes (1983) subsequently extended Brenner and Davies transgressive-regressive model to the subsurface in southeastern Alberta. In this area, the lower member closely resembles the lower shale member at the Swift type section. However, the upper member, informally termed the ribbon sands by Hayes, differs from strata at the type section. It consists of interbedded mudstone and very fine sandstone (dominantly lenticular to wavy bedding), with uncommon sandstone-rich strata that occur locally within the unit. Similar to Brenner and Davies' model, the sandstone-rich bodies were interpreted to be the result of high-energy storms. However, the mechanism responsible for their deposition and distribution was not described in detail. Hayes also noted that the ribbon sands are marked

Figure 1.10. Stratigraphic nomenclature of Jurassic and Cretaceous strata in southeastern Alberta. Although the Morrison Formation is present locally in southeastern Alberta, it was not observed in this study (modified from Leckie and Smith, 1992).

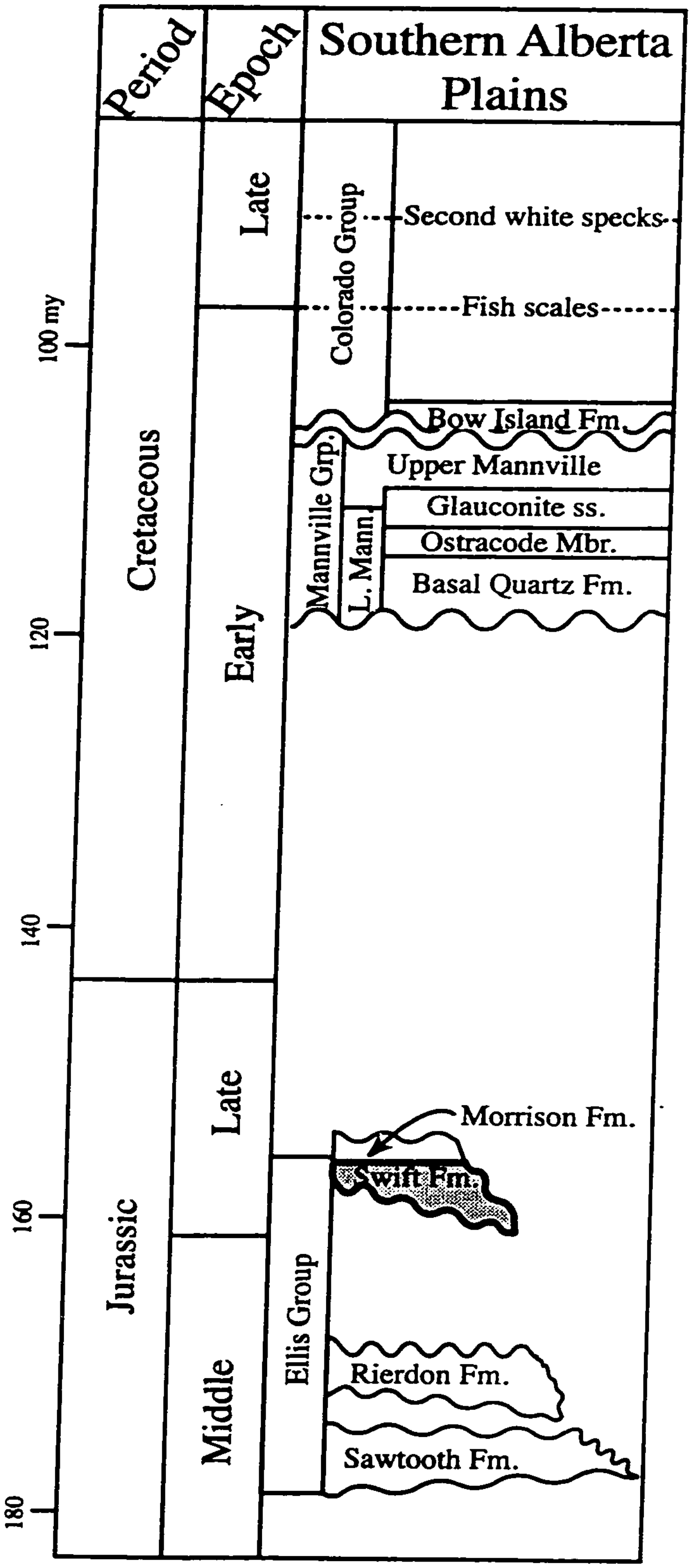
Period
Epoch
Southern Alberta Plains
Cretaceous
Jurassic
Late
Early
Late
Middle
100 my
120
140
160
180
Colorado Group
Second white specks
Fish scales
Bow Island Fm.
Mannville Grp.
Upper Mannville
L. Mann
Glauconite ss.
Ostracode Mbr.
Basal Quartz Fm.
Morrison Fm.
Swift Fm.
Ellis Group
Rierdon Fm.
Sawtooth Fm.

by a sharp colour change from dark to light coloured mudstone interbeds. The nature of this change, however, was poorly understood but was thought to be possibly related to environmental changes in the basin from anoxic to oxic conditions. Subaerial exposure between deposition of the dark and light ribbon sands was not ruled out however, although no signs of subaerial exposure were reported. In this thesis, a slightly modified version of Hayes's terminology is adopted, recognizing a lower shale member and an upper ribbon sandstone.

Although few in numbers, other studies on the Swift Formation can be found. Brooke and Braun (1972) described the microfauna from Jurassic strata in southern Saskatchewan and north-central Montana. Also, Radella and Galuska (1966) described the Flat Coulee oil field in northern Montana, where the Swift Formation is the main oil and gas producer. Hydrocarbons are produced from two narrow, elongated, porous, sandstone-rich bodies, that trend roughly northeast-southwest, each encased dominantly in mudstone. The main producing horizon occurs at about 16 m above the Rierdon-Swift contact; a secondary horizon is about 10 m lower. The depositional mechanisms for the sandstone bodies were not discussed in that study. More recently, Leckie *et al.*, (1997) studied the Success Formation in southwestern Saskatchewan as part of a larger study. The Success was subdivided into two members; the S1 and S2 (Christopher, 1974; Hayes, 1983; Christopher, 1984; Poulton, 1984, 1989; Leckie *et al.*, 1997). The S1 consists of interlaminated very fine sandstone and grey to black siltstone with common sphaerosiderite and accessory glauconite (Poulton, 1984), and was shown to be the laterally equivalent to the ribbon sandstone (Hayes, 1983). The S2 is laterally equivalent to the Basal Quartz Formation.

1.5 Sequence stratigraphy

Sequence stratigraphy, developed in large part by the Exxon Production Research Group in the early 1980's, is a stratigraphic tool commonly used to correlate sedimentary rocks. The fundamental unit is a depositional sequence which is defined as a "relatively conformable succession of genetically related strata bounded by unconformities and their correlative conformities" (Van Wagoner *et al.*, 1990). Sequences are made up of parasequences, which in turn formulate parasequence sets. A parasequence is a "relatively conformable succession of genetically related beds and bedsets bounded by marine-flooding surfaces and their correlative surfaces" (Van Wagoner *et al.*, 1990). A parasequence set, on the other hand, is a "succession of parasequences which form a distinctive stacking pattern that is bounded by major marine flooding surfaces and their correlative surfaces" (Van Wagoner *et al.*, 1990). Parasequence sets may be aggradational, progradational or retrogradational and are related to changes of sediment flux and accommodation space in the basin. Sequences and their stratal constituents are interpreted to form in response to the interaction between eustasy, subsidence, sediment supply and basin physiography (Posamentier and Allen, 1993). In the Western Canada Foreland Basin, the interplay between subsidence and sediment supply played a significant role in depositional style.

Prior to the development of sequence stratigraphy, Sloss (1963) had subdivided Phanerozoic strata of the North American craton into six sequences. Each sequence was bounded by craton-wide, and most probably world-wide unconformities that passed laterally into their correlative conformities. Presently, these sequences are considered to be second order cycles in the terminology of Plint *et al.* (1992). Middle Jurassic to Lower Cretaceous strata in the western Interior of North America forms Sloss's lower Zuni Sequence. In western Canada, it includes the Ellis, Mannville, Colorado and Alberta groups. In this area, several third order and fourth order cycles have also been identified within the lower Zuni Sequence. However, despite these numerous studies, the sequence stratigraphic framework of the Swift Formation (Ellis Group) is still largely unknown.

1.6. Currents in shallow marine environments

Numerous types of currents occur in shallow marine environments such as continental shelves, epeiric seas, and the shallow part of foreland basins. These flows are the principle component of sediment transport, deposition and erosion in the shallow marine and include oceanic, tidal, and storm-generated currents. The influence of shallow marine currents on the sedimentary record has long been recognized in both modern and ancient environments (Swift *et al.*, 1971; Hamlin and Walker, 1979; Knight *et al.*, 1986; Walker, 1984). Recently, advances in our understanding of these processes, and in particular combined flow, have much improved our interpretation of the ancient shallow marine sedimentary record (e.g. Duke, 1990; Arnott, 1992). However, the preserved record of shallow marine systems is commonly complicated by the effects of periodic changes in relative sea level (Walker and Plint, 1992). Significant erosion is commonly associated with falling and rising of relative sea level, thereby modifying the distribution and geometry of the original deposits.

Because the Swift Formation is interpreted in this thesis to have been deposited in a low-energy marine environment characterized by periodic increases in both wave and tidal energy, a more detailed discussion on shallow marine processes is warranted. This section reviews briefly each of the three principal kinds of currents that affect sediment entrainment and dispersal in shallow marine environments: 1) oceanic currents, 2) tidal currents, and 3) meteorological currents. This is followed by a discussion on sedimentation characteristics in tide- and storm-dominated environments.

1.6.1 Oceanic currents

Ocean currents are the result of thermohaline circulation or wind-forcing. Thermohaline circulation is produced by density differences related to salinity gradients and thermal stratification of the water column. These currents are deep and relatively slow (typically 1 – 2 cm/sec at depths of 1500 to 2000 m) (Gross, 1977). Furthermore, they typically have a complex array of flow directions that are partially related to deflection caused by the rotation of the earth (Corialis effect), physiography of the coastline, and topography of the ocean floor.

Wind-driven currents constitute the second main kind of ocean currents. Wind-driven currents are related to atmospheric wind patterns and hence, are relatively shallow flows, although with time they progressively deepen due to turbulent mixing of the water. Global wind patterns develop because of uneven heating of the atmosphere by the Sun. Because of the Corialis effect, air is deflected to the right in the Northern Atmosphere and to the left in the Southern Atmosphere. As a result, the global wind patterns produced consist of prevaling trade winds and westerlies. Trade winds blow steadily toward the equator from the northeast in low northern latitude (<30°), and from the southeast in low southern latitudes (<30°). Mid-latitude westerlies blow from the west, away from the equator. Shearing by this large-scale atmospheric wind system produces the shallow wind-driven oceanic currents.

Oceanic currents generally occur oceanward of the shelf break, and as a result only effect the outer part of some continental shelves. Major ocean currents are generally not narrowly confined flows but instead consist of numerous filamentary flows with meanders and eddies; commonly when meanders grow too large they can become detached from the main current and are advected toward the adjacent continental shelf. Approximately 3% of modern continental shelves are dominated by strong, one dimensional oceanic currents, which operate most effectively on the outer shelf near the shelf break (Walker, 1984; Boggs, 1987). Modern examples of ocean currents include the Gulf Stream system, the Algulhas Current along the southeast African continental shelf and the Panama and North Equatorial currents that parallel the northeastern coast of South America. Generally, ocean currents contribute little new sediment to continental shelves but are able to rework and redistribute significant amounts of relict shelf sediment.

1.6.2 Meteorological currents

Currents in shallow marine environments are strongly affected by meteorological forces, principally wind. When wind blows over a body of water, energy is transferred to the water surface , which in turn results in the formation of non-periodic surface waves. In deep water, surface waves start growing when wind speeds exceeds 1 m/s. Waves continue to grow with increasing wind speeds, until they reach speeds equal to one third the wind speed. Beyond this, waves continue to grow in size, wavelength, and speed but at diminishing rates (Open University Course Team, 1989). There are three reasons why wave growth ceases before it reaches speed of wind. Firstly, some wind energy is dissipated by friction. Secondly, some of the energy transferred onto the water surface produces surface currents, and thirdly, some energy is lost as a result of white-capping (breaking of the tip of the wave crest). Wave size is also related to fetch. Areas with large fetch, (e.i. oceans) can support the development of large waves. On the other hand, smaller bodies of water, such as enclosed seas (smaller fetch), form comparatively smaller waves because much of the energy generated by wind shear stress is quickly dissipated nearshore instead of being transferred for wave growth.

Water particles in waves in deep water move essentially in a circular orbit. At the surface, the diameter of the orbits corresponds to the wave height. With depth, orbital diameter decreases exponentially and at a depth of ~ 1/2 the surface wavelength, is only 5% of the surface diameter (Fig. 1.11a). It is important to note that these orbits are not completely closed, and, as a result, there is a small net displacement that takes place in the trough, causing a wave-drift current (Fig. 1.11c). In shallow water, where depth is less than half the wavelength, orbits become progressively more elliptical and flatter with depth (Fig. 1.11b). Close to the sea floor, the orbital water motion is degraded to an asymmetrical to-and-fro rectilinear motion that causes a net onshore movement of sediment.

1.4.2 Tidal currents

Along coastlines, tides are special types of waves characterized by a rhythmic rise (flood tide) and fall (ebb tide) of sea level over several hours. Tides are generated by the comnined gravitational forces of the Moon and Sun. The Moon exerts the strongest tide-generating force, which is 0.54 greater than that of the Sun because, despite its smaller mass, it is approximately 360 times closer to the Earth (Open University Course Team, 1989). Tidal range is highest when the Sun, Moon, and Earth are nearly aligned such as during the full and new moons, and form what are termed spring tides. Conversely, when the Sun and Moon are at right angles, during the first and third quarters, their forces counteract one another and the resulting tidal range is smallest; termed neap tides. Because the relative motions of the Earth, Sun, and Moon are complex, their effects on tidal events are equally complex. Furthermore, the magnitude of tides is also modified by the distribution of continents, and the physiography of the ocean floor. In addition, weather patterns can also

Figure 1.11 Orbital motion in wind-generated oceanic waves (modified from Open University Course Team, 1989).

Figure 1.11a) Water particle motion in deep-water waves. Note the exponential decrease in orbital diameter with depth.

Figure 1.11b) Water particle motion in deep-water waves. Wave orbits are not completely closed, which results in wave-drift currents.

Figure 1.11c) Water particle motion in shallow-water waves. Orbits become progressively more elliptical with depth, eventually degrading to to-and-fro motion at the bed.

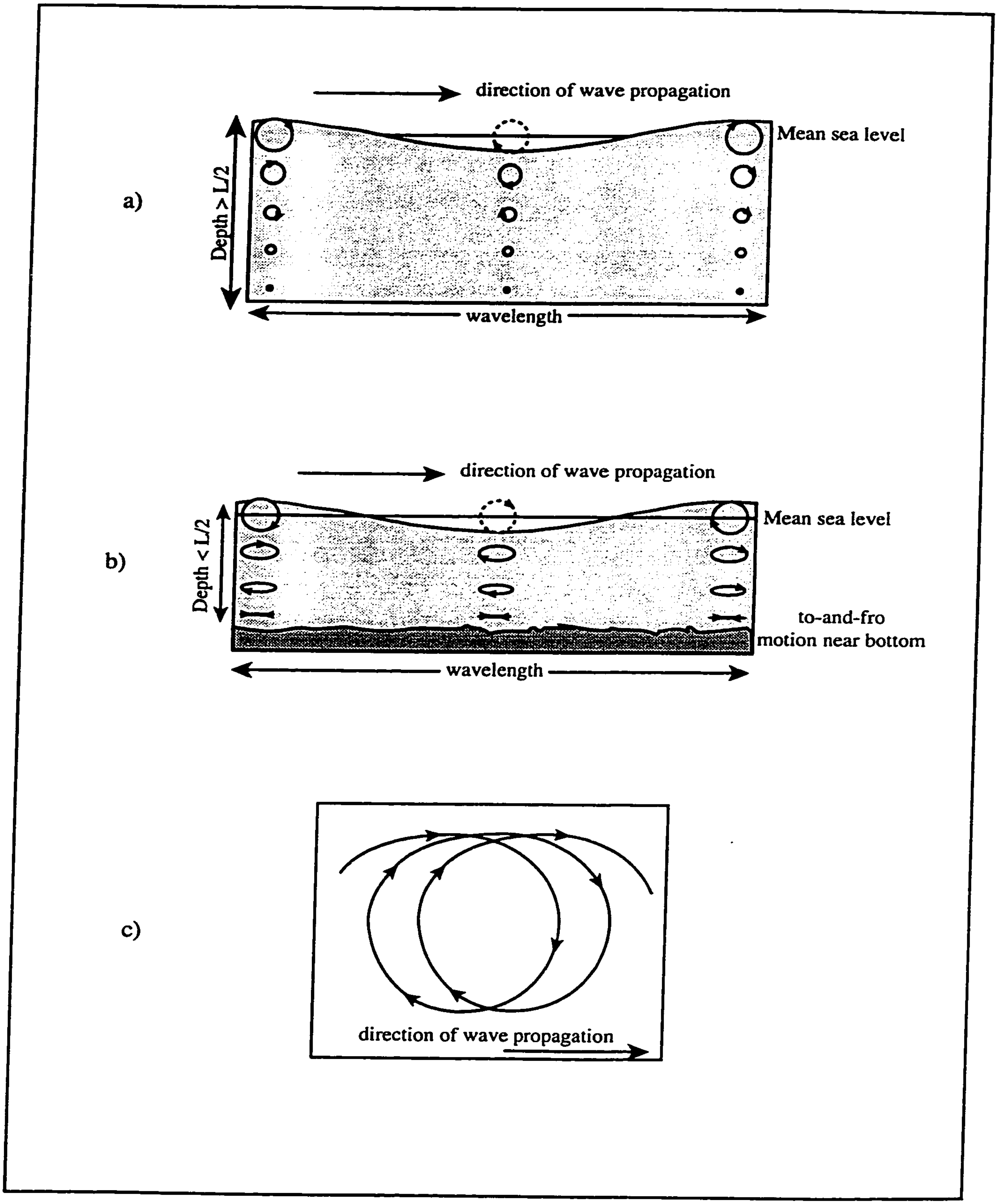
direction of wave propagation
Mean sea level
a)
Depth > L/2
wavelength
direction of wave propagation
Mean sea level
b)
Depth < L/2
to-and-fro
motion near bottom
wavelength
c)
direction of wave propagation

amplify tidal magnitude. The numerous variables that affect tides makes modelling difficult, and therefore the equilibrium theory of tides presented below assumes an idealized Earth, completely covered by deep water of uniform depth. Although this theory does not provide a complete explanation of the tidal phenomenon it does serve as a useful first approximation.

Tides are related to two forces: 1) the gravitational attraction of the Moon, which is strongest on the side of the Earth facing the Moon and 2) the centripetal force, which is caused by the eccentric revolution of the Earth around the centre of mass of the Earth-Moon system. Contrary to the gravitational force, the centripetal force exerts equal intensity on all points on and within the Earth. The vector sum of the gravitational and centripetal forces pulls the water in the oceans towards the Moon and towards the side opposite to the Moon, forming two bulges (Fig. 1.12a). Because the Earth rotates, the bulges appear to travel around the Earth as two waves, causing water to rise and fall semi-diurnally (twice a day). Typically, one of the semidiurnal tides will be higher (dominant tide) than the second, which follows approximately 12 hours later (subordinate tide). The cause of this inequality is related to the declination of the Moon. The Moon's orbit is inclined at an angle of 28° with respect to the Earth's equatorial plane. In other words, the line that joins the centre of the Earth to that of the Moon varies from 0° to 28° on either side of the equator over a period of 27.32 days (Kvale *et al.*, 1998) (Fig. 1.12b). The daily inequality in semidiurnal tidal range is greatest when the declination of the Moon is highest. On the other hand, the dominant and subordinate tides are equal when the Moon is over the equator. Not all coastal areas are characterized by semidiurnal tides. Depending on coastal geometry, some areas record only diurnal tides (one tide per day) because the subordinate tide is damped out by destructive interference.

Because tide-generating forces are small, measurable tides are entirely formed in the open oceans, where the tidal range is typically less than 1 metre. Smaller bodies of water such as enclosed seas (e.g. the Mediterranean Sea) or water overlying continental shelves, cannot develop significant tides of their own. Tidal currents observed on continental shelves are the result of ocean tidal waves propagating onto adjacent shelves. As the tidal waves shoal onto the shelf and/or converge in coastal embayments, the tidal prism is concentrated

Figure 1.12 Origin of tides and tidal ranges.

Figure 1.12a) The derivation of tide-producing forces on Earth. The centrifugal force is equal at all points on Earth whereas gravitational forces are strongest on the side of the Earth immediately beneath the Moon (modified from Dalrymple, 1992).

Figure 1.12b) The Moon's orbit does not parallel the earth's equator. This declination (max 28°) produces unequal diurnal tides at mid-latitudes (modified from Open University Course Team, 1989).

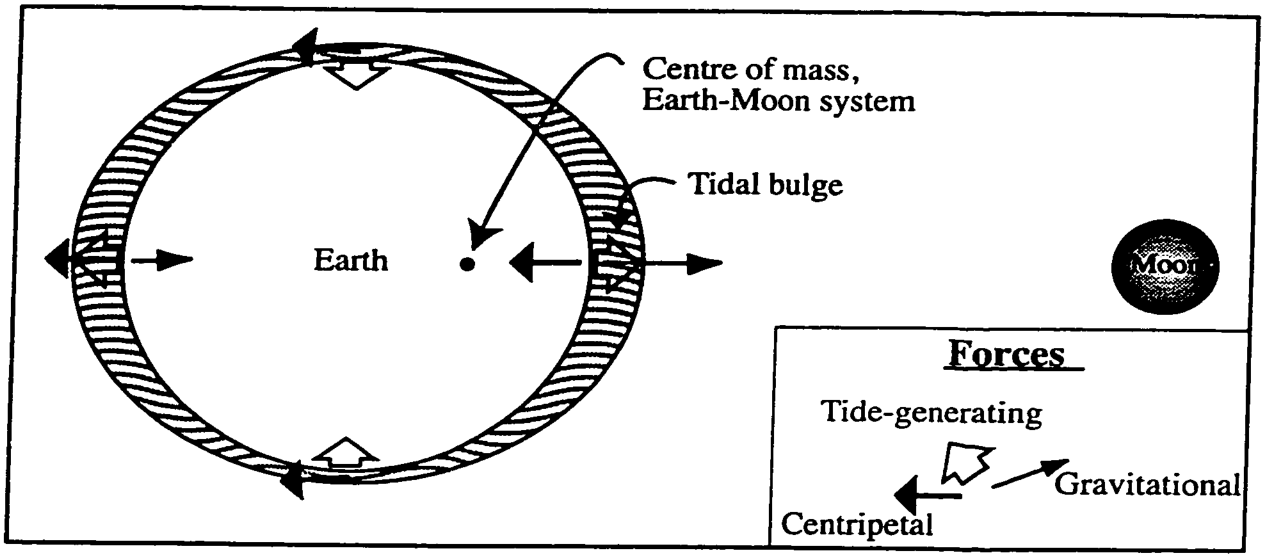
Centre of mass,
Earth-Moon system
Tidal bulge
Earth
Moon
Forces
Tide-generating
Gravitational
Centripetal

(a)

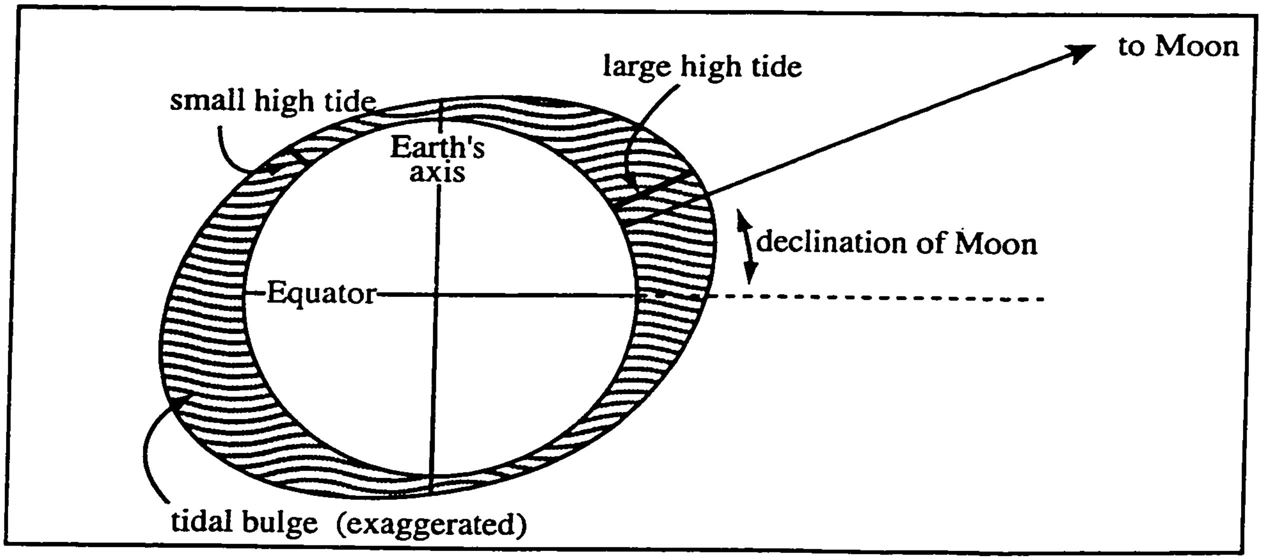
to Moon
large high tide
small high tide
Earth's axis
declination of Moon
Equator
tidal bulge (exaggerated)

(b)

into a smaller cross-sectional area and, as a result, the tidal range and current speeds increase.

Coastline settings have been subdivided into three groups according to their tidal ranges: 1) macrotidal (> 4 m range), 2) mesotidal (2-4 m range), and 3) microtidal (< 2m range). Areas characterized by macrotidal tides are typically dominated by tidal processes whereas mesotidal and microtidal areas are generally dominated by wave processes. However, in sheltered settings, where wave action is limited, or in constricted areas such as straits, tidal inlets, and estuaries, where tidal current speeds are generally increased, tides can control the spatial and temporal characteristics of bed-load sediment transport and deposition, even in microtidal settings. For Example, Chesapeake Bay on the east coast of the United States is microtidal (1 m tidal range) but, because its mouth is very small relative to its size, it has near-surface tidal current speeds comparable to macrotidal areas, ranging from 0.5 to 1 m/s (Dalrymple, 1992). Tidal currents are further amplified if the natural period of the body of water (the back and forth motion in the absence of a moving force) coincides with the tidal period, as in the case of the Bay of Fundy. Approximately 17% of the present day continental shelves are affected by strong tidal currents (Walker, 1984).

1.7. Sedimentation in shallow marine environments

1.7.1. Sedimentation in wave-dominated settings

Wave-induced sedimentation dominates in shallow marine environments where tidal processes are weak or absent. During fairweather, wave ripples may form above fairweather wave base (5–15 metres depth), providing that bottom velocities are high enough to move sediment. Small-scale orbital currents create eddies that throw sediment into suspension alternately on the landward and seaward side of the ripple crest. The forward and backward orbital wave velocities, however, are not always equal, and, consequently, oscillation ripples are not always symmetrical in cross-section, and so asymmetrical forms commonly develop. In addition, wave ripples tend to have form discordant cross-lamination. Symmetrical ripples commonly have unidirectional cross-lamination and asymmetrical ripples may have either symmetrical (chevron) or unidirectional cross-lamination (De Raaf *et al.*, 1977). Wave ripples are further distinguished by an undulating lower boundary rather than a flat base, which is more typical of current ripples. Ripple height and wave length generally increase with bottom orbital velocity. Oscillatory ripples generally have wavelengths ranging from 10 cm to 2 m, and heights ranging from about 3 to 25 cm. At higher orbital velocities, generally coincident with storms, sharp-based units containing hummocky cross-stratification (HCS) are produced in fine-grained sediment. HCS is a large scale, low angle style of cross-stratification characterized by swales (concave-up) and hummocks (convex-up) that formed under moderately strong, relatively long period waves. With a further increase of orbital velocity, HCS (gradationally?) is replaced by flat-based plane beds (sheet flows).

Storms are responsible for most increases in bottom orbital velocity and, despite the relatively short period of time storm conditions persist, their effects on sediment erosion, transport, and deposition, and hence the sedimentary record, are disproportionately large. During fairweather, sand tends to move onshore, steepening the beach profile. During storms, however, the beach profile is eroded and flattened, the shoreface is eroded and sediment transported offshore. Deposits from these high-energy events typically consist of a sharp base overlain abruptly by an upward-fining succession that displays a decrease in the size of sedimentary structures. These features are generally interpreted to indicate deposition under waning flow conditions.

1.5.2. Sedimentation in tide-dominated settings

Tides exert a significant influence on the sedimentary characteristics of a large number of many different depositional environments including deltas, estuaries, barrier islands, and shelf settings. Because of the regular rise and fall of the tide, and related waxing and waning of tidal current speed, tidal deposits commonly exhibit a regular alternation of sand and mud layers, forming what are termed tidal rhythmites. Tidal rhythmites are small-scale sedimentary deposits characterized by rythmically stacked sets of mud-draped ripples or intercalated siltstone and mudstone layers. In the terminology of Reineck and Singh (1980), these sets form cosets that can be classified as lenticular, wavy, or flaser bedding. Each individual layer was deposited in response to changing current velocities associated,

Figure 1.13 Variations in tidal current speed during one tidal cycle produces tidal rhythmites. In this idealized example, semi-diurnal tides are subequal in strength and, as a result, bedload transport occurs during both flood and ebb tides. Mud drapes are then deposited during the intervening slack water stage (modified from Dalrymple, 1992).

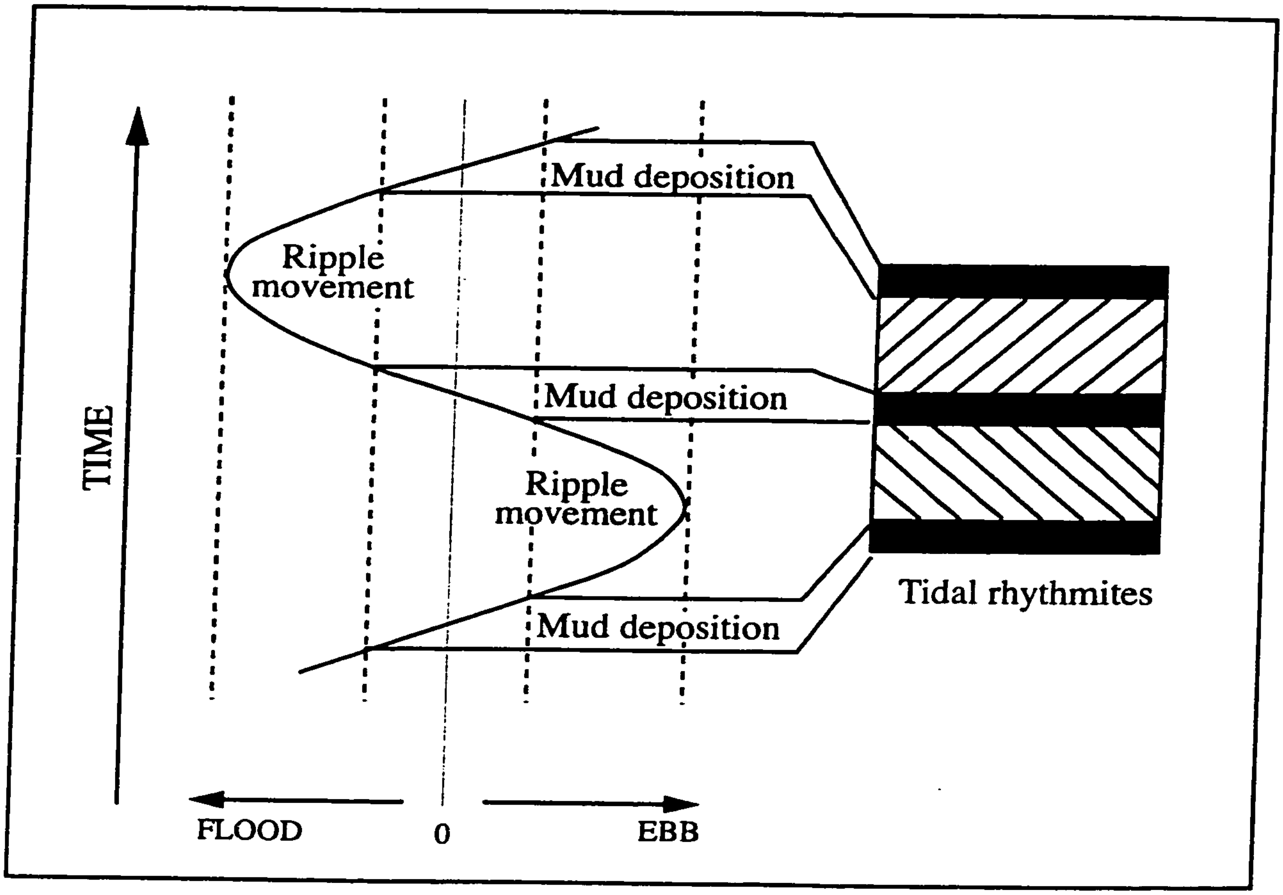
Mud deposition
Ripple movement
Mud deposition
Ripple movement
Mud deposition
TIME
Tidal rhythmites
FLOOD
0
EBB

with ebb and flood tides and the intervening slack water stages (Fig. 1.13). More commonly however, tidal rhythmites are composed almost entirely of either ebb or flood events, because most tidal systems are either flood- or ebb-dominated and the subordinate current is too weak to cause bedload transport (Kvale *et al.*, 1998). The layers also progressively thicken and thin in response to the spring-neap tidal cycle. Thicker sand layers correspond to higher high tides (spring tides), whereas thinner sand layers reflect lower high tides (neap tides). Presently, modern tidal rhythmites have only been observed in fresh to brackish water environments with large tidal ranges (> 3 metres) (Kvale *et al.*, 1998).

Where tidal currents are stronger, large scale bedforms develops. Active, large scale subaqueous dunes occur on numerous macrotidally influenced continental shelves (Belderson *et al.*, 1982; Stride *et al.*, 1982; Dalrymple, 1984; Davies *et al.*, 1992; Davies *et al.*, 1993). Within these dunes, stratification formed by the dominant tide is preferentially preserved. This is because the subordinate tidal current strength is generally lower and high speed tidal currents are maintained for a shorter period of time during the subordinate tide. As a result, less sediment is transported during the subordinate tide and thinner bedforms develop. Commonly, these deposits are almost completely eroded during the next tidal cycle and evidence for their presence is generally only preserved in the troughs of the tidal bundle (set deposited during the dominant tide).

Where sediment supply is ample and tidal currents sufficiently strong (> 1 m/s), linear tidal sand ridges (sand banks) may form, such as those in the North Sea. Tidal ridges cover large areas in tide-dominated shallow marine settings (~ 1000 km^2). They are generally 10 – 120 km long, 7.5 to 40 m high, have spacings of 1 – 30 km, and are oriented at about 20° to the principal tidal flow (Houbolt, 1968; Stride *et al.*, 1982; Twichell, 1983). Sand ridges are interpreted to form from reworked shelf sediment, which is transported downcurrent along tidal transport pathways. They display various types of cross-bedding, dominantly large scale, and may either coarsen or fine upward depending on sea level history. Numerous sand ridges on continental shelves have become moribund (inactive) as a result of post glacial eustatic rise and are now overlain only by small scale ripples, storm deposits or mud. Recently, however, some tidal sand ridges, such as those in the Celtic Sea, have been reinterpreted as erosional remnants related to lowstand erosion (Berné *et al.*, 1998). In the Celtic Sea, intense erosion of lowstand estuarine/deltaic deposits or sharp-based shorelines by tidal currents has lead to the development of shore-oblique ridges. These tidal ridges, therefore, most probably are the result of erosional rather than constructional processes.

Different tidal bedforms develop in specific zones along the dominant tidal current pathway on continental shelves, reflecting differences in the strength of the local tidal currents. In the direction of decreasing tidal current speed these zones are: 1) furrows and gravel waves where erosion is strongest, 2) flow-parallel sand ribbons where sediment is by-passed and there is no net sediment loss or gain, 3) extensive sand sheets with abundant dunes or sand ridges, 4) rippled sand sheets, 5) isolated sand patches, and 6) a zone of mud accumulation, if wave-induced currents permit deposition of fine-grain material (Fig. 1.14).

1.5. Paleosols

Following withdrawal of the Oxfordian sea, a regionally extensive soil horizon developed across the top of the Swift Formation. Because pedogenic processes significantly modified the texture and mineralogy of the upper part of the Swift Formation, a brief review of paleosols is deemed necessary and, therefore, is presented next.

A paleosol is the remains of an ancient soil. It may be buried by later deposits or be subaerially exposed but is no longer subject to the original pedogenic conditions. In terms of paleopedology, a soil consists of material formed at the surface of a planet (or similar body) and is altered in situ by chemical, physical and biological processes (Retallack, 1990). Paleosols are relatively common in the geologic record, although in some cases they are not easily recognized because of post-pedogenic processes such as diagenetic alteration and mineralization, or erosion by wave/tide ravinement processes.

The most diagnostic attributes of paleosols are: 1) fossil roots or root traces, 2) soil horizons, and 3) soil structures. Fossil roots are the best criteria for recognizing paleosols in sedimentary successions because they are evidence that plants were once present, and therefore, regardless of its appearance, it was once a soil (Retallack, 1990). However, the use

Figure 1.14 Block diagram of bedforms showing the streamwise variations in tide-generated sedimentary structures on a modern continental shelf with the corresponding near surface, mean tidal current speeds. Furrows, gravel beds, and sand ribbons are formed dominantly by erosion of palimpset sediment. Downcurrent, large and small dunes form from sediment sourced upcurrent. With decreasing tidal current speeds, smaller bedforms are generated (rippled sands sheet and sand patches) (modified from Belderson *et al.*, 1982)

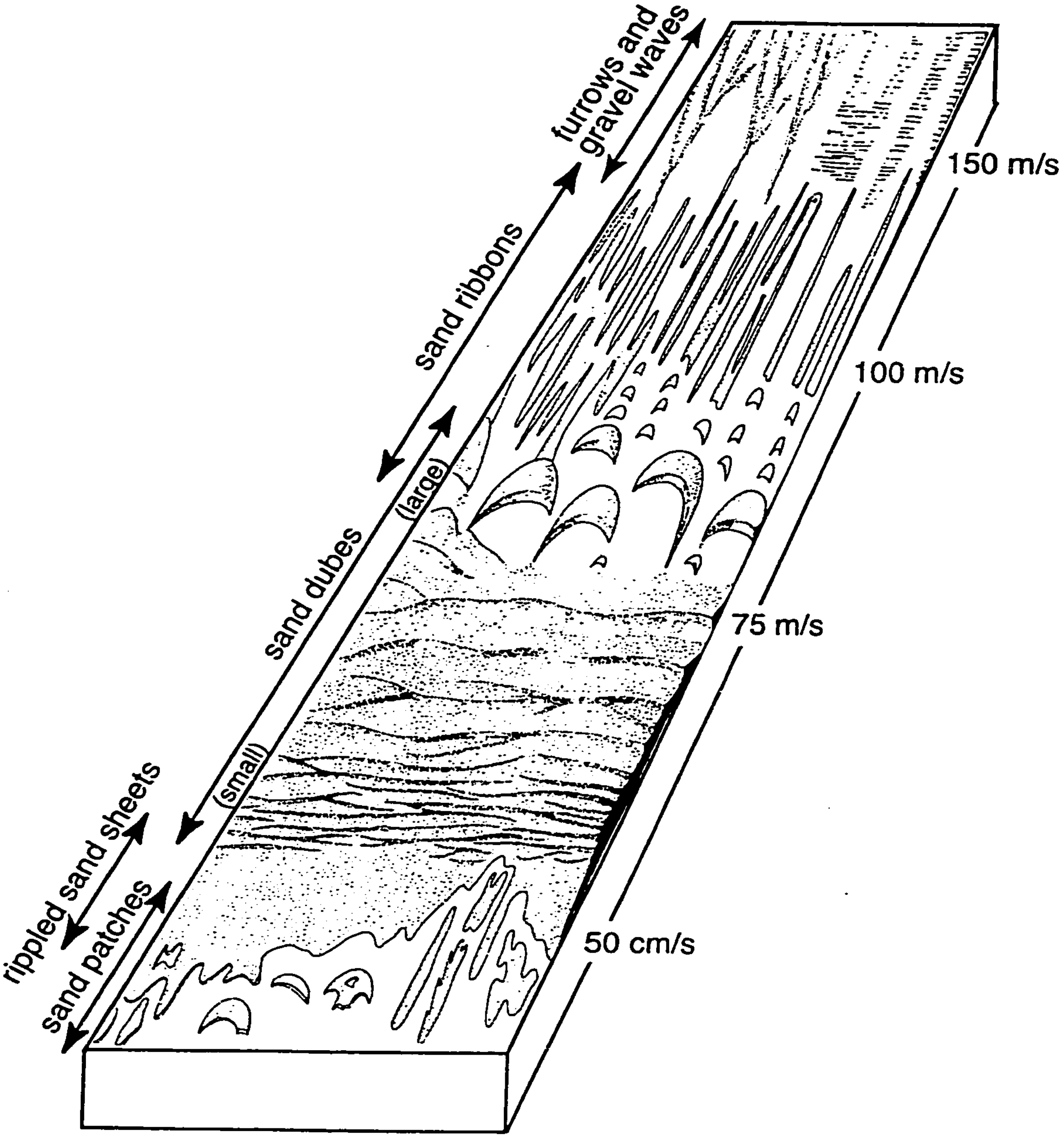
furrows and
gravel waves
sand ribbons
(large)
sand dubes
(small)
rippled sand sheets
sand patches
150 m/s
100 m/s
75 m/s
50 cm/s

of root traces for the recognition of paleosols is limited to strata younger than Silurian, when the first vascular plants appeared (Retallack, 1985). Fossil roots are easily recognized when their organic material is preserved. Moreover, a rooted paleosol may also be recognized even if the organic matter has been completely decomposed, because root traces are commonly defined by infills of clay or calcite. These root traces are generally differentiated from burrows by their branching and tapering characteristics. The patterns of root traces also provide useful information on the former drainage, vegetation type, and original indurated parts of a paleosol.

Other features in many paleosols are soil horizons. Numerous types of soil horizons exist, each reflecting the different conditions under which the soil formed. For example, a clayey B horizon (Bt horizon) forms under forest vegetation in warm humid climates, and a calcareous B horizon (Bk horizon) develops in weakly weathered soils in dry climates (Retallack, 1988). Certain paleosol horizons are unique and have specific names. For example, ganisters are silicified quartz sandstones (E horizon) that are penetrated by root traces and underlie coal seams. The principal paleosol horizons and their subordinate descriptors are summarised in Table 1.1. Although the top of a paleosol profile is usually sharply defined, contacts between successively lower horizons are typically diffuse. Sharp contacts between lower horizons may occur if relict bedding has not been completely destroyed by soil processes. The uppermost (A and E) horizons are generally thin (< 50 cm). The subsurface (Bt and Bk) horizons are thicker, generally less than 2 metres thick, and the slightly altered C horizon much thicker still, and depends in large part on the duration of soil formation.

Although some soil profiles may appear massive and featureless, closer observation commonly reveals numerous soil structures. Perhaps the most striking soil structures are soil peds. Peds are aggregates of soil confined between cracks, roots, burrows, or other soil openings. They are regularly distributed within a given soil profile and are classified by their size, shape, and angularity (Fig. 1.15a). Commonly, there is an upward gradation in the size of soil peds from blocky to granular and crumb peds. The gradation is most likely related to degree of burrowing activity and associated of organic compounds, such as polysaccharides

Table 1.1 Major horizons in paleosols, subordinate features and shorthand labels (modified from Retallack, 1988)

Category	Term	Description
Master Horizons	O	Surface accumulation of organic materials (peat, lignite, coal) overlying clayey or sandy part of soil
	A	Usually has roots and a mixture of organic and mineral matter; forms the surface of those paleosols lacking an O horizon
	E	Underlies an O or A horizon and appears bleached because it is lighter colored, less organic, less sesquioxidic, or less clayey than underlying material
	B	Underlies an A or E horizon; appears enriched in some material compared to underlying and overlying horizons (because it is darker colored, more organic, more sesquioxidic, or more clayey); or more weathered than other horizons
	K	Subsurface horizon so impregnated with carbonate that it forms a massive layer
	C	Subsurface horizon, slightly more weathered than fresh bedrock; lacks properties of other horizons, but shows mild mineral oxidation, limited accumulation of silica, carbonates, soluble salts, or moderated gleying
	R	Consolidated and unweathered bedrock
Subordinate descriptors referred to in this chapter	g	Evidence of strong gleying, such as pyrite or siderite nodules
	h	Illuvial accumulation of organic matter
	k	Accumulation of carbonates less than for K horizon
	n	Evidence of accumulated sodium, such as domed columnar peds or halite casts
	o	Residual accumulation of sesquioxides
	t	Accumulation of clay
	s	Illuvial accumulation of sesquioxides
	y	Accumulation of gypsum crystals or crystal salts

Figure 1.15 Soil structures

Figure 1.15a Classification and principal causes for the formation of different soil peds (modified from Retallack, 1990).

Figure 1.15b Stages in the formation of the Bt horizon. Soil peds and roots progressively destroy original bedding. In a well developed Bt horizon, primary sedimentary features are no longer discernible (modified from Retallack ,1990).

a)

SKETCH	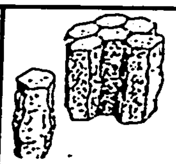	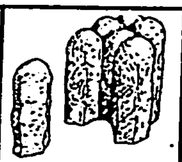	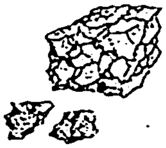	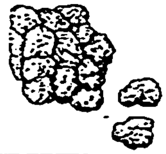	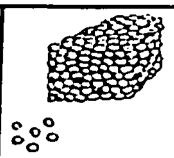	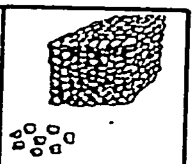
TYPE	Prismatic	Columnar	Angular blocky	Subangular blocky	Granular	Crumb
DESCRIPTION	Elongate Flat top Vertical	Elongate Domed top Vertical	Equant Sharp interlocking edges	Equant Dull interlocking edges	Spheroidal Slightly interlocking edges	Rounded Spheroidal Not interlocking
USUAL HORIZON	Bt	Bn	Bt	Bt	A	A
MAIN LIKELY CAUSES	Swelling and shrinking related to wetting and drying	Swelling and shrinking Abundant erosion by percolating water	Cracking around roots and burrows Swelling and shrinking related to wetting and drying	As for angular blocky More erosion and illuvial clays	Active bioturbation Clay skins, sesquioxide, and organic matter	As for granular Fecal pellets and relict soil clasts

b)

STAGES IN THE FORMATION OF Bt HORIZONS

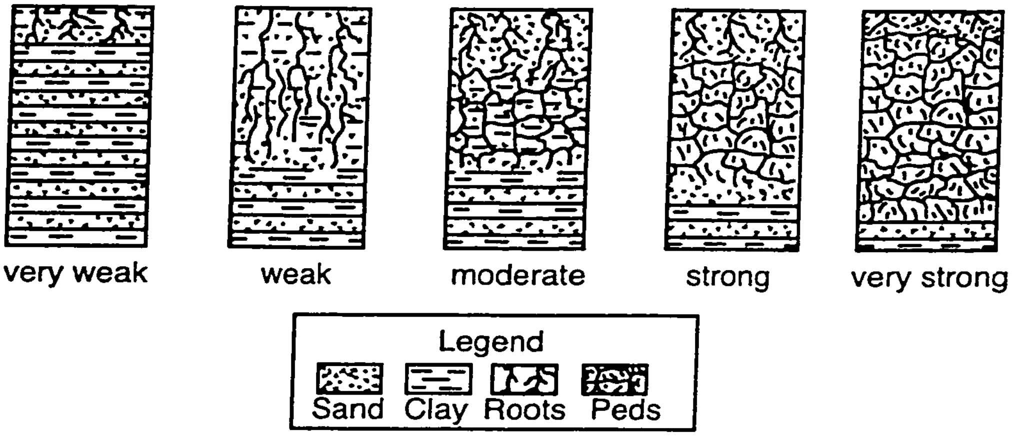

that binds ped surfaces (Retallack, 1990). Crumb peds, in part, may represent fecal pellets.

The surface of soil peds is further characterized and modified by cutans. These structures are very useful for identifying paleosols because commonly they are the only indication that peds were once present. In ancient soil profiles, cracks between peds are rarely preserved because of compaction. Cutans form in these cracks and vary greatly in composition, and include clays skins (argillans), iron-stained surfaces (ferrans), iron and aluminium oxides (sesquans), iron and manganese oxides (mangans), soluble salts such as gypsum (soluans), calcite (calcans), opal or chalcedony (silans), or organic matter (organans). The composition of the cutan is a good indicator of the original chemical conditions in the paleosol. For example, non-calcareous, nonclayey, ferruginous cutans indicate acidic and highly oxidizing conditions generally found in well drained sandy soils in humid climates. Cutans form by three distinct processes: illuviation, diffusion, or by shearing in the soil. Illuvial cutans form by successive gravitational infiltration (elluviation) and deposition (illuviation) of fine-grained material, and hence are commonly laminated. Diffusion cutans are composed of modified ped material and have a sharp outer boundary and a gradational inner boundary with the unaltered ped. Stress cutans are less well defined but are generally indicated by slickensides. Slickensides can form in clayey soils by swell-shrink processes related to repeated wetting and drying cycles or by the abrasion of adjacent soil peds during burial.

Glaebules are also common structures in soil profiles and include nodules and concretions. They are sharply-defined, highly irregular to nearly spherical isolated lumps of soil that are chemically as widely variable as cutans. Concretions and nodules are differentiated by their internal structure. Concretions have concentric layers and form as a result of discontinuous, often seasonal growth. Nodules, on the other hand, are massive and represent continuous growth or recrystallization. Some nodules are characterized by cracks radiating outward from their center. These cracks develop as a result of a change in volume, which commonly takes place during irreversible drying. Although glaebules are abundant and conspicuous features in soils, they are not unique of them; they also form at the sea floor (manganese nodules), in shallow lakes (lime balls), and during deep burial (siderite nodules and concretions) (Coleman, 1985).

The development of a soil is the result of the combination of physical, chemical, and biological processes (Retallack, 1990). Physical processes cause the disintegration of rocks and sediments, for example by expansion, clay swelling, freezing in periglacial environments and fire heating of coal resulting in decay-resistant charcoal. Soil-forming chemical reactions result in the decomposition of parent material, and include hydrolysis, oxidation, hydration, and dissolution. The reverse reaction of alkalization, reduction, dehydration, and precipitation also occur in soils. Hydrolysis is the reaction by which cation-rich mineral grains are altered into clay minerals plus cations, and is principally controlled by soil acidity. Oxydation particularly affects iron-rich minerals, which alter to iron oxides. Hydration and dehydration involves the addition and loss of water, respectively, within part of the mineral lattice (e.g. gypsum and anhydrite). Dissolution is a reaction by which a mineral passes into solution as separate. Biological activity also contributes significantly to the soil forming process, and includes humification (plant decay), nutrient availability for plant productivity, and bioturbation.

Physical, chemical, and biological processes combine to form one of six soil-forming regimes. Common regimes include gleization, podzolization, lessivage, ferralitization, calcification and salinization (Fig 1.16). Only lessivage is described in more detail because, as discussed in chapter 3, it is the soil-forming regime interpreted to have controlled pedogenesis across the top of the Swift Formation. Lessivage is the process by which the upper horizons of the soil profile (E) is leached and the subsurface B-horizon is enriched in clay. Commonly, the E horizon becomes lighter in colour and the B horizon darkens. Evidence of illuviated clays can be observed in thin sections as laminated argillans with a high birefringent clay fabric. In addition, the clayey B horizon is generally matrix supported. Soils formed by lessivage tend to be neutral to moderately acidic and, consequently, they are dominated by hydronium (H_3O^+) rather than aluminium (Al^{3+}) ions, which, in turn promotes the development of stable clay minerals. Large exchangeable ions (K^+, Mg^{2+}, Ca^{2+}, Na^{2+}) are also removed from weatherable minerals by hydrolysis and, with time, can be removed from

Figure 1.16 Common soil-forming regimes. a) ferralization occurs in well drained soils of wet tropical climates. Intense weathering produces a uniform soil profile, depleted in exchangeable cations, and enriched in clay, sesquioxides, and kaolinite; b) lessivage occurs in neutral, clay-rich soils of humid climates. Abundant illuvial clays accumulate in the B-horizon, and exchangeable cations are generally removed by groundwater; c) podzolization takes place in acidic, sandy soil ($pH < 5$) of humid climates. It is characterized by extensive leaching, removal of large exchangeable cations by groundwater, and translocation of Al and Fe oxides and organic matter to the B-horizon; d) gleiziation is the principal process in waterlogged soils, where anaerobic conditions favour the preservation of organic matter and chemically unstable minerals. Also, precipitation of ferric irons minerals (pyrite and siderite) aided by anaerobic bacteria is widespread; e) calcification occurs in well drained soils of semi-arid climates and is characterized by abundant accumulation of Ca^{2+} minerals in the subsurface and little loss of exchangeable cations. These soils are typically fertile and support grasslands and grassy woodlands; f) salinization is characterized by the accumulation of salts (halite and gypsum) in well drained soils in arid climates. As a result, these soils are highly alkaline (pH 9 - 11) and can only support a small number of plant types (cacti and desert shrubs) (modified from Retallack, 1990).

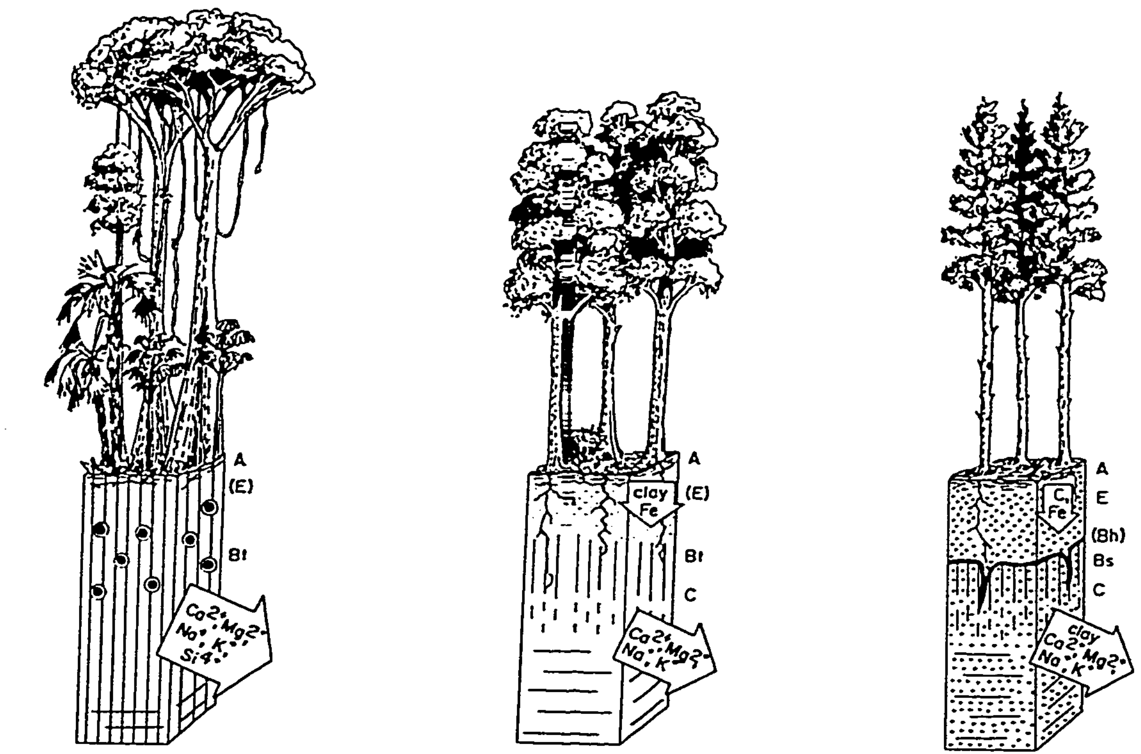

a) Ferrallitization b) Lessivage c) Podzolization

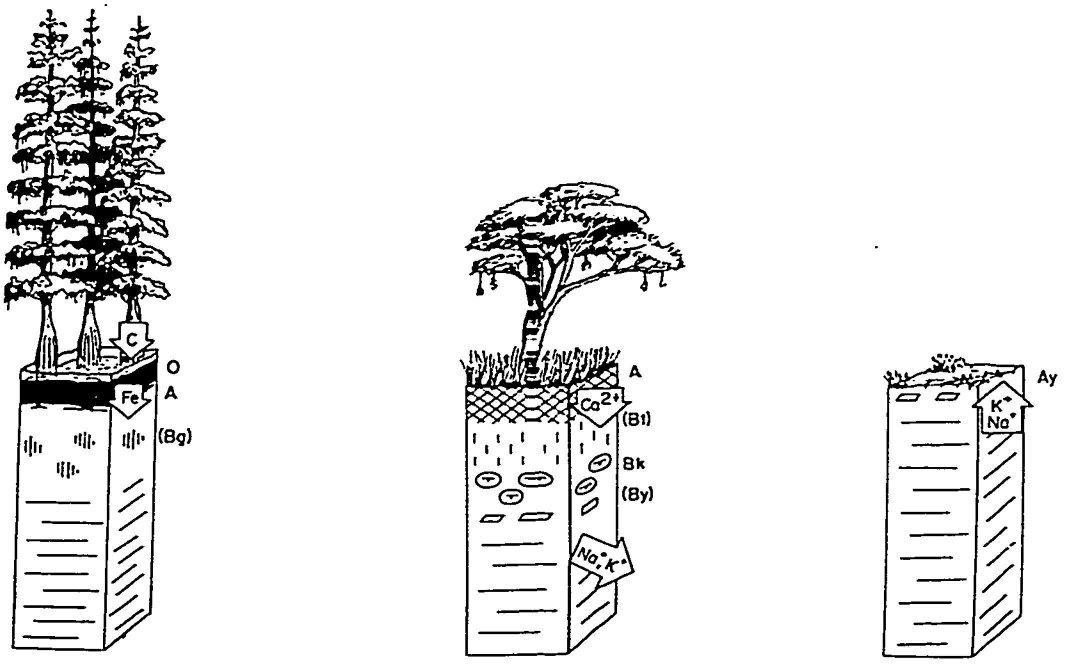

d) Gleiziation e) Calc ification f) Salinization the soil profile. The process of lessivage is favoured in strata rich in minerals that weather to clay (e.g. shales or basalts). Also, lessivage is favoured in areas where the surface vegetation creates small amounts of acid-generating phenolic compounds and resins such as in a deciduous broadleaf woodland.

Soils form on time scales ranging from days to millions of years. Organic layers (A horizon) form in only tens to hundreds of years whereas a deeply weathered horizon requires millions of years to form. No single soil feature can provide a quantitative measure of time for paleosol development. However, a general qualitative estimate can be formulated based on: 1) the amount of carbonate in a calcareous horizon (Bk) of a aridland paleosol, 2) the amount of peat accumulation (O) in waterlogged paleosols, and 3) the abundance of clay skins in the B-horizon of humid climates paleosols. The accumulation of illuvial clays in the Bt horizon takes time and several stages of development can be recognized (Fig. 1.15b). In very weakly developed soils, there is little to no evidence of clay accumulation and bedded strata are characterized only by root traces. With time, weakly developed soils form as strata become fragmented and space is made available for argillans to accumulate. Within these soils, much relict bedding remains. In moderately developed soils, peds are better defined, argillans are more abundant and relict bedding is uncommon and can only be detected by subtle grain size changes in hand specimens. In a strongly developed soil, argillans are abundant, the Bt horizon is thicker, and there are no traces of relict bedding. With further development, the Bt horizon thickens to well over 1 metre, and commonly, the A horizon thins or is lost to erosion. Strongly developed paleosols commonly coincide with major unconformities.

Chapter 2

Sedimentology and stratigraphy of the Swift Formation (Upper Jurassic) in southeastern Alberta: sedimentation in an open marine basin to a microtidally-influenced intracontinental strait

Introduction

Presently, the depositional history and sequence stratigraphic framework of the Upper Jurassic Swift Formation is poorly understood. The formation was first defined by Cobban (1945) from exposures in northern Montana. He devised an informal two-fold subdivision for the Swift and recognized a lower shale member and an upper sandstone member. The Swift Formation was subsequently correlated with subsurface strata in southern Alberta by Weir (1949). Much later, Brenner and Davies (1974) proposed a depositional model for the Swift in Montana and Wyoming that consisted of a basal mudstone succession deposited during an initial transgressive phase, conformably overlain by sandy offshore bars and flaser bedded interbar facies deposited during a regressive phase. Local coquinoid sandstone-filled channels that incised into offshore bars were interpreted as high-energy events related to storms. Hayes (1983), in turn, extended Brenner and Davies' transgressive-regressive model for the Swift into the subsurface in northern Montana and southeastern Alberta. In this area, the lower member closely resembles the lower shale member at the Swift type section. However, the upper member differs significantly by its abundant mud content and as a result, Hayes termed it the ribbon sands. In this study, we adopt a modified version of Hayes' nomenclature and recognize the lower shale member and the upper ribbon sandstone. The ribbon sandstone is predominantly lenticular to wavy bedded with locally developed sandstone-rich bodies. Although Hayes suggested that the sandstone-rich facies in the ribbon sandstone were deposited during high-energy events, he did not discuss in detail the physical controls responsible for the deposition and distribution of the sand-size fraction. Hayes also noted that the ribbon sandstone was systematically marked by a sharp colour change from dark to light coloured mudstone, but the origin of the change was poorly understood.

Because of the paucity of detailed studies on the Swift Formation in southeastern Alberta, the distribution of its sandy reservoir strata and the stratigraphic significance of the colour change, if any, currently remain enigmatic. Consequently, the Swift is generally viewed as a low-priority target for hydrocarbon exploration even though oil and gas are presently being co-produced from its sandstone-rich facies in the Manyberries, Pakowki Lake and Black Butte pools in southeastern Alberta and in the Flat Coulee pool in Northern Montana, where it is the main oil producer. Because of its hydrocarbon potential, additional investigations regarding the depositional history of the Swift Formation are warranted. Furthermore, since many "offshore bars" have recently been re-interpreted to be lowstand (Plint, 1988; Walker and Plint, 1992; Pattison and Walker, 1992; Walker and Bergman, 1993; Ainsworth and Pattison, 1994; Walker and Wiseman, 1995), the sequence stratigraphic framework of the Swift needs to be addressed. The objectives of this study are therefore threefold: 1) develop a detailed sedimentological model for the Swift Formation in southeastern Alberta, 2) resolve its sequence stratigraphic framework and 3) determine the transport and depositional mechanisms for the sandstone-rich, reservoir, and potential reservoir facies.

Study Area and Methodology

The study area is located in southeastern Alberta, east of the Whitlash paleovalley (Cretaceous) and comprises the area between Townships 1 to Township 10 and from Ranges 1 to 10 W4 (Fig. 2.1). In this area, over 2150 wells penetrate Jurassic strata. From these, approximately 450 wells were selected (Fig. 2.2) to form a grid of 20 wireline cross-sections. In addition, 68 cores were examined and described in bed-by-bed detail (Appendix 1) that then were used to calibrate geophysical log signatures. Also, 37 samples were selected for petrographic examination (Appendix 2) and 16 samples additional samples were collected for geochemical analyses (by X-ray fluorescence and isotope analyses) (Appendix 3).

Geological Setting and Regional Stratigraphy

Deposition of the Swift Formation occurred during the Columbian-Nevadan Orogeny, which coincided with the collision between the Intermontane Superterrane and the western

Figure 2.1 Location of study area and distribution of well control. The study area is bounded to the west by the Saskatchewan – Alberta border, to the south by the Canada – U.S.A. border, and to the west by the deeply incised Lower Cretaceous Whitlash Valley. Lines of north-south and east-west cross-sections are outlined.

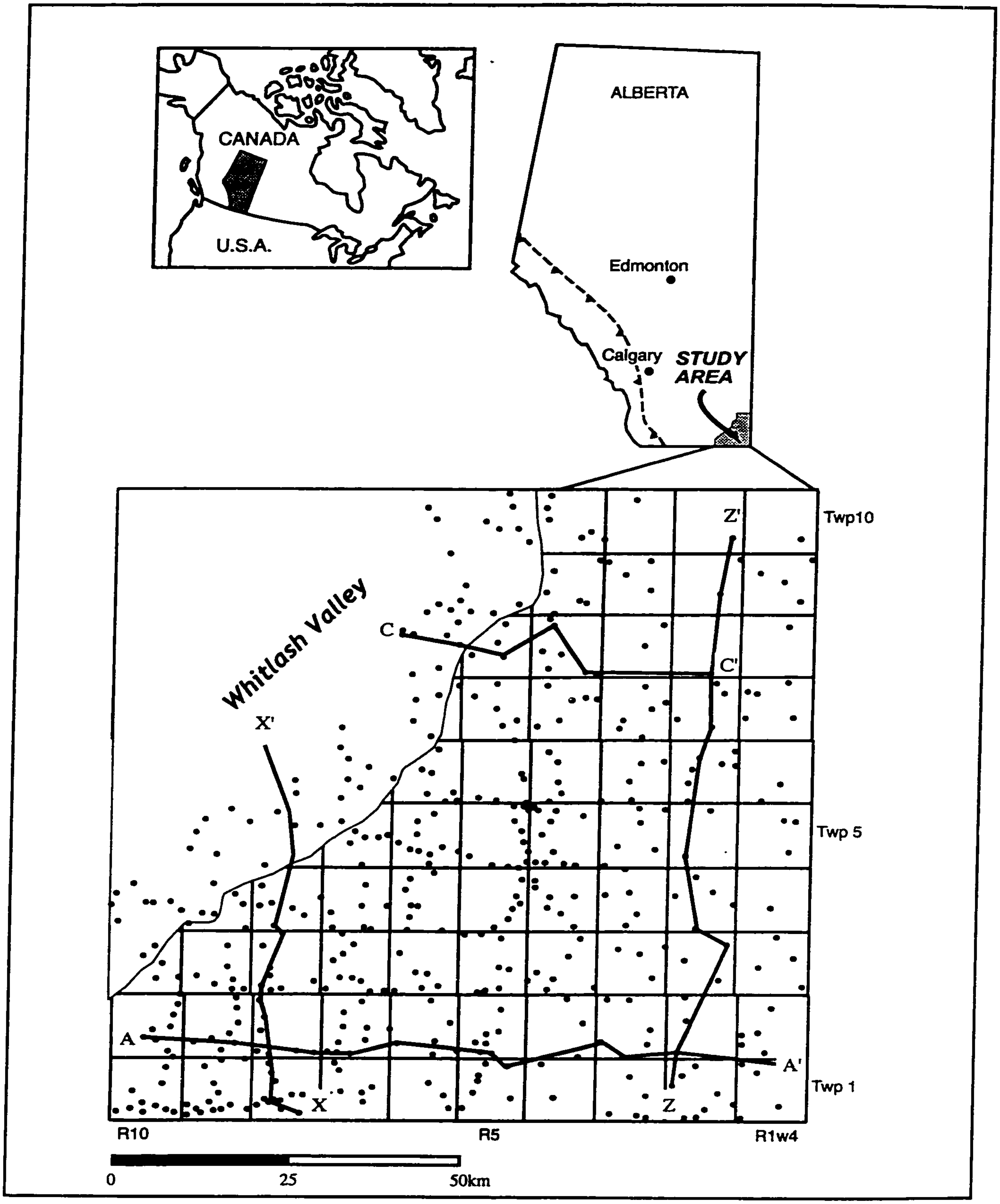
CANADA
U.S.A.
ALBERTA
Edmonton
Calgary
STUDY AREA
Whitlash Valley
C
C'
X'
X
Z'
Z
A
A'
Twp10
Twp 5
Twp 1
R10
R5
R1w4
0
25
50km

margin of the North American Plate (Leckie and Smith, 1992). Tectonic thickening and related lithospheric flexure formed a narrow, northwest-southeast elongated foreland basin, a portion of which is termed the Alberta Trough. During the Late Jurassic, a southward transgression of the northern Boreal sea inundated the trough and eventually flowed eastward, across the Sweetgrass Arch and into the ancestral intracratonic Williston basin through an east–west trending strait that eventually became over 300 km wide (Imlay, 1980; fig. 10) (Fig. 2 2). The exact position of the initial breach over the arch remains unclear, but is generally taken to be close to the international border (Brenner and Davies, 1974, Imlay, 1980; Hayes, 1983). During the Late Jurassic, the Sweetgrass Arch was a major positive topographical feature in southeastern Alberta that significantly influenced marine circulation, sedimentation patterns and erosional processes (Christopher, 1964; Brennar *et al.*, 1974; Hayes, 1983). The arch consists of several sub-components. In north-central Montana it includes the northwest-plunging South Arch and the northwest-striking Kevin-Sunburst Dome. Northward the arch extends into southern Alberta and may also include the northeast-plunging Bow Island Arch (Hayes, 1983; Podruski, 1988; Arnott *et al.*, 1995) (Fig. 2.3). In addition, the study area overlies the Medicine Hat Block, a Precambrian terrane bounded to the north and west by the Vulcan Low, which represents an ancestral collisional suture zone, and, to the south is separated from the Wyoming Craton by a Proterozoic shear zone termed the Great Falls Tectonic Zone, (Ross *et al.*, 1991) (fig. 2.3).

Although strata in the study area are essentially undeformed, there is a consistent steep dip toward the northeast. This was caused by kilometre-scale uplift related to Eocene, alkalic igneous intrusion in the Sweetgrass Hills complex in north-central Montana (Fig. 2.4). Although these domal structures are centered in north-central Montana, they are not restricted to that area and isolated intrusions also occur elsewhere in southeastern Alberta and southwestern Saskatchewan (Podruski, 1988) (Fig. 2.3). Another anomaly occurs in townships 8 and 9, range 4w4, where Mississippian and Jurassic strata occur consistently at higher stratigraphic levels than equivalent adjacent strata (Fig. 2.5). This anomalous feature represents the uplifted central core of a relatively small crater (10 km in diameter) that was formed by a Late Cretaceous to Early Tertiary meteorite impact (Sawatsky, 1976; Grieve *et*

Figure 2.2 Paleogeography of North America during the Oxfordian (Late Jurassic). Note the wide epeiric strait that connected the Alberta Trough in the west to the intracratonic Williston Basin in the east. The boundaries of the marine portion of the Williston Basin during the Late Jurassic have not yet been well established. Modified from Imlay, 1980.

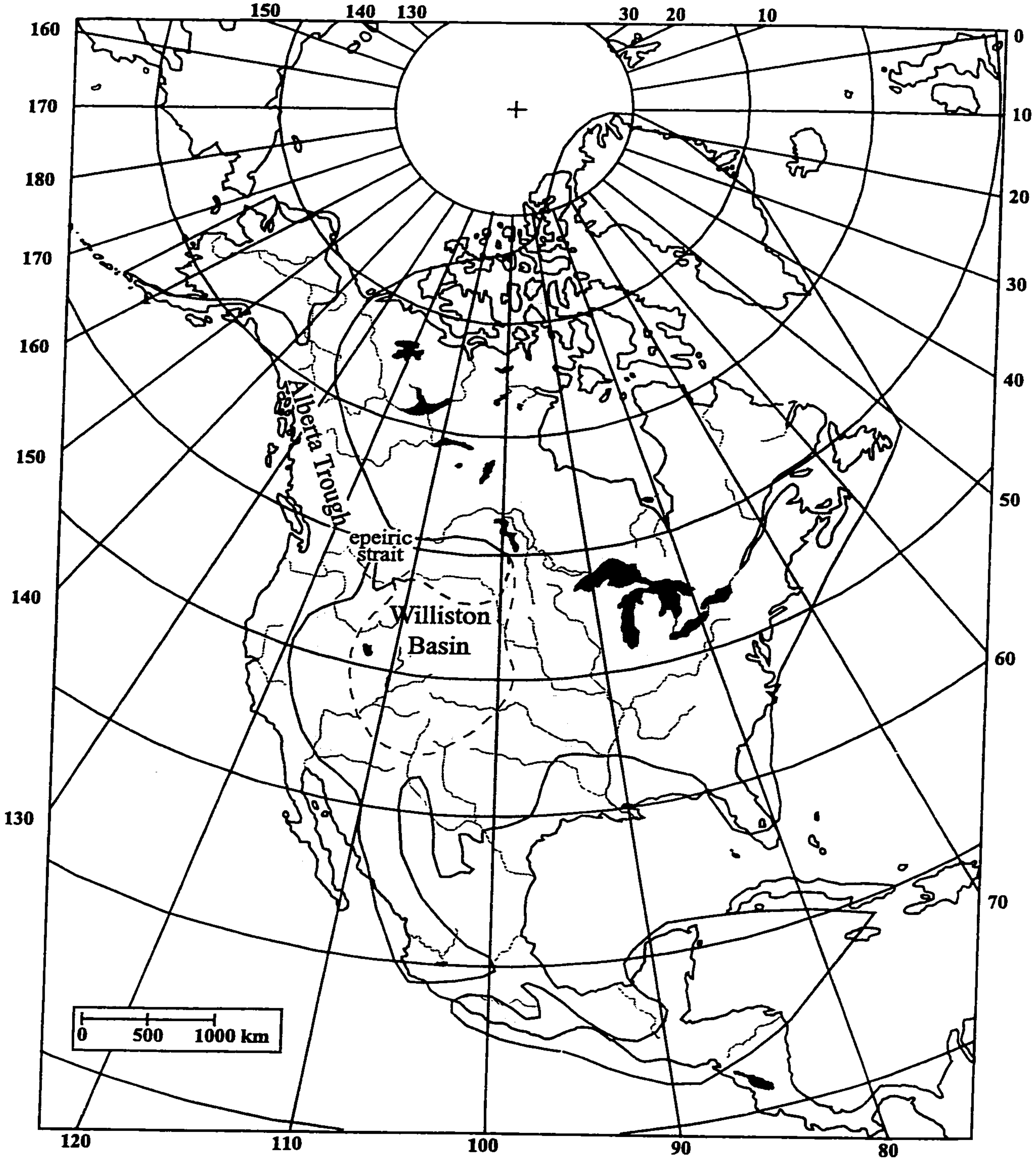

150
140
130
30
20
10
160
170
180
170
160
150
140
130
0
10
20
30
40
50
60
70
120
110
100
90
80
Alberta Trough
epeiric strait
Williston Basin
0
500
1000 km

Figure 2.3 Map illustrating the principal tectonic elements in proximity to the study area.

(A) Distribution of sub-components of the Sweetgrass Arch in southeastern Alberta and north-central Montana, and location of domal structures in proximity to the arch. Note the change in trend of the arch near the international border from northwest to northeast-southwest. Adapted from Podrusky, 1988; and Arnott *et al.*, 1995.

(B) Map of tectonic domains that form the basement rocks in southeastern Alberta and north-central Montana. The study area overlies part of the Archean Medicine Hat Block. The Vulcan Low and Great Fall Tectonic Zone bound the Medicine Hat Block and represents ancient suture zones along which movement may have been reinitiated during the Columbian-Nevadan Orogeny. Wy: Wyoming Craton; GTZ: Great Fall Tectonic Zone; MHB: Medicine Hat Block; VL: Vulcan Low; LoB: Loverna Block; L: Lacombe Domain; R: Rimbey High. Modified from Ross *et al.*, 1991.

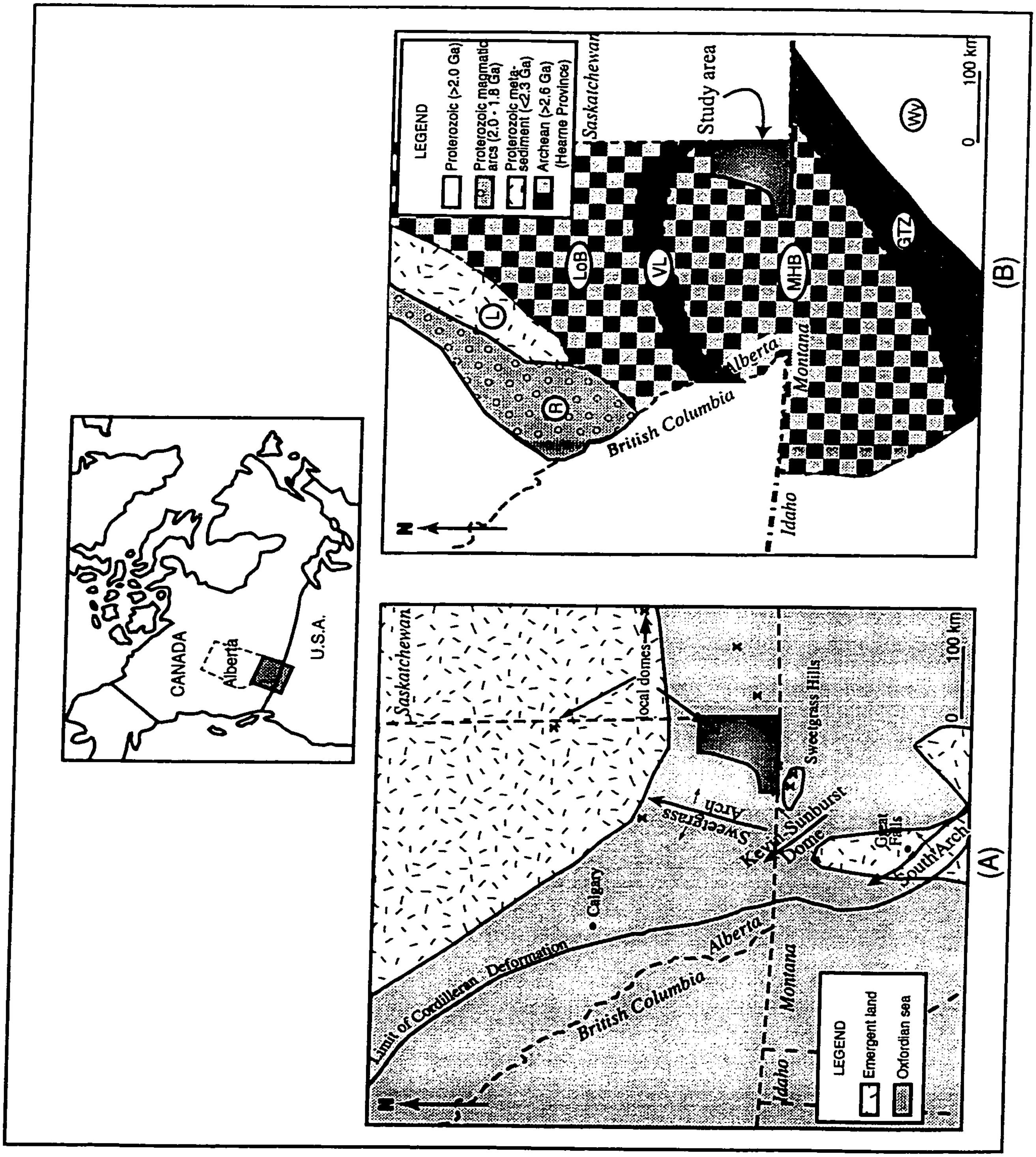
CANADA
Alberta
U.S.A.
(A)
N
Limit of Cordilleran Deformation
Saskatchewan
Calgary
British Columbia
Alberta
Idaho
Montana
local domes
Sweetgrass Arch
Kevin-Sunburst Dome
Sweetgrass Hills
Great Falls
South Arch
0
100 km
LEGEND
Emergent land
Oxfordian sea
(B)
N
LEGEND
Proterozoic (>2.0 Ga)
Proterozoic magmatic arcs (2.0 - 1.8 Ga)
Proterozoic meta-sediment (<2.3 Ga)
Archean (>2.6 Ga) (Hearne Province)
Saskatchewan
Study area
R
L
LoB
VL
MHB
GTZ
Wy
British Columbia
Alberta
Montana
Idaho
0
100 km

Figure 2.4 Structure map of the top of the Rierdon Formation in southeastern Alberta depicting steep, northeast dipping strata. The anomalous dip direction and dip angle is related to Tertiary alkaline igneous intrusion in the Sweetgrass Hills of northern Montana.

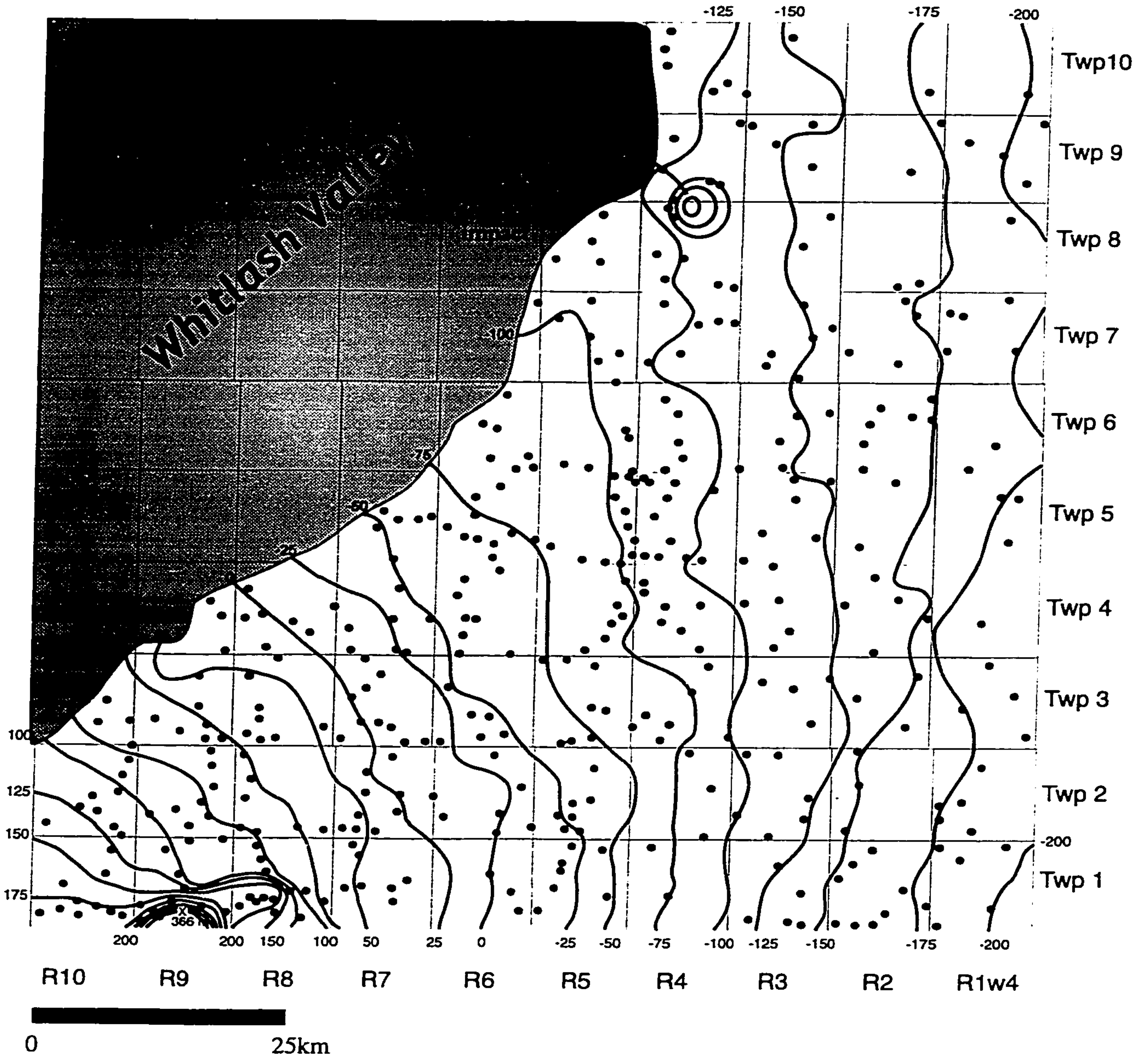
Whitlash Valley
-125
-150
-175
-200
Twp10
Twp 9
Twp 8
Twp 7
Twp 6
Twp 5
Twp 4
Twp 3
Twp 2
Twp 1
-200
-100
-75
-50
-25
100
125
150
175
366
200
200
150
100
50
25
0
-25
-50
-75
-100
-125
-150
-175
-200
R10
R9
R8
R7
R6
R5
R4
R3
R2
R1w4
0
25km

Figure 2.5 Composite drawing illustrating location and vertical displacement of strata in the Eagle Butte meteorite impact structure (twps. 8 and 9, range 4w4). Significant displacement is evident in the central uplift portion of the crater. Modified from Grieve *et al.*, 1998.

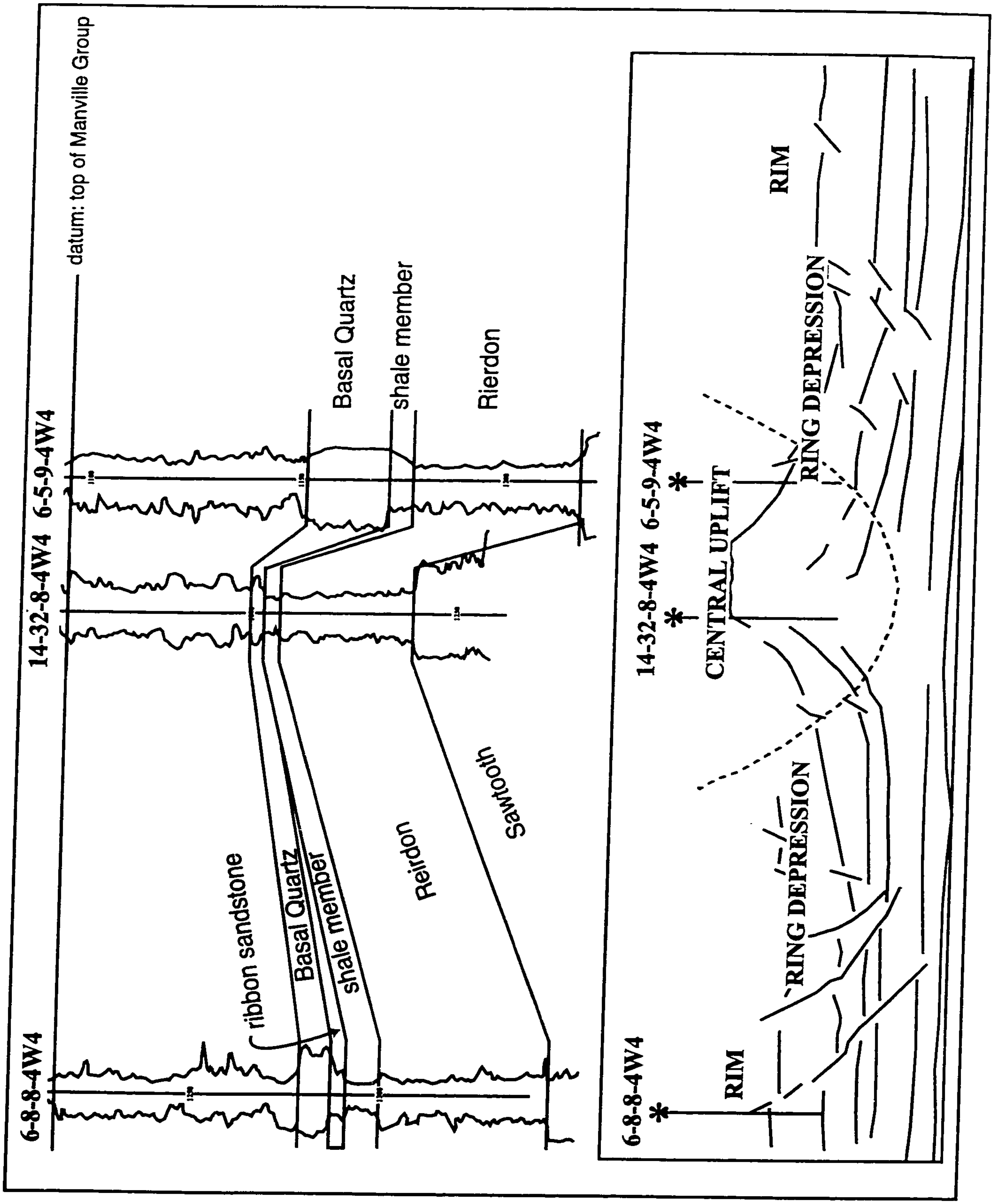

datum: top of Manville Group
6-8-8-4W4
14-32-8-4W4
6-5-9-4W4
ribbon sandstone
Basal Quartz
shale member
Reirdon
Sawtooth
Basal Quartz
shale member
Rierdon
6-8-8-4W4
14-32-8-4W4
6-5-9-4W4
RIM
RING DEPRESSION
CENTRAL UPLIFT
RING DEPRESSION
RIM

al., 1998; Ezeji-Okoye, 1985). Other meteorite craters such as the Viewfield and Red Wing structures in the Williston Basin, and the Ames structure in Major County, Oklahoma, form significant reservoirs from fractures that radiate outward from the crater (Hamm and Olsen, 1992; Donofrio, 1997; Grieve *et al.*, 1998). To date, however, no hydrocarbon production is associated with the small impact crater in this study area.

The Oxfordian Swift Formation was deposited in the Williston Basin during the fourth of five Jurassic marine transgressions over the Western Interior of North America (Imlay, 1980). In the study area, it is the youngest formation of the Jurassic Ellis Group, which comprises the Sawtooth, Rierdon and Swift formations. The Oxfordian Swift unconformably overlies Bathonian calcareous to mixed carbonate-siliciclastic mudstone of the Rierdon Formation (Christopher, 1974) and, in turn, is unconformably overlain by Lower Cretaceous fluvial sandstone, mudstone, and siltstone of the Basal Quartz (Lower Mannville Group) (Fig. 2.6). The top of the Swift is marked by the sub-Cretaceous unconformity, which represented a period of extensive subaerial weathering and a hiatus of approximately 35 Ma. (Gradstein *et al.*, 1996). This was followed by substantial erosion by stream downcutting and valley incision during the Aptian (Hayes, 1983). The Swift has been subdivided into two informal members: 1) a basal non-calcareous dark shale with thin siltstone laminae termed, the shale member and 2) wavy to lenticular bedded mudstone, siltstone and sandstone here termed the ribbon sandstone (Cobban, 1945; Imlay, 1980; Hayes, 1983).

Facies and Facies Associations

In this study, based on lithology, primary physical and biogenic sedimentary structures and bounding contacts, eight lithofacies have been identified in strata of the Swift Formation (Table 2.1). In addition, two unconformably bounded facies associations are recognized and, stratigraphically upwards are: 1) shale member and 2) ribbon sandstone.

Figure 2.6 Stratigraphic nomenclature of Jurassic and Cretaceous strata in southeastern Alberta. Modified from Leckie and Smith, 1992.

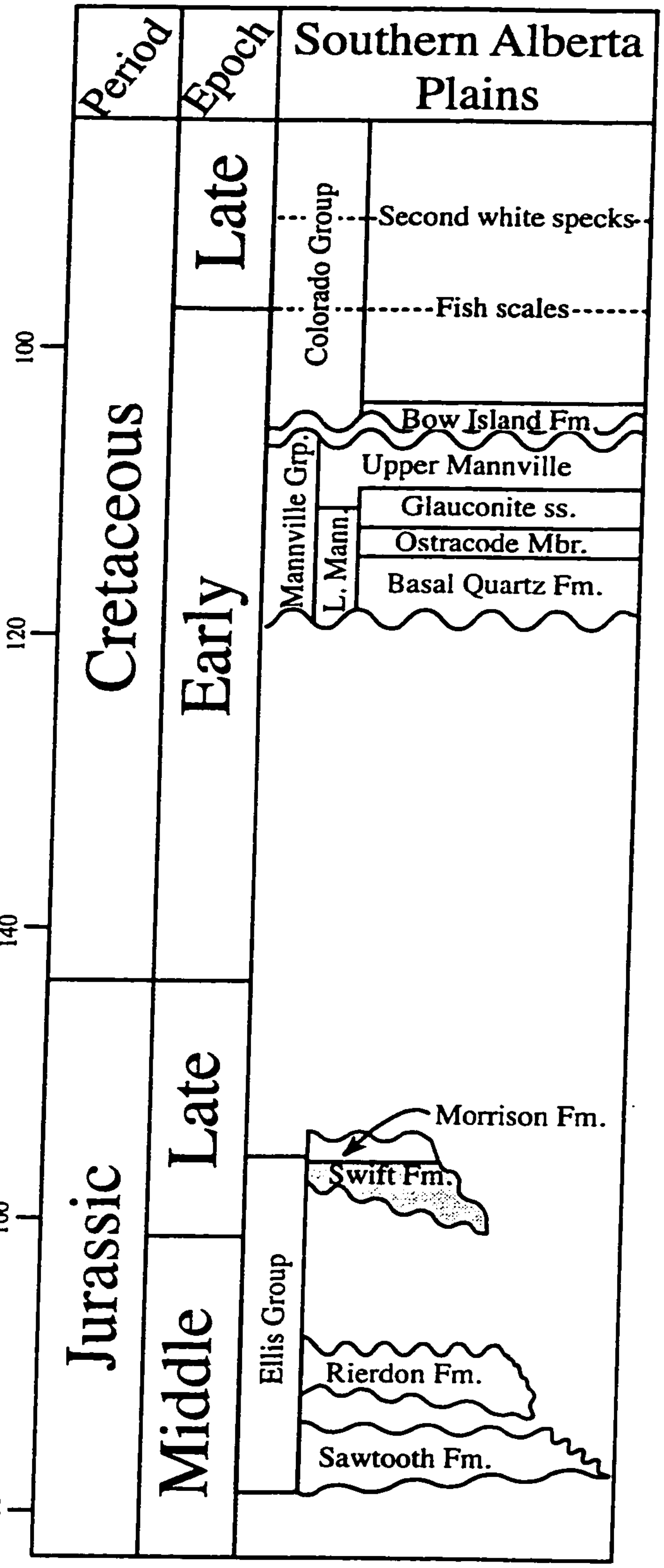
Period
Epoch
Southern Alberta Plains
Cretaceous
Late
Early
Jurassic
Late
Middle
100
120
140
160
180
Colorado Group
Second white specks
Fish scales
Bow Island Fm.
Mannville Grp.
Upper Mannville
L. Mann.
Glauconite ss.
Ostracode Mbr.
Basal Quartz Fm.
Morrison Fm.
Swift Fm.
Ellis Group
Rierdon Fm.
Sawtooth Fm.

Table 2.1 Summary of lithofacies descriptions and interpretations for the shale member (Sequence 1) and ribbon sandstone (Sequence 2) of the Swift Formation.

Litho-facies	Name	Description	Interpretation	Lithofacies Association
1	Shale with uncommon silt laminae	Black shale with rare thin (<1mm) siltstone laminae. Commonly glauconitic. Common *Helminthopsis* burrows.	Deposition from suspension in a low-energy open marine setting. Siltstone laminae deposited by high-energy events related to storms.	Shale member
2	Low-angle cross-stratified sandstone	Low-angle cross-stratified siltstone beds 5 to 15 cm thick. Isolated *Planolites, Chondrites, Teichnichnus, Skolithos.*	Hummocky cross-stratified siltstone deposited on an offshore shelf by high-energy long-period storm waves. Burrows formed by opportunistic organisms	
3	Chert pebble conglomerate	Dispersed black chert pebbles or cm-thick pyritized and glauconitic coarse sandstone. Overlies both Rierdon shale & shale member.	Areally extensive transgressive lag; reworked lowstand deposits.	Ribbon sandstone
4	Interstratified mudstone and sandstone	Non-cyclic, wavy to lenticular bedded strata. Unidirectional foresets with varying angles of dip. Low diversity trace fossil assemblage Synaeresis cracks, coalified wood fragments.	Deposition predominantly from suspension in a brackish water strait. Bed-load sediment starved. Uncommon bed-load transport related to both weak tide and wave currents.	
5	Small-scale cross-stratified sandstone	Thin sets (1 - 5 cm) of bundled lenses (5a) or herringbone cross-stratified sandstone (5b) Common thin mud flasers. Laterally and vertically discontinuous.	Combined-flow ripples produced by: 5a) negligeable tidal and weak oscillatory currents related to storms and 5b) microtidal (spring tides) and weak oscillatory currents.	
6	Quasi-planar laminated sandstone	Thin (< 5 cm) planar laminated fine sandstone. Downlapping basal contact. Uncommon.	Combined-flow high-energy storm beds (with stronger oscillatory component).	
7	Massive very fine sandstone	Thin (< 3 cm) massive sandstone interbeds. Uncommon.	The origin of Lithofacies 7 remains enigmatic.	
8	Paleosol	Macroscopically massive, off-white strata. Abundant sphaerosiderite nodules increasing in size and abundance upwards.	Pedogenically altered ribbon sandstone.	

Facies Association 1 – Shale Member

Facies Association 1 unconformably overlies the Rierdon Formation and is unconformably overlain by the ribbon sandstone. It consists of a conformable, slightly upward-fining succession up to 30 metres thick that comprises lithofacies 1, 2, and 3. Lithofacies 1 occurs also in the ribbon sandstone facies association.

Lithofacies 1 – Chert Pebble Conglomerate

Chert pebble conglomerate occurs at the base of both the shale member and the ribbon sandstone (see later). It consists typically of centimetre-thick, matrix-supported conglomerate composed of well-rounded black chert pebbles in a pyritized, poorly-sorted glauconitic fine sandstone matrix (Fig. 2.7a). In places it occurs as scattered black chert pebbles encased in black shale. Although Hayes, (1983) reported belemnites in similar strata, none were observed in this study. In core, basal contacts are erosional and are either planar or show several centimetres of relief (gutter casts?). As in earlier studies, the areal distribution of this lithofacies is difficult to determine. In large part, this can be attributed to two reasons. Firstly, these strata are commonly too thin to be detected by conventional geophysical tools and secondly, cores rarely penetrate the contact, because thick intervals of shales are seldom continuously cored by petroleum companies.

Lithofacies 1 is interpreted to be a transgressive lag formed by wave ravinement during an episode of rising relative sea level. In general, transgressive lags are thin (< 0.6 m) and overlie marine flooding surfaces, which commonly are coincident with unconformities (Van Wagoner *et al.*, 1990). Because of its anomalously coarse-grained texture, thinness and stratigraphic position (overlies an unconformity), it is likely that the thin conglomerate at the base of the shale member is the result of shoreface erosion that took place during the initial transgression of the Oxfordian sea into the study area. Chert pebbles in Lithofacies 1 were possibly derived from Upper Paleozoic chert-carbonate lithologies such as the Permian Phosphoria Formation, which are locally absent in Montana (Peterson, 1972, Brenner and

Davies, 1974) or the lower part of the Madison limestone which contains abundant chert nodules (Christopher, 1984).

Dispersed chert pebbles at the base of the ribbon sandstone are also interpreted to overlie a flooding surface coincident with an unconformity. However, the source of the chert pebbles is problematic. Aside from the thin layer of pebbles at the base of the shale member, no pebbles occur in the thick succession of shale and siltstone that make up the shale member. In this case, the pebbles are likely the remnants of reworked lowstand deposits. This interpretation is supported by the physiography along the top of the shale member (see later discussion; Fig. 2.17). Elongate, several metre-deep scours were most probably formed by a lowstand fluvial channel network that incised the top of the shale member.

Lithofacies 2 – Dark Shale

Lithofacies 2 consists of 1 - 20 m of horizontally laminated black shale with rare to uncommon thin siltstone laminae (Fig. 2.7b). It unconformably overlies greenish-grey calcareous shale of the Rierdon Formation or conformably overlies Lithofacies 1. Although bioturbation is uncommon, ***Helminthopsis*** and rare ***Rhyzocorallium*** burrows are observed in mudstone beds. Green to dark green authigenic glauconite is common to abundant in isolated lenses.

Lithofacies 2 is interpreted to have been deposited from suspension in a low-energy setting below storm wave base. Siltstone laminae were probably deposited by the distal remnants of high-energy sediment-transport associated with storms. In addition, the observed ichnofossil assemblage is dominated by grazing and deposit-feeding structures, consistent with a low energy, distal marine setting (Ekdale *et al.*, 1984). Furthermore, the abundance of green to dark green authigenic glauconite, which forms during the late stages of organic material alteration, suggests deposition in a sediment-starved marine environment (Amorosi, 1995). Commonly, these conditions occur on marine flooding surfaces in the transgressive systems tract and during early highstand (Amorosi, 1995).

Figure 2.7. Lithofacies of the shale member (Sequence 1).

Figure 2.7a) Lithofacies 1: thin matrix-supported chert pebble conglomerate. The matrix is composed of sideritized, glauconitic fine sand. Well 8-34-6-6w4, (1158 m depth).

Figure 2.7.b) Lithofacies 2. Friable dark shale intercalated with thin hummocky cross-stratified siltstone (Lithofacies 3). Well 3-2-4-6w4, (956 - 954.5 m depth).

Figure 2.7c) Low angle cross-stratification interpreted to be hummocky cross-stratification deposited during high-energy, long period wave events (storms). Well 3-2-4-6w4, (955.6 m depth).

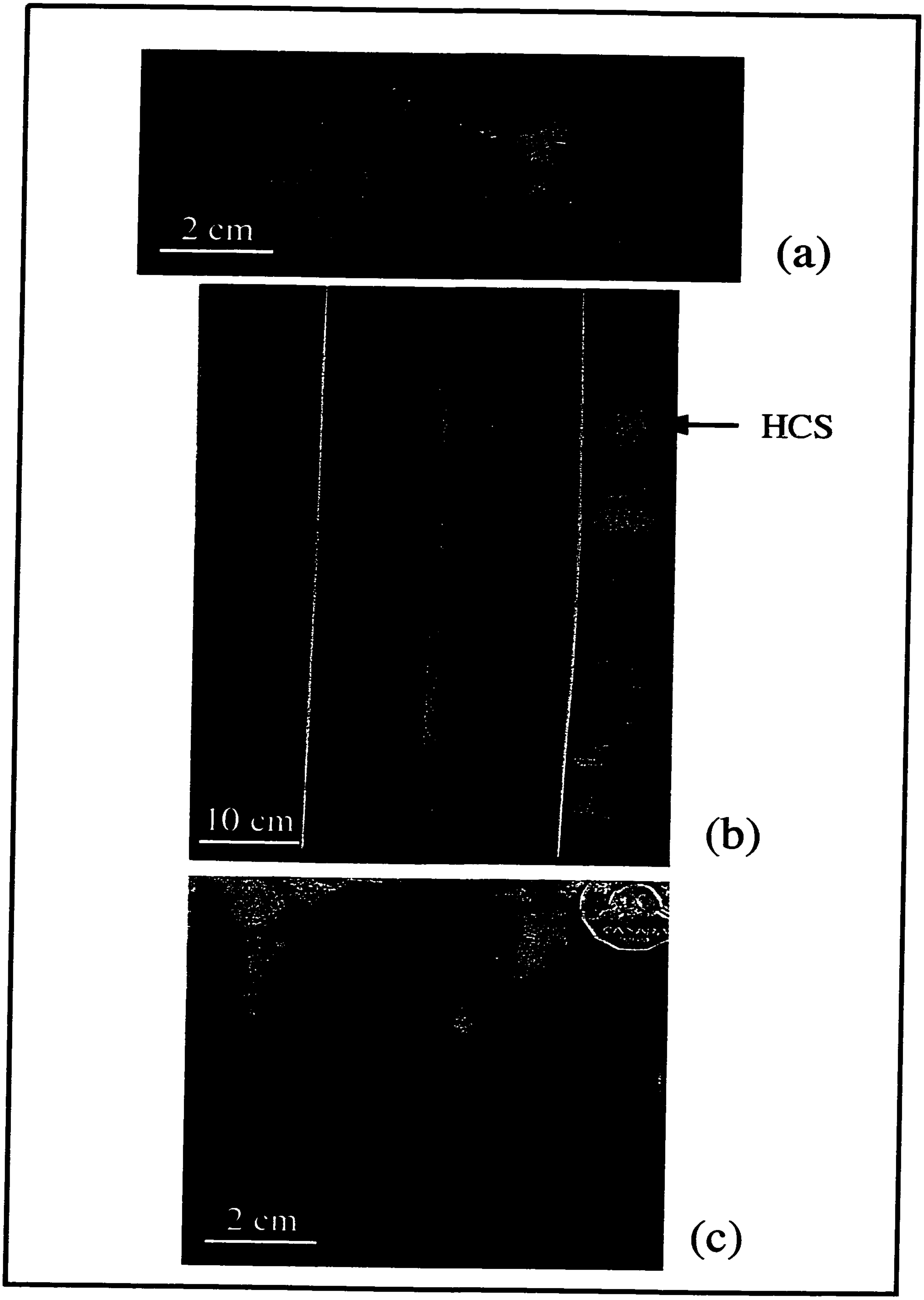
2 cm
(a)
HCS
10 cm
(b)
2 cm
(c)

Lithofacies 3 – Low Angle Cross-Stratified Siltstone

Lithofacies 3 consists of low angle cross-stratified siltstone (Fig. 2.7c). Although rare, it has been observed intercalated with dark shales of Lithofacies 2. Notably, Lithofacies 3 is absent in the overlying ribbon sandstone. Beds range from 5 - 15 cm thick (average 10 cm), are erosionally based and are commonly pyritized or sideritized. Laminae generally exhibit a distinctive undulation and locally form a noticeable fanning within discrete sets (consistent upward decrease in angle of dip of the cross-stratification). Isolated burrows are common and include *Skolithos*, *Planolites*, *Chondrites* and *Teichichnus*.

Lithofacies 3 is interpreted to represent sharp-based, hummocky cross-stratified siltstone that was deposited in an offshore environment during storms that formed high-energy, long period waves. Accordingly, burrows are interpreted to have been formed by opportunistic organisms that exploited the change in ecological conditions, principally a change in the nature of the substrate, and temporarily replaced the endemic tracemaking behaviours (e.g. Pemberton and Frey 1984).

Facies Association 2 – Ribbon Sandstone

Facies Association 2 consists of thee ribbon sandstone and comprises lithofacies 1 and 4 to 8. Facies Association 2 always overlies Facies Association 1, where present, and although the contact is unconformable, it is commonly difficult to identify in core. On geophysical well logs, however, the contact is generally sharp and particularly well defined on resistivity and neutron-porosity logs (see Fig. 2.13).

Lithofacies 4 – Interstratified Mudstone, Siltstone, and Sandstone

The ribbon sandstone is composed mostly of Lithofacies 4, which consists of thickly interlaminated to thinly bedded mudstone and siltstone or sandstone. Bulk composition ranges from 95% glauconitic mud and 5% sand (lenticular bedding) to 30% mud and 70% sand (flaser bedding). Volumetrically, however, Lithofacies 4 is mostly lenticular to wavy bedded, following the terminology of Reineck and Singh (1980) (Fig 2.8a). Sand interbeds are composed mostly of very fine sand, although coarse silt and uncommon medium sand interlaminae also occur. They are generally 0.3 - 2 cm thick and are characterized by wavy lamination and intercalated continuous to discontinuous small-scale trough cross-stratified sets. Discontinuous sets, which are more common than continuous sets, average 5 cm in length (i.e. less than the width of a core) and typically thin laterally into wavy lamination. Within individual sets, cross-stratification is typically unidirectional and commonly shows a systematic increase followed by a decrease in the angle of dip of the stratification (i.e. in the direction of bedform migration) (Fig. 2.8c). The change in angle can be observed within the width of a typical 3 inch (7.6 cm) core, and occurs in both discontinuous and continuous sets. Basal contacts are flat or more commonly are gently undulating, which causes sets to pinch and swell laterally. Soft sediment deformation, mostly in the form of small load casts, is locally developed. In addition, interbeds commonly are marked by reactivation surfaces. Bioturbation intensity ranges from uncommon to abundant (Fig. 2.8b) but consistently is characterized by a low diversity assemblage dominated by small (<3 mm diameter) *Planolites*, *Teichnichnus*, *Cylindrichnus*, *Skolithos*, inclined *Arenicolites*, rare robust *Thalassinoides* (?) and rare small *Chondrites* burrows. Crenulated synaeresis cracks are also common in mudstone interbeds. Fully marine trace fossils of the *Zoophycos* ichnofacies are distinctly absent from the ichnofossil assemblage. In addition, mudstone interbeds are barren of benthic or planktonic microfauna. Micropaleontological analysis did, however, reveal common small coalified wood fragments within the dark gray mudstone of Lithofacies 4.

The high mud content and common glauconite in Lithofacies 4 indicate that low-energy conditions prevailed during deposition. However, rhythmically bedded siltstone and sandstone also indicates that energy conditions regularly fluctuated in the study area. Moreover, common reactivation surfaces suggest that flow directions or mechanisms regularly changed in the basin. Although rhythmic bedding and reactivation surfaces are not indicative of any particular depositional environment (Reineck and Singh, 1980), they are common in tidal deposits. The cross-stratification in the sandstone interbeds is unidirectional and therefore, may have been caused by tidal currents. More significantly, however, is the

Figure 2.8 Lithofacies 4. Interstratified mudstone, siltstone, and sandstone.

Figure 2.8a) Typical lenticular bedded strata in the ribbon sandstone characterized by interbeds of wavy laminated siltstone and discontinuous, small scale cross-stratified fine sandstone (narrow arrow). Note crenulated synaeresis crack (thick arrow) and low diversity trace fossil assemblage composed of common small *Planolites* (Pl) and less common *Teichnichnus* (Te). Well 6-2-4-7w4 (890 m depth).

Figure 2.8b) Non-typical strongly bioturbated lenticular bedded strata. Despite the abundance of trace fossils, the diversity remains low. *Cylindrichnus*: Cy; inclined *Arenicolites*: Ar; and *Planolites*: Pl. Well 6-12-6-6w4 (1023.5 m depth).

Figure 2.8c) Detailed cross-section of small scale cross-stratified fine sandstone. Note the decrease in the angle of dip of the stratification toward the right, suggesting that current strengths were variable. These bedforms are interpreted to have been formed by combined flows with a weak oscillatory component and a variable-speed tidal component. Well 7-6-4-7w4 (855.5 m depth).

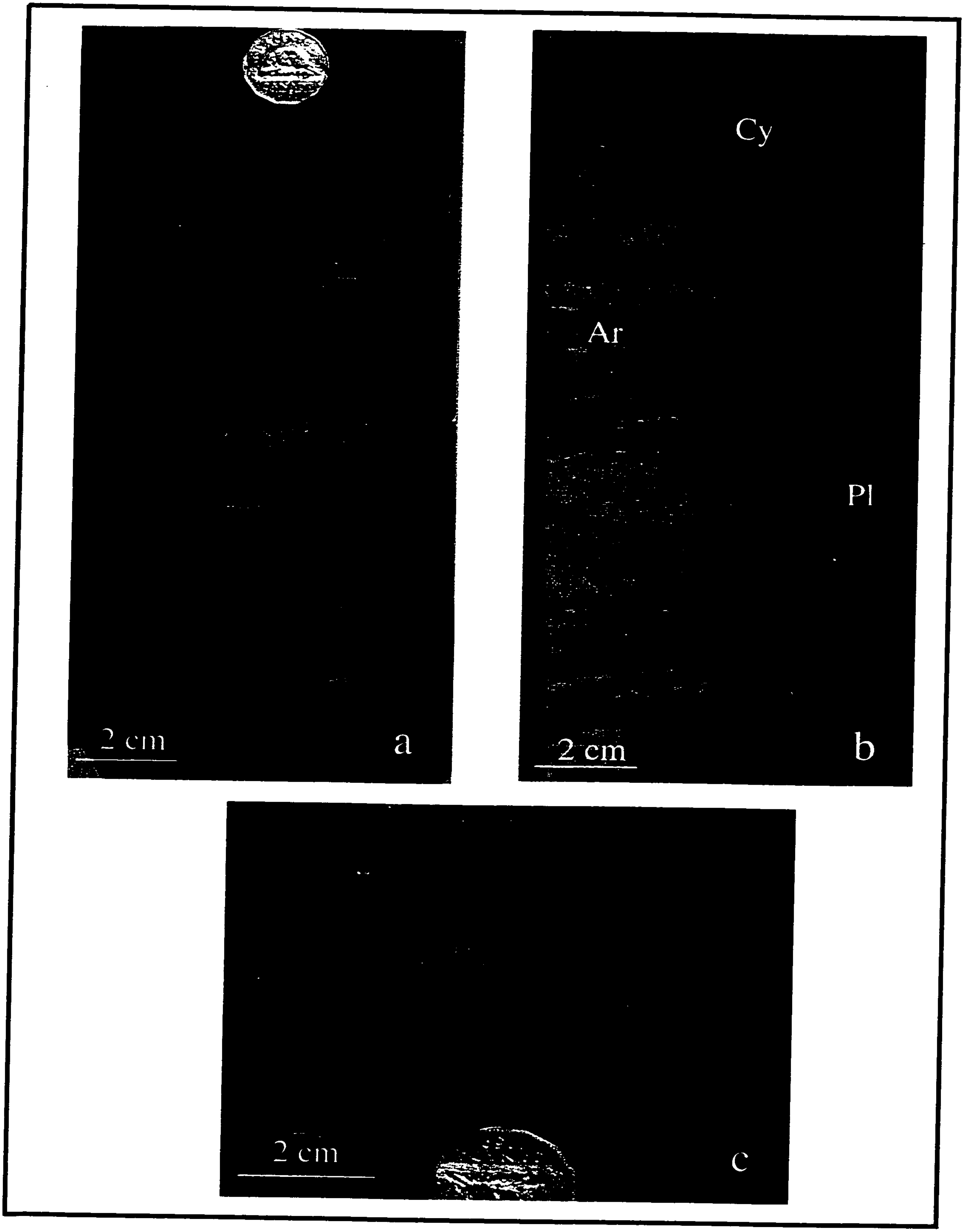
2 cm
a
Cy
Ar
Pl
2 cm
b
2 cm
c

systematic change in angle of dip of the stratification, which indicates that bedform migration was influenced by variable-speed unidirectional currents. Incipient current ripples are characterized by low-angled cross-stratification, but as flow speed increases and the bedform builds towards its equilibrium morphology, the foreset angle progressively increase in dip. As current speeds wane, however, foreset laminae progressively decrease in angle of dip. The consistent change in angle of dip, therefore, likely resulted from increasing then decreasing tidal current speed during a half tidal cycle. Also, the common occurrence of systematically inclined *Arenicolites* burrows in sandstone interbeds is suggestive of tidally influenced sedimentation. Polychaete worms that inhabit tidal environments commonly incline their U-shaped burrows as a strategy to rid their burrows of fecal material (M. Gingras, pers. comm., 1998).

Origin of Tidal Currents in the Study Area

During deposition of the ribbon sandstone, the study area was located in a strait that connected the Alberta Trough with the Williston Basin to the east (Fig. 2.2); the strait most likely formed because of reactivated uplift of the Sweetgrass Arch. Straits are commonly characterized by amplified tidal currents as tidal waves are funneled through a physiographically narrower area (Howarth, 1982). Although tidal currents in straits are commonly strong and capable of significant erosion or forming large scale bedforms (dunes), (e.g. Keller *et al.*, 1963; Kranck, 1972; Davies *et al.*, 1992; Anastas *et al.*, 1997; Ikehara, 1998), owing to differences in strait physiography, including width, length, depth and coastline morphology, and/or or characteristics of the local tide wave (combined effect of the progressive and standing tide waves), local tidal currents can also be much weaker and highly complex. In the case of the Swift, tidal currents, although amplified, are interpreted to have always remained weak and only reached velocities near the critical threshold for very fine sand. Furthermore, the typical short length (<5 cm) of individual sets suggests that during a half tidal cycle, tidal currents were amplified to threshold velocity for only a short period of time. The small amount of tidal amplification is probably because of the broadness of the strait, which may have been as much as 300 km during the Late Oxfordian (Imlay, 1980, fig. 10).

Despite the interpreted significance of tides, tidal rhythmites were not observed, which, in turn, suggests that bed-load transport was not controlled entirely by tidal currents. The common wavy basal contacts and lateral pinching and swelling of set thickness are characteristics more indicative of oscillatory conditions related to surface-gravity waves, which is likely related to storms. However, high-energy wave-formed sedimentary structures, like HCS, which are observed in strata of the shale member, are notably absent in the ribbon sandstone. These observations, therefore, suggest that wave energy, like tidal current energy, was also generally low, most probably because long-period, high-energy surface-gravity waves could not be formed in this part of the Swift basin, which was narrow and ~shallow, and/or extrabasinal waves (and wave energy) were extensively attenuated as they were propagated through the strait. Accordingly, in the absence of the other flow component, neither the tidal nor the oscillatory flow could independently initiate and maintain bed-load transport. Instead a combined-flow regime with a combined unidirectional (tidal current) and oscillatory (wave) flow component was necessary in order to initiate bed-load transport and permit small-scale bed forms to grow on the sea floor. Most cross-stratification in Lithofacies 4, therefore, is interpreted to have been formed by low-energy combined-flow ripples (cf. Arnott and Southard 1990) whose migration alternated with periods of suspension mud deposition.

Evidence for a Brackish Water Setting

Lithofacies 4 is characterized by an atypical ichnofossil assemblage. Ordinarily, under open marine conditions, interstratified sandstone and mudstone are thoroughly reworked by benthic fauna and hence, physical sedimentary structures, are rarely preserved (Hunter *et al.*, 1979; Howard *et al.*, 1981). In Lithofacies 4, however, physical sedimentary structures are well preserved and bioturbation is characterized by a low diversity, generally low abundance ichnofossil assemblage dominated by small, simple, horizontal and vertical burrows. The admixture of trace fossils common to both the *Cruziana* and *Skolithos* ichnofacies, combined with their small size, low diversity, and generally low abundance are suggestive of an ecologically stressed environment, commonly related to brackish water conditions (Ekdale *et al.*, 1984; Frey *et al.*, 1985; Wightman *et al.*, 1987; Beynon *et al.*, 1988). Additionally, common synaeresis cracks in mudstone beds may also suggest that salinity fluctuations were prevalent in the study area. Although the origin of these subaqueous shrinkage cracks is presently equivocal (Tanner, 1998), synaeresis cracks are commonly abundant in strata interpreted to have been deposited in tidally influenced brackish water settings (Wightman *et al.*, 1987; Beynon *et al.*, 1988). In addition, mudstone interbeds are barren of microfauna, which further suggests that water in the study area was brackish. Foraminifera that inhabit brackish waters are typically agglutinated and owing to post-depositional (post-morten) disaggregation, have low preservation potential (Owen Dixon, pers. comm., 1998). Despite their poor preservation potential however, brackish-water tolerant microfaunal assemblages have been documented in strata equivalent to the ribbon sandstone further to the east in Saskatchewan (Brooke and Braun, 1972). Brackish water conditions can also be inferred based on the local climatic conditions during the Oxfordian, which were probably warm and rainy (Imlay, 1980). Abundant precipitation would have resulted in significant fresh water input by rivers that bordered the low-energy strait, which in turn would have considerably reduced the salinity of the strait and consequently, its faunal and floral content. Also, the abundance of small coalified wood fragments observed in mudstone interbeds suggests a landmass nearby. Carbonaceous material was probably flushed into the strait by rivers discharging from highlands to the north (craton) and south (Belt Island Trend). Owing to the general low abundance of sandstone in ribbon sandstone, much of the bed-load flux was probably maintained in marginal marine settings. Suspended sediment, which at times consisted of sediment up to fine sand, would have formed buoyant effluent plumes that transported sediment some distance offshore where it later became reworked and redistributed by basinal processes (see below).

Lithofacies 5 – Small-Scale Cross-Stratified Sandstone

Lithofacies 5 consists of small-scale trough cross-stratified fine to medium sandstone with common mud drapes. It is only locally developed and occurs at several different stratigraphic horizons within the ribbon sandstone where it forms units up to 8 m thick. Lithofacies 5 has been further subdivided into two subfacies based on differences in internal stratification.

Subfacies 5a – Cross-Stratified Sandstone

Subfacies 5a is characterized by approximately 1 cm-thick bed sets with undulating basal contacts. The sets are up to 20 cm thick and consist mostly of bundled lenses (see De Raaf *et al.*, 1977) with bimodal internal stratification (Fig. 2.9a). Chevron upbuilding is rare. Bioturbation is uncommon and consists exclusively of *Planolites*. Subfacies 5a is generally gradationally overlain or underlain by Subfacies 5b.

Bundled lenses, chevron upbuilding and the consistent bidirectionality of the cross-laminae within a single set are characteristic of symmetrical oscillatory ripples, and therefore, Subfacies 5a is interpreted to have been deposited by purely oscillatory flows. Strata of Subfacies 5a, however, are uncommon in the ribbon sandstone, and most probably were deposited during high-energy storms that coincided with periods of negligible tidal current; these latter conditions occurred during short-duration slack water stage or longer-term neap tide periods. However, the wave-formed structures in Subfacies 5a suggests that tidal currents had a negligible effect on bed-load transport, despite their interpreted predominance in the basin. When storms coincided with slack water stage, subfacies 5a and 5b are interstratified. If, on the other hand, storms coincided with neap tides, only Subfacies 5a was deposited.

Subfacies 5b – Herringbone Cross-Stratified Sandstone

Subfacies 5b is characterized by small-scale unidirectional cross-stratified sets with flat to slightly undulatory basal contacts. Sets are less than 1 cm thick and mud drapes are preserved locally between them. Cross laminae dip consistently at high angles and in

Figure 2.9 Lithofacies 5. Small-Scale Cross-Stratified Fine Sandstone

Figure 2.9a) Lithofacies 5a. Cross-stratified sandstone with undulating basal contacts and bundled lenses interpreted to have been formed by combined flow currents with both weak oscillatory and tidal components, possibly during neap tide. Well 6-2-4-7w4 (879 m depth).

Figure 2.9b) Lithofacies 5b. Herringbone cross-stratification. Note the bidirectionality of individual sets (arrows). Distribution of Lithofacies 5b, appears to be random and does constitute cyclic bedding. These bedforms are interpreted to have been formed by combined flows with a dominant microtidal component, possibly during spring tide. Well 6-2-4-7w4 (881 m depth).

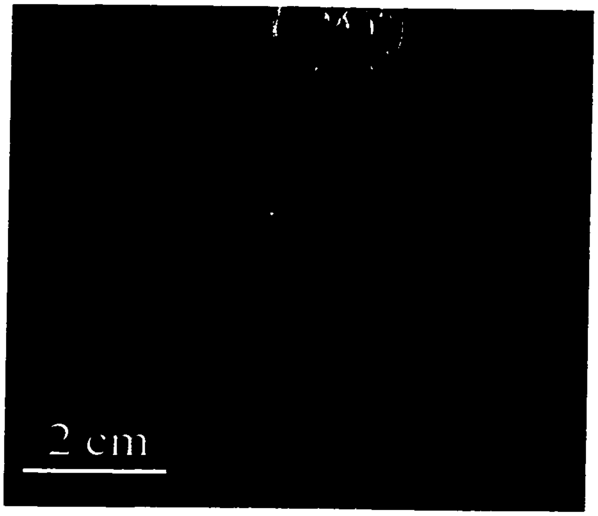

(a)

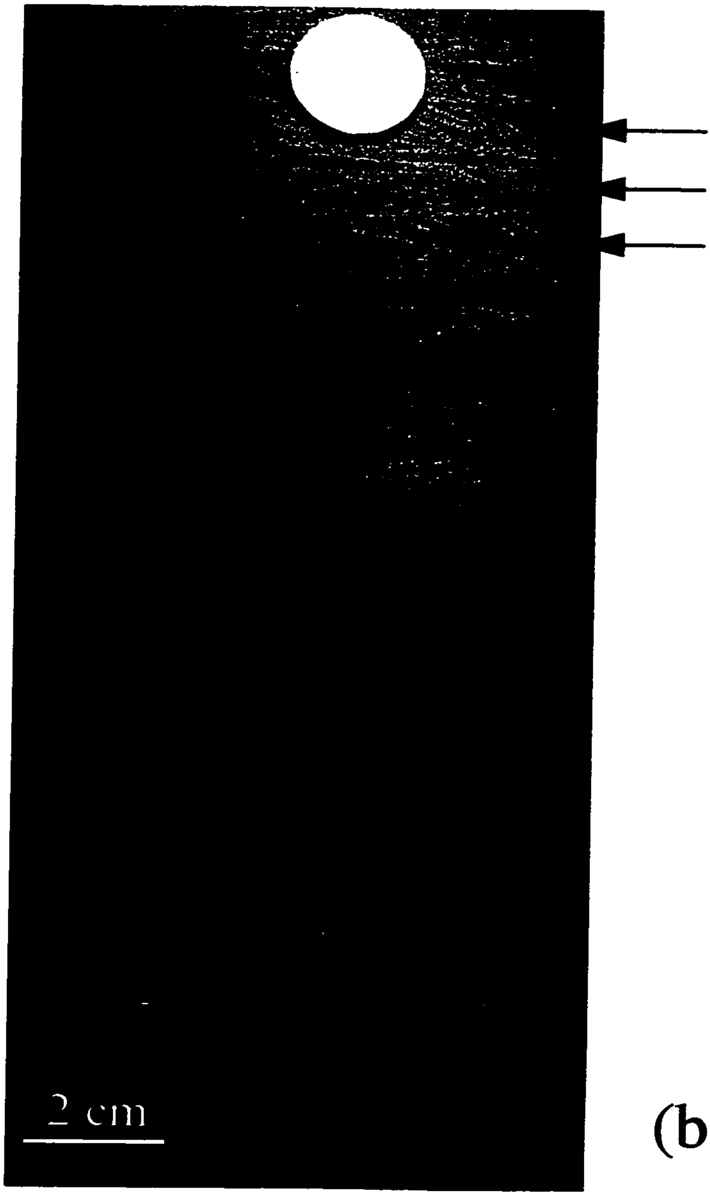

(b)

contrast to Lithofacies 4, generally do not change along the length of an individual set. Significantly, cross-stratification in superjacent sets commonly dip in the opposite direction (Fig. 2.9b). Subfacies 5b is commonly associated with Subfacies 5a and generally, gradationally overlies it.

The common bidirectionality of cross-stratification indicates that deposition of Subfacies 5a was influenced significantly by reversing tidal currents. However, because tidal currents were generally weak in the study area, an increase in tidal current strength alone, for example during spring tide periods, would likely have been insufficient to develop the observed herringbone cross-stratification. Moreover, if spring tidal currents were sufficiently strong to independently create Subfacies 5b, then intuitively these strata should be cyclically, or at the very least abundantly distributed throughout the Swift succession, which they are not. Increases in both the tidal and oscillatory components, therefore, were most probably necessary to generate strata of Subfacies 5b, which in turn necessitated the temporal and spatial coincidence of spring tide and high-energy storm conditions. Combined flows with a varying tidal component can form cross-stratification with unidirectional cross-laminae and undulatory basal contacts. Under these conditions, comparatively high unidirectional flow speeds (spring tide) and high oscillatory speeds (storm waves) formed the sufficiently energetic conditions for combined flow ripples to rapidly grow, develop steep slipfaces (high angle cross-stratification), and migrate preferentially in the direction of net bed shear stress during half of each tidal cycle (cf. Davies *et al.*, 1988; Duke *et al.*, 1991).

Lithofacies 6 – Quasi-Planar Laminated Sandstone

Lithofacies 6 forms uncommon to rare, sharp-based interbeds in the ribbon sandstone. It is characterized by planar laminated fine to medium grained sandstone and forms beds that range from 3 - 15 cm thick. Laminae are generally sub-parallel to the basal contact, although rare examples of shallow dipping laminae downlapping onto the basal contact were observed (Fig. 2.10a). Abundant shale rip-up clasts are common at the bottoms of the thicker sets. Bioturbation was not observed. Generally, Lithofacies 6 is sharply overlain by Lithofacies 5.

Figure 2.10 High-energy deposits of the ribbon sandstone (Sequence 2)

Figure 2.10a) Lithofacies 6. Rare quasi-planar laminated sandstone form sharp based, 3 – 15 cm thick interbeds in the ribbon sandstone. Note the shallow dipping laminae downlapping near the basal contact. Lithofacies 6 is interpreted to be high-energy combined flow plane beds formed during storms. Well 8-29-5-6w4 (955 m depth).

Figure 2.10b) Lithofacies 7. Uncommon massive medium sandstone with common shale rip-up clasts near the basal contact. Note pyritized seam. The origin of the Lithofacies 7 remains enigmatic. Well 6-23-7-3w4 (1429m depth).

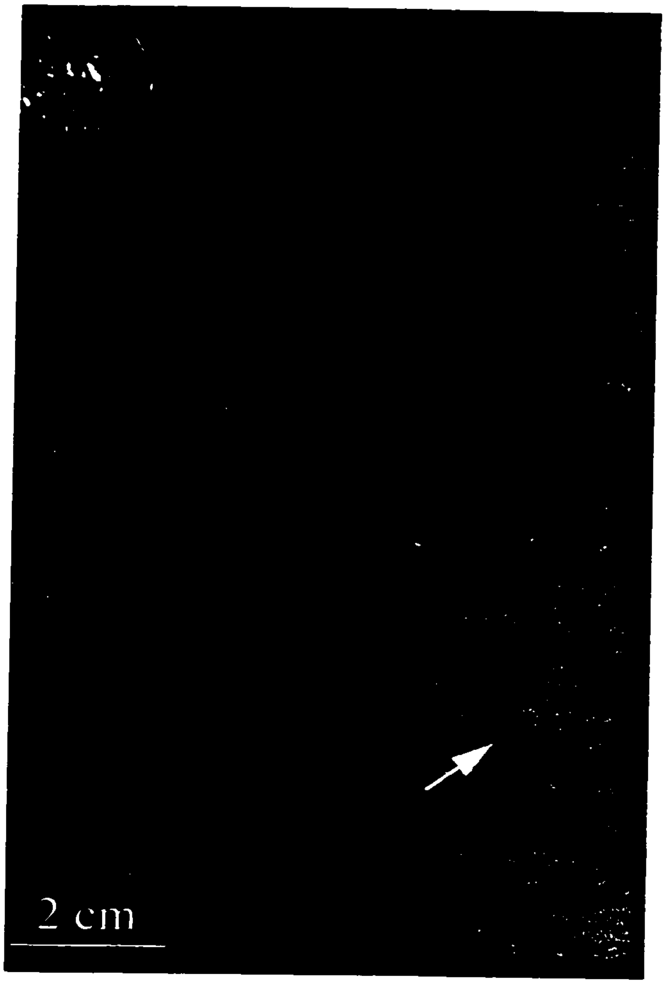

(a)

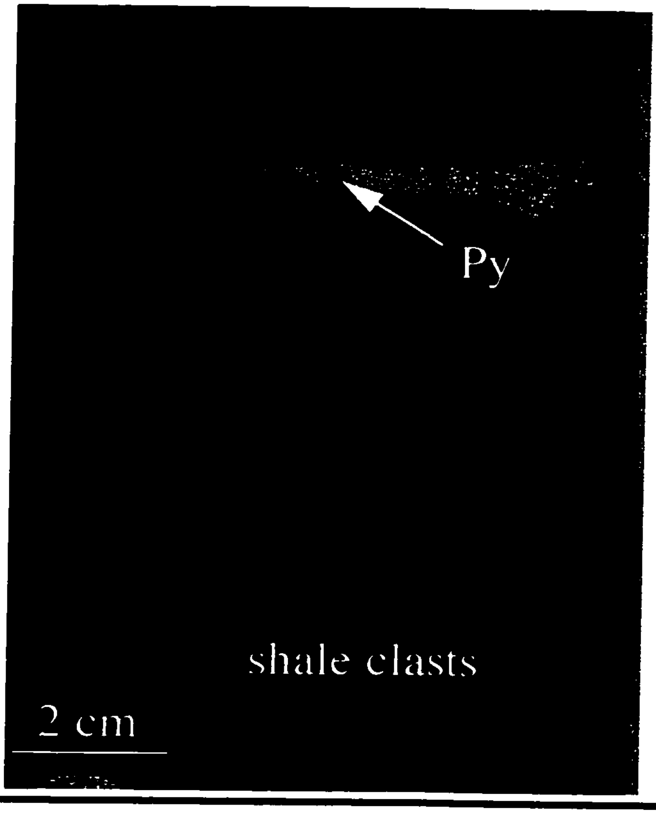

(b)

Planar lamination is formed either by unidirectional or oscillatory upper flow regime currents. However, as stated previously, high-energy unidirectional or oscillatory conditions are interpreted to have not existed during deposition of the ribbon sandstone. On the other hand, Lithofacies 6 was probably formed by high-energy combined flow currents. Combined flow planar bedding (quasi-planar-lamination) is characterized by subtle, metre-scale undulation of the "planar" laminae and is deposited under high-energy combined flow conditions (Arnott and Southard, 1990; Arnott, 1992). Because the undulation is a large scale feature, its observation in core is not possible. However, quasi-planar-lamination commonly exhibits shallow dipping laminae downlapping onto the basal contact, which was observed in core. Lithofacies 6 is also generally overlain by small-scale cross-stratified sandstone of Lithofacies 5, suggesting deposition from waning flows. Beds of Lithofacies 6, therefore, are interpreted to consist of high-energy combined flow plane bed (quasi planar lamination) deposited during rare, larger than normal storms that formed higher speed, longer-period oscillatory currents that combined with spring tidal currents (alternatively, high energy oscillatory currents may have been formed by swell waves generated by major storms in the Alberta Trough or Williston Basin, but most of this energy would have likely been attenuated along the length of the strait).

Lithofacies 7 – Massive sandstone

Lithofacies 7 consists of fine to medium massive sandstone (Fig. 2.10b). Beds have sharp basal contacts and range from 3 to 15 cm thick. Poorly organized shale rip-up clasts are present locally at the base of thicker beds. Lithofacies 7 is typically associated with other sandy lithofacies of the ribbon sandstone. The origin of massive beds is poorly understood and consequently, they are difficult to interpret. Massive beds can form as a result of intense bioturbation, which thoroughly reworks the sediment into a structureless, massive bed. However, highly bioturbated beds typically display a distinctive mottled texture, which was not observed in Lithofacies 7. Furthermore, bioturbation intensity is generally low to absent in the ribbon sandstone, including high-energy deposits, and as such, Lithofacies 7 is unlikely the result of intense bioturbation. Alternatively, massive beds can be primary features that form when sediments are deposited very rapidly from suspension or from highly concentrated sediment dispersions, commonly associated with sediment gravity flows (Boggs, 1987). However, the energy needed to transport medium sand in suspension is extremely high, and given the overall physical conditions in the depositional basin, such high energy currents are unlikely to have developed. Some massive beds, however, are not completely structureless, but have weakly developed structures that can be detected using X-radiographic or staining techniques (Boggs, 1987). Such techniques were not undertaken because only one small sample was retrieved from core. Nonetheless, Lithofacies 7 may be composed of macroscopically invisible medium-scale cross-bedding or planar lamination that would likely have been deposited during high-energy storms. The origin of Lithofacies 7, therefore, presently remains enigmatic.

Lithofacies 8 – Altered ribbon sandstone

Lithofacies 8 occurs at the top of the Swift Formation and consists of light-coloured ribbon sandstone. It invariably overlies gradationally(decimetre scale) or abruptly strata of Lithofacies 4, 5, or 6 and, in turn is unconformably overlain by continental deposits of the Basal Quartz (Mannville Group). Lithofacies 8 is areally extensive but varies significantly in thickness, ranging from 0 to a few meters thick where it has been completely to partly removed by Basal Quartz erosion, up to 15 m thick where Basal Quartz erosion is assumed to have been negligible. At the base of Lithofacies 8 strata are similar to those of Lithofacies 4, 5 or 6 described above, but differ in that mudstone interbeds or drapes are light instead of dark in colour. These strata are then gradationally overlain by diffusely interstratified material, most notably in the mudstones, and in its upper part by abundant microscopic clay/silt argillans and possible rare root traces highlighted by rusty reaction rims.

The altered ribbon sandstone is interpreted to be a paleosol that developed at the unconformity marking the top of the Swift Formation following withdrawal of the Oxfordian sea from the study area. Because of the long period of time needed to form well-developed soils, paleosols are commonly associated with unconformities (Retallack, 1990). In this study, the sub-Cretaceous unconformity spans a period of approximately 35 My (Gradstein *et*

Figure 2.11 Altered ribbon sandstone

Figure 2.11a) Sharp colour change from dark to light ribbon sandstone. Well 10-36-5-5w4 (1176 m depth).

Figure 2.11b) The interstratification that characterizes the ribbon sandstone progressively becomes more difficult to discern and gradually merges into pedogenically altered, massive-appearing, beige strata. Well 8-29-5-6w4 (~945m depth).

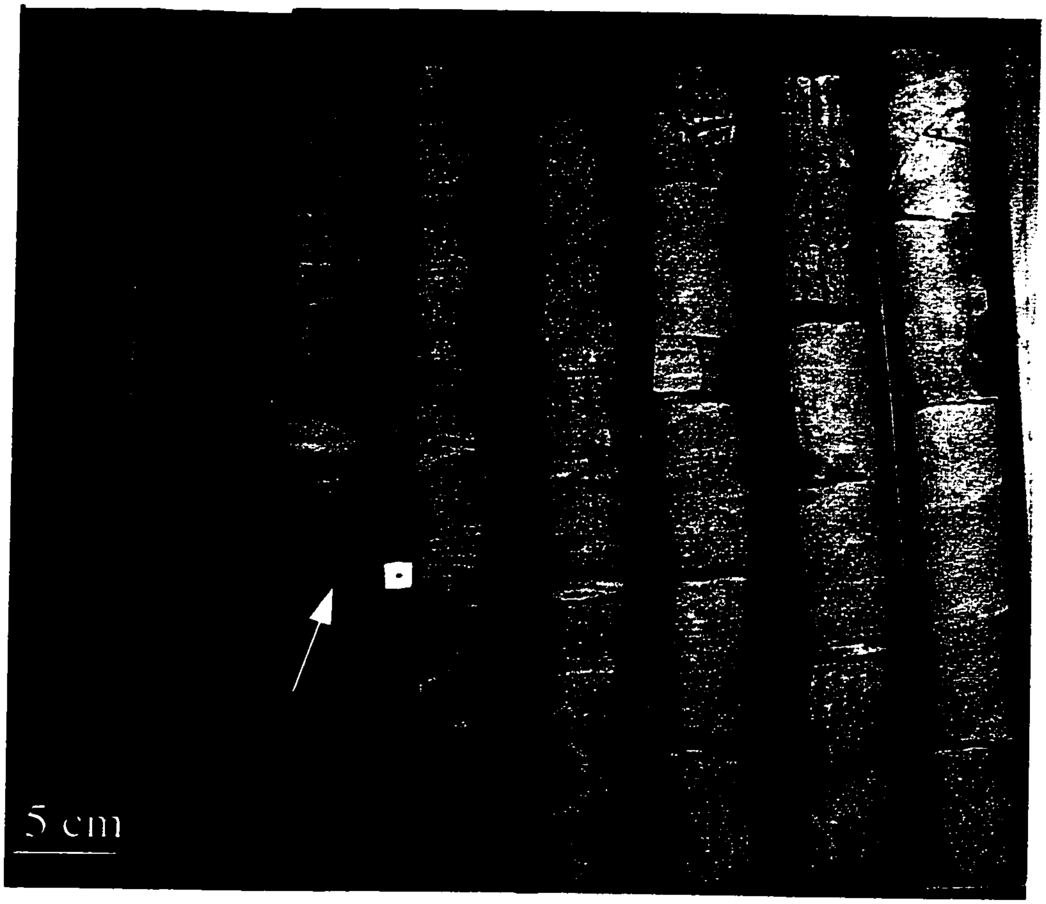

(a)

(b)

al., 1996) and therefore, represents sufficient time for paleosol development. In southeastern Alberta, the Swift paleosol consists predominantly of pedogenically altered strata of Lithofacies 4. Its sharp to gradational lower contact with dark-coloured strata represents the contact between unaltered, organic-rich bedrock (dark-coloured strata) and the overlying C-horizon consisting of slightly altered bedrock in which all organic material has been completely degraded. In turn, the gradational contact between the light coloured ribbon sandstone and overlying structureless strata represents the contact between the C- and B-horizon (more altered bedrock) in the soil profile. Other horizons commonly observed in paleosols (e.g. E and A horizons) are interpreted have been removed by later Early Cretaceous fluvial erosion. Glaebules, such as sphaerosiderite, which locally are abundant in strata of Lithofacies 8, have previously been shown to be common in paleosols, but notably are not exclusive to them (Coleman, 1985; Retallack, 1990; Morad, 1998). However, other indicators of pedogenesis were observed in strata of Lithofacies 8 and include rare root traces and soil structures, such as peds and argillans. Argillans (clay skins) are emplaced by elluviated silt and mud particles into cracks between soil peds (natural aggregates of soil material) (Retallack, 1990) and generally accumulate in the Bt horizon of a soil profile. During burial diagenesis the peds were compacted and formed massive appearing strata. Slickensides were formed also by the compaction and abrasive interaction of adjacent peds during burial. In addition to all these processes, extensive pedogenic leaching caused primary sedimentary structures to become significantly obscured or in many places obliterated. Details on ribbon sandstone pedogenesis are given in Chapter 3.

Significant also is the marked increase in radioactivity at the base of Lithofacies 8. (Figure 2.12). Here radioactivity is related to organically bound uranium at the base of the paleosol -- the origin of this horizon is discussed in detail in Chapter 3. In these strata uranium is presumed to have been derived from unpreserved thin layers of Lower Cretaceous volcanic ash. Although Aptian or older Cretaceous bentonites have not been observed in southern Alberta, volcanic activity was nonetheless widespread during the Early Cretaceous. Barremian (128 Ma) tuff layers are prominent in the Bighorn Basin in Wyoming (May *et al.*, 1995) and indicates that volcanic activity occurred between deposition of the Swift

Figure 2.12 Geophysical well log (well 10-36-5-5w4) showing the abrupt rightward deflection on the gamma-ray curve, which coincides with the dark and light ribbon sandstone contact. The source of the deflection is related to organically bound uranium. Uranium derived from volcanic ash layers was mobilized by ground water during soil leaching, and reprecipitated along a redox front at the light and dark ribbon sandstone contact.

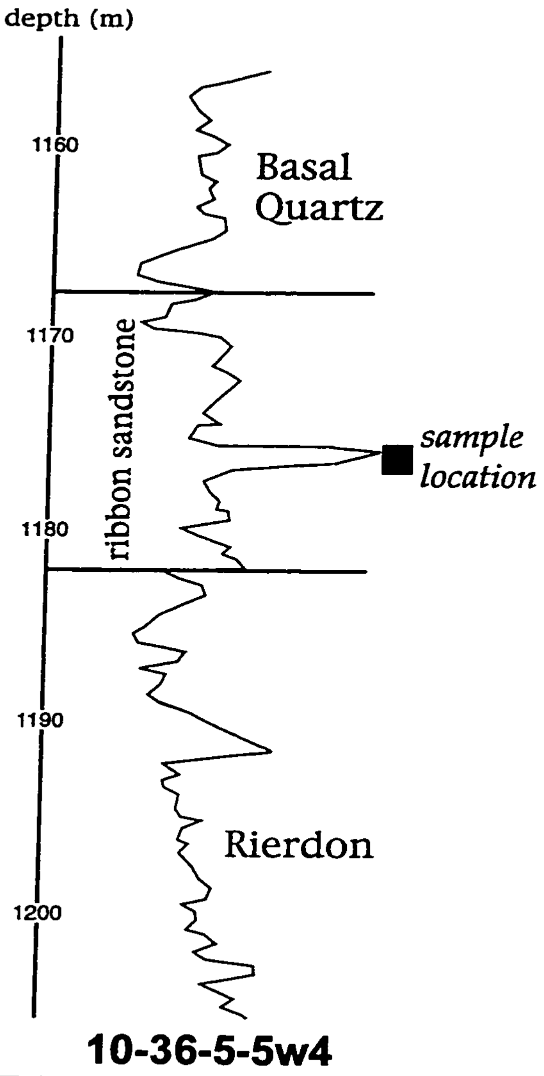

depth (m)	U ppm
1175.68	<1.0
1175.80	5.4
1175.85	24.5
1175.95	29.1
1176.05	14.5
1176.25	10.3
1176.45	6.2
1176.65	1.2
1176.85	2.3
1177.05	< 1.0

Formation and the overlying Basal Quartz. Volcanic ash emitted from volcanoes located west and south of the study area could have been easily transported downwind to southeastern Alberta where they were deposited as thin laminae. Uranium was leached from the tuff layers at the surface (under oxidizing conditions) and formed highly soluble uranyl compounds that were transported vertically through the soil profile by downward-percolating meteoric fluids. At depth, however, reducing conditions caused the uranium to be adsorbed onto organic material present along the upper surface of Lithofacies 4 strata (this surface, in fact, represents an ancient redox front). The depth of the redox front, and hence the stratigraphic position of the radioactive marker horizon was controlled by primary and secondary permeability heterogeneities within the soil profile (composed of altered (light-coloured) ribbon sandstone). This, in turn, controlled patterns of groundwater flux and circulation, and as a consequence, caused the radioactive layer to form at variable depth in the subaerially exposed Swift succession, even locally.

Geophysical Well Log Character

The Swift Formation is characterized by various well log signatures, some of which resemble those of the underlying Rierdon Shale and overlying Basal Quartz. Consequently, strata of the ribbon sandstone have commonly been misinterpreted. A discussion of geophysical well log attributes is therefore deemed necessary.

The shale member typically exhibits the well log character of a shale. It is distinguished by its high gamma count, high neutron porosity (related to bound water), low resistivities (~ 4 ohms) and a spontaneous potential curve that typically defines the shale line. Locally, the SP deflects to the left, which coincides with the occurrence of hummocky-cross-stratified sandstone strata (Lithofacies 3) (e.g. 3-2-4-6w4) (Fig. 2.13a). South of Township 8, the shale member is easily distinguished from the Rierdon Shale, which typically forms a 'shoulder' because of relatively lower API values and high resistivity indicative of lime mud. North of Township 8, however, there is a facies change in the Rierdon Shale, which becomes more siliciclastic in character, and the well-developed "shoulder" is no longer present. The increase in siliciclastic content is probably related to the increasing proximity to the land (craton) and detrital sediment. As a result, the Rierdon - shale member boundary is more difficult to determine.

The log signature of the ribbon sandstone, on the other hand, resembles that of a siltstone, with higher resistivity, lower API values, and lower bulk density and neutron porosity (Fig. 2.13a-e). Typically, the shale member - ribbon sandstone contact is abrupt and only in Ranges 1 and 2, south of Township 4 does it appear gradational. The ribbon sandstone exhibits a number of different log profiles, including upward-unchanging, upward-fining, and upward- coarsening successions (Fig. 2.13b, c, and e). The areal distribution of these different profiles appears to show no recognizable organization, and all three signatures can occur within an area of 1 square mile. Also, uncommon "clean" sandstone units (API <60) are observed at different stratigraphic intervals within the ribbon sandstone. These units are typically less than 5 metres thick, are laterally discontinuous and have either a sharp basal contact or grade upward from mudstone to more sandstone-rich strata.

Many logs show an upward-sandier profile in the ribbon sandstone that begins above the high gamma peak that separates the dark and light ribbon sandstone (Fig. 2.13b, c, and e). This signature, however, is unreliable because it corresponds to Lithofacies 8, which has been extensively chemically altered. Exchangeable cations such as radioactive potassium (K^{40}) have effectively been leached from strata by hydrolytic reactions and as a result, gamma counts are typically lower than those in the underlying, unaltered ribbon sandstone (see section on colour change). Similarly, resistivity values gradually increase and bulk density and neutron porosity generally decrease stratigraphically upwards from the colour change. These signatures are related to loss of bound water by chemical alteration and to argillan infiltration. The apparent upward-cleaning trend in the ribbon sandstone therefore reflects a change in crystal chemistry instead of an upward decrease in mud content. Ribbon sandstone is overlain by the Basal Quartz Formation, which consists of fluvial sandstones exhibiting a well log character consistent with a "clean" sandstone: low API values, a leftward deflection on the spontaneous potential curve and high resistivities (Fig. 2.13b). Locally however, many of these sandstones have been extensively pedogenically altered and, because of the abundance of grain-rimming clay cutans (clay skins) there is a systematic

Figure 2.13 Geophysical log illustrating various log character of the Swift Formation. a) Thick shale member with interbeds of HCS (note the abrupt decrease in gamma counts and increase in resistivity in underlying Rierdon); b) sharp contact between the shale member and the ribbon sandstone marked by decreases in gamma counts and increase in resistivity; strata of the ribbon sandstone are characterized by various stacking patterns including c) upward-coarsening (less mud), d) upward-fining (getting muddier), and e) aggrading; f) many logs show an upward-coarsening profile above the deflection on the gamma curve.

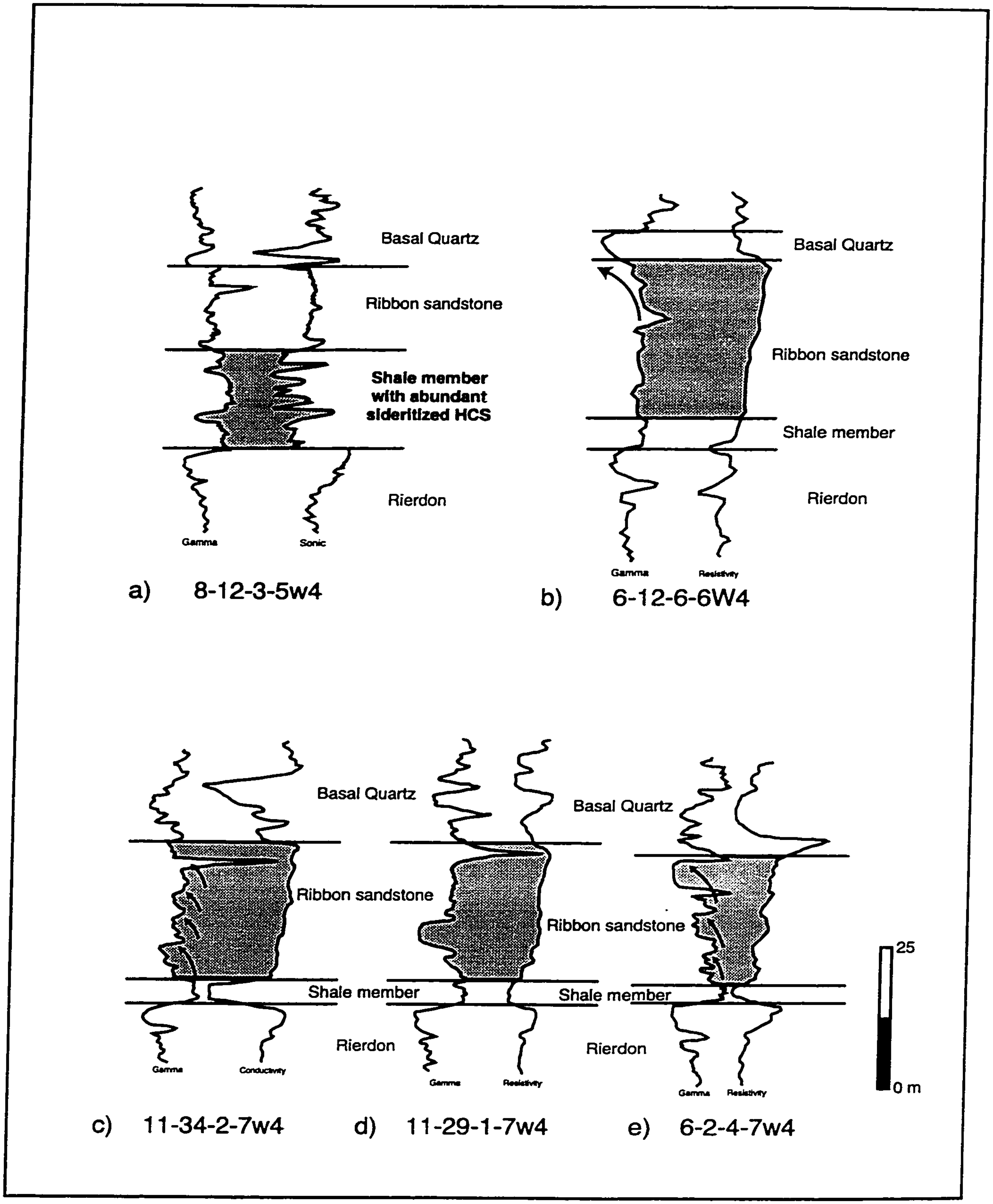
Basal Quartz
Ribbon sandstone
Shale member with abundant sideritized HCS
Rierdon
Gamma
Sonic
a) 8-12-3-5w4
Basal Quartz
Ribbon sandstone
Shale member
Rierdon
Gamma
Resistivity
b) 6-12-6-6W4
Basal Quartz
Ribbon sandstone
Shale member
Rierdon
Gamma
Conductivity
c) 11-34-2-7w4
Basal Quartz
Ribbon sandstone
Shale member
Rierdon
Gamma
Resistivity
d) 11-29-1-7w4
Gamma
Resistivity
e) 6-2-4-7w4
25
0 m

lowering of the gamma counts, which, in turn causes it to be similar to the log profile in the underlying ribbon sandstone (Fig. 2.13e). Nonetheless, Basal Quartz strata can usually be distinguished from the ribbon sandstone on the resistivity curve and the contact between the two generally lies at the inflection point between increasing and then decreasing resistivity. Elsewhere, Mannville strata also have well log signatures similar to the ribbon sandstone, but can be distinguished from it by its higher neutron porosities, bulk densities and lower resistivity associated with Cretaceous paleosols or pedogenically altered continental deposits (Fig. 2.13c).

Lateral Facies Relationships

Three-dimensional facies relationships were examined by using a series of north-south and east-west oriented cross-sections, isopach maps, and slice maps.

Choice of Datum

The choice of an appropriate stratigraphic datum is important because it forms the basis for accurate and meaningful correlations. Choosing a suitable datum in this study, however, was problematical because regionally extensive correlatable marker beds, such as basin-wide marine flooding surfaces unrelated to unconformities, are absent in both the Swift and the overlying lower part of the Mannville Group. In addition, the Ostracode zone, which is a commonly used stratigraphic horizon throughout much of southern Alberta, is absent in the study area. Furthermore, the top of the Mannville, which represents a basin-wide transgressive surface, is an unreliable stratigraphic datum because of the significant variability in the thickness of the Mannville succession. Mannville strata within the study area, thins to the north by approximately 40 metres over a distance of about 100 kilometres (Fig. 2.14a). This thinning is interpreted to be related to the development of a subsiding half-graben (Medicine Hat Block), hinged to the north along the Precambrian Vulcan Low (Fig. 2.14b). Asymmetrical subsidence is interpreted to have been caused by reactivation of the Proterozoic Great Falls Tectonic Zone in northern Montana related to the ongoing Columbian Orogeny. Although subsidence likely commenced during the Late Jurassic, rates were likely

Figure 2.14 Rierdon to Mannville isopach map and Precambrian basement terranes and structures in southeastern Alberta

Figure 2.14a) Isopach map of combined Rierdon, Swift and Mannville strata illustrating a northward thinning of the strata by ~40 metres. A combined stratal thickness was chosen to avoid complications related to thickness variations caused by deep Lower Cretaceous fluvial incision.

Figure 2.14b) Precambrian terranes in the subsurface of Alberta, northeast British Columbia, and northern Montana. The study area overlies the Medicine Hat Block, which is interpreted to have formed a subsiding half-graben hinged to the north along the Vulcan Low during the Late Jurassic to Early Cretaceous. Based on isopach maps, subsidence rates were highest in the early Early Cretaceous (modified from Ross *et al.*, 1991).

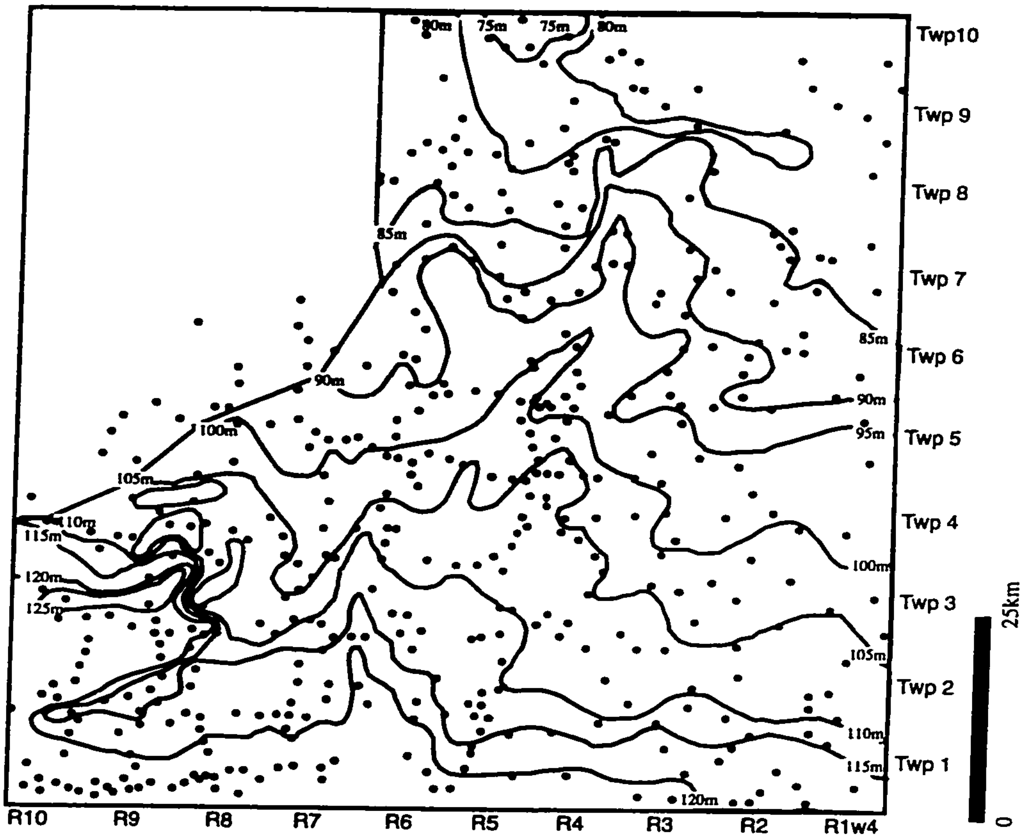

80m
75m
75m
80m
85m
85m
90m
90m
95m
100m
100m
105m
105m
110m
110m
115m
115m
120m
120m
125m
Twp10
Twp 9
Twp 8
Twp 7
Twp 6
Twp 5
Twp 4
Twp 3
Twp 2
Twp 1
R10
R9
R8
R7
R6
R5
R4
R3
R2
R1w4
25km
0

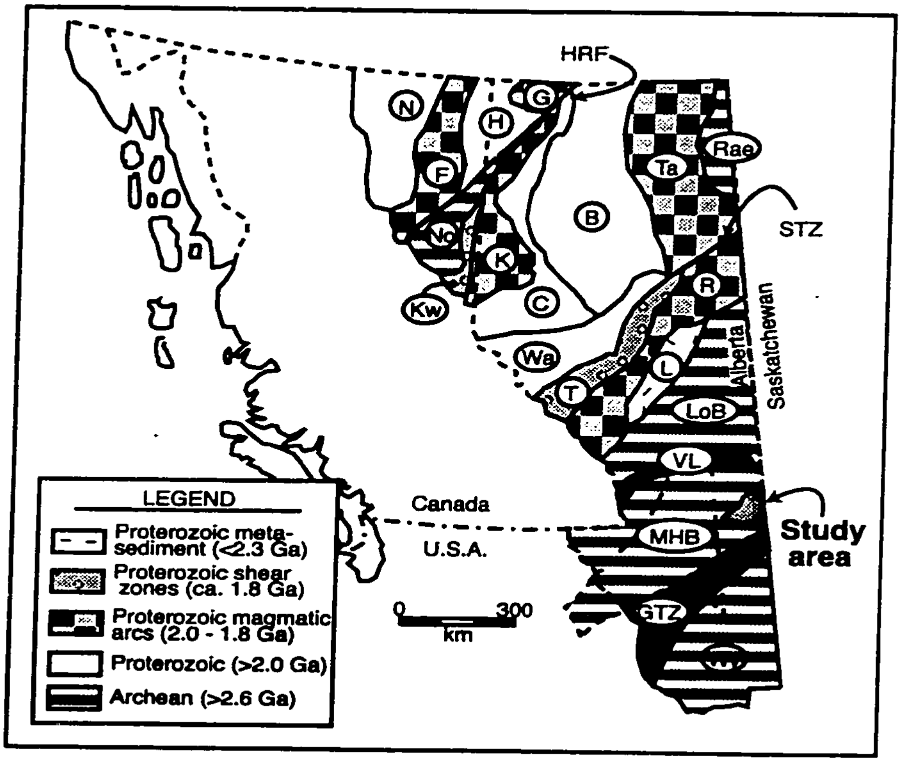

HRF
N
G
H
F
Ta
Rae
B
STZ
No
K
Kw
C
R
Wa
L
T
LoB
Alberta
Saskatchewan
VL
Canada
U.S.A.
MHB
Study area
GTZ
0
300
km
LEGEND
Proterozoic meta-sediment (<2.3 Ga)
Proterozoic shear zones (ca. 1.8 Ga)
Proterozoic magmatic arcs (2.0 - 1.8 Ga)
Proterozoic (>2.0 Ga)
Archean (>2.6 Ga)

highest in the Early Cretaceous because significant depositional thickness variations were observed only for the Lower Cretaceous Mannville Group succession. Therefore, the top of the Mannville is a poor choice of datum to correlate Swift strata. Another alternative is the top of the Rierdon Formation. Although this surface is marked by a major unconformity that spans approximately 5 Ga. (Gradstein *et al.*, 1996), thickness of the Rierdon succession varies little throughout the study area, and regional mapping shows surface topography to be negligible (Fig. 2.15). The top of the Rierdon Formation, therefore, has been chosen as the stratigraphic datum in this study.

Sequence 1 – Shale Member

Sequence 1 consists of the shale member. It comprises three and possibly four upward-coarsening parasequences, each averaging approximately 4 metres thick. On geophysical well logs, marine flooding surfaces that bound the parasequences are locally difficult to identify because the coarsest facies in the shale member (Lithofacies 3) does not systematically correspond to the uppermost part of the parasequence. Furthermore, these beds tend not to be areally extensive. Parasequences generally stack in a subtle upward-fining trend, forming a retrograding parasequence set, and suggest a long-term deepening of the marine basin. Within the study area, Sequence 1 varies from 0 to 30 metres thick, with strata most thickly preserved in the southeast (Fig. 2.16; Z–Z'). It generally thins to the west as it onlaps the Sweetgrass Arch, suggesting that the arch was a positive topographical feature during the Late Jurassic. A slight thinning toward the north is also observed, and may be related to asymmetrical subsidence of the Precambrian Medicine Hat Block toward the south, which lasted at least until the end of Mannville time. Alternatively, the thinning may be an artefact of the misidentification of the top of the Rierdon Formation. In this area (north of Township 8) the diagnostic "Rierdon shoulder" is no longer recognizable and because no cores are available in this part of the study area, differentiating siliciclastic Rierdon shale from Swift shale on geophysical well logs alone is problematical (Fig. 2.16, line Z-Z'). Nevertheless, in spite of these complications, thinning of the shale member is most probably real for two reasons. Firstly, between townships 1 and 7, where the Rierdon shoulder is well

Figure 2.15 Isopach map depicting minor thickness variations in the Rierdon Formation.

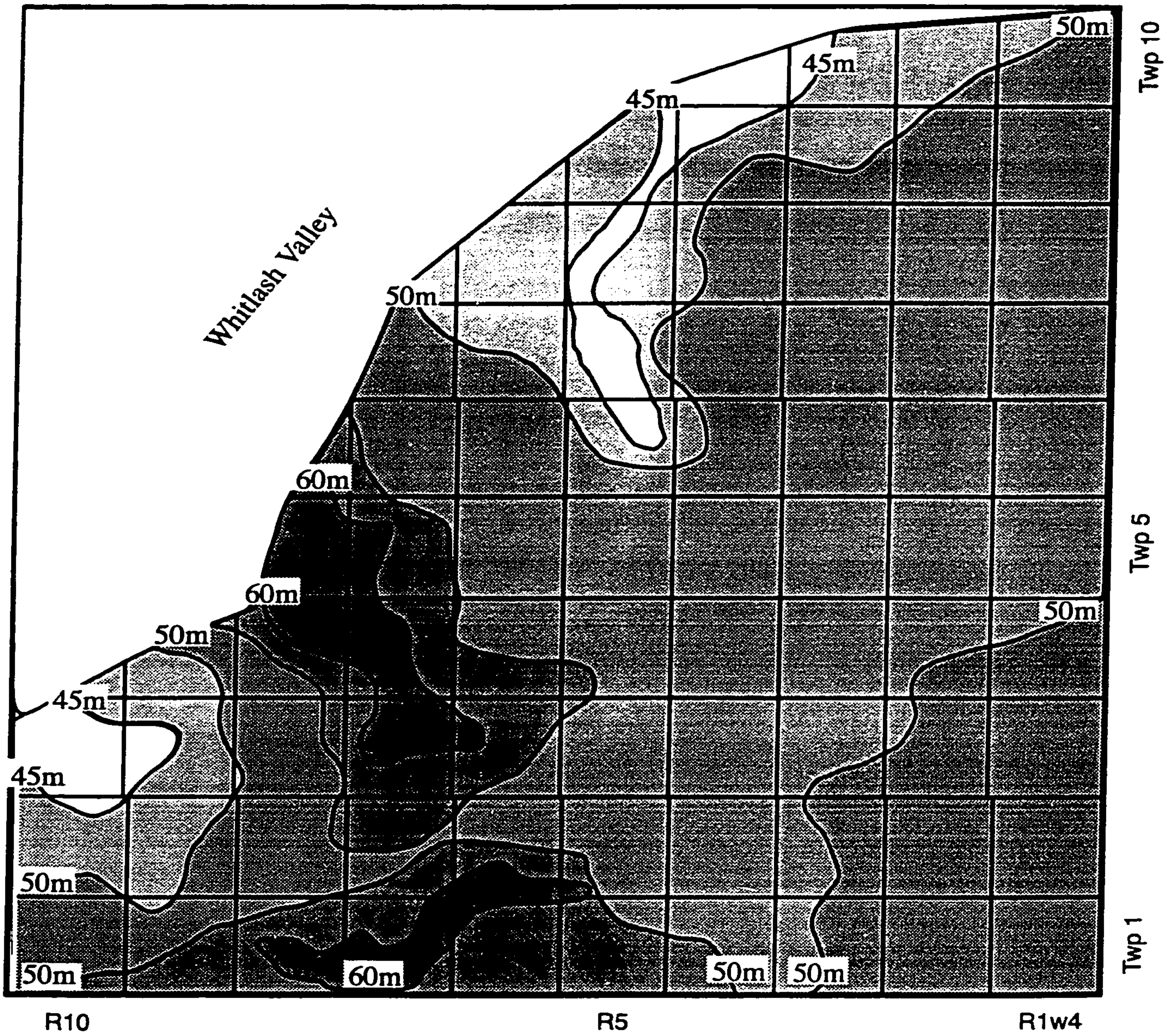

Whitlash Valley
50m
45m
45m
50m
60m
60m
50m
45m
45m
50m
50m
60m
50m
50m
50m
Twp 10
Twp 5
Twp 1
R10
R5
R1w4

Figure 2.16 West to east and north-south cross-sections illustrating variable stacking patterns in the ribbon sandstone (i.e. prograding, retrograding and aggrading). These laterally discontinuous stratal successions formed because of spatial and temporal variations in sediment deposition and related built-up and temporary maintenance of low-energy combined-flow sand banks. Line of section is shown in Figure 1.

Note that the Rierdon shale south of Township 8 (line Z – Z') forms a 'shoulder' because of relatively lower API values indicative of lime mud. North of Township 8, however, there is a facies change in the Rierdon shale, which becomes more siliciclastic in character, and the well development 'shoulder' is no longer present. Here, discerning Rierdon shale from the shale member is more difficult.

Also, note that strata in the central uplift of the impact crater (14-32-8-4w4; line C – C') appear to be compacted and opposed to being uplifted. Compare to Figure 2.6, which clearly illustrates the uplifted structure by using the top of the Mannville Group as a datum. The choice of datum, therefore must be done carefully by keeping in mind the specific objectives.

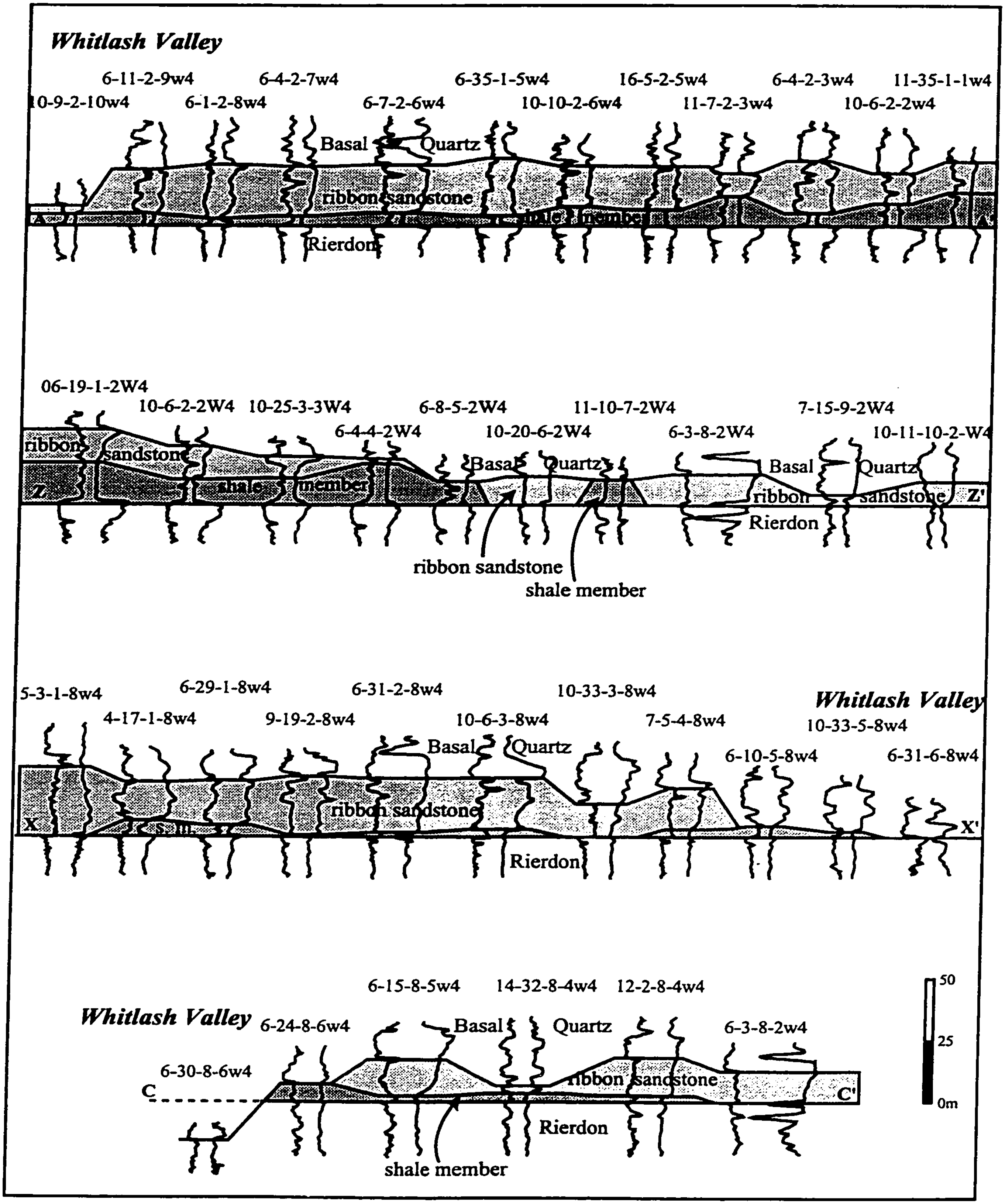
Whitlash Valley
6-11-2-9w4
6-4-2-7w4
6-35-1-5w4
16-5-2-5w4
6-4-2-3w4
11-35-1-1w4
10-9-2-10w4
6-1-2-8w4
6-7-2-6w4
10-10-2-6w4
11-7-2-3w4
10-6-2-2w4
Basal
Quartz
ribbon sandstone
shale member
Rierdon
A
A'
06-19-1-2W4
10-6-2-2W4
10-25-3-3W4
6-8-5-2W4
11-10-7-2W4
7-15-9-2W4
6-4-4-2W4
10-20-6-2W4
6-3-8-2W4
10-11-10-2-W4
ribbon
sandstone
shale
member
Z
Basal
Quartz
Basal
Quartz
ribbon
sandstone
Z'
Rierdon
ribbon sandstone
shale member
5-3-1-8w4
6-29-1-8w4
6-31-2-8w4
10-33-3-8w4
Whitlash Valley
4-17-1-8w4
9-19-2-8w4
10-6-3-8w4
7-5-4-8w4
10-33-5-8w4
6-10-5-8w4
6-31-6-8w4
Basal
Quartz
ribbon sandstone
X
s. m.
X'
Rierdon
6-15-8-5w4
14-32-8-4w4
12-2-8-4w4
Whitlash Valley
6-24-8-6w4
Basal
Quartz
6-3-8-2w4
6-30-8-6w4
C
ribbon sandstone
C'
Rierdon
shale member
50
25
0m

developed, a minor (5 m) northward thinning of shale member strata is observed; and secondly, thickness of the Rierdon Formation north of Township 8 reported from this study is similar to thicknesses previously reported to the east in southwestern Saskatchewan (Christopher, 1974).

The upper surface of the shale member shows a highly irregular paleotopography typified by a network of narrow (~ 1.5 km) interconnected meandering scours that are up to 15 metres deep. The nature and origin of these scours is discussed next.

Evidence for Oxfordian Channel Incision

The upper surface of the shale member is characterized by multiple, deep, narrow, elongated, sinuous, northeast-southwest trending scours (Fig. 2.17). These scours trend approximately normal to the east-west trending Oxfordian strait (Fig. 2.2). Scours of this scale are formed by a limited number of processes including: 1) erosion in an open marine setting, 2) erosion along transgressive shorefaces, and 3) fluvial erosion in a subaerial environment (Walker and Plint, 1992). In an open marine setting, erosion usually occurs during storms, but typically is only local and no more than a few metres deep. Conversely, erosion related to transgressive shorefaces commonly form deep scours. These scours, termed stillstand incisions, form during periods of reduced rate of relative sea level rise, and have a distinctive asymmetrical profile (parallel to depositional dip), and typically subparallel the regional shoreline trend (Walker and Plint; 1992). Other possible causes for deep scours include submarine erosion related to strong tidal currents (Huthnance, 1982; Berné *et al.*, 1998) and erosion by channelized tidal currents such as tidal inlets. Although tidal currents are interpreted to have been important during deposition of the overlying ribbon sandstone, it remains unlikely that tidal activity eroded these scours for two reasons. Firstly, tidal currents generally create relatively straight and elongate scours and secondly, deep tidal scours are generated by high-velocity currents. However, stratigraphic evidence of high–energy tidal current erosion or deposition is lacking in Swift strata in this study or in the literature from adjacent areas. The relatively narrow width, long length, multiple number and overall meandering and interconnected nature of the scours are all characteristics consistent

Figure 2.17 Isopach map of the shale member showing highly irregular paleotopography. Note the multiple, deep (< 15 m), narrow, elongated, sinuous, northeast-southwest trending scours. Scours are interpreted to have resulted from the incision of subaerial fluvial channels.

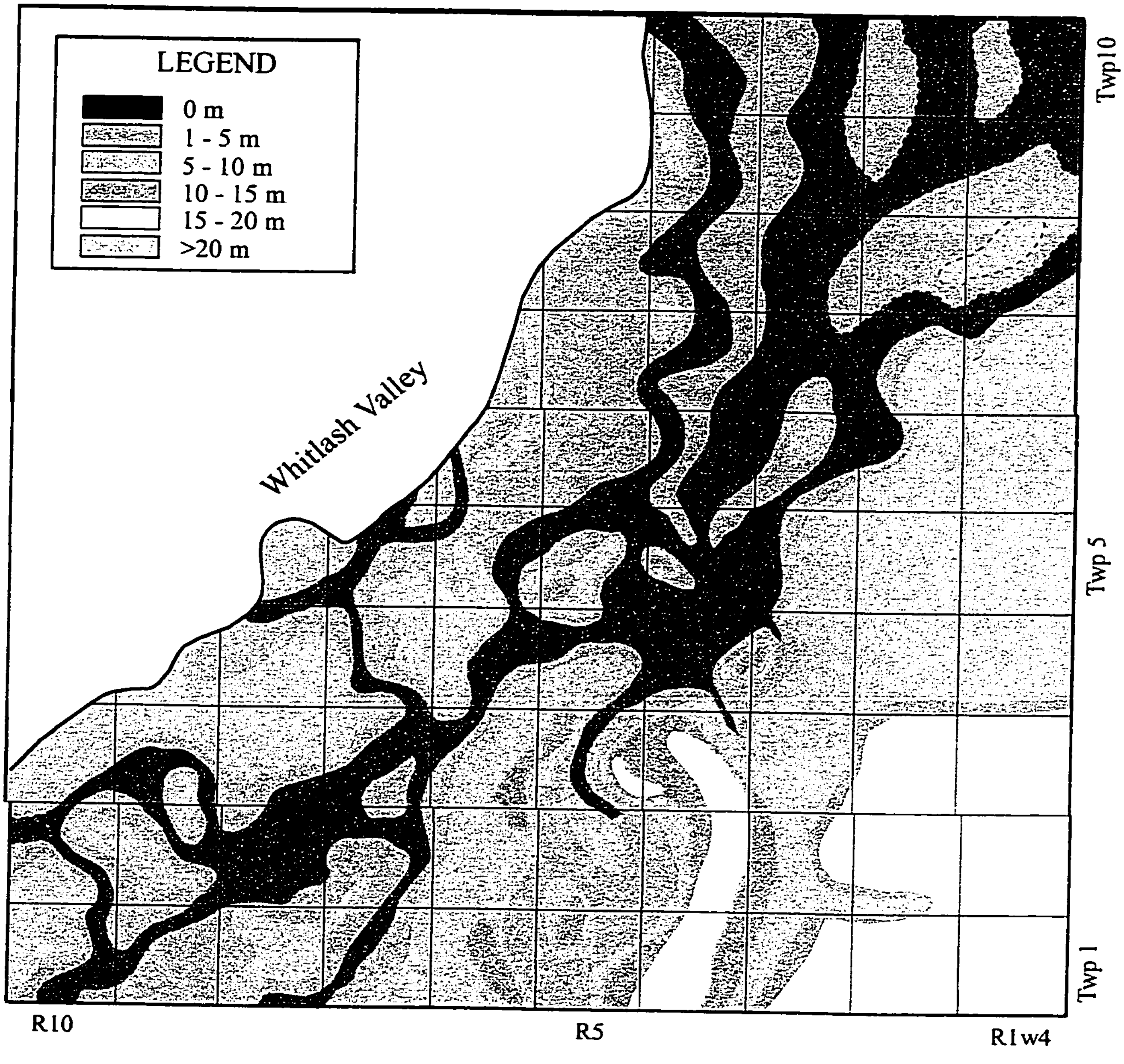
LEGEND
0 m
1 - 5 m
5 - 10 m
10 - 15 m
15 - 20 m
>20 m
Whitlash Valley
Twp10
Twp 5
Twp 1
R10
R5
R1w4

with incision by subaerial fluvial systems. It is therefore interpreted that deposition of the shale member was terminated by a fall of relative sea level that exposed these strata to fluvial erosion.

Sequence 2 – Ribbon Sandstone

Sequence 2 consists of the ribbon sandstone. It unconformably overlies Sequence 1, and in turn is unconformably overlain by the Basal Quartz and other continental deposits of the Mannville Group. Sequence 2 varies considerably in thickness in the study area (Fig. 2.18). Some of this variability is related to the significant paleotopography along the top of Sequence 1 (see discussion above), however, much of it is related to post-depositional erosion created by Aptian fluvial channel (Basal Quartz). An extreme example of this is the Whitlash Valley (Fig. 2.16) where channels have eroded most of the Jurassic succession and locally, incise Mississippian carbonates. In the highland area to the east of the Whitlash Valley, channel incision is less extreme, but nonetheless has removed some, and in some places, all Swift strata. In these areas, therefore, it is difficult to determine the original geometry of Sequence 2 and, in order to do so, data points with thick Basal Quartz sandstone were disregarded.

Lowstand deposits that ideally would overly the sequence boundary are notably absent in the ribbon sandstone. Instead, only a thin, coarse-grained lag (Lithofacies 1) was observed in core, at the base of Sequence 2. The lack of lowstand deposits in southeastern Alberta is attributed to their erosional reworking and removal during the subsequent transgression. The coarse transgressive lag is then overlain by a comparatively thick succession of ribbon sandstone.

Stratal patterns in Sequence 2 vary significantly in character, even locally, and include upward-coarsening, upward-fining, and aggrading successions. Individual stratal packages are generally less than 10 metres thick and significantly, cannot be correlated for more than several kilometres in any direction (Fig. 2.16 and Appendix 4). Similarly, less common sandstone-rich facies (reservoir facies) (Lithofacies 5, 6 and 7), which are

Figure 2.18 Present-day distribution and thickness of the ribbon sandstone showing considerable thickness variation. Some of the variability is related to the significant paleotopography along the top of the shale member; however, much of it is related to post-depositional erosion created by Aptian channel incision (Basal Quartz).


?
?
?
20
20
15
10
5
0
15
10
5
0
15
10
25
5
20
30
15
5
10
15
10
10
0
15
15
5
10
15
25
30
25
25
20
15
R10
R5
R1w4
Twp10
Twp 5
Twp 1

Figure 2.19 Residual isopach map of the ribbon sandstone in which data points with thick Basal Quartz sandstone were disregarded. The remaining data suggest that strata of the ribbon sandstone initially infilled topographic lows incised into the top of the shale member, and subsequently formed a uniformly thick sheet-like deposit across the study area.

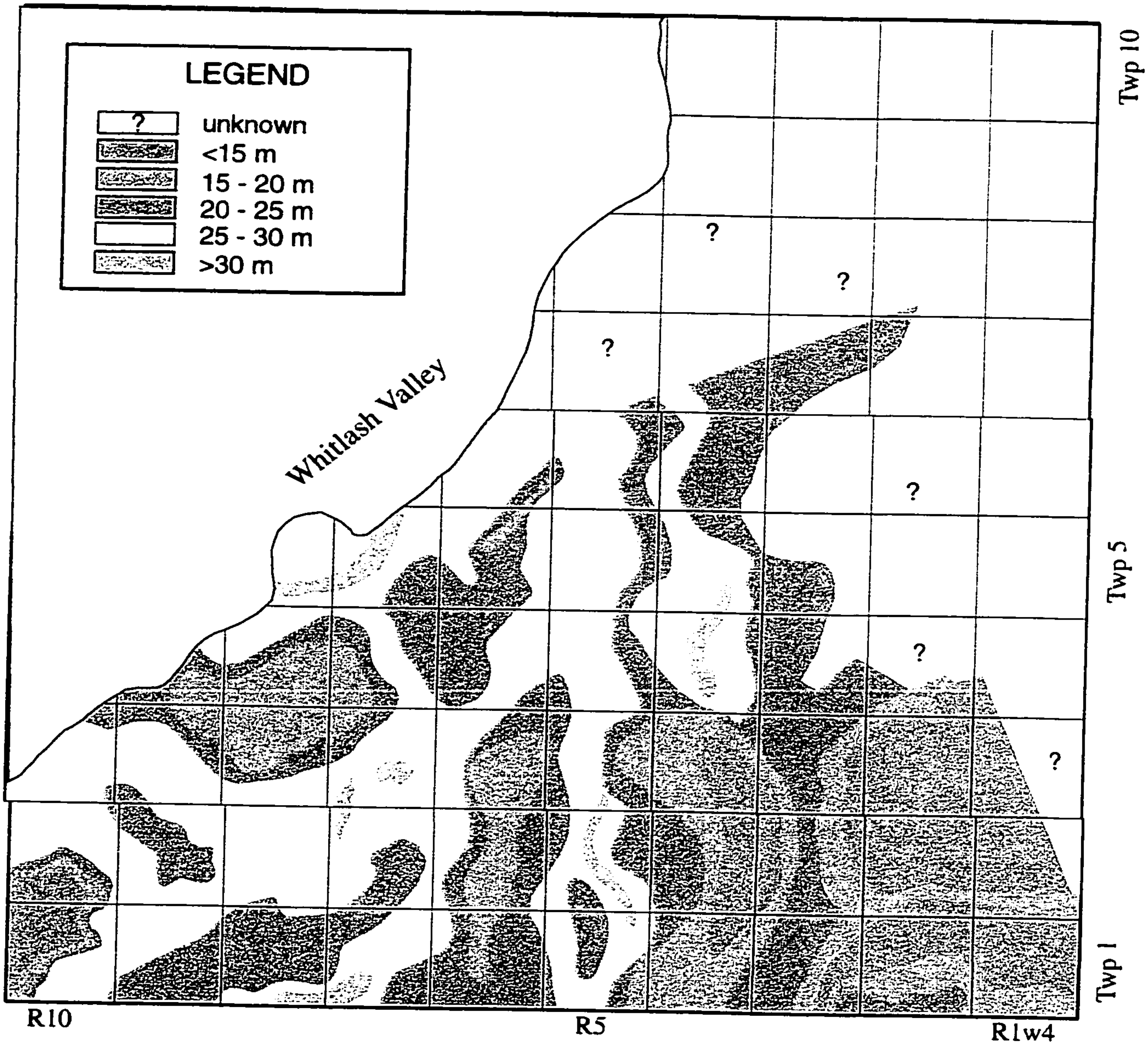
LEGEND
? unknown
<15 m
15 - 20 m
20 - 25 m
25 - 30 m
>30 m
Whitlash Valley
?
Twp 10
Twp 5
Twp 1
R10
R5
R1w4

developed at stratigraphic positions that relate closely to the kind of stratal package in which they occur, are also only locally correlatable. Marine successions that are characterized by upward-changes in grain size or mud content are commonly interpreted to be parasequences (Van Wagoner *et al.*, 1990). Parasequences form under shoaling depositional conditions and are bounded above and below by marine flooding surfaces related to "abrupt" rises of relative sea level, which were not observed for the stratal packages in the ribbon sandstone. Stratal sacking patterns also show variability, and although they are dominantly aggradational, less common retrogradational and progradational stacking patterns were also observed (Fig. 2.13c-e). As pointed out by Posamentier and Allen (1993), different stacking patterns form from differences in the interplay between eustacy, subsidence, sediment supply, and basin physiography. The synchronous development of different kinds of stratal packages (see above) and stacking patterns in the ribbon sandstone suggests that they are unrelated to changes of relative sea level, or related accommodation space. Sediment flux can also be the primary control of stratal architecture. Church and Gawthorpe (1997) documented a wide range of coeval stacking patterns within the same systems tract in strata of the Late Numerian of northern England and attributed this variability to changes in sediment supply related to varying sediment transport pathways. In strata of the ribbon sandstone, however, stratal packages and stacking patterns are unlikely to have been formed as a result of varying sediment transport pathways because bed-load transport was controlled by low-energy combined flows with a significant, albeit weak unidirectional component related to microtidal currents, which would have been equally distributed within the strait. Their development, instead, is interpreted to be the result of the spatial and temporal variability in patterns of sediment deposition and related formation and lateral migration of positive topographical elements on the sea bed, termed (subtidal) sand banks (see next).

Because stratal architecture of the Swift Formation is largely unrelated to changes of relative sea level, stratigraphic techniques, like sequence stratigraphy, provide little aid in stratal correlation. Alternatively, slice techniques proved useful in delineating the lateral and vertical (spatial and temporal) distribution of sandstone-rich lithofacies. Slice maps with a five-metre sampling interval proved to be the most effective, and identified a large number of variably shaped, discontinuous small pods of sandstone, or sand banks, that diminish in number and size stratigraphically upwards (Fig. 2.20 and Appendix 5). Where well developed, banks are up to 8 m thick and of the order of 25 km^2 (Fig 2.20a). Those that formed early during Sequence 2, and are found within the first 15 metres above the Rierdon Formation (the datum), have a moderate length:width ratio because their lateral development was confined by north-east trending lowstand channels (Fig. 2.20b). However, once these channels were infilled by ribbon sandstone sediment, developing sand banks could migrate both laterally and longitudinally and, as a result, sand banks that formed during late Sequence 2 time (15 to 30 meters above the Rierdon Formation) have a low length:width ratio (Fig. 2.20c). It is important note that these interpreted sand bank morphologies are based mostly on geophysical log interpretation. Because of the abundance of mudstone throughout the entire Swift succession, even in the sandstone-rich horizons, the profile of some geophysical logs have been profoundly affected, especially the gamma-ray log. As a consequence gamma-ray values in sandstone-rich horizons (locally ground-truthed with core) are generally >45 API units. In contrast interbank deposits have only slightly higher API values, generally taken to be ≥75 API, which makes differentiating interbank from bank strata on geophysical logs difficult, which in turn can profoundly affect the interpreted shape of the sand bank buildup. Sand banks within the ribbon sandstone show no discernible preferred spatial distribution across the study area other than the early lateral confinement within lowstand channels. Each bank is interpreted to have become initiated on the sea bed and built upward and laterally by the preferential deposition of sand-rich strata (lithofacies 5, 6, 7). At the same time mud-rich strata (Lithofacies 4) continued to accumulate in the interbank areas, but at a slower rate. In addition to up-building, sand banks also migrated laterally; the trajectory of migration was determined by the resultant of local rates of lateral bank migration and bed aggradation. Significantly, the shape of ribbon sandstone banks is notably different from elongated subtidal sand banks, or ridges, observed/interpreted in both the modern and the ancient parts of the wave- and tide-dominated marine environments. This difference is interpreted to reflect the markedly different physical regime under which the Swift banks existed: a bed-load sediment starved, low-energy combined-flow regime. Under these

Figure 2.20 Detailed diagrams of sand banks in the ribbon sandstone.

(A) East-West and North-South cross sections showing spatial and temporal discontinuity of sandstone-rich facies in the ribbon sandstone. Line of section is shown in both B and C.

(B & C) Stacked five metre slice maps showing the spatial and temporal distribution of sandstone rich facies in the ribbon sandstone. Note the moderate length:width ratio of sand banks that developed early during Sequence 2 (A) versus the low length ratio of later formed sand banks (B). This change in sand bank morphology is related to a change from development in laterally confining lowstand channels to development on a sea floor marked by negligible topography, where the banks could migrate both laterally and longitudinally.

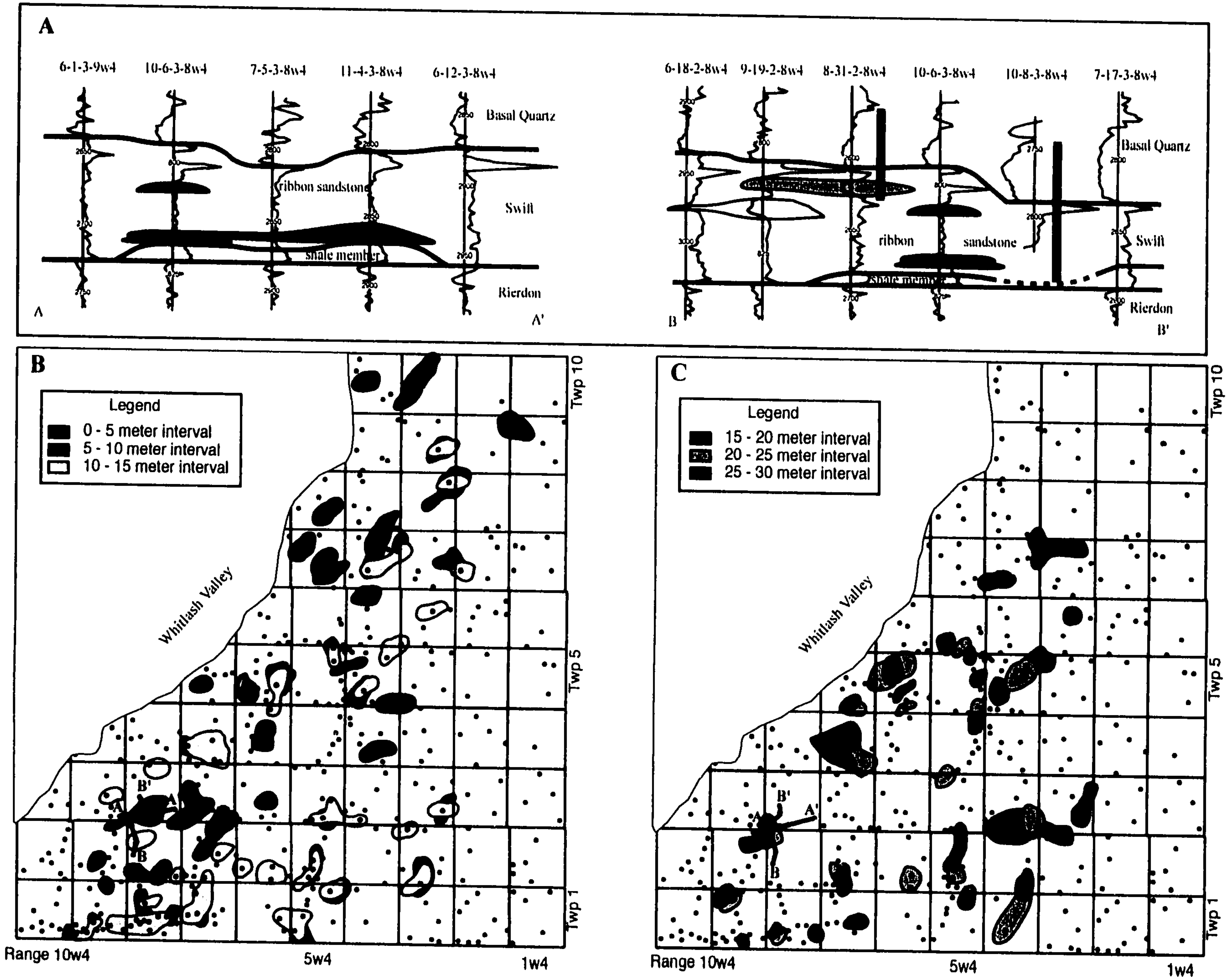
A
6-1-3-9w4
10-6-3-8w4
7-5-3-8w4
11-4-3-8w4
6-12-3-8w4
Basal Quartz
ribbon sandstone
Swift
shale member
Rierdon
A
A'
6-18-2-8w4
9-19-2-8w4
8-31-2-8w4
10-6-3-8w4
10-8-3-8w4
7-17-3-8w4
Basal Quartz
ribbon
sandstone
Swift
shale member
Rierdon
B
B'
B
Legend
0 - 5 meter interval
5 - 10 meter interval
10 - 15 meter interval
Whitlash Valley
Twp 10
Twp 5
Twp 1
Range 10w4
5w4
1w4
C
Legend
15 - 20 meter interval
20 - 25 meter interval
25 - 30 meter interval
Whitlash Valley
Twp 10
Twp 5
Twp 1
Range 10w4
5w4
1w4

conditions the preferential direction of bed-load sediment transport and subsequent deposition was determined by the relative strength of the variable speed, but directionally consistent, low-energy tidal currents and the wind-generated oscillatory currents, which most probably varied more widely in both speed and direction (at times the oscillatory current may have been oriented at a very high-angle to the tidal current). As a result, sand bank depositional history, and consequent morphology, was governed principally by deposition of bed-load sediment during short-term sedimentation events that were not always directionally consistent, for instance when the oscillatory component dominated.

Depositional History

The Oxfordian Swift Formation in southeastern Alberta comprises two unconformably bounded sequences. The shale member was unconformably deposited over the Bathonian Rierdon Formation during the fourth of five Jurassic marine transgressions over the Western Interior of North America. The contact between the two units is not only characterized by a marked difference in lithologies from calcareous, fossiliferous shales to clastic shales but also by a thin basal chert-pebble/belemnite conglomerate (Cobban, 1945; Brenner and Davies; 1974; Hayes, 1983) interpreted to be an areally extensive transgressive lag. The shale member comprises up to four parasequences that show a subtle upward-fining stacking pattern, which were deposited in overall deepening, fully marine conditions. Within this basin, high-energy, long period waves were periodically developed and deposited hummocky-cross-stratified siltstone. The basin was therefore not physically nor chemically restricted during this time as opposed to during Sequence 2 time. Sequence 1 is interpreted to be composed entirely of sediments deposited during the transgressive system tract, firstly, because it is composed of a retrogradational parasequence set, which is characteristic of the transgressive systems tract and secondly, because a maximum flooding surface that forms the base of the highstand was not observed in strata of Sequence 1. Maximum flooding surfaces are commonly marked by condensed sections and can be recognized on geophysical logs as a marker bed or in core as thin, highly fossiliferous, phosphatic and glauconitic strata (Cant, 1992; Amorosi, 1995). These attributes, however, were not observed in the shale member.

Deposition of Sequence 1 was terminated during the late transgressive systems tract by a fall of relative sea level that exposed these strata to fluvial erosion. The mechanisms responsible for this change are unknown, but are most probably related to renewed tectonic activity and vertical uplift along the Sweetgrass Arch. During the subsequent lowstand, multiple, northeast-southwest trending meandering channels incised into Sequence 1 as they flowed toward the new paleoshoreline. The exact location of the lowstand shoreline, however, is unknown, either because it lies beyond the study area, was eroded by wave ravinement processes during the following rise in relative sea level, or eroded by Lower Cretaceous channel incision. In the depositional model proposed by Brenner and Davies (1974), channelized sandstones with conglomeratic bases were documented to have incised into strata equivalent to the shale member landward of the depocenter, near the Belt Island Trend in southwestern Montana. During lowstand, these channels would also have incised into the shale member as they made their way to a new paleoshoreline somewhere in the northeast. Imlay (1980) also documented a regression during the Early Middle Oxfordian, which was followed by a fifth Jurassic marine transgression that is recorded by a limy, locally oolitic ripple-marked sandstone in southern Wyoming (Windy Hill Sandstone Member of the Sundance Formation). It is proposed here that the unconformity observed in Wyoming can be traced northward into southeastern Alberta at the top of the shale member and that the Windy Hill Sandstone is the lateral equivalent of the ribbon sandstone. Despite the presence of lowstand channels, lowstand deposits were not observed in core and, even though they may be preserved, they most probably are rare. Wave ravinement processes are interpreted to have thoroughly reworked both lowstand deposits and the underlying shale member, leaving only a lag consisting of few scattered chert pebbles. At the same time, the channels were most probably widened.

With transgression came significant changes in physical and chemical conditions in the study area. These changes are related to modifications in basin configuration and the development of a strait, which likely formed as a result of vertical tectonic movement along the Sweetgrass Arch. Within this newly configured basin, long-period oscillatory waves no longer developed, and combined flows, with a weak but significant tidal current component and a low-energy oscillatory component related to storm waves, became the principal mechanism for sediment transport. Furthermore, brackish waters prevailed as a result of abundant freshwater discharge into the strait from rivers in nearby highlands to the south (Belt Island trend) and north (craton). It is important to note that during deposition of Sequence 2, the basin in the study area was mud dominated and starved of sand-size sediment, sedimentation rates were low, and thick and areally extensive sand-rich deposits did not accumulate. Small, irregular-shaped sand banks were deposited locally as a result of spatial and temporal variations in patterns of sediment deposition and lateral migration of the banks. The net result of the spatial variability in sand deposition is the formation of a number of different stratal patterns (upward-coarsening, -fining, -aggrading), even locally. These discrete stratal patterns are notoriously laterally discontinuous, and furthermore stack vertically to form equally variable stratal assemblages that consist of aggrading, prograding or retrograding stacking patterns, again, even locally. Because of variable stacking patterns, the absence of biostratigraphic markers in the ribbon sandstone, and post-Oxfordian erosion and chemical alteration (pedogenesis), the assignment of systems tracts to Sequence 2 is difficult. Despite these complications, the ribbon sandstone in the study area appears to be dominated by transgressive deposits because they 1) overlie an unconformity 2) are dominantly aggradational and do not show overall progradation that is typical of highstand deposits and 3) sand content appears to diminish stratigraphically upwards, suggesting overall deepening conditions, although this may be partially a function of Lower Cretaceous erosion. The absence of highstand deposits may be attributed to a forced regression brought on by renewed tectonic uplift in the study area, and/or to post-depositional erosion or pedogenic alteration of highstand deposits or simply because highstand deposits did not develop because of lower sediment flux.

Diagenetic History

Following the withdrawal of the Oxfordian Sea, a soil profile developed in strata of the Swift Formation, which modified their original chemistry and texture. As a consequence, the geophysical log signatures in the altered ribbon sandstone are not reliable for correlation purposes. Within the Swift profile, only the Bt and C horizons are preserved. The absence of organic material indicates that the Jurassic soil was mildly oxidizing and the abundant illuviation cutans (clay skins) that occur in the Bt horizon suggest that it was also seasonably dry. Thin volcanic ash layers are interpreted to have been deposited above Swift paleosols during the Barremian. They were subsequently chemically altered, during which time their uranium content was leached and mobilized by downward percolating meteoric waters. Upon encountering organic material in the dark mudstone of the unaltered ribbon sandstone, the uranium was adsorbed by the dead organic matter, forming a marker horizon on the gamma ray log. This horizon, however, only indicates an ancient redox front and depth of pedogenic alteration and, as opposed to hot shales, is without chronostratigraphic significance.

Conclusions

The Swift Formation is characterized by two unconformably bounded sequences. Sequence 1 consists of the shale member and was deposited in a low energy environment where high-energy, long-period oscillatory waves readily developed during storms and deposited hummocky cross-beds. The shale member consists of a retrogradational parasequence set deposited during transgression. The shale member, in turn, is unconformably overlain by Sequence 2, which consists of the ribbon sandstone. The contact is characterized by deep scours (< 15 metres) and is overlain by a thin, matrix-supported chert-pebble conglomerate interpreted to be a regionally extensive transgressive lag. Lowstand deposits were not observed in core but may be due to the lack of core in this interval. Locally, lowstand deposits may be preserved but are nevertheless rare. During transgression, erosion by waves thoroughly reworked both lowstand and underlying shale member strata, and resulted in the widening of lowstand channels. The ribbon sandstone is interpreted to consist mostly of mud-dominated transgressive deposits emplaced in a physically and chemically restricted strait that connected the Alberta Trough and the Williston Basin. The strait likely developed as a result of renewed uplift along the Sweetgrass Arch. Long-period oscillatory waves did not develop in this area and brackish waters prevailed. Bed-load sediment, which consisted mostly of fine and very fine sand, was transported principally by combined flows composed of a low speed tidal current and a low energy oscillatory component related to storms. Although tidal currents were probably amplified as they were funneled through the wide strait, they were still beneath the threshold velocity for even very fine sand. Only with the input of an oscillatory flow component, albeit at no time strong, did bed-load transport occur. Differential deposition of bed-load sediment formed and temporarily maintained many small, irregularly shaped sand banks in the study area. Consequently, sandier facies are laterally discontinuous and individual stratal packages vary in character (i.e. aggrading, prograding or retrograding). The stratal architecture, therefore, did not form in response to changes of relative sea level but instead to spatial and temporal variations in the patterns of deposition of sand-rich strata and the resultant local rates of lateral bank migration and bed aggradation.

Chapter 3

Nature and origin of an areally extensive radioactive marker horizon in the Swift Formation, southeastern Alberta

Introduction

Radioactive layers in a stratigraphic succession form easily identifiable marker horizons. In many cases these horizons coincide with important bounding surfaces, and where areally extensive form a useful stratigraphic reference horizon, or datum. For example, radioactive shales, commonly termed hot shales, are thin hemipelagic or pelagic sediments that accumulated very slowly on the shelf. These sediments form condensed sections, and commonly are interpreted to be associated with regional marine transgression; their tops mark the maximum flooding surface and the top of the transgressive systems tract (Loutit *et al.*, 1988). Other studies, however, have suggested that not all condensed sections form in deep water nor do they coincide with the maximum flooding surface (Leckie *et al.*, 1990). Nevertheless, irrespective of origin, condensed sections form during episodes of rising relative sea level and form readily recognizable horizons commonly used as stratigraphic data.

Radioactive marker horizons have also been shown to coincide with unconformities. During lowstand (fall of relative sea level), channels incise down-dip and transport heavy accessory minerals basinward. Some of these minerals are radioactive (e.g. zircons, uraninite) and form placers near the base of the channel fill. Even though this type of marker bed is typically not laterally extensive it nonetheless highlights the uncomformity, especially where the incised valley is infilled by transgressive lower-shoreface strata or marine mudstone.

This chapter provides a detailed description and interpretation of a radioactive horizon in the subsurface Upper Jurassic Swift Formation in southeastern Alberta (Fig. 3.1). The origin of this horizon, however, is interpreted to be unrelated to changes of relative sea

Figure 3.1. Map illustrating the location of the study area in southeastern Alberta and location of samples for the geochemical analyses: A (10-36-5-5w4) and B (6-19-3-9w4). Small dots indicate individual wells used in the study, also the line of cross-section (A-A') illustrated in Figure 4 is shown. The study area is bounded to the west by the Saskatchewan-Alberta border, the south by the Canada-U.S. border, the west by the deeply incised Lower Cretaceous Whitlash paleovalley, and to the north by Township 10.

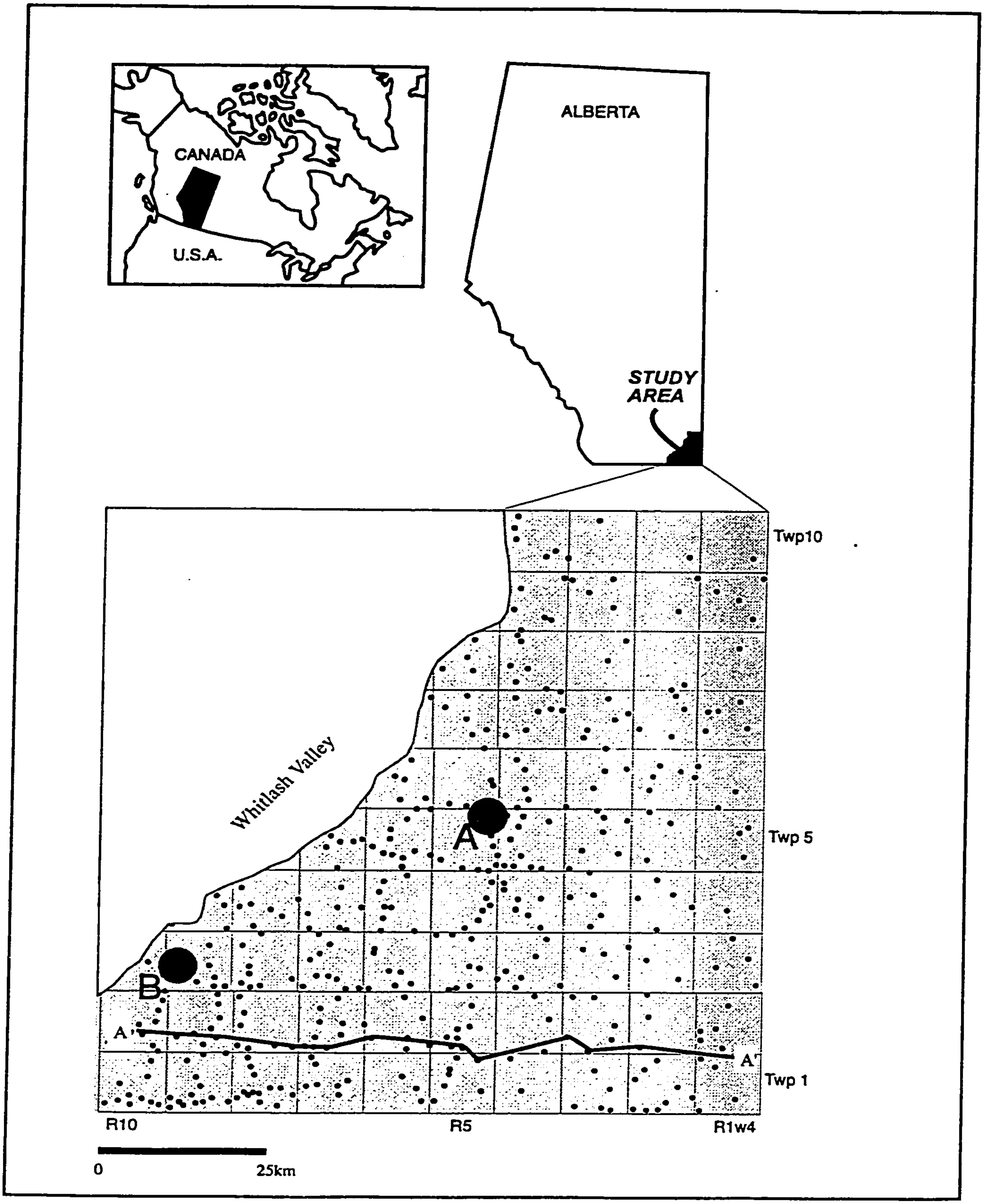
CANADA
U.S.A.
ALBERTA
STUDY AREA
Whitlash Valley
A
B
A
A'
Twp10
Twp 5
Twp 1
R10
R5
R1w4
0
25km

level, condensed sections, or erosional unconformities, but instead to pedogenic processes during subaerial exposure. Furthermore, this pedogenic horizon formed at variable depth beneath the paleoland surface, even locally, and therefore would represent an unsuitable datum for stratigraphic correlation.

Geological Setting and Local Stratigraphy of the Swift Formation

In southeastern Alberta, the subsurface Upper Jurassic (Oxfordian) Swift Formation is the youngest formation of the Jurassic Ellis Group. It unconformably overlies Bathonian calcareous to mixed carbonate-siliciclastic mudstone of the Rierdon Formation (Christopher, 1974) and in turn, is unconformably overlain by Lower Cretaceous fluvial sandstone and floodplain mudstone of the Basal Quartz (Lower Mannville Group) (Fig. 3.2). The Swift was deposited in the ancestral intracratonic Williston Basin and records the transition from a passive continental margin to a foreland basin during the early stages of the Columbian-Nevadan Orogeny (Leckie and Smith, 1992). Tectonic thickening and related lithospheric flexure formed a narrow, northwest-southeast elongated foreland basin, a portion of which is termed the Alberta Trough. During the Late Jurassic, southward transgressing marine conditions inundated the trough, and eventually flooded parts of the Williston Basin by way of an east-west-trending strait that had breached the crest of the Sweetgrass Arch (Imlay, 1980) -- the study area occurs in the north-central part of the strait.

The study area is located in southeastern Alberta, east of the Whitlash paleovalley (Cretaceous) and comprises the area between Townships 1 to 10 and from Ranges 1 to 10 W4 (Fig. 3.1). In this area the Swift Formation is interpreted to consist of two unconformably bounded sequences (for details see Chapter 2). The shale member is characterized by a thin basal pebble layer, overlain by black, organic-rich shale with minor interbeds of hummocky cross-stratified siltstone. Trace fossils form a deep shelf assemblage dominated by *Helminthopsis* in mudstone strata and *Planolites* in siltstone. The shale member is then unconformably overlain by the ribbon sandstone, a microtidally influenced, bed-load-sediment starved, mudstone-dominated succession. Trace fossils include an assemblage of small *Planolites*, *Teichichnus*, *Cylindrichnus*, *Chondrites*, *Skolithos* and inclined *Arenicolites*

Figure 3.2. Stratigraphic nomenclature of Jurassic and Lower Cretaceous strata in southeastern Alberta. Although the Upper Jurassic Morrison Formation unconformably overlies the Swift Formation in some parts of southeastern Alberta, it is absent in the study area. Instead, Swift strata are unconformably overlain by sandstone and mudstone of the Lower Cretaceous Basal Quartz Formation (modified from Leckie and Smith, 1992).

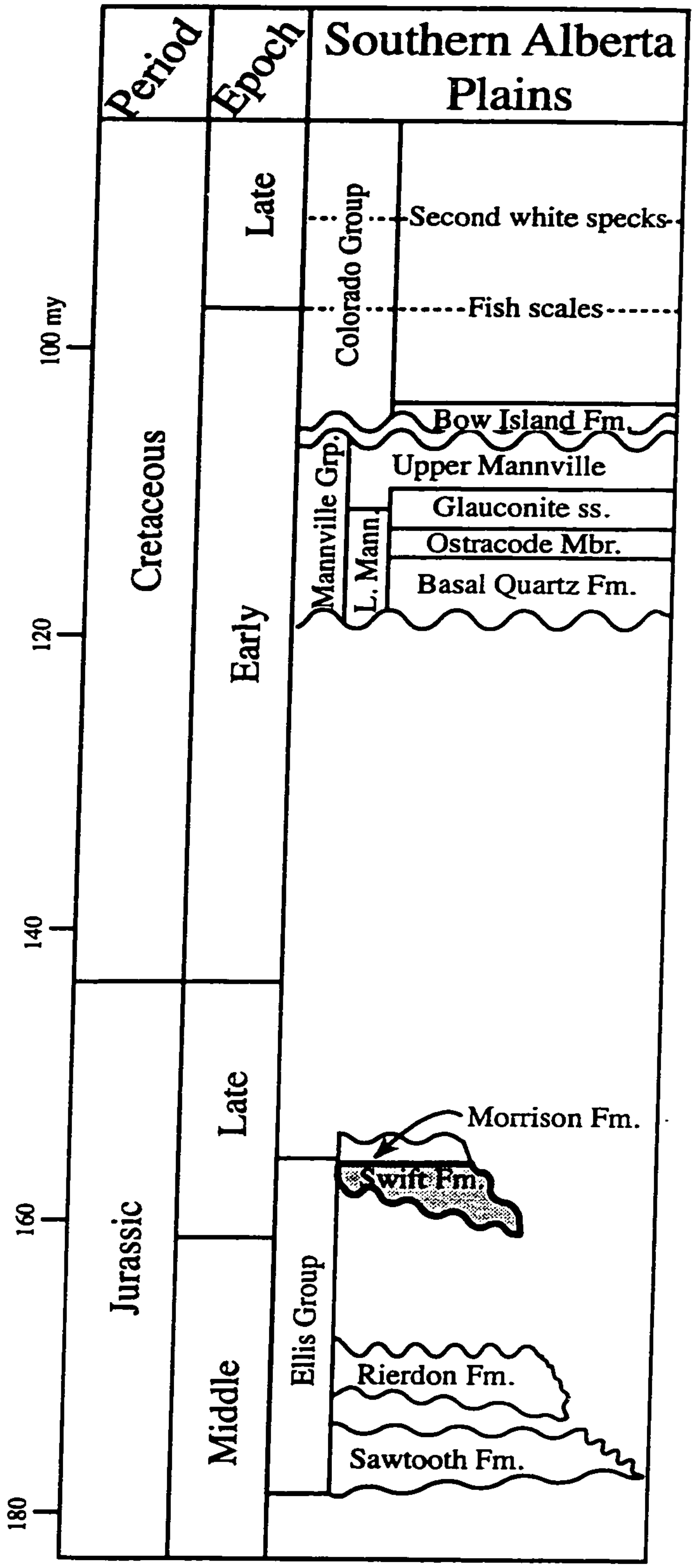
Period
Epoch
Southern Alberta Plains
Cretaceous
Jurassic
Late
Early
Late
Middle
100 my
120
140
160
180
Colorado Group
Second white specks
Fish scales
Bow Island Fm.
Mannville Grp.
Upper Mannville
L. Mann.
Glauconite ss.
Ostracode Mbr.
Basal Quartz Fm.
Morrison Fm.
Swift Fm.
Ellis Group
Rierdon Fm.
Sawtooth Fm.

burrows. Both laterally and vertically, the ribbon sandstone consists of stacked, several-meter-thick stratal units that coarsen upward, fine upward, or remain unchanged upward. This lateral and vertical variability is interpreted to be have been controlled by spatial and temporal variations in bed-load sediment depositions that resulted in the initiation, build-up, and lateral migration of irregular shaped, low-energy combined flow sand banks. Also of note in the ribbon sandstone is the common occurrence of a single thin (< 2 m) interval characterized by anomalously high gamma-ray counts (as detected on gamma-ray geophysical logs). This interval, which occurs generally in the upper part of the succession, coincides also with a distinctive change from dark-colored ribbon sandstone to bleached white ribbon sandstone, and it is this interval that is the focus of this chapter.

The top of the Swift Formation is marked by an unconformity that represents a hiatus of approximately 35 my (Gradstein and Ogg, 1996). During this time strata of the Swift were subaerially exposed and profoundly altered (see below). Later, during the Aptian (Early Cretaceous), significant erosion by stream downcutting and valley incision occurred (Hayes, 1983) and extensively eroded exposed Swift strata. The present-day distribution of the Swift Formation, therefore, consists only of an erosional topography preserved in Early Cretaceous highland areas.

Methodology

Samples for geochemical analysis were collected across the high gamma-ray interval and from only two wells. X-ray fluorescence was performed on 14 samples collected from a 4 metre interval spanning the color change horizon in the New Jordan *et al.* well (10-36-5-5w4) in the Manyberries area (Fig. 3.1). This well was selected because the log 'gamma kick' is well developed and core was easily calibrated to the geophysical well log signature. Crushed bulk rock samples were heated at 100°C for approximately 12 hours to remove any unbound water. Samples were subsequently combusted at 500° C to remove all organic matter before being analysed using XRF. Remaining fresh samples were analyzed for organic matter content by elemental analysis. Samples were first crushed and then reacted with 10% hydrochloric acid at 80°C for 2 hours to eliminate inorganic carbon present principally as calcite cement and sphaerosiderite. Samples were subsequently analysed in a NC 2500 elemental analyser. Carbon isotopes values were obtained from sphaerosiderite sampled from the ribbon sandstone in the 10-36-5-5w4 (1170 to 1177 m) well and the 6-19-3-9w4 (845 m) well (Fig. 3.1). Samples were crushed and reacted with phosphoric acid for 2 hours at 50° C, after which gases were evacuated, to eliminate CO_2 produced from dissolved calcite or dolomite. Reactions were continued for 36 hours at 50° C and gases were subsequently collected and analysed for carbon isotopes.

Stratigraphic Position of the Radioactive Marker Bed

The radioactive marker horizon in the Swift Formation occurs throughout most of southeastern Alberta except where eroded by younger deeply incised Lower Cretaceous channel fills. Characterized by an abrupt rightward deflection on the gamma ray log, it occurs generally within the upper half of the ribbon sandstone (Fig. 3.3B). The deflection extends over a thin stratigraphic interval, commonly less than 2 metres thick, and has variable intensity, ranging from slightly higher than background ribbon sandstone (~100 API) to anomalously high gamma counts of up to 225 API units. This deflection is not observed in all wells, but does occur in over 75% of the ~450 wells in which ribbon sandstone is present (a total of 600 wells were used in the study, but Cretaceous channel incision has completely eroded ribbon sandstone in ~150 wells). Above the marker horizon, the gamma ray curve commonly shows a gradual decrease in API, suggesting the occurrence of an upward-sandier (less mudstone) trend (Fig. 3.3B). However, upward changes in mud content or sediment grain size were **not** observed in core (Fig. 3.3C), and the trend is interpreted to be the result of post-depositional alteration (see below). The gamma kick coincides also with an abrupt to gradual upward change in color from dark to light mudstone interlaminae (Fig. 3.3A). As suggested earlier by Hayes (1983), the color change is related to a change in the abundance of organic matter from high in dark mudstone to absent in light mudstone. For example, in the course of a standard microfossil analysis, which were found to be absent in Swift strata, small dark resinous wood fragments were observed to be common in dark mudstone but absent in light-colored mudstone (C. Henderson, pers. comm., 1996). Interestingly, measured weight

Figure 3. Composite diagram depicting the main characteristics and geochemical attributes of the radioactive marker horizon in the Swift Formation (columns A-E). In core, the radioactive horizon coincides with an abrupt to slightly gradational (~ 10 cm) upward change in color from dark to light colored mudstone interbeds (A; arrow), which is related to an upward-change in the abundance of organic material (E). Generally, no other changes in lithology occur across this horizon (C). On geophysical well logs, the radioactive horizon (B; arrow) is shown to be typically thicker, generally of the order of 2 m thick. Intensity varies from slightly higher than background values to in excess of 225 API units. Above the radioactive marker horizon, the gamma ray logs commonly show an upward decrease in radioactivity. This is related to the removal of highly mobile radioactive K^{40} during pedogenesis. Other indicators of pedogenesis include conspicuous concave-upward laminated argillans (D, top photo) and sphaerosiderite nodules (D, lower photo). In the latter photo, note the discontinuous concentric layer of pyrite (dark band) within the siderite nodule. This suggests fluctuating Eh conditions during siderite precipitation within the paleosol horizon.

10-36-5-5w4

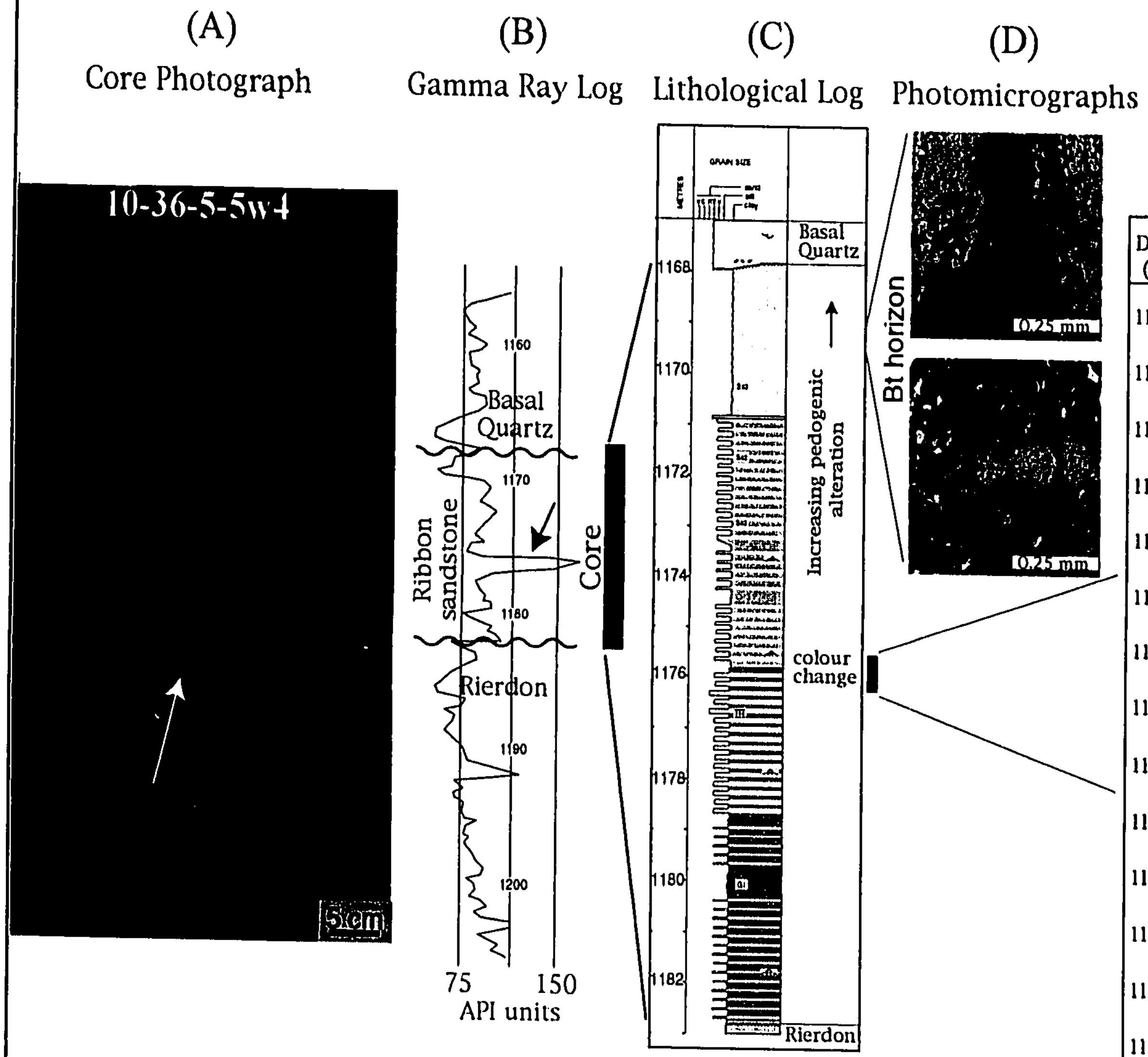

(E)
Geochemistry

Depth (m)	Organic C %	K2O %	Fe2O3 %	U ppm	$\delta^{13}C_{PDB}$
1170	0.21	0.407	0.692	0	
1172.25	0.29	0.757	3.962	1.38	-8.31
1173.5	0.19	0.982	2.848	0	-13.23
1174.75	0.23	0.892	1.684	0	-12.4
1175.5	0.29	1.437	1.419	0	
1175.8	0.34	1.259	1.405	0	
1175.95	3.95	1.375	1.018	23.14	
1176.05	1.91	1.327	1.066	30.5	
1176.1	1.59	1.480	1.742	14.45	
1176.3	1.92	1.570	1.626	10.32	
1176.5	2.18	1.687	1.547	6.2	
1176.7	2.47	1.920	1.379	1.15	
1176.9.	1.89	1.943	1.241	2.27	
1177.1	1.74	2.071	1.051	0	

* **well 6-19-3-9w4** 845m below the surface & 10 cm below the BQ	$\delta^{13}C_{PDB}$ -23.00

loss following combustion was similar for dark- and light-colored mudstones (average 5.8%), despite the supposed greater abundance of organic carbon content in dark colored mudstone. This apparent inconsistency is most probably because of high weight loss in light-colored mudstone related to the dehydration of clay minerals and partial combustion of carbonate minerals, both of which are common in these strata. In order to accurately determine the presence or absence of organic material in light- and dark-colored strata, therefore, samples were analyzed by an elemental analyser. These data show that organic carbon content is approximately an order of magnitude higher in dark- compared to light-colored mudstone (average 2% and 0.25%, respectively) (Fig. 3.3E). Note that because the instrument's precision for measuring CO_2 is ± 0.3%, organic carbon values in the light ribbon sandstone may be as high as 0.6%, but are more probably closer to 0%.

As mentioned above, Hayes (1983) suggested that the color change was related to an upward decrease in organic content. This, in turn, was interpreted to be related to changes in the chemistry of the Oxfordian sea from a non-oxidizing environment where organic material was preserved, to more-oxidizing conditions during deposition of the light-colored ribbon sandstone. However, changes in physical or biogenic sedimentary structures, suggestive of changes in physical and ecological conditions, were not observed across the color change. Moreover, the color change occurs at different stratigraphic levels throughout the study area (Fig. 3.4), suggesting that it is unrelated to changes in depositional conditions. Stratigraphically upwards from the color change, the interstratification that typifies the light ribbon sandstone becomes progressively more difficult to discern and gradually merges into massive-appearing, beige strata in which primary sedimentary structures are no longer distinguishable (Figs. 3.3A,C). These uppermost, massive strata are generally less than 2 metres thick and contain common small (< 1 mm) sphaerosiderite nodules.

Evidence for Pedogenic Alteration

The origin of the radioactive horizon and the overlying succession of light ribbon sandstone are interpreted to be the result of post-depositional pedogenic alteration and related leaching processes. Fossil soils, or paleosols, are relatively common in the geologic record

Figure 3.4. Stratigraphic cross-section using gamma-ray and resistivity geophysical well logs (see Fig. 3.1 for location of cross-section). Note the variable depth of the radioactive marker horizon, which is interpreted to be related to permeability heterogeneities in the ribbon sandstone and its influence on pedogenic processes (see text for details).

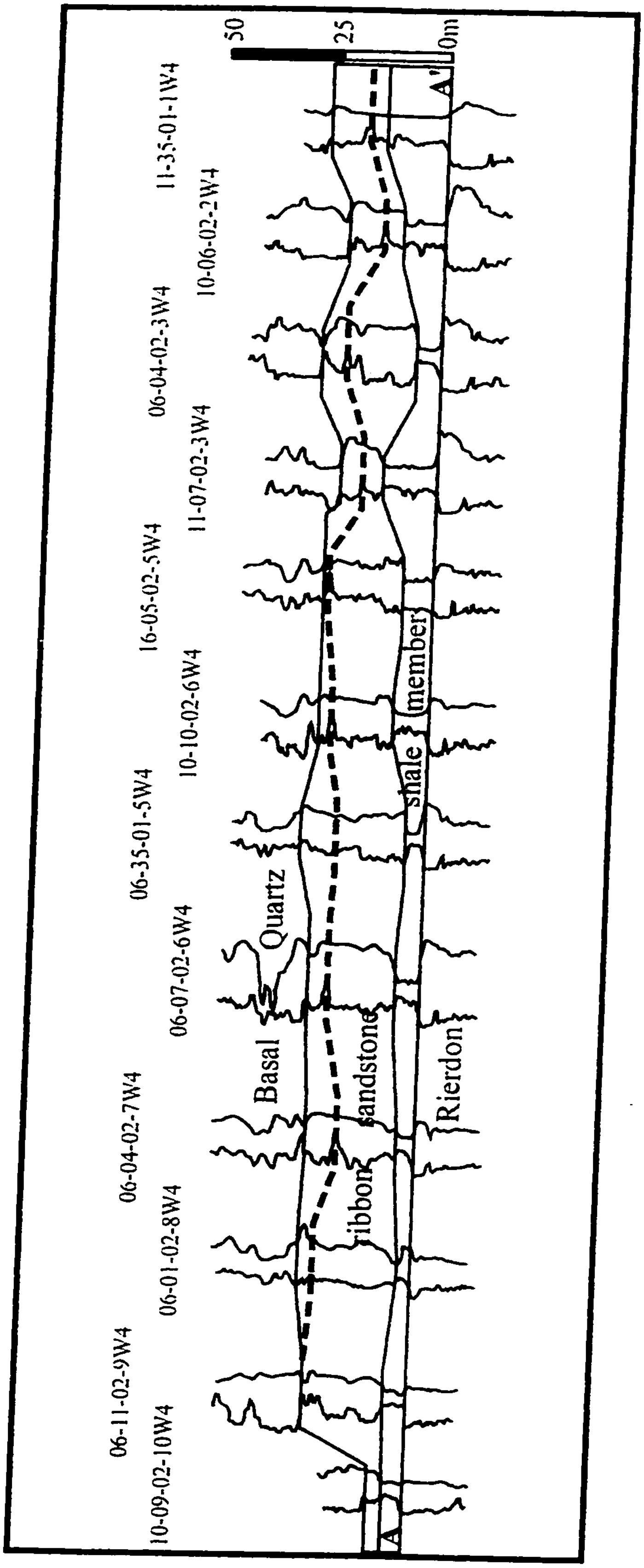
10-09-02-10W4
06-11-02-9W4
06-01-02-8W4
06-04-02-7W4
06-07-02-6W4
06-35-01-5W4
10-10-02-6W4
16-05-02-5W4
11-07-02-3W4
06-04-02-3W4
10-06-02-2W4
11-35-01-1W4
Basal Quartz
ribbon sandstone
Rierdon shale member
A
A'
50
25
0m

and their tops commonly coincide with unconformities (Retallack, 1990). However not all unconformity surfaces are underlain by paleosols. In many cases, the paleosol has been eroded completely by later fluvial or wave/tide ravinement processes. In addition, paleosols are not always easy to recognize. During burial, paleosols can be modified significantly by groundwater flowing through a porous overburden (Pavich and Obermeier, 1985), which in turn commonly results in significant alteration and mineralization in the underlying soil layer (Retallack, 1983) and, as a consequence, many diagnostic soil features, such as soil horizons and soil structures become masked. As discussed earlier, the top of the ribbon sandstone, which in the study area marks the top of the Swift Formation, represents a major unconformity surface and a hiatus of approximately 35 my. It would seem reasonable, therefore, that a well developed paleosol would have formed across the top of the Swift Formation. However, because of extensive Lower Cretaceous fluvial erosion, evidence of pedogenesis has been locally removed. Moreover, distinguishing between Lower Cretaceous and Swift paleosols is generally difficult, although Lower Cretaceous paleosols are generally coarser grained, and darker because of more abundant macroscopic coalified material.

Rootlets are notably absent from the ribbon sandstone, although rare, equivocal root traces were observed in the beige "massive" strata in the uppermost part of the succession. Furthermore, well developed, soil horizons were not recognized in core. Stratigraphically downwards an idealized soil profile consists of 1) a surficial rooted, organic-rich A horizon, 2) bleached, organic- and clay-poor E horizon, 3) a B horizon that is either dark in color because of organic or clay enrichment or light in color because of intense weathering, 4) carbonate-rich K horizon, and 5) the lowermost C horizon, consisting of mildly oxidized, slightly more weathered rock than unaltered bedrock (Retallack, 1990). In the case of the Swift, only the B and C horizons of the paleosol profile are interpreted to be present. The A horizon was not preserved, most probably because of Early Cretaceous erosion. Evidence of a B-horizon, on the other hand, is suggested by abundant microscopic laminated argillans present in the uppermost part of the ribbon sandstone (Fig. 3.3D). Argillans, or clay skins, form by elluviation of fine-grained sediment, principally silt and/or mud, into cracks between soil peds (Retallack, 1990). Generally, this occurs in the clayey B horizon (Bt horizon) of a soil profile, and can be up to 2 m thick (Retallack, 1990). The beige, massive-appearing strata in the upper part of the ribbon sandstone, therefore, is interpreted to represent the preserved Bt-horizon of an ancient soil profile. The massive appearance most likely developed because of compaction during burial. Similarly, locally developed slickensides probably formed by the abrasive interaction of adjacent soil peds during burial. The discernible interstratified light ribbon sandstone gradationally underlies the Bt horizon. Like the Bt horizon, it too lacks organic material, which indicates mild oxidation and is interpreted to represent the soil C horizon. The C horizon, in turn, is underlain by unaltered dark ribbon sandstone.

In core the light and dark ribbon sandstone contact is generally sharp but locally is gradational over less than 20 cm. In addition, the contact occurs at different stratigraphic horizons, suggesting that pedogenic alteration reached different stratigraphic depths in the study area (Fig. 3.4). Variable depth of pedogenic alteration is related to primary and secondary permeability heterogeneities within the ribbon sandstone, which controlled local patterns of groundwater flux and circulation. For example, in areas where more permeable sandstone-rich strata occur near the top of the Swift Formation, the color change occurs stratigraphically lower in the Swift succession. The color change, and associated deflection of the gamma ray curve, is the result of post-depositional processes, and therefore has no chronostratigraphic significance. Accordingly, these changes are not related to primary physio-chemical changes during deposition of the Swift. Significant also is the fact that geophysical well log signatures in the several meter-thick unit above the gamma kick, in particular the gamma ray curve, are an unreliable indication of lithology. On gamma-ray logs, an upward decrease in gamma counts is generally interpreted to indicate an upward-increase in sand content (upward coarsening). In the case of the Swift, however, lower gamma counts in highly altered Swift strata are not related to a change in lithology but rather because exchangeable cations, principally radioactive potassium (K^{40}), have been extensively leached and removed from the succession (Fig. 3.3E).

Geochemical Analysis

Uranium and Thorium Distribution

X-ray fluorescence was used to identify the elemental source causing the high radioactivity (API values) within the marker horizon. Five possible sources were considered: potassium (K^{40}), which is generally present in clay minerals and potassium feldspars, thorium, detrital uranium, or authigenic uranium. Results show that uranium occurs in concentrations up to 30 ppm at the marker horizon and then decreases rapidly to < 1 ppm both stratigraphically upwards and downwards (Fig. 3.3E). Thorium content, on the other hand, is relatively constant and averages ~10 ppm. Similarly, potassium remains constant at the marker horizon and averages ~1.4%. Because thorium is insoluble in water, and remains stable during diagenesis, any thorium present is considered to be of detrital origin. Furthermore, previous workers have suggested that, at the time of deposition, the ratio of detrital thorium to uranium is constant (Myers and Wignall, 1987; Leckie *et al.*, 1990). Variations in this ratio, therefore, are taken to be related to post-depositional changes in uranium content. In the case of the Swift Formation, authigenic uranium is interpreted to be the source of the radioactivity at the marker horizon. Under oxidizing conditions, uranium forms highly soluble uranyl compounds that are commonly mobilized by leaching processes (Langmuir, 1978; Galloway, 1978; Guilbert and Park, 1986). In reducing conditions however, uranium precipitates as uraninite (UO_2) or carnotite ($K_2 (UO_2)_2 (VO_4)_2$) or is sorbed onto organic material. In strata of the Swift, uranium could have been derived from two possible sources: 1) thin, unpreserved layers of Lower Cretaceous volcanic ash, and/or 2) was present originally in the mudstone interbeds. Aptian or older Lower Cretaceous volcanic deposits are absent in southern Alberta but Barremian (128 Ma) tuff layers are prominent to the south in the Bighorn Basin in Wyoming (May *et al.*, 1995). It is therefore reasonable to assume that volcanic ash was transported downwind into southeastern Alberta where some was deposited as thin layers. Alternatively, the uranium may have been present in the mudstone interbeds and subsequently was mobilized and concentrated at the redox front between the light and dark ribbon sandstone. However, in spite of the limited data set, results from XRF analysis indicate that uranium was most probably all authigenic. Uranium concentration quickly diminishes to <1 ppm below the marker horizon, and suggests that background uranium content in unaltered ribbon sandstone is negligible. Uranium, therefore, is interpreted to have been leached from Lower Cretaceous volcanic ash layers and subsequently was mobilized by oxidizing, meteoric waters. Groundwater percolated slowly downward through Swift strata until it reached a redox front at the light - dark ribbon sandstone contact. Here uranium was reduced and sorbed onto organic matter, forming organo-uraniferous mineraloids. With time, the redox front most probably migrated slowly downward. As a result, previously formed organo-uraniferous mineraloids became oxidized and organic matter was decomposed. Uranium was then remobilized and transported to the underlying redox front, where it was immediately reprecipitated. This process would have continued progressively until strata were buried below the zone affected by meteoric water.

Authigenic Iron Minerals

In addition to changes in uranium content across the color boundary, there is also a change in authigenic iron mineral composition. Different iron minerals are associated with the different colored mudstone interbeds in the ribbon sandstone. Disseminated authigenic pyrite and glauconite are present locally in dark ribbon sandstone but are notably absent in the light ribbon sandstone. Thin section analyses indicate that the principal iron-bearing mineral in the light ribbon sandstone is siderite, which occurs as sphaerosiderite nodules or as smaller-sized disseminated siderite, and generally increases in size (0.25 mm to 1mm) and abundance stratigraphically-upward. Glauconite is a Fe(III)-rich silicate mineral that commonly forms from the alteration of fecal matter at the sediment-water interface in marine environments with low sedimentation rates. Below this interface oxygen is generally absent and pyrite commonly precipitates, aided by the activity of sulfate-reducing bacteria (Berner, 1985). Therefore, despite their differences in oxidation state, both glauconite and pyrite likely formed at or near the sea floor and originally were most probably present throughout the entire Swift succession. The absence of glauconite and disseminated pyrite, and the presence of siderite in light ribbon sandstone strata are the result of post-depositional chemical alteration and iron recycling. During subaerial exposure glauconite was chemically altered, releasing ferric iron into solution. Despite being a ferric iron clay mineral, and therefore already in its oxidized state, glauconite can be further altered when exposed to aggressive fluids. Sufficiently aggressive fluids are interpreted to have been present in the soil profile because of the ubiquitous occurrence of tripolitic chert (leached chert), which is significantly more abundant in altered Swift (light ribbon sandstone) strata. At the same time that glauconite was being altered, pyrite, which was exposed to oxygen and oxygenated water, also was being chemically altered. As a result, pyrite was oxidized, which released sulfate and ferrous iron ions into solution:

$$FeS_2 + 7/2\ O_2 + H_2O \dashrightarrow Fe^{2+} + 2\ SO_4^{2-} + 2\ H^+ \qquad (1)$$

Subsequently, Fe^{2+} was oxidized to Fe^{3+}:

$$2\ Fe^{2+} + 1/2\ O_2 + 2\ H^+ \dashrightarrow 2\ Fe^{3+} + H_2O \qquad (2)$$

During this period of chemical alteration, organic material was being decomposed by microbial action. Oxygen concentrations within the groundwater or soil profile, however, were highly variable and oxygen was periodically completely consumed by bacteria. Respiring microorganisms also increased the local soil pCO_2. As a result, ferrous iron was likely repeatedly oxidized to ferric iron and then reduced again to ferrous iron. Ferrous iron subsequently reacted with CO_3^{2-} and precipitated siderite:

$$CO_2 + H_2O \dashrightarrow H_2CO_3 \qquad (3)$$

$$H_2CO_3 \dashrightarrow HCO_3^- + H^+ \qquad (4)$$

$$HCO^{3-} \dashrightarrow H^+ + CO_3^{2-} \qquad (5)$$

$$CO_3^{2-} + Fe^{2+} \dashrightarrow FeCO_3 \qquad (6)$$

Locally, however, where small amounts of sulfate ions were present, ferrous iron reprecipitated principally as discontinuous rings of pyrite around siderite concretions (Fig. 3.4D):

$$Fe^{2+} + 2\ SO_4^{2-} + 2\ H^+ \dashrightarrow FeS_2 + 7/2\ O_2 + H_2O \qquad (7)$$

This interpretation is based also on changes in siderite observed within the profile, which generally increases in size and abundance stratigraphically upwards. Because siderite precipitates in reducing, anoxic, non-sulfidic conditions (Krumbein and Garrels, 1952; Berner, 1981), its presence in the pedogenically altered sandstone indicates that oxygen was at times completely consumed prior to precipitation of siderite. Importantly, XRF data indicate that iron content increases by about 3% stratigraphically upwards from the color change (Fig. 3.3E). This observation suggests that iron was not derived exclusively from pyrite and glauconite in the Swift succession. Ferrous iron (Fe^{2+}) is readily mobile in solution and intuitively, an external source also likely contributed to total iron content in the light ribbon sandstone.

Four siderite samples were analyzed for carbon isotopes in order to determine the early diagenetic conditions in the Swift paleosol profile (Fig. 3.3E). However, because of the small number of samples, these data should be treated with caution. Marine plankton generally has $\delta^{13}C$ values of about $-20\ ^0/_{00}$, whereas atmospheric CO_2 is about $-7\ ^0/_{00}$ (Drever, 1997). Carbon isotope analyses for siderite in the Swift show that both sphaerosiderite and disseminated siderite are depleted in $\delta^{13}C$ although sphaerosiderite, which generally occurs higher stratigraphically, is less depleted (Fig. 3.3E). In addition, there appears to be a gradual decrease in $\delta^{13}C$ value stratigraphically downward from approximately $-8\ ^0/_{00}$ (sphaerosiderite) to $-23\ ^0/_{00}$ (disseminated siderite), which corresponds closely to the $\delta^{13}C$ value of marine plankton. This decrease is probably related to the input of isotopically lighter atmospheric CO_2 in the upper part of the light ribbon sandstone. Downward, the influence of atmospheric CO_2 gradually weakened until the carbon isotope signature resembled that of the original marine organic matter.

Analogue Model: Uranium Roll-front Deposits

The different authigenic minerals present in the ribbon sandstone form a vertical stratigraphic succession that upward consists of pyrite and glauconite, uraniferous mineraloids, and siderite. Interestingly, this vertical succession is similar to the horizontal mineralized zones in uranium roll-front deposits described from Wyoming (Guilbert and

Figure 5. Analogue model for the precipitation of authigenic uranium and siderite in the Swift Formation: uranium roll-front deposits from Wyoming. In this example, the observed lateral change in mineralized zones from iron oxides (hematite), to iron carbonates (siderite), to uraninite, and then to iron sulfides (pyrite) are related to geochemical gradients from oxidizing to reducing in the downflow direction (left to right). Modified from Guilbert and Park,1986.

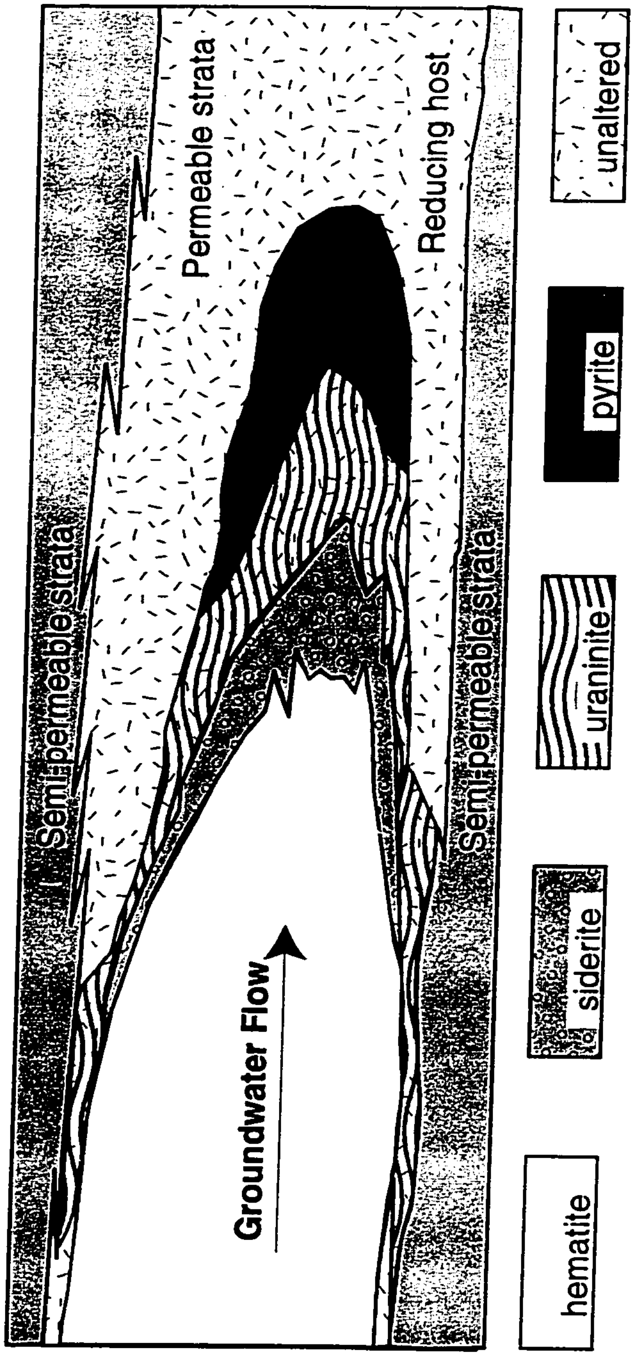
Semi-permeable strata
Permeable strata
Reducing host
Semi-permeable strata
Groundwater Flow
hematite
siderite
uraninite
pyrite
unaltered

Park, 1986), although the latter is much larger in scale. In the Wyoming example uranium roll-front deposits occur in permeable channel sandstones that are underlain and overlain by impermeable strata. They typically are crescent- or S-shaped in cross-section and are generally less than 20 m thick but can extend laterally for several tens of meters along the upper and lower limbs of the deposit. The ore is interpreted to occur along a redox front. Here, migrating, uranium-bearing, oxidizing fluids encounter a regionally reduced host, commonly because of the presence of organic matter. The uranium is then precipitated as uraninite or is sorbed onto the organic material. Roll-front deposits are further characterized by mineralized zones that consist of a hematite- and magnetite-rich core at the trailing edge of the orebody (concave side), followed in the downflow direction by an alteration envelope with siderite and goethite, the uranium orebody, and then an ore-stage pyrite zone at the leading edge of the roll-front deposit (convex side) (Fig. 3.5). This zonation is interpreted to be related to geochemical gradients (from oxidizing to reducing conditions) in the direction of the flow system within the aquifer (Galloway, 1978). Similar geochemical gradients are interpreted to have controlled the distribution of secondary minerals in pedogenically-altered Swift strata. In this case, a siderite-rich horizon passes downward to the uranium layer, which marks the redox front, and then farther downward to locally pyritic unaltered dark ribbon sandstone.

Discussion

The radioactive horizon in the ribbon sandstone forms a regionally extensive marker horizon in southeastern Alberta that is interpreted to be related to post-depositional pedogenic alteration and mineralization. These changes occurred in two stages, which significantly modified the primary mineralogy and texture of the ribbon sandstone (Fig. 3.6).

Stage one consisted of pedogenic alteration. Following withdrawal of the Oxfordian sea from the study area, Swift strata became subaerially exposed and formed a soil in the upper part of the succession. Because of extensive pedogenesis, primary sedimentary structures were destroyed. Abundant clay coatings (argillans) indicate elluvial deposition in the Bt horizon of the developing paleosol. Also, oxidizing conditions, related to atmospheric

Figure 6. Schematic diagram illustrating the two stage, early diagenetic history of the Swift Formation. Stage one began with early diagenetic precipitation of glauconite on the Oxfordian seafloor and pyrite under reducing conditions in the underlying sediment. Later subaerial exposure causes these minerals to be altered and sphaerosiderite to be precipitated. Stage two consisted of uranium mineralization during late pedogenesis. Uranium, derived from unpreserved volcanic ash layers was leached, mobilized and sorbed onto organic material at the redox front. With time, the redox front migrated farther downward, causing uranium to be dissolved and reprecipitated stratigraphically lower. Eventually the redox front stabilized – its topography preserved by the mineralized uranium layer.

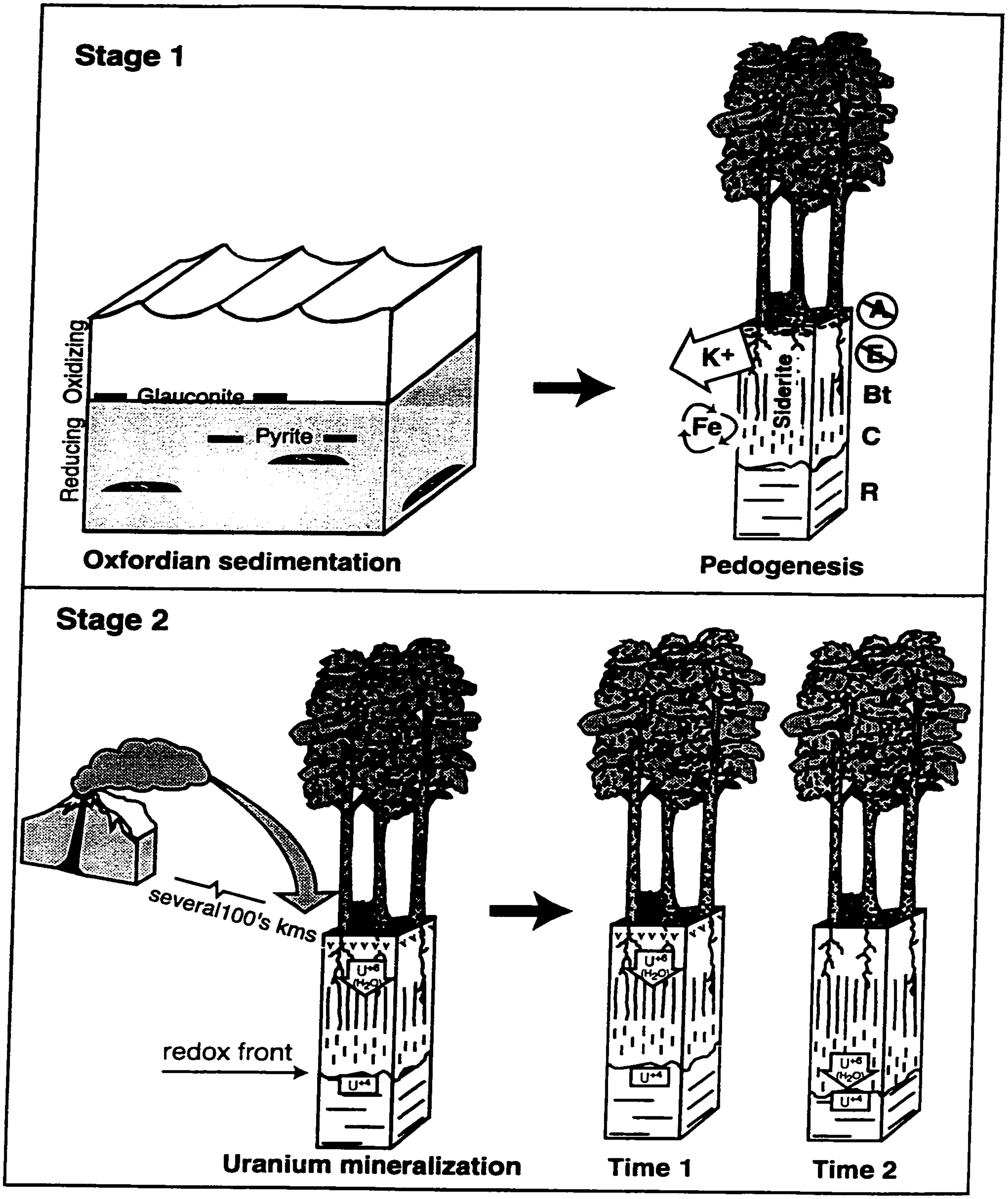
Stage 1
Oxidizing
Reducing
Glauconite
Pyrite
Oxfordian sedimentation
K+
Fe
Siderite
A
E
Bt
C
R
Pedogenesis
Stage 2
several100's kms
redox front
U+6 (H2O)
U+4
Uranium mineralization
Time 1
Time 2

oxygen in pores and dissolved in meteoric waters, aided oxygen-respiring microbes to decompose dead organic matter. Alteration of chemically unstable minerals such as feldspars and clay minerals, plus the oxidation of authigenic pyrite, and the chemical weathering of glauconite occurred in this pedogenically altered horizon. Carbon dioxide concentrations were locally elevated, mostly as the by-product of bacterial respiration. At the same time, oxygen was regularly depleted, and at times eliminated by respiring microbes. The combination of high pCO_2 and anaerobic conditions, combined with the presence of ferrous iron in solution created the conditions necessary for the precipitation of sphaerosiderite. The observed upward increase in the size of siderite nodules is coincident with an increase in the amount of time for crystal growth. Also, some sphaerosiderite nodules contain discontinuous concentric layers of pyrite, which suggests that geochemical conditions (Eh and pH) within the soil profile commonly fluctuated (Fig. 3.3D).

Stage two was an episode of uranium mineralization. Thin volcanic ash layers were probably deposited during the Barremian. Uranium was leached from these deposits and mobilized downward by meteoric water. Upon reaching the reducing environment at the top of the unaltered, organic-rich dark ribbon sandstone, uranium was sorbed onto the organic matter. With time, the redox front likely migrated slowly downward as organic material at the top of the dark ribbon sandstone was progressively oxidized. At the same time, uranium was being continuously remobilized and then reprecipitated stratigraphically lower until the redox front was buried beneath the influence of atmospheric oxygen. The variable depth of pedogenic alteration in the study area is most likely related to local differences in groundwater flux through the Swift succession, which in turn was controlled by primary (depositional) and secondary (pedogenic alteration) permeability heterogeneities. As a result, the marker horizon that separates the dark and light ribbon sandstone has no chronostratigraphic significance but only marks an ancient redox front and the depth of pedogenic alteration.

Significance of Recognizing Pedogenic Alteration

Recognizing the effects of pedogenesis is important because it has a significant impact on stratal mineralogy and texture. Because of mineralogical and textural changes, geophysical well log profiles of pedogenically altered successions are no longer indicative of primary depositional features, and therefore, are generally unreliable for correlation purposes. For example, above the radioactive marker horizon in the Swift, the gamma ray curve is typically characterized by API values that gradually decrease stratigraphically upwards. Because sandstone-rich horizons are present locally at this stratigraphic horizon, this signature could easily be mistaken for an overall upward-sandier trend indicative of upward-shoaling depositional conditions. However, as shown earlier, this "upward sandier" trend formed as a result of secondary pedogenic alteration and the preferential removal of large exchangeable ions like radioactive K^{40} from the soil profile (Fig. 3.3E). This, in turn, reduced the API value but had no effect on the (primary) sand:mud ratio, which remained unchanged. In addition, the underlying marker horizon could also be misinterpreted as a significant bounding surface such as a maximum flooding surface or, alternatively, an unconformity marking a change in physio-chemical conditions within the depositional basin. However, this surface represents an ancient redox front that formed at variable depth within a soil profile, and therefore, does not approximate a horizontal surface, nor represent a surface with stratigraphic significance.

Summary

Radioactive marker horizons in mud-dominated successions generally make useful and reliable stratigraphic data, because commonly they correspond with maximum flooding surfaces. In this study, however, the readily recognizable radioactive horizon in the Swift Formation is interpreted to be the result of post-depositional alteration. Following withdrawal of the Oxfordian sea, the top of the Swift Formation was subaerially exposed for approximately 35 my, during which time significant pedogenic alteration took place. A soil profile developed, of which only the lowermost Bt (altered ribbon sandstone) and C horizons (light ribbon sandstone), and unaltered bedrock (dark ribbon sandstone) are locally preserved.

Pedogenic alteration penetrated to variable depth in the study area because of heterogeneities related to primary permeability differences within the ribbon sandstone. Iron recycling was a prominent process in the soil profile. Iron, derived in part from oxidized authigenic pyrite and chemically altered glauconite, was reprecipitated as siderite in altered ribbon sandstone because of high pCO_2 created by bacterial respiration and atmospheric input.

During late pedogenesis, uranium was leached from unpreserved (Barremian?) volcanic ash deposits and subsequently mobilized by slow, downward-migrating meteoric groundwater. Upon encountering a redox front at the top of the underlying unaltered, more organic-rich dark ribbon sandstone, uranium was sorbed onto organic matter within the mudstone and formed organo-uraniferous mineraloids. This suggests that the radioactive marker horizon within the Swift Formation does not correspond to a significant (primary) stratigraphic discontinuity, but instead to a horizon of post-depositional pedogenic alteration. In addition, because of its variable stratigraphic position, this horizon does not approximate a horizontal surface, and therefore would represent an unreliable stratigraphic datum. Furthermore, geophysical well log signatures above the marker horizon are unreliable because they represent mineralogically altered strata. This is particularly true for the gamma ray log, which commonly shows an "upward-sandier" trend, which generally would be interpreted to represent upward-coarsening related to upward shoaling depositional conditions. In fact, this trend is the result of post-depositional leaching and removal of K^{40} ions causing a concomitant reduction of gamma-ray counts.

Chapter 4

Conclusions

The Oxfordian Swift Formation in southeastern Alberta is composed of two unconformably bounded sequences: the shale member and the ribbon sandstone. Each member is characterized predominantly by fine grained sediment and small-scale physical sedimentary structures. Large scale sedimentary structures and medium sand are rare. The contact between the Rierdon Formation and the shale member is characterized by a marked difference in lithologies from fossiliferous calcareous shale to siliciclastic shale. A thin chert-pebble conglomerate was locally observed at the base of the member and is interpreted to be an areally extensive transgressive lag. The shale member comprises up to four parasequences that form a retrogradational parasequence set, suggestive of a long-term deepening of fully marine conditions. Within this basin, high-energy, long period waves readily developed and deposited hummocky-cross-stratified siltstone. The basin was therefore not physically or chemically restricted during this time. Deposition of Sequence 1 was terminated during the late transgressive systems tract by a fall of relative sea level that exposed these strata to fluvial erosion. The cause(s) for this abrupt fall in relative sea level is unknown, but may be related to renewed tectonic activity and uplift of the Sweetgrass Arch.

During the following lowstand (base of Sequence 2), multiple northeast-southwest trending meandering channels incised into the top of Sequence 1 as they flowed toward a new paleoshoreline. The location of the lowstand shoreline is unknown, because it either lies beyond the study area or it was eroded by wave ravinement processes during the following rise in relative sea level or later, by Lower Cretaceous fluvial systems. Despite the presence of lowstand channels, however, lowstand deposits were not observed. Wave ravinement processes during the subsequent rise in relative sea level are interpreted to have thoroughly reworked both lowstand deposits and the underlying shale member, leaving only a few scattered chert pebbles in newly widened lowstand channels. Associated also with transgression were significant changes in the physical and chemical conditions in the marine basin within the study area. These changes are related to modifications in basin configuration and the development of a strait, which likely formed as a result of rejuvenated uplift of the Sweetgrass Arch, possibly related to the onset of the Columbian-Nevadan Orogeny. Within this newly configured basin, brackish waters prevailed as a result of voluminous freshwater discharge from rivers in nearby highlands to the south (Belt Island trend) and north (craton). In addition, the basin was incapable of developing long-period oscillatory waves. Instead, sand was principally transported by combined flows with variable speed, but invariably weak tidal currents and a weak oscillatory component related to storm waves. During Sequence 2, the basin in the study area was mud dominated and bedload sediment starved, sedimentation rates were low, and thick and areally extensive sand-rich deposits did not accumulate. Differential deposition of bed-load sediment formed and temporarily maintained many small, irregularly shaped sand banks that occur throughout the Swift succession. The depositional history of the sand banks was controlled by the relative contribution of the wave (oscillatory) versus tidal (unidirectional) flow components on the combined-flow regime, which in turn controlled the short-term direction of bed-load sediment transport and subsequent deposition. The net result of the spatial variability in sand deposition is the formation of a number of different stratal patterns (upward-coarsening, -fining, -aggrading), and a stratal architecture characterized by the synchronous development of aggrading, prograding and retrograding stacking patterns, which are completely unrelated to changes in relative sea level.

In the study area, strata of the ribbon sandstone are marked by a distinctive abrupt to gradual (decimetre scale) upward change in colour from black to light grey mud interlaminae, which is commonly marked by a narrow and abrupt rightward deflection of the gamma ray curve. The colour transition is related to an upward change in the abundance of organic matter, which is high in the dark ribbon sandstone and absent in the light. Changes in physical or biogenic sedimentary structures were not observed across the colour boundary, which suggests that physical and ecological conditions remained constant across the boundary between deposition of the light and dark ribbon sandstone. Upwards from the colour change, the interstratification that typifies the light ribbon sandstone becomes progressively more difficult to discern and gradually merges into massive-appearing, beige-coloured strata with abundant siderite nodules.

The origin of the colour change and associated deflection of the gamma curve is interpreted to be related to a two stage process. Stage one consisted of pedogenic alteration. Following withdrawal of the Oxfordian sea from the study area, Swift strata became subaerially exposed and formed a soil in the upper part of the succession. Because of extensive pedogenesis, abundant elluvial clay coatings (argillans) were deposited in the Bt horizon of the developing soil and primary sedimentary structures were destroyed. Only the Bt-and C-horizons of the Swift paleosol profile are preserved and are represented by light Ribbon Sandstone and 'massive' strata, respectively. Also, oxidizing conditions in the soil, related to atmospheric oxygen in pores and dissolved in meteoric waters aided oxygen-respiring microbes to decompose organic matter. In addition, chemically unstable minerals were altered, such as feldspars and clay minerals, authigenic pyrite was oxidized and glauconite was chemical weathered, supplying abundant ferric iron to local pore waters. Because carbon dioxide concentrations were locally elevated, mostly as the by-product of bacterial respiration and, at the same time, oxygen was regularly depleted or eliminated by respiring microbes, ferric iron in solution was reduced and precipitated as sphaerosiderite ($FeCO_3$). The observed upward increase in the size of siderite nodules is coincident with an increase in the amount of time for crystal growth.

Stage two constitutes uranium mineralization. Thin volcanic ash layers were deposited over the Swift soil, probably during the Barremian. Uranium was leached from these deposits and mobilized downward by oxidizing meteoric water. Upon reaching the reducing environment at the top of the unaltered, organic-rich dark Ribbon Sandstone, uranium was sorbed onto the organic matter. With time, the redox front likely migrated slowly downward as organic material at the top of the dark Ribbon Sandstone was progressively oxidized. At the same time, uranium was being continuously remobilized and then reprecipitated stratigraphically lower until the redox front was buried beneath the influence of atmospheric oxygen. The variable depth of pedogenic alteration in the study area most likely reflects differences in groundwater flux through the Swift succession, which in turn was controlled by primary (depositional) and secondary (pedogenic alteration) permeability heterogeneities. As a result, the colour change and associated radioactive marker horizon in the ribbon sandstone has **no** chronostratigraphic significance, nor does it record significant physico-chemical changes during deposition of the Swift, but only indicates the depth of pedogenic alteration.

References

Ainsworth, R.B., and Pattison, S.A.J., 1994. Where have all the lowstands gone? Evidence for attached lowstand systems tracts in the Western Interior of North America: Geology, vol. 22, p. 415 – 418.

Anastas, A.S., Dalrymple, R.W., James, N.P., and Nelson, C.S., 1997. Cross-stratified calcarenites from New Zealand: subaqueous dunes in a cool-water, Oligo-Miocene seaway. Sedimentology, vol. 44, p. 869 – 891.

Amorosi, A., 1995, Glaucony and sequence stratigraphy: a conceptual framework of distribution in siliciclastics sequences. Journal of Sedimentary Research, vol. B65, no. 4, p. 419 - 425.

Arnott, R.W.C., 1992. Quasi-planar-laminated beds in the Lower Cretaceous Bootlegger Member, north-central Montana: evidence of combined-flow sedimentation. Journal of Sedimentary Petrology, vol. 63, no.3, p. 488 – 494.

Arnott, R.W.C., Hein, F.J., and Pemberton, S.G., 1995. Influence of the ancestral Sweetgrass Arch on sedimentation of the Lower Cretaceous Bootlegger Member, north-central Montana. Journal of Sedimentary Research, vol. B65, no. 2, p. 222-234.

Arnott, R.W.C. and Southard, J.B., 1990. Exploratory flow-duct experiments on combined-flow bed configurations, and some implications for interpreting storm-event stratification. Journal of Sedimentary Petrology, vol. 60, no. 2, p. 211 – 219.

Belderson, R.H., Johnson, M.A., and Kenyon, N.H., 1982. Bedforms. *In* A.H. Stride, ed., Offshore Tidal Sands: Processes and Deposits, Chapman and Hall, New York, p. 27 – 57.

Berné, S., Lericolais, G., Marsset, T., Bourillet, J.F., and DeBatist, M., 1998. Erosional offshore sandsridges and lowstand shorefaces: examples from tide- and wave-dominated environments of France. Journal of Sedimentary Research, vol. 68, no. 4, p. 540 - 555.

Berner, R.A., 1981. A new geochemical classification of sedimentary environments. Journal of Sedimentary Petrology, vol. 51, no. 2, p. 359 – 365.

Berner, R.A., 1985. Sedimentary pyrite formation: an update. Geochimica Cosmochimica Acta, vol. 48, p. 605 – 615.

Beynon, B.M., Pemberton, S.G., Bell, D.D. and Logan, C.A., 1988. Environmental implication of ichnofossils from the Lower Cretaceous Grand Rapids Formation, Cold Lake Oils Sands Deposits. *In* D.P. James and D.A. Leckie, eds., Sequences, Stratigraphy, Sedimentology: Surface and Subsurface. Canadian Society of Petroleum Geologists, Memoir 15, p. 275 – 290.

Boggs, S.Jr., 1987. Principles of Sedimentology and Stratigraphy. Merrel Publishing Co., Prentice-Hall, New Jersey, 784 p.

Brenner, R.L. and Davies, D.K., 1974. Oxfordian sedimentation in the Western Interior United States, American Association of Petroleum Geologists Bulletin, vol. 58, no. 3, p. 407 - 428.

Brooke, M., and Braun, W.K., 1972. Biostratigraphy and microfaunas of the Jurassic system of Saskatchewan. Saskatchewan Department of Mineral Resources Report 161, 83 p.

Cant, D.J., 1988. Regional structure and development of the Peace River arch, Alberta; a Paleozoic failed-rift system? Bulletin of Canadian Petroleum Geology, vol. 36, p. 284 – 295.

Cant, D.J., 1992. Subsurface Facies Analysis. *In* R.G. Walker and N.P. James, eds., Facies Models: Response to Sea Level Change. Geological Association of Canada, p. 27 - 45.

Christopher, J.E., 1964. The Middle Jurassic Shaunavan Formation of southwestern Saskatchewan. Saskatchewan Department of Mineral Resources Report 95, 96 p.

Christopher, J.E., 1974. The Upper Jurassic Vanguard and Lower Cretaceous Mannville groups of southwestern Saskatchewan. Saskatchewan Department of Mineral Resources Report 151, 349 p.

Christopher, J.E., 1984. The Lower Cretaceous Mannville Group, northern Williston Basin region, Canada. *In*: D.F. Stott, and D.J. Glass, eds., The Mesozoic of Middle North America, Canadian Society of Petroleum Geology, Memoir 9, p. 109-126.

Church, K.D. and Gawthorpe, R.L., 1997. Sediment supply as a control on the variability of sequences: an example from the Late Numerian of northern England. Journal of the Geological Society, vol. 154, p. 55 - 60.

Cobban, W.A., 1945. Marine Jurassic formations of Sweetgrass Arch, Montana. American Association of Petroleum Geologists Bulletin, vol. 29, p. 1262 – 1303.

Coleman, M.L., 1985. Geochemistry of diagenetic non-silicate minerals: kinetic considerations. Philosophical transactions of the Royal Society of London, A315, p. 39-56.

Coleman, M.L., Hedrick, D.B., Lovley, D.R., White, D.C., and Pye, K., 1993. Reduction of Fe (III) in sediments by sulphate-reducing bacteria. Nature, vol. 361, p. 436 - 438.

Coney, P.J., Jones, D.L., and Monger, J.W.H., 1980. Cordilleran suspect terrane. Nature, vol. 288, p. 329 – 333.

Dalrymple, R.W., 1992. Tidal depositional systems. *In* R.G. Walker and N.P. James, eds., Facies Models: Response to Sea Level Change. Geological Association of Canada, p. 195 – 218.

Davies, A.G., Soulsby, R.L., and King, H.L., 1988. A numerical model of the combined wave and current bottom boundary layer. Journal of Geophysical Research, vol. 93, p. 491 – 508.

Davies, Jr.R.A. and Balson, P.S., 1992. Stratigraphy of North Sea tidal sand ridge. Journal of Sedimentary Research, vol. 62, no.1, p. 116 – 121.

Davies, Jr.R.A., Klay, J., and Jewell, P., 1993. Sedimentology and stratigraphy of tidal sands ridges southwest Florida inner shelf. Journal of Sedimentary Research, vol. 63, no. 1, p.91 – 104.

DeRaaf, J.F.M., Boersma, J.R., and van Gelder, A., 1977. Wave-generated structures and sequences from a shallow marine succession, Lower Carboniferous, County Cork, Ireland. Sedimentology, vol. 24, p. 451 – 483.

Donofrio, R.R., 1997. Survey of hydrocarbon-producing impact structures in North America: exploration results to date and potential for discovery in Precambrian basement rocks. *In* K.S. Johnson and J.A. Campbell, eds., Ames Structure in Northwest Oklahoma and Similar Features: Origin and Petroleum Production (1995 Symposium), Circular 100, Oklahoma Geological Survey, Norman, OK, p. 17 – 29.

Drever, J.I., 1997. The Geochemistry of Natural Waters. Surface and Groundwater Environments. Prentice Hall, third edition, 436p.

Duke, W.L., 1990. Geostrophic circulation of shallow marine turbidity currents? The dilemma of paleoflow patterns in storm-influences prograding shoreline systems. Journal of Sedimentary Petrology, vol. 60, p. 870 – 883.

Duke, W.L., Arnott, R.W.C., and Cheel, R.J., 1991. Storm-sandstones and hummocky cross-stratification: new evidence on a stormy debate. Geology, vol 19, p. 625 – 628.

Ekdale, A.A., Bromley, R.G., and Pemberton, S.G., 1984. Ichnology. Society of Economic Paleontologists and Mineralogists, Short Course no.15, 317p.

Eziji-Okoye, S., 1985. The origin of the Eagle Butte structure. Unpublished report for PanCanadian Petroleum, 75p.

Fermor, P.R. and Moffat, I.W., 1992. Tectonics and structure of the Western Canada foreland basin. *In* R.W. Macqueen and D.A. Leckie, eds., Foreland Basins and Fold Belts, American Association of Petroleum Geologists Memoir 55, p 81 – 105.

Fisher, C.A., 1909. Geology of the Great Falls coal field, Montana. United States Geological Survey Bulletin 390.

Folk R.L., Andrews, D.B., and Lewis, D.W., 1970. Detrital sedimentary rock classification and nomenclature for use in New Zealand. New Zealand Journal of Geology and Geophysics, vol. 13, p. 937 – 968.

Frey, R.W. and Pemberton, S.G., 1985. Biogenic structures in outcrops and cores. 1. Approaches to ichnology. Bulletin of Canadian Petroleum Geology, vol. 33, p. 72-115.

Gabrielse, H., 1985. Major dextral transcurrent displacements along the northern Rocky Mountain trench and related lineaments in north-central British Columbia. Geological Society of American Bulletin, vol. 94, p. 1 –14.

Galloway, W.E., 1978. Uranium mineralization in a coastal-plain fluvial aquifer system: Catahoula Formation, Texas. Economic Geology, vol. 73, p. 1655 – 1676.

Gawthorpe, R.L., Fraser, A.J., and Collier, R.E.L.L., 1994. Sequence Stratigraphy in active extensional basins: implications for the interpretations of ancient basin-fills. Marine and Petroleum Geology, vol. 11, p. 642 - 658.

Gradstein, F.M. and Ogg, J.G., 1996. A Phanerozoic time scale. Episodes 1996, vol. 19, no.'s 1 & 2.

Grieve, R.A.F., Therriault, A.M., and Kreis, L.K., 1998. Impact structures of the Western Sedimentary Basin of North America: new discoveries and hydrocarbon resources. *In* J.E. Christopher, C.F. Gilboy, D.F. Paterson and S.L. Bend, eds., Eight International Williston Basin Symposium, Saskatchewan Geological Society Special Publication no. 13, p. 189 – 201.

Gross, G.M., 1977. Oceanography a view of the Earth. Prentice-Hall, New Jersey, 497 p.

Guilbert, J.M. and Park, Jr. C.F., 1986. The Geology of Ore Deposits. 4th ed., W.H. Freeman & Co., Chap. 20, p. 910 – 921.

Hamlin, A.P., and Walker, R.G., 1979. Storm-dominated shallow marine deposits: the Fernie-Kootenay (Jurassic) transition, southern Rocky Mountains. Canadian Journal of Earth Sciences, vol. 16, p. 1673 – 1690.

Hamm, H. and Olsen, R.E., 1992. Oklahoma Arbuckle lime exploration centered on burial astrobleme structure. The Oil and Gas Journal, vol. 90, no. 16, p. 113 (114).

Haq, B.U., Hardenbol, J., and Vail, P.R., 1987. Chronology of fluctuating sea levels since the Triassic. Science, vol. 235, p. 1156 – 1167.

Hayes, B.J.R., 1983, Stratigraphy and petroleum potential of the Swift Formation (Upper Jurassic), southern Alberta and north-central Montana. Bulletin of Canadian Petroleum Geology, vol. 31, no. 1, p. 37 - 52.

Herbaly, E.L., 1974. Petroleum geology of the Sweetgrass Arch. American Association of PetroleumGeologists Bulletin, vol. 58, p. 2227 – 2244.

Hoffman, P.F., 1988. United plates of America: the birth of a craton. Annual Review of Earth and Planetary Sciences, vol. 16, p. 543 – 604.

Houbolt, J.J.H.C., 1968. Recent sediments in the southern Bight of the North Sea. Geologie en Mijnbouw, vol. 47, p. 245 – 273.

Howard, J. D., and Reineck, H.-E., 1981. Depositional facies of high energy beach-to-offshore sequence: comparison with low-energy sequence. American Association of Petroleum Geology Bulletin, vol. 65, p. 807-830.

Howarth, M.J., 1982. Tidal currents forces and the ocean's response. *In* A.H., Stride, ed., Offshore tidal sands, processes and deposits. Chapman and Hall, New York, p. 10 – 26.

Hunter, R. E., Clifton, H. E., and Phillips, R. L., 1979. Depositional processes, sedimentary structures, and predicted vertical sequences in barred nearshore systems, southern Oregon coast. Journal of Sedimentary Petrology, vol. 49, p. 711-726.

Huthnance, J.M., 1982. On the formation of sands banks of finite extent. Estuarine, Coastal and Shelf Science, vol. 15, p. 277 - 299.

Ikehara, Ken, 1998. Sequence stratigraphy of tidal sand bodies in the Bungo Channel, southwest Japan. Sedimentary Geology, vol. 122, p. 233 –244.

Imlay, R.W., 1980. Jurassic paleobiogeography of the conterminous United States in its continental setting. U.S. Geological Survey Professional Paper 1062, 134 p.

Irving, E., and Yole, R.W., 1972. Paleomagnetism and the kinematic history of mafic and ultramafic rocks in fold mountain belts; Canadian Earth Physics Branch Publication, vol. 42, p. 87-95.

Irving, E., Monger, J.W.H., and Yole, R.W., 1980. New paleomagnetic evidence for displacement terranes in British Columbia. *In* D.W. Strangway, ed., The continental crust and its mineral deposits. Geological Association of Canada Special Paper 20, p. 441 – 456.

Jervey, M., 1992. Siliciclastic sequence development in foreland basins, with examples from the Western Canada foreland basin. *In* R.W. Macqueen and D.A. Leckie, eds., Foreland Basins and Fold Belts. American Association of Petroleum Geologists Memoir 55, p. 47 - 80.

Kauffman, E.G., 1984. Paleobiogeographic and evolutionary dynamic responses in the Cretaceous Western Interior Seaway of North America. *In* G.E.G. Westermann, ed., Jurassic –Cretaceous biochronology and biogeography of North America. Geological Association of Canada Special Paper 27, p. 273 – 306.

Keller, G.H. and Richards, A.F., 1963. Sediments of the Malacca Strait, southeast Asia. Journal of Sedimentary Petrology, vol. 37, no. 1, p. 102 – 127.

Knight, R.J. and McLean, J.R., eds., 1986. Shelf sands and sandstones. Canadian Society of Petroleum Geologists, Memoir 11, 347 p.

Kranck, K., 1972. Tidal Current Control of Sediment Distribution in Northumberland Strait, Maritime Provinces. Journal of Sedimentary Petrology, vol. 42, no. 3, p 596-601.

Krumbein, W.C. and Garrels, R.M., 1952. Origin and classification of chemical sediments in terms of pH and oxidation-reduction potentials. Journal of Geology, vol. 60, p. 1 – 33.

Kvale, E.P, Sowder, K.H., and Hill, B.T., 1998. Modern and ancient tides. Booklet to accompany Modern and Ancient Tides poster. Society for Sedimentary Geology and the Trustees of Indiana University, 10p.

Langmuir, D. and Herman, J. S., 1980. The mobility of thorium in natural waters at low temperatures. Geochimica Cosmochemica Acta, vol. 44, p. 1753 – 1766.

Leckie, D.A., 1986. Rates, controls and sand-body geometries of transgressive-regressive cycles: Cretaceous Moosebar and Gates formations, British Columbia. American Association of Petroleum Geologists Bulletin, vol. 70, p. 516 – 535.

Leckie, D.A., and Cheel, R.J., 1989. The Cypress Hills Formation (upper Eocene to Miocene): a semi-arid braidplain deposit resulting from intrusive uplift. Canadian Journal of Earth Science, vol. 26, p. 1918 – 1931.

Leckie, D.A., Singh, C., Goodarzi, F., and Wall, J. H., 1990. Organic-rich, radioactive marine shale: a case study of a shallow-water condensed section, Cretaceous Shaftesbury Formation, Alberta, Canada. Journal of Sedimentary Petrology, vol. 60, no.1, p. 101 – 117.

Leckie, D.A. and Smith, D.G., 1992. Regional setting, evolution and depositional Cycles of the Western Canada Foreland Basin. *In* Macqueen, R. W. and Leckie, D. A., eds., Foreland Basins and Fold Belts, American Association of Petroleum Geologists, Memoir 55, p. 9-46.

Leckie, D.A., Vanbeselaere, N.A., and James, D.P., 1997. Regional sedimentology, sequence stratigraphy and petroleum geology of the Mannville Group; southwest Saskatchewan. *In* D.P. James and S.G. Pemberton, eds., Petroleum geology of the Cretaceous Mannville Group, Western Canada, Canadian Society of Petroleum Geologists Memoir 18, p. 211 - 262

Loutit, T.S., Hardenbol, J., Vail, P.R., and Baum, G. R., 1988. Condensed sections: the key to age determination and correlation of continental margin sequences. *In* Wilgus, C.K., Hastings, B.S., Kendall, C., Posamentier, H.W., Ross, C.A., and Van Wagoner, J.C., eds., Sea-Level Change – An Integrated Approach: Society of Paleontologists and Mineralogists Special Publication 42, p. 183-213.

Martisen, O.J. and Helland-Hansen, W., 1995. Strike variability of clastic depositional Systems: does it matter for sequence stratigraphic analysis?. Geology, vol. 23, p. 439 – 442.

Masters, J.A., 1984. Lower Cretaceous oil and gas in western Canada. *In* J.A. Masters, ed., - Elmworth- Case Study of a Deep Basin Gas Field. American Association of petroleum Geologists Memoir 38, p. 1 – 38.

May, M.T., Furer, L.C., Kvale, E.P., and Suttner, L.J., 1995. Chronostratigraphic and tectonic significance of Lower Cretaceous conglomerates in the foreland basin of central Wyoming. *In* Steven Dorobek and Gerald Ross, eds., Stratigraphic Evolution of Foreland Basins, Society of Paleontologists and Mineralogist Special Publication no. 52, p. 97 – 110.

Monger, J.W.H., 1989. Overview of the Cordilleran orogeny. *In* Ricketts, B.D., ed., Western Canada Sedimentary Basin; A Case Study. Canadian Society of Petroleum Geology, chapter 2, p. 9 – 32.

Monger, J.W.H., and Ross, C.A., 1971. Distribution of fusulinaceans in the western Canadian Cordillera: Canadian Journal of Earth Science, vol. 8, p. 259-278.

Morad, S., 1998. Carbonate cementation in sandstones: distribution patterns and geochemical evolution. *In* S. Morad, ed., Carbonate cementation in sandstones. International Association of Sedimentologists Special Publication 26, p. 1 – 26.

Myers, K.J., and Wignall, P.B., 1987. Understanding Jurassic organic-rich mudrocks – new concepts using gamma ray spectrometry and paleoecology: examples from the Kimmeridge clay of Dorset and the jet rock of Yorkshire. *In* J.K. Leggett and G.G. Zuffa, eds., Marine Clastic Sedimentology: London, Graham and Trotman, p. 172-189.

Neumeier, U., 1998. Tidal dunes and sand waves in deep outer shelf environments, Bajocian, S.E. Jura, France. Journal of Sedimentary Research, vol. 68, p. 507 – 514.

O'Neill, J.M. and Lopez, D.A., 1985. Character and regional significance of Great Falls tectonic zone, east-central Idaho and Wyoming. American Association of Petroleum Geologists Bulletin, vol. 69, p. 437 – 447.

O'Neill, J.M., Duncan, M.S., and Zartman, R.E., 1988. An Early Proterozoic gneiss dome, Highland Mountains, Montana. *In* S.E. Lewis and R.B. Berg, eds., Precambrian and Mesozoic plate margins: Montana, Idaho and Wyoming. Montana Bureau of Mines and Geology, Special Publication 96, p. 81 – 88.

Open University Course Team, 1989. Waves, tides and shallow water processes. Oxford, Pergamon Press, 187 p.

Pattison, S.A.J. and Walker, R.G., 1992. Deposition and interpretation of long, narrow sandbodies underlain by a basinwide erosion surface: Cardium Formation, Cretaceous Western Interior Seaway, Alberta, Canada. Journal of Sedimentary Research, vol. 62, no. 2, p. 292 – 309.

Pavich, M.J. and Obermeier, S.F., 1985. Saprolite formation beneath coastal plain sediments near Washington, D.C. Bulletin of the Geological Society of America, vol. 96, p. 886-900.

Pemberton, S.G., and Frey R.W., 1984. Ichnology of a storm-influenced shallow-marine sequence: Cardium Formation (Upper Cretaceous) at Seebee, Alberta. *In* D.F. Stott and D.J. Glass, eds., The Mesozoic of middle North America. Canadian Society of Petroleum Geologists Memoir 9, p. 281 – 304.

Peterson, J.A., 1972. Jurassic System. *In* Geologic Atlas of the Rocky Mountains: Rocky Mountain Association of Geologists, p. 177-189.

Plint, A.G., 1988. Sharp-based shoreface sequences and "offshore bars" in the Cardium Formation of Alberta: their relationship to relative changes in sea level. *In* C.K. Wilgus, B.S. Hastings, C.G. Kendall, H.W. Posamentier, C.A. Ross, and J.C. Van Wagoner, eds., Sea Level Changes – An Intergral Approach, Society of Paleontologists and Mineralogists Special Publication no. 42, p. 357 – 370.

Plint, G. A, Eyles, N., Eyles, C., and Walker, R. G., 1992, Control of sea level change. *In* R.G. Walker and N.P. James, eds., Facies Models - Response to Sea Level Change, Geological Association of Canada, p. 15 – 25.

Podruski, J.A., 1988, Contrasting character of the Peace River and Sweetgrass arches, Western Canada Sedimentary Basin, Canada, Geoscience Canada, vol. 15, p. 94 - 97.

Posamentier, H.W. and Allen, G.P., 1993. Variability of the sequence stratigraphic model: effects of local basin factors. Sedimentary Geology, vol. 86, p. 91-109.

Poulton, T.P., 1984, Upper Absaroka to Lower Zuni: The transition to the foreland basin. *In* D.F. Stott, and D.J. Glass, eds., The Mesozoic of Middle North America. Canadian Society of Petroleum Geology, Memoir 9, p. 233 - 267.

Poulton, T.P., 1989. Upper Absaroka to Lower Zuni: the transition to the foreland Basin. *In* Brian D. Ricketts, ed., Western Canada Sedimentary Basin. A case history. Canadian Society of Petroleum Geologists, p. 233 – 247.

Price, R.A., 1981. The Cordilleran thrust and fold belt in the southern Canadian Rocky Mountains. *In* K.R. McClay and N.J. Price, eds., Thrust and nappe tectonics: Geological Society of London Special Publication 9, p. 427 – 448.

Price, R.A., Monger, J.W.H., and Roddick, J.A., 1985. Cordilleran cross-section: Calgary to Vancouver, trip 3. *In* D. Templeman-Kluit, ed., Field guides to geology and mineral deposits in the southern Canadian Cordillera. GSA Cordilleran Section Meeting, Vancouver, British Columbia, Geological Association of Canada Special paper 6, p. 7 – 25.

Radella, F.A. and Galuska, G.R., 1966. The Swift Formation of Flat Coulee field Liberty County, Montana. *In* S.E. Cox, ed., Jurassic and Cretaceous Stratigraphic Traps, Sweetgrass Arch Symposium, Billings Geological Society 17th annual field conference guidebook, p. 202 – 219.

Reineck, H.-E. and Singh, I.B., 1980. Depositional Sedimentary Environments. 2nd ed., New York, Springer Verlag, 549 p.

Retallack, G.J., 1983. Late Eocene and Oligocene paleosols from Badlands National Park, South Dakota. Geological Society of America Special Paper no. 193.

Retallack, G.J., 1985. Fossil soils as grounds for interpreting the advent of large plants and animals on land. Philosophical Transactions of the Royal Society of London, vol. B309, p. 93 – 259.

Retallack, G.J., 1988. Field recognition of paleosols. *In* J. Reinhart and W.R. Sigleo eds., Paleosols and weathering through geologic time: principles and applications. Geological Society of America Special Paper no. 216, p.1-20.

Retallack, G.J., 1990. Soils of the Past. An Introduction to paleopedology. Unwin Hyman, 520 p.

Roddick, J.A., 1983. Geophysical review and composition o the Coast Plutonic Complex, south of latitude 55° N. *In* Circum-Pacific Plutonic Terranes. Geological Society of America, Memoir159, p. 195 – 212.

Ross, G.M., Parrish, R.R., Villeneuve, M.E., and Bowring, S.A., 1991. Geophysics and geochronology of the crystalline basement of the Alberta Basin, western Canada. Canadian Journal of Earth Science, vol. 28, p. 512 – 522.

Rudkin, R.A., 1964. Lower Cretaceous. *In* R.G. McCrossan and R.P. Glaister, eds., Geological history of Western Canada. Calgary, Alberta, Alberta Society of Petroleum Geologists, p. 157 – 168.

Sawatsky, H.B., 1976. Two probable Late Cretaceous astroblemes in western Canada – Eagle Butte, Alberta and Dumas, Saskatchewan. Geophysics, vol. 41 no. 6, p. 1261 – 1271.

Silbering, N.L. and Jones, D.L., 1987. Lithotectonic terrane maps of the North American Cordillera. United States Geological Survey Miscellaneous Field Studies Maps 1874 A,B,C,D, scale 1:2,500,000.

Sloss, L.L., 1963, Sequences in the cratonic Interior of North America. Geological Society of America Bulletin, vol. 74, p. 93 -114.

Stockmal, G.S., Cant, D.J., and Bell, J.S., 1992. Relationship of the stratigraphy of the Western Canada foreland basin to Cordilleran tectonics: insights from geodynamic models. *In* R.W. Macqueen and D.A. Leckie, eds., Foreland Basins and Fold Belts American Association of Petroleum Geologists Memoir 55, p. 107 – 124.

Stott, D.F., 1968. Lower Cretaceous Bullhead and Fort St. John groups between Smoky and Peace rivers, Rocky Mountain Foothills, Alberta and British Columbia. Geological Survey of Canada Bulletin 152, 279 p.

Stott, D.F., 1973. Lower Cretaceous Bullhead Group between Bullmoose Mountain and Tetsa River, Rocky Mountain Foothills, northeastern British Columbia. Geological Survey of Canada Bulletin 219, 228 p.

Stride, A.H., Belderson, R.H., Kenyon, N.H., and Johnson, M.A., 1982. Offshore tidal deposits: sandsheets and sandbank facies. *In* A.H. Stride, ed., Offshore Tidal Sands: Processes and Deposits, Chapman and Hall, New York, p. 95 – 125.

Swift, D.J.P., Stanley, D.J., and Curray, J.R., 1971. Relict sediments on continental shelves: a reconsideration. Journal of Geology, vol. 79, p. 322 – 346.

Tanner, P.W.G.,1998. Interstratal dewatering origin for polygonal patterns of sand-filled cracks: a case study from late Proterozoic metasediments of Islay, Scotland. Sedimentology, vol. 45, p. 49 – 89.

Tempelman-Kluit, D.J., 1979. Transported cataclasite, ophiolite and granodiorite in Yukon: evidence of arc-continent collision. Geological Survey of Canada Paper 79-14, 27 p.

Tipper, H.W., 1981. Offset of an upper Pliensbachian geographic zonation in the North American Cordillera by transcurrent movement. Canadian Journal of Earth Science, vol. 18, p. 1788 - 1792.

Tovell, W.M., 1958. The development of the Sweetgrass Arch, southern Alberta. Geological Association of Canada Proceedings, vol. 10, p. 19 – 30.

Twichwell, D.C., 1983. Bedforms distributions and inferred sand transport on Georges Bank, United States Atlantic continental shelf. Sedimentology, vol. 30, p. 295 – 710.

Van Wagoner, J.C., Mitchum, R.M., Campion, K.M., and Rahmanian, V.D., 1990. Siliciclastic sequence stratigraphy in well logs, cores, and outcrops: concepts for high-resolution correlation of time and facies, American Association of Petroleum Geologists Methods in Exploration Series, no. 7, 55 p.

Walker, R.G., 1984. Shelf and shallow marine sands. *In* R.G. Walker, ed., Facies Models. Geoscience Canada, reprint series 1, second edition, p. 141 – 169.

Walker, R.G. and Bergman, K.M., 1993. Shannon Sandstone in Wyoming. A shelf-ridge complex reinterpreted as lowstand shoreface deposits. Journal of Sedimentary Petrology, vol. 63, no. 5, p. 839 – 851.

Walker, R.G. and Plint, A.G., 1992. Wave-and Storm- Dominated Shallow Marine Systems. *In* R.G. Walker and N.P. James, eds., Facies Models: Response to Sea Level Change, Geological Association of Canada, p. 219-238.

Walker, R.G. and Wiseman, T.R, 1995. Lowstand shorefaces, transgressive incised shorefaces, and forced regressions: examples from the Viking Formation, Joarcam Area, Alberta. Journal of Sedimentary Research, vol 65B, no. 1, p. 132 – 141.

Weir, J.D., 1949. Marine Jurassic formations of southern Alberta Plains. American Association of Petroleum Geologists Bulletin, vol. 33, p. 547 – 563.

Wightman, D.M., Pemberton, S.G., and Singh, C., 1987. Depositional modeling of the upper Mannville (Lower Cretaceous), east central Alberta: implications for the recognition of brackish water deposits. *In* Reservoir Sedimentology. Society of Economic Mineralogists and Paleontologists Special Publication 40, p. 151-181.

Wright, G.N, McMechan, M.E., and Potter, D.E.G., 1994. Structure and architecture of the Western Canada Sedimentary Basin. *In* G.D. Mossop and I. Shetsen comps., Geological Atlas of the Western Canada Sedimentary Basin. Canadian Society of Petroleum Geology and Alberta Research Council, p. 25 – 40.

Appendix 1

Stratigraphic Columns and Miscellaneous Lithological Data

Wells	Cored depth	Observed Lithologies	General Comments
Township 1			
16-6-1-8w4	3092 - 3120'	Dark and light ribbon sandstone and Basal Quartz sandstone	
6-7-1-8w4	928 - 935.5m	Dark and light ribbon sandstone	
6-8-1-8w4	3156 - 3208'	Rierdon, shale member, dark and light ribbon sandstone, BQ	1" core
5-17-1-8w4	2866 - 3167'	Rierdon, D. and sandy D. Swift, L. Swift, Jurassic paleosol, "A"	1" core
9-17-1-8w4	2930 - 3018' & 3190 - 3264'	Rierdon, Swift shale member, D. Swift, L. Swift, paleosol, "A"	1" core
6-29-1-8w4	3060 - 3088m	Swift shale member, 4' Light Swift, "A" sandstone	
6-32-1-8w4	915 - 933m	Dark and light ribbon sandstone	
16-29-1-9w4	2900 - 3074' & 3153 - 3161'	Dark Swift, Swift Fluvial, Light Swift	1" core
11-34-1-9w4	2971 - 2991'	rooted? siltstone - BQ sandstone	
16-5-1-10w4	872 - 881m	Rierdon, Swift shale member, Light Swift, paleosol, "A"	
6-36-1-10w4	2810 - 2832'	Light Swift	
Township 2			
16-5-2-5w4	1012 - 1021m	Dark ribbon sandstone, fines up	3" core
2/15-15-2-7w4	825.25 - 843.5 m	Light ribbon sandstone, paleosol, BQ sandstone	4" slabbed, rec. 11.75m
11-6-2-8w4	2940 - 3220'	Rierdon Shale, dark and light ribbon sandstone, Jur? paleosol	1" core
7-29-2-8w4	2818.5 - 2760'	Dark and light ribbon sandstone, BQ sandstone	
6-31-2-8w4	2565 - 2630'	Light ribbon sandstone, Swift sandstone, BQ sandstone	
14-25-2-10w4	2645 - 2572'	Rierdon, shale member, dark and light ribbon sandstone, BQ	1" core
Township 3			
12-14-3-5w4	1041.2 - 1052m	Dark and light ribbon sandstone, paleosol, BQ sandstone	slabbed core
14-31-3-5w4	938.3 - 999.3m	Dark and light ribbon sandstone, BQ sandstone	
16-32-3-5w4	1004.5 - 1023.5m	Dark and light ribbon sandston, Jurassic? and Cretaceous? paleosols	
7-34-3-5w4	1045 - 1054m	Dark ribbon sandstone	
6-15-3-6w4	3078 - 3080'	Dark and light ribbon sandstone, Jurassic? and Cretaceous? paleosols	
10-20-3-7w4	2875 - 2879'	Dark ribbon sandstone, glauconitic mudstone, BQ sandstone	logged boxes 7 - 9; 1" core
10-28-3-7w4	2870 - 2930'	Dark ribbon sandstone, mudstone, paleosol, "A" sandstone	
11-4-3-8w4	2775 - 2825'	Dark and light ribbon sandstone, BQ sandstone, floodplain deposits?	only logged boxes 7 - 12
10-8-3-8w4	2745 - 2845'	Dark and light ribbon sandstone, paleosol, BQ	slabbed
6-11-3-9w4	2685 - 2732'	Light ribbon sandstone, BQ sandstone	
6-19-3-9w4	2772 - 2783'	Light ribbon sandstone, BQ sandstone	
Township 4			
10-9-4-4w4	1102.8 - 1107.6m	Dark and light ribbon sandstone, Jurassic? Cretaceous? paleosol, BQ	
8-22-4-4w4	1053.6 - 1071.6m	Dark and light ribbon sandstone, BQ sandstone with coal seam	
6-30-4-4w4	1078.5 - 1094m	Dark and light ribbon sandstone, BQ sandstone	
8-4-4-5w4	1032 - 1050m	Dark and light ribbon sandstone, paleosol	
6-11-4-5w4	1040 - 1042.75m	Floodplain deposits, BQ sandstone	slabbed and plugs tested
14-14-4-5w4	1073 - 1086m	Dark and light ribbon sandstone, BQ sandstone	
8-23-4-5w4	1123 - 1132m	Dark and light ribbon sandstone, BQ sandstone	slabbed 3" core
8-35-4-5w4	1050 - 1067m	Dark and light ribbon sandstone, paleosol	slabbed

3-2-4-6w4	947 - 965m	Rierdon shale, shale member, Dark and light ribbon sandstone	
2/6-16-4-6w4	905 - 923m	Lacustrine? BQ sandstone	
6-2-4-7w4	2879 - 2900'	Sandy Swift, dak ribbon sandstone, more sandy Swift	
7-6-4-7w4	2750 - 2808'	Dark ribbon sandstone, BQ, Lacustrine	slabbed and plugs tested
10-7-4-7w4	2814 - 2853'	Dark and light ribbon sandstone , Jurassic?, Cretaceous? paleosol, BQ	
6-1-4-9w4	2852 - 2883'	Dark and light ribbon sandstone, BQ sandstone	
2/10-8-4-9w4	2924 - 2880'	BQ sandstone, mudstone (floodplain deposits?)	
Township 5			
14-9-5-4w4	1173.3 - 1181.7m	paleosol, BQ, mudstone. NO SWIFT	
15-29-5-4w4	1214 - 1232.25m	Rierdon shale, Light ribbon sandstone, paleosol	
10-31-5-4w4	1212 - 1225m	Rierdon shale, dark and light ribbon sandstone, BQ sandstone	
6-35-5-4w4	4258 - 4300'	Light ribbon sandstone, BQ sandstone	
4-1-5-5w4	1063 - 1081'	Dark and light ribbon sandstone, BQ sandstone	
16-1-5-5w4	1120 - 1134m	Dark and light ribbon sandstone, BQ sandstone	
7-13-5-5w4	1119 - 1143m	Dark and light ribbon sandstone, rubbly Cretaceous paleosol	
10-36-5-5w4	1168 - 1183m	Dark and light ribbon sandstone, pink BQ sandstone	
8-29-5-6w4	940 - 958m	Dark and light ribbon sandstone , sandy Swift, BQ sandstone	
6-34-5-6w4	968 - 986m	Dark and light ribbon sandstone, sandy Swift	
Township 6			
10-5-6-4w4	1290 - 1311.8m	Rierdon shale, BQ sandstone	
16-4-6-5w4	1074.5 - 1083.5m	Light ribbon sandstone , BQ sandstone	
14-5-6-5w4	1055 - 1091m	Rierdon shale, dark and light ribbon sandstone	slabbed and plugs
6-1-6-6w4	1040 - 1051m	Shale member, dark ribbon sandstone	
2/6-2-6-6w4	1021 - 1030m	Dark and light ribbon sandstone, BQ sandstone	
6-12-6-6w4	1051 - 1069m	Dark and light ribbon sandstone , BQ sandstone	
11-21-6-6w4	1045 - 1064m	BAT sandstone	
8-34-6-6w4	1147 - 1163m	Shale member, dark and light ribbon sandstone, coal, paleosol	
13-5-6-7w4	2970 - 2995'	sandy Light Swift, BQ sandstone, paleosol	
15-22-6-7w4	3135 - 3158'	BQ? NO SWIFT	1" core
9-29-6-7w4	2392 - 2450'	fining up sandy succession, Cretaceous	mud coated 1" core
6-31-6-8w4	3067 - 3090'	Rierdon shale, Horsefly sandstone	1" core
Township 7			
6-23-7-3w4	4650 - 4700'	Dark and light ribbon sandstone	
10-4-7-8w4	3060 - 3054'	Rierdon Shale, BQ sandstone	
4-28-7-9w4	931 - 936	paleosol, BQ sandstone	Cores 3 & 4
Township 8			
6-1-8-4w4	4052 - 4101'	Dark and light ribbon sandstone, BQ	
6-27-8-9w4	900 - 917.25m	Rierdon shale, BQ sandstone, mudstone	logged to 907m
Township 9			
14-19-9-7w4	925 - 934m	BQ sandstone	
6-31-9-7w4	890 - 905m	paleosol, BQ sandstone	

LEGEND

LITHOLOGY

⛆ SAND/SANDSTONE

⛆ SILT/SILTSTONE

⛆ sandy silt

▤ SHALE/MUDSTONE

▤ silty shale

CONTACTS

——— Sharp

〰〰〰 Scoured

ssssssss Bioturbated

PHYSICAL STRUCTURES

⌣ - Trough Cross-strat.

≈ - Wavy Parallel Bedding

∿ - Convolute Bedding

⇅ - Slickensides

⌒ - Combined-Flow Ripples

»»» - Herringbone Cross-strat.

@ - Chaotic Bedding

≡ - Quasi-planar lamination

≂ - Hummocky Cross-strat.

ℿ - Synaeresis Cracks

LITHOLOGIC ACCESSORIES

······· - Sand Lamina

Sid - Siderite

Py - Pyrite

Lth - Lithoclasts

- - - - - Shale Lamina

Gl - Glauconitic

▰▰▰ - Rip Up Clasts

■ - -Carbonaceous shale clasts

●●●● - Pebbles/Granules

Kaol - Kaolinitic

-■-■- - Coal Fragments

▭▭▭ - -Carbonaceous lamina

ICHNOFOSSILS

⽕ - Rootlets

U - Arenicolites

⊠ - Chondrites

0 - Skolithos

≋ - Escape Trace

8 - Teichichnus

⊂⊃ - Planolites

Ϙ - Cylindrichnus

ᗰ - Helminthopsis

FOSSILS

⌄ - Brachiopods

⊖ - Molluscs (undifferentiated)

⋈ - Fish Remains

@ - Cephalopods

Ⓣ - Fish Scales

BIOTURBATION

■ Abundant

■ Common

■ Moderate

■ Rare

□ Barren

CMG Black Butte

16-6-1-8w4

Remarks: dark ribbon sandstone - altered light ribbon sandstone - Basal Quartz sandstone
Cored Interval 3092 - 3120 ft
Recovered 28 ft

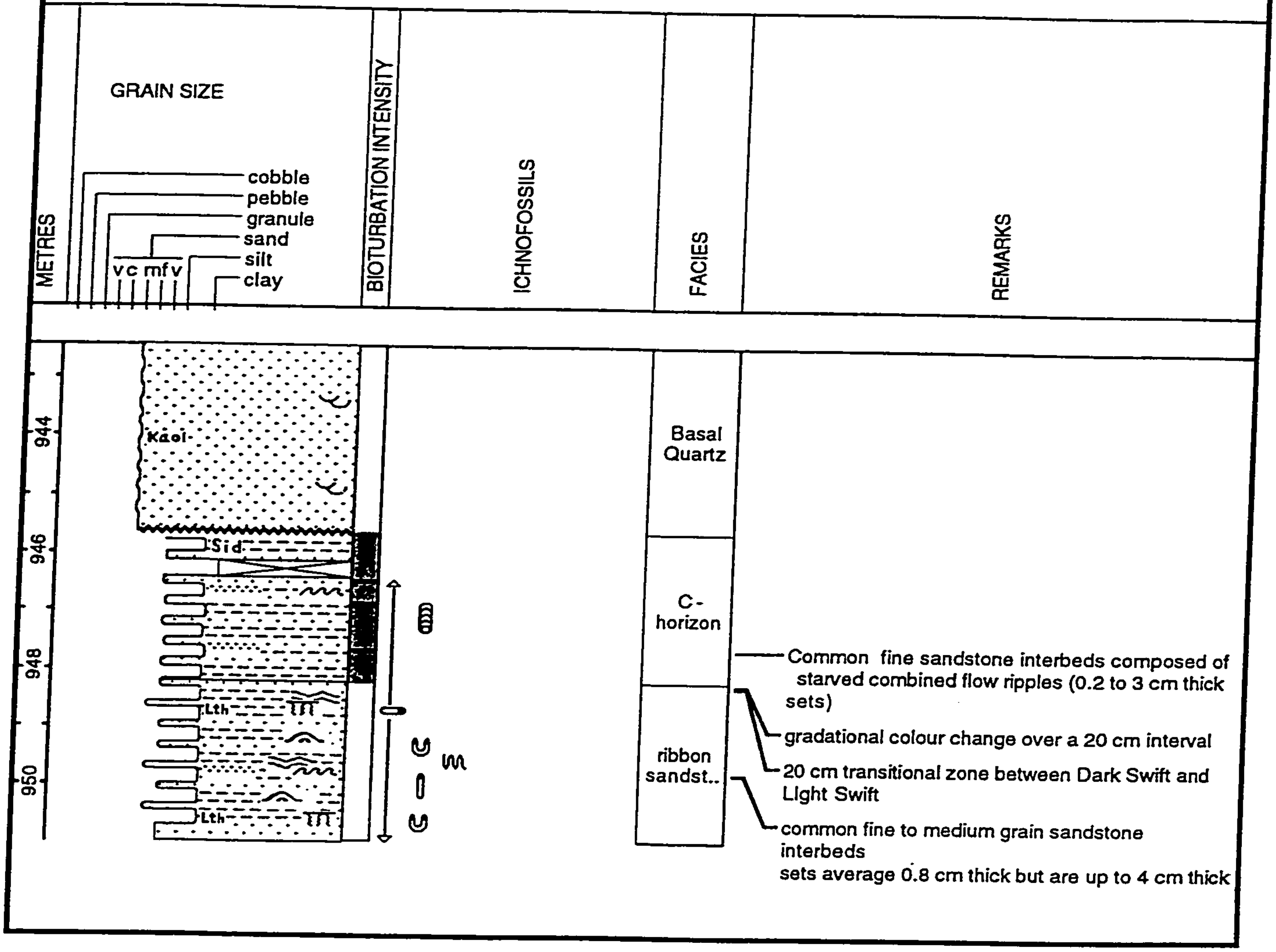

Common fine sandstone interbeds composed of starved combined flow ripples (0.2 to 3 cm thick sets)

gradational colour change over a 20 cm interval

20 cm transitional zone between Dark Swift and Light Swift

common fine to medium grain sandstone interbeds
sets average 0.8 cm thick but are up to 4 cm thick

Roan CMG Black Butte
6-7-1-8w4

Remarks: Dark Swift - Light Swift

Cored interval 928 - 935.5 m
recovered 7.5 m
? boxes

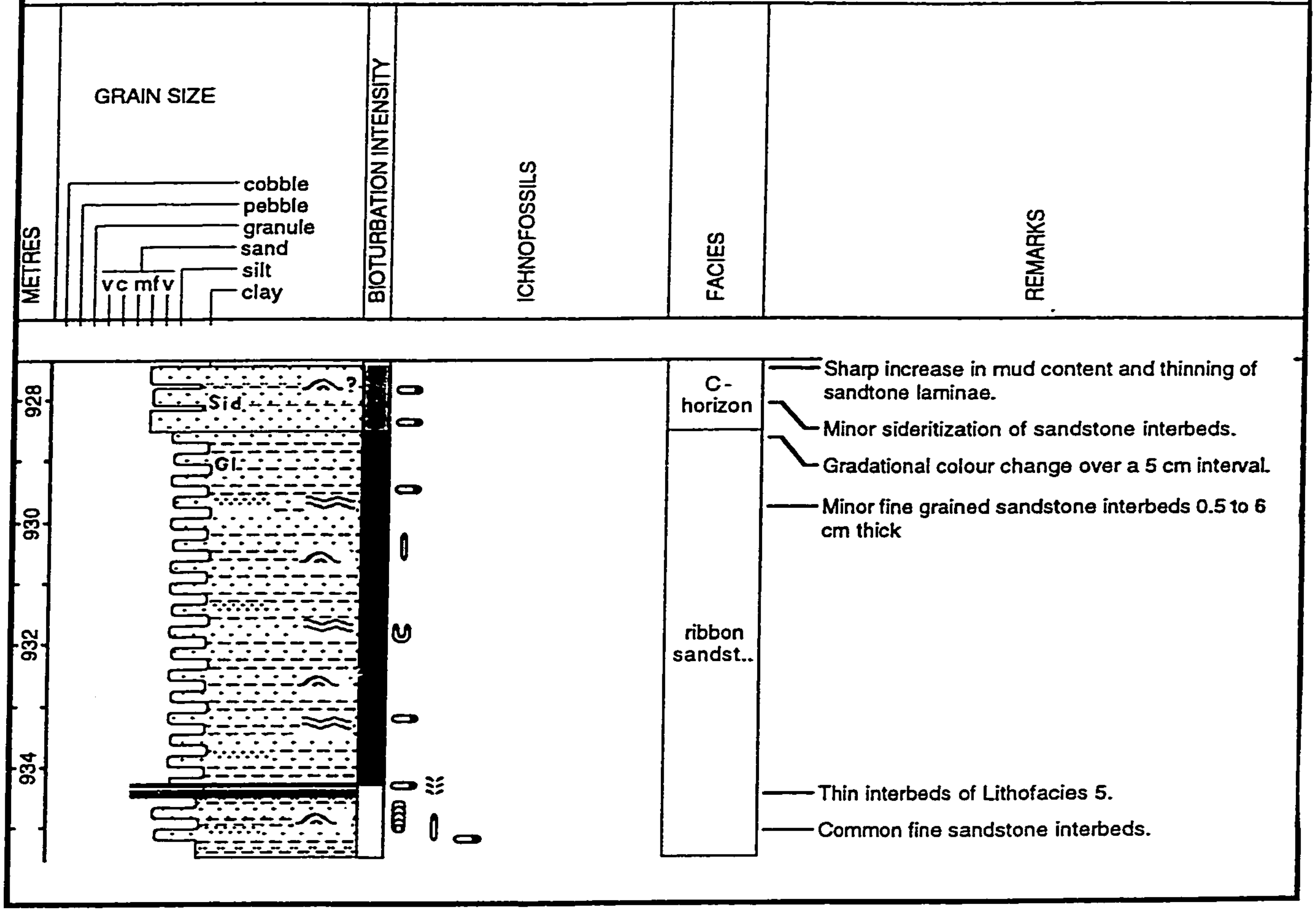

Sharp increase in mud content and thinning of sandtone laminae.

Minor sideritization of sandstone interbeds.

Gradational colour change over a 5 cm interval.

Minor fine grained sandstone interbeds 0.5 to 6 cm thick

Thin interbeds of Lithofacies 5.

Common fine sandstone interbeds.

HB
6-8-1-8w4

Remarks: Wireline core (1")
Cored interval 3156 - 3208
Boxes 2 - 9

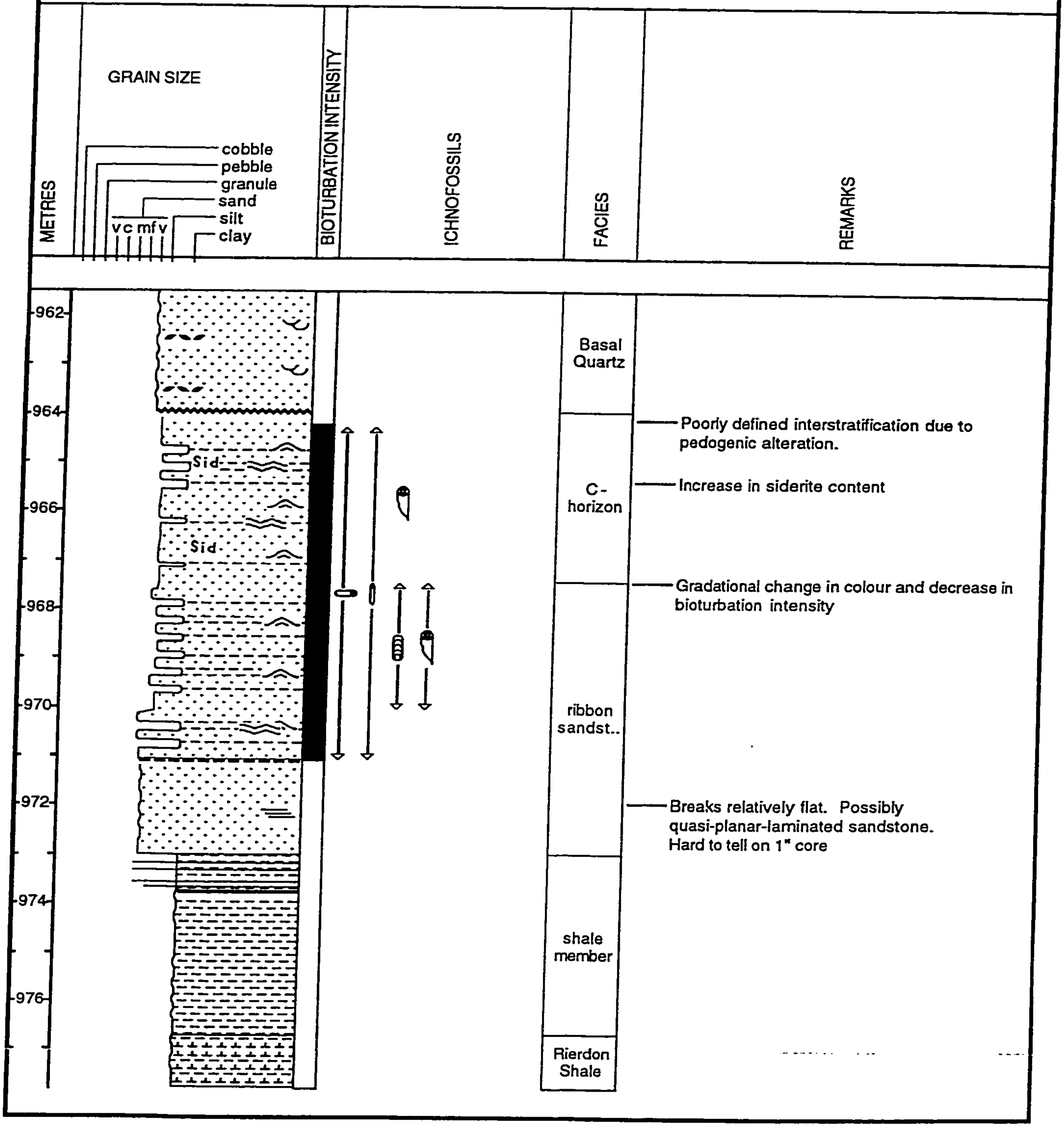

Poorly defined interstratification due to pedogenic alteration.

Increase in siderite content

Gradational change in colour and decrease in bioturbation intensity

Breaks relatively flat. Possibly quasi-planar-laminated sandstone. Hard to tell on 1" core

McColl Union

5-17-1-8w4

Remarks: Wireline core (1")
Cored interval 2866 - 3167' ; boxes 16-28
Rierdon Shale- dark ribbon sandstone (retrogradational stacking pattern) -
altered light ribbon sandstone

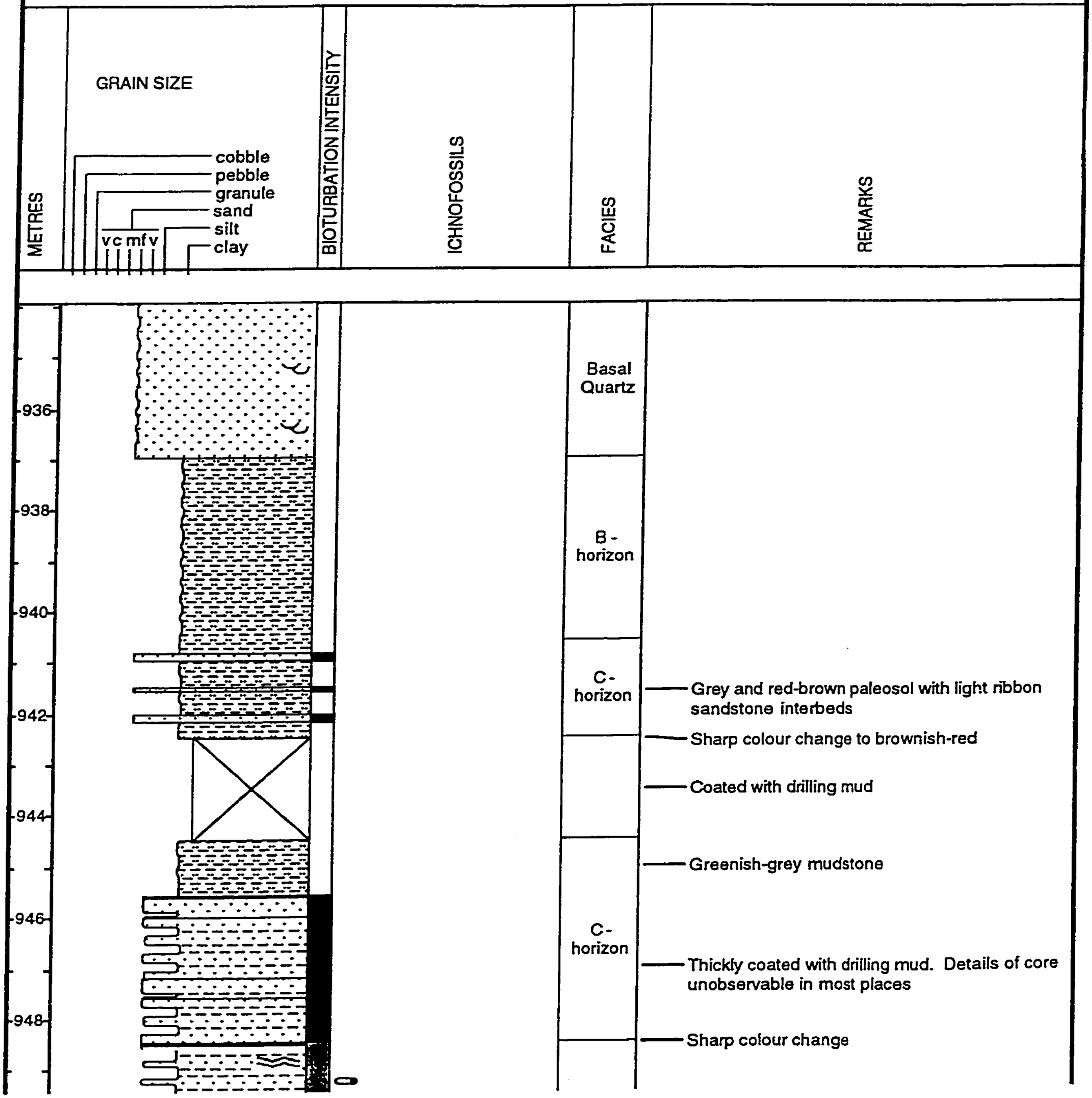

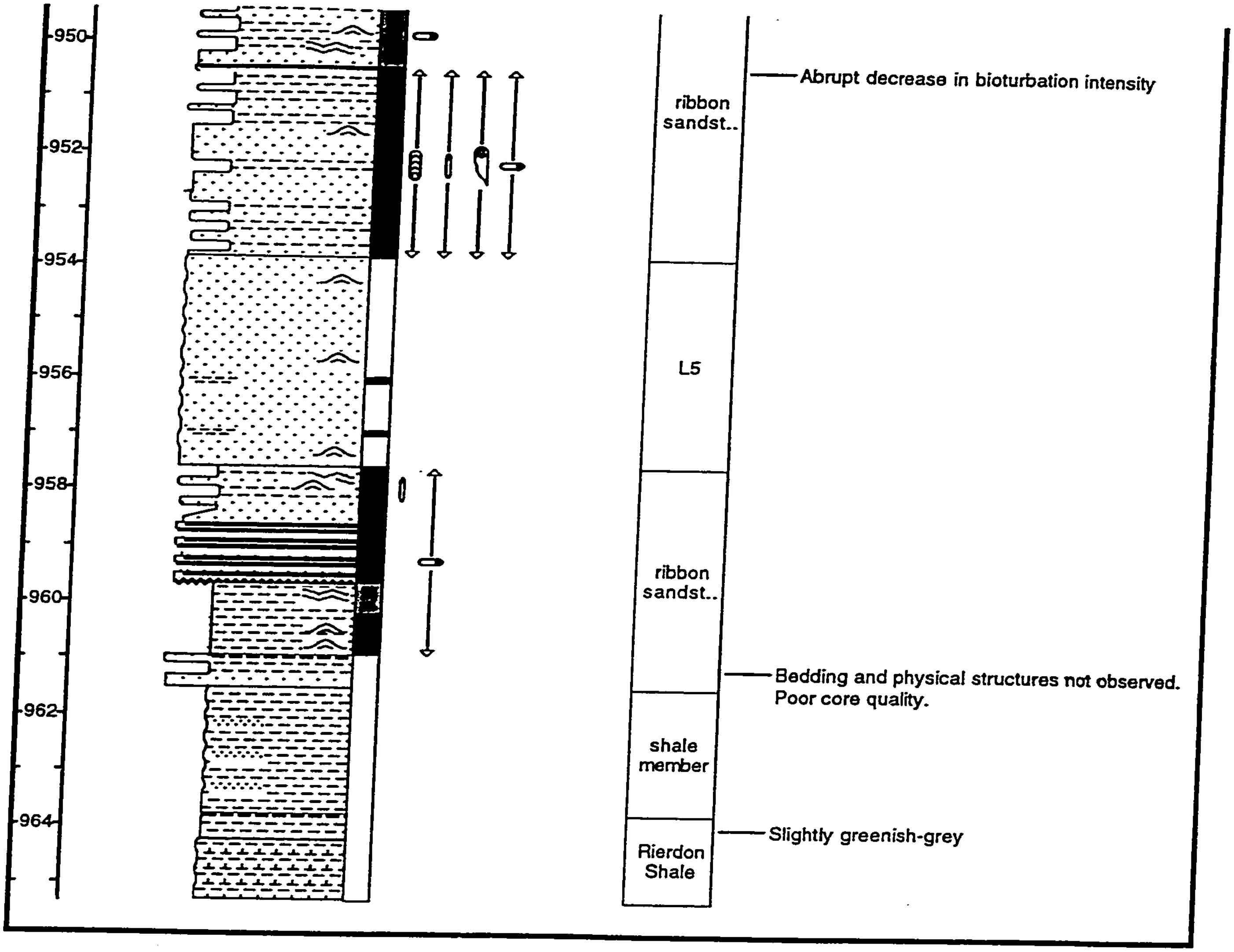
950
952
954
956
958
960
962
964
ribbon sandst..
L5
ribbon sandst..
shale member
Rierdon Shale
Abrupt decrease in bioturbation intensity
Bedding and physical structures not observed. Poor core quality.
Slightly greenish-grey

9-17-1-8w4

Remarks: Wireline core (1") - good condition
Rierdon - shale member - dark ribbon sandstone - light ribbon sandstone - paleosol - Basal Quartz - mudstone.
Cored intervals: 2930 - 3018' (11 boxes) - Swift and BQ
3190 - 3264' (8 boxes) - Rierdon Shale

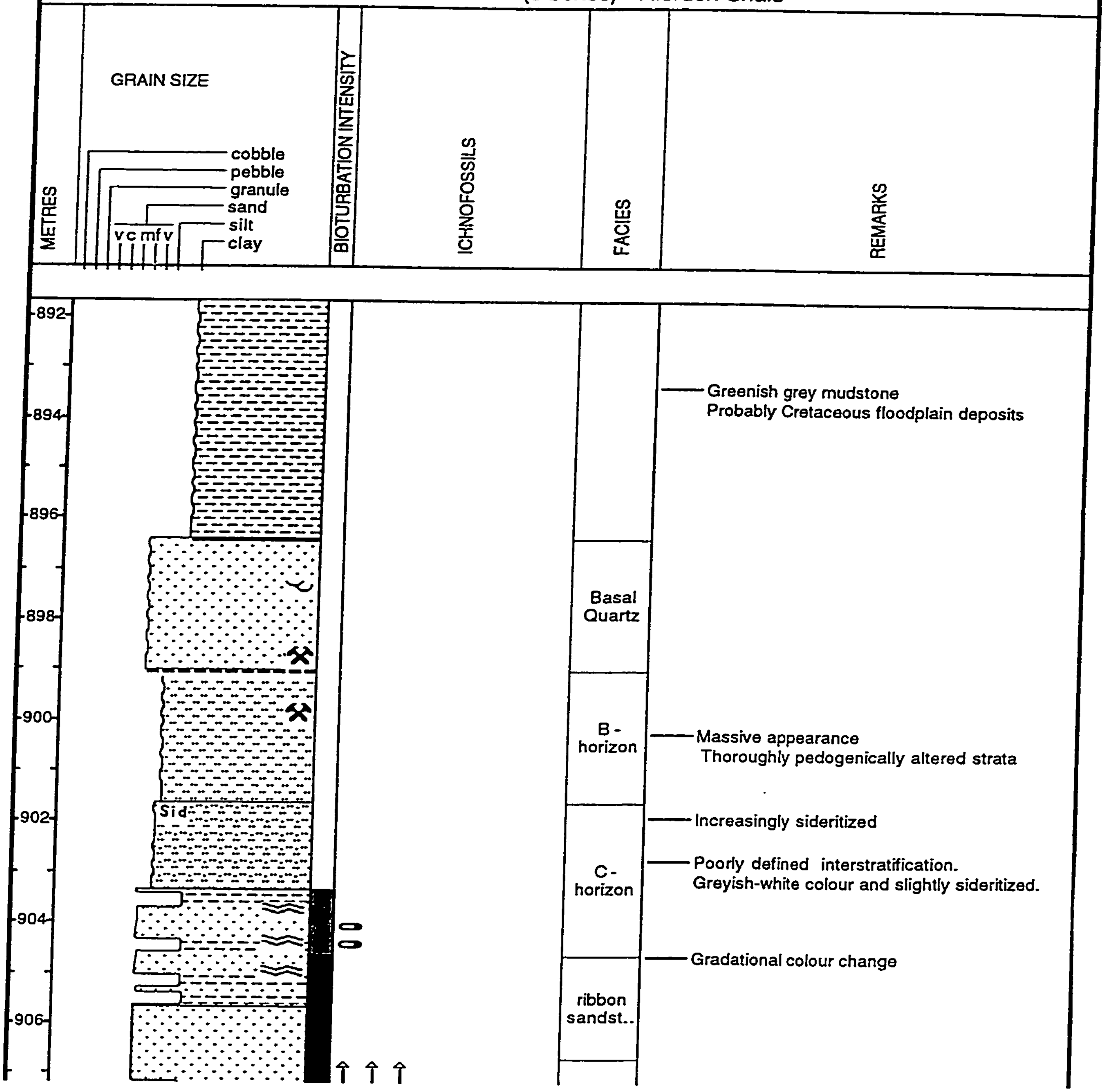

—Greenish grey mudstone
Probably Cretaceous floodplain deposits

—Massive appearance
Thoroughly pedogenically altered strata

—Increasingly sideritized

—Poorly defined interstratification.
Greyish-white colour and slightly sideritized.

—Gradational colour change

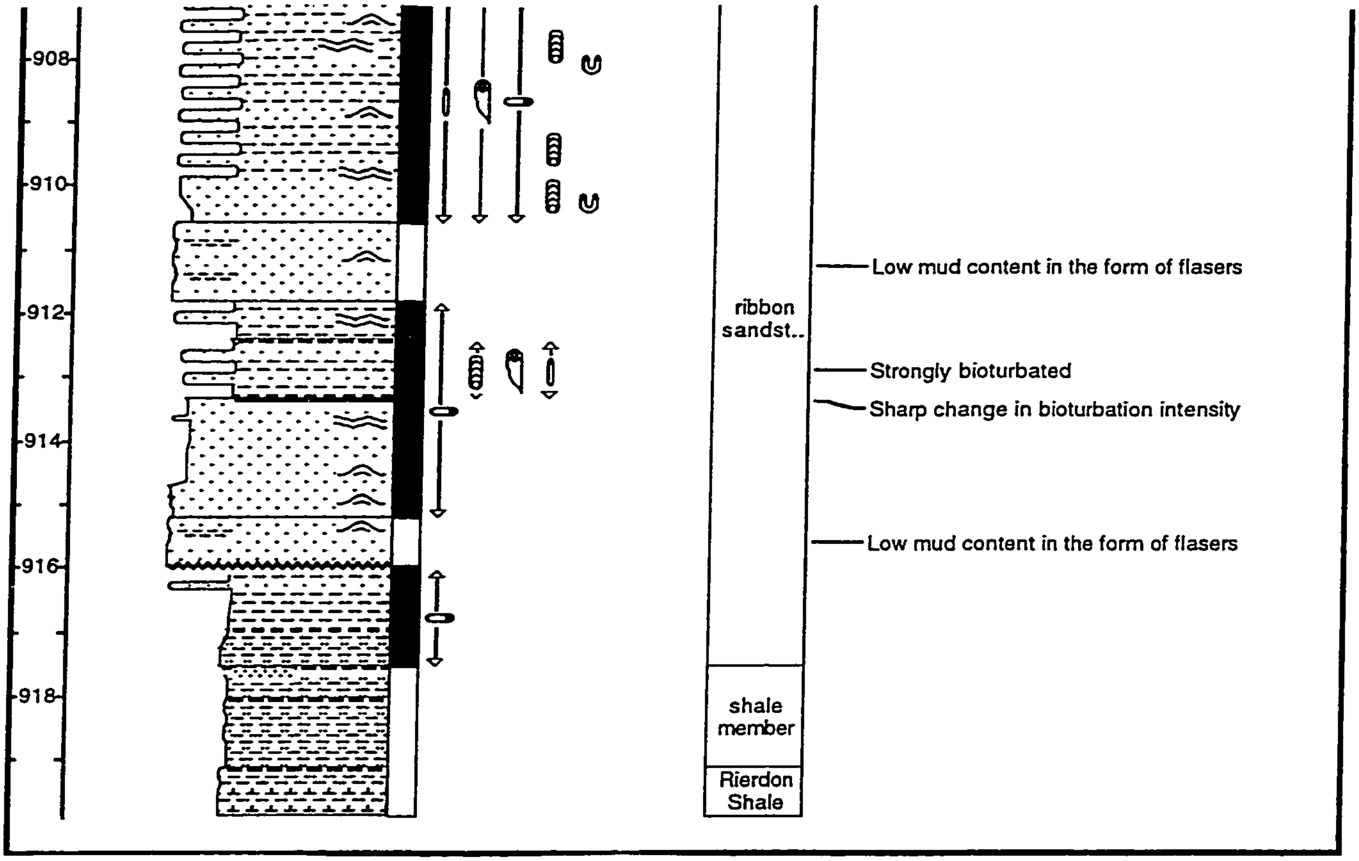
908
910
912
914
916
918
ribbon sandst..
shale member
Rierdon Shale
Low mud content in the form of flasers
Strongly bioturbated
Sharp change in bioturbation intensity
Low mud content in the form of flasers

Canadian Montana gas

6-29-1-8w4

Remarks: (silty mudstone) - paleosol - Basal Quartz
Cored interval: 3060 - 3088' - 7 boxes

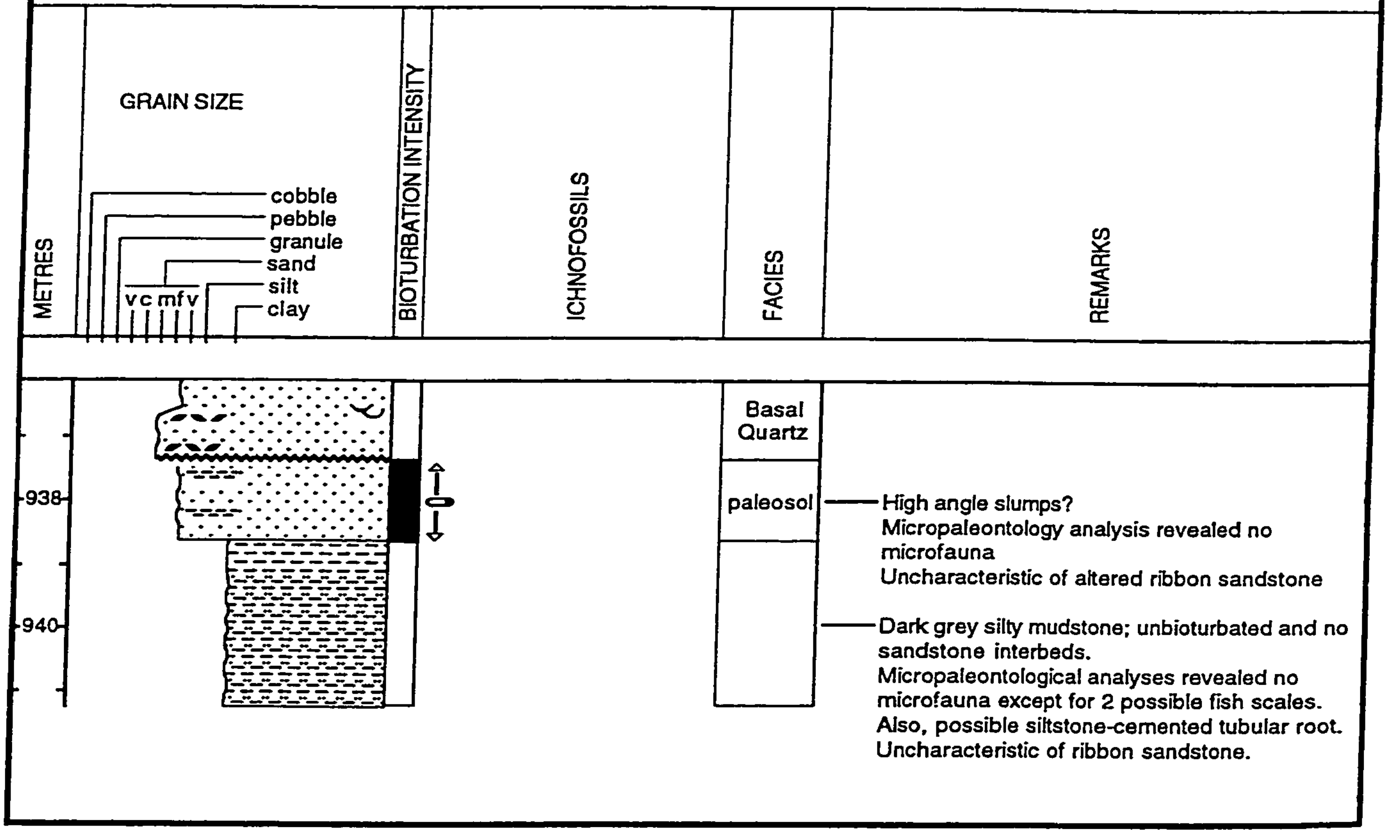

High angle slumps?
Micropaleontology analysis revealed no microfauna
Uncharacteristic of altered ribbon sandstone

Dark grey silty mudstone; unbioturbated and no sandstone interbeds.
Micropaleontological analyses revealed no microfauna except for 2 possible fish scales.
Also, possible siltstone-cemented tubular root.
Uncharacteristic of ribbon sandstone.

N Cont et al.

6-32-1-8w4

Remarks: dark ribbon sandstone - altered light ribbon sandstone - Basal Quartz
Cored interval 915 - 933 m; recovered 18 m
16 boxes - logged boxes 14 to 16

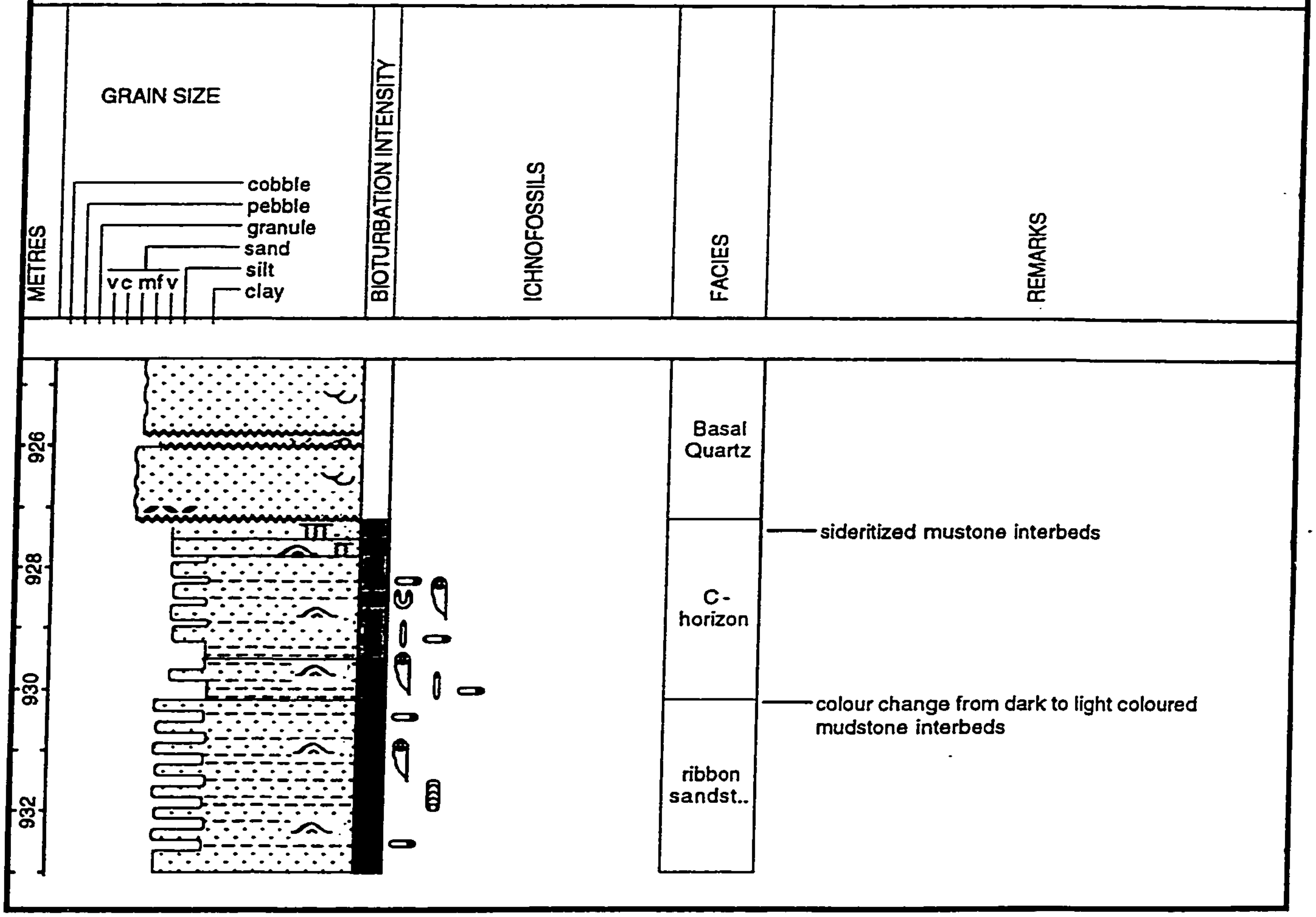

McColl F. Union
16-29-1-9w4

Remarks: Wireline core (1")
dark ribbon sandstone - light ribbon sandstone - Basal Quartz succession with probable channel abandonment
Cored interval 2900-3074' and 3153-3161'

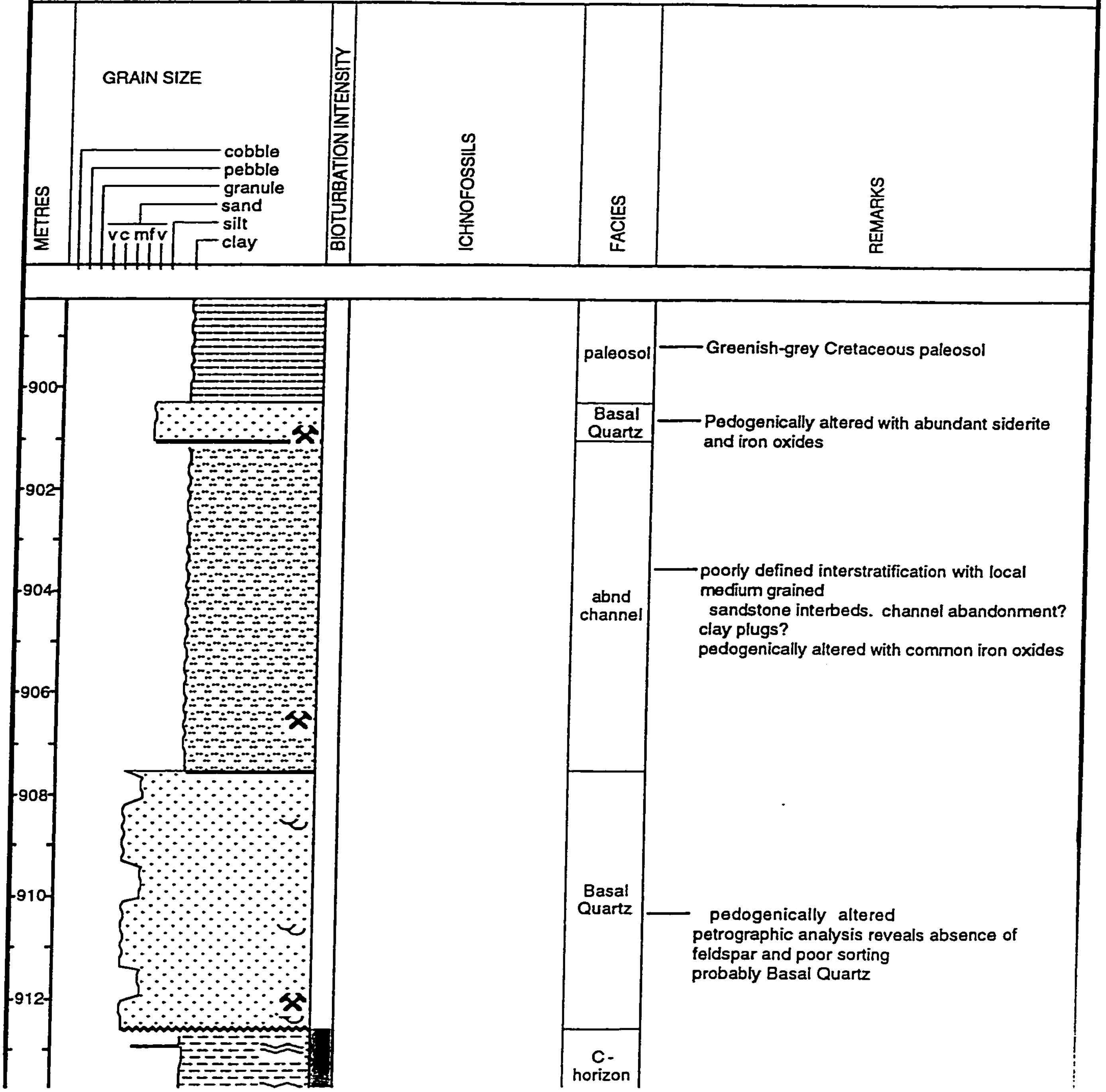

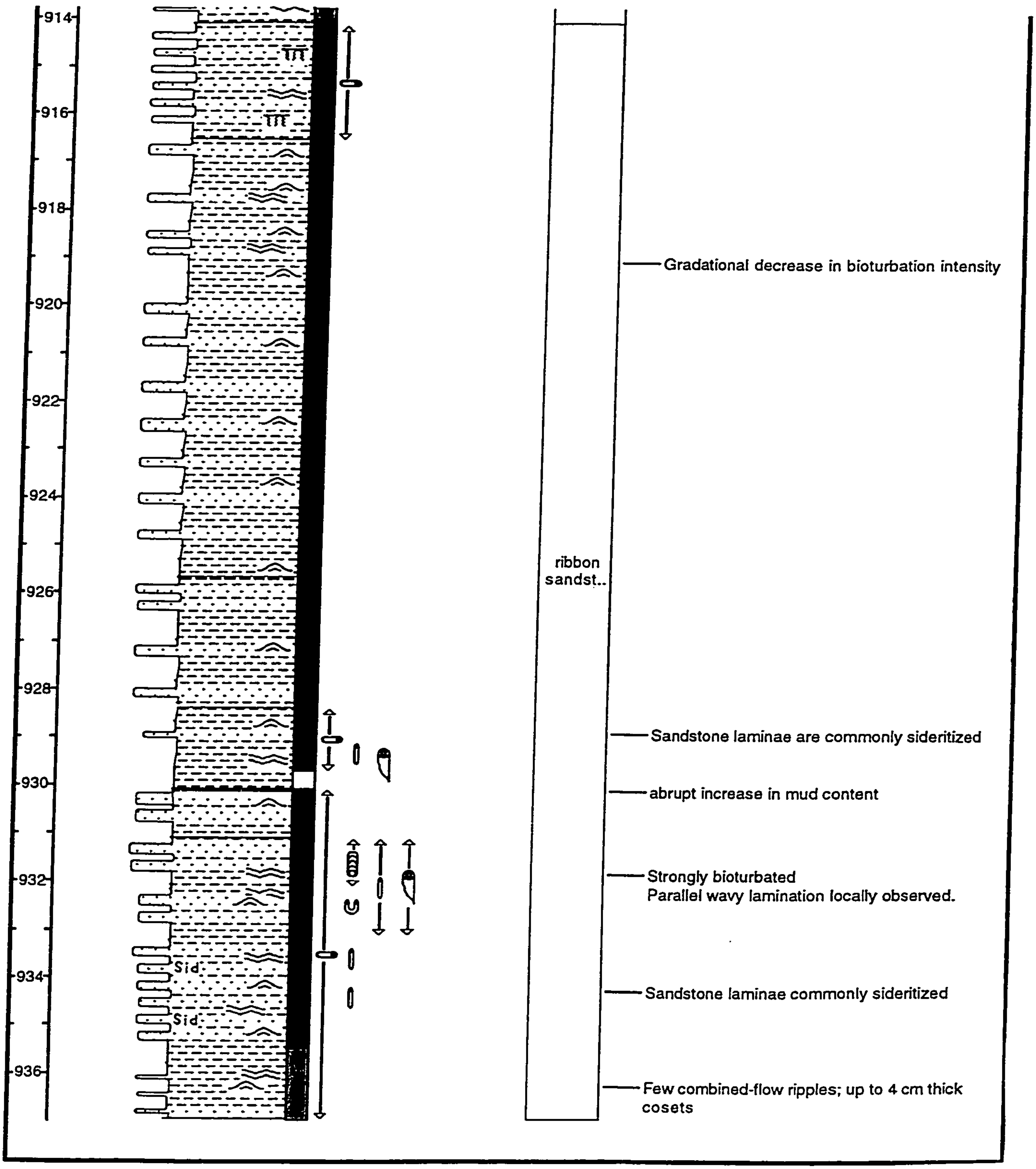

Gradational decrease in bioturbation intensity

Sandstone laminae are commonly sideritized

abrupt increase in mud content

Strongly bioturbated
Parallel wavy lamination locally observed.

Sandstone laminae commonly sideritized

Few combined-flow ripples; up to 4 cm thick cosets

Domtar Mission Knappen

16 -5-1-10w4

Remarks: Rierdon shale, glauconitic shale member? - thin dark ribbon sandstone - altered light ribbon sandstone, channel lag overlain by Basal Quartz sandstone and floodplain paleosols
14 boxes
Cored interval: 866 - 881m
rec. 15.25 m

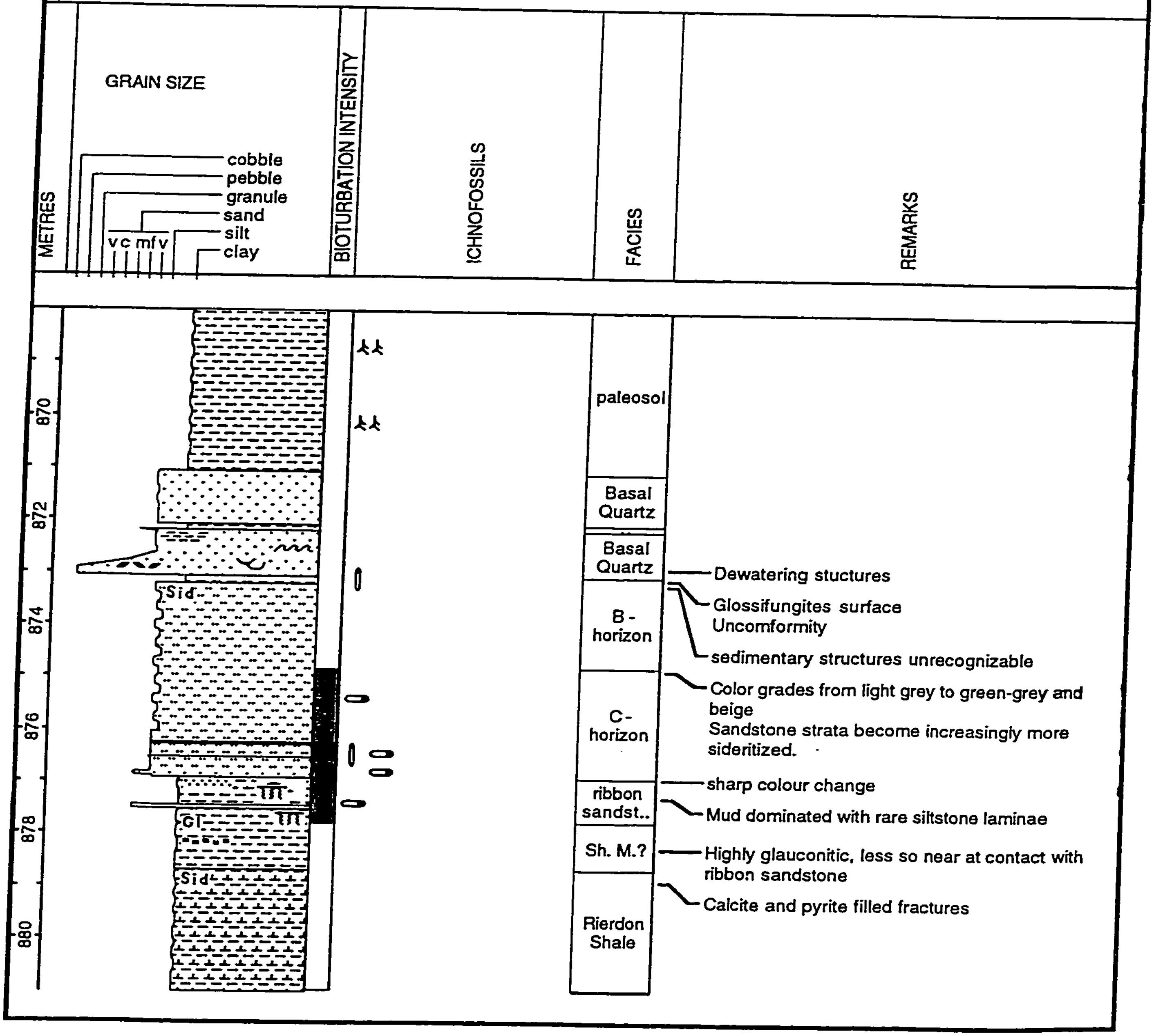

Altex et al. Sapphire
16-5-2-5w4

Remarks: 3" core
Cored interval 1012 - 1021m; recovered 8.66 m; 6 boxes
Dark Ribbon Sandstone

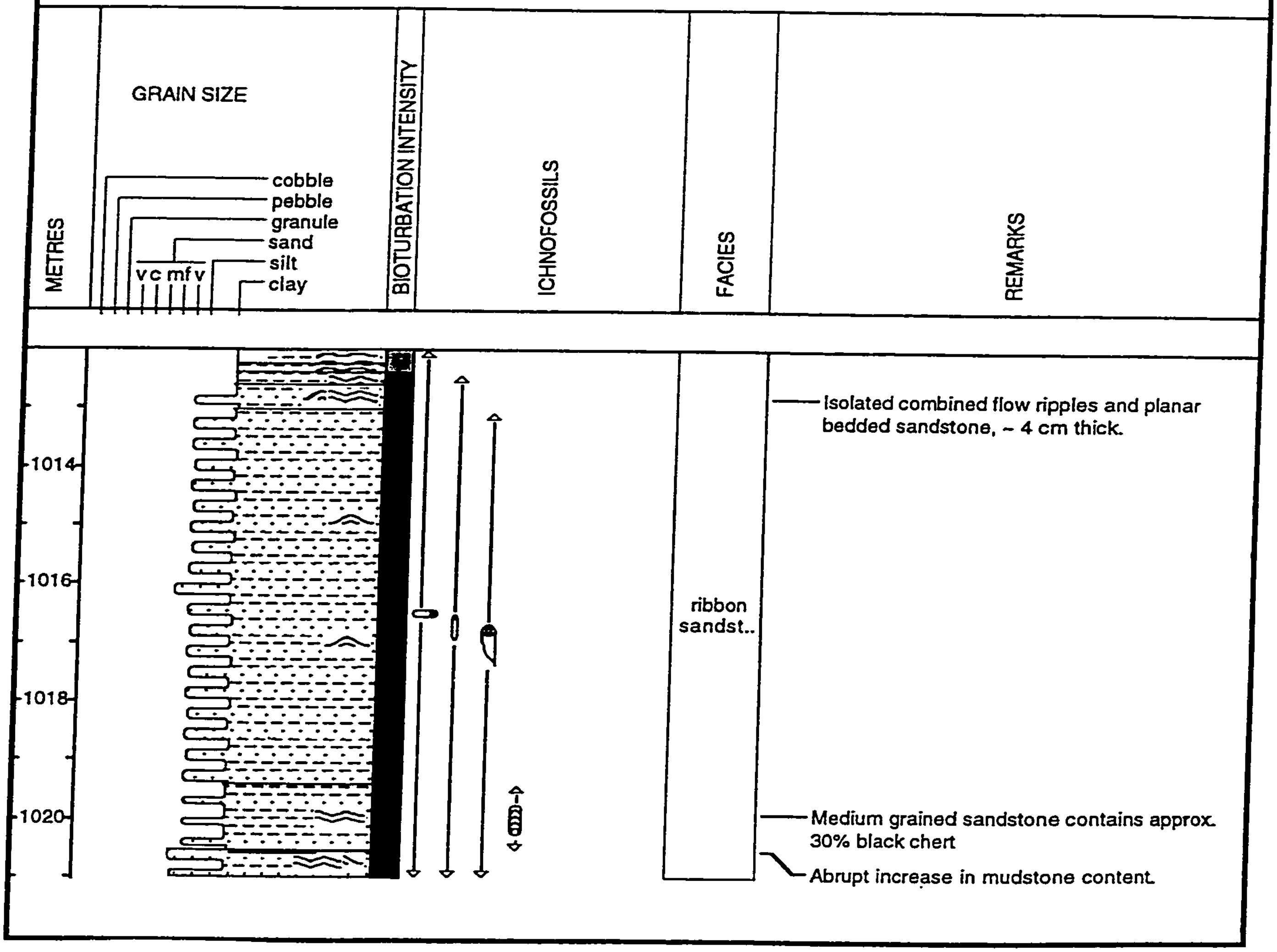

Home Scurry Pendor

15-15-2-7w4

Remarks: light ribbon sandstone - paleosol - Basal Quartz
Cored interval: 825.25 - 843.5m; recovered 11.75m
11 boxes of slabbed 4" core

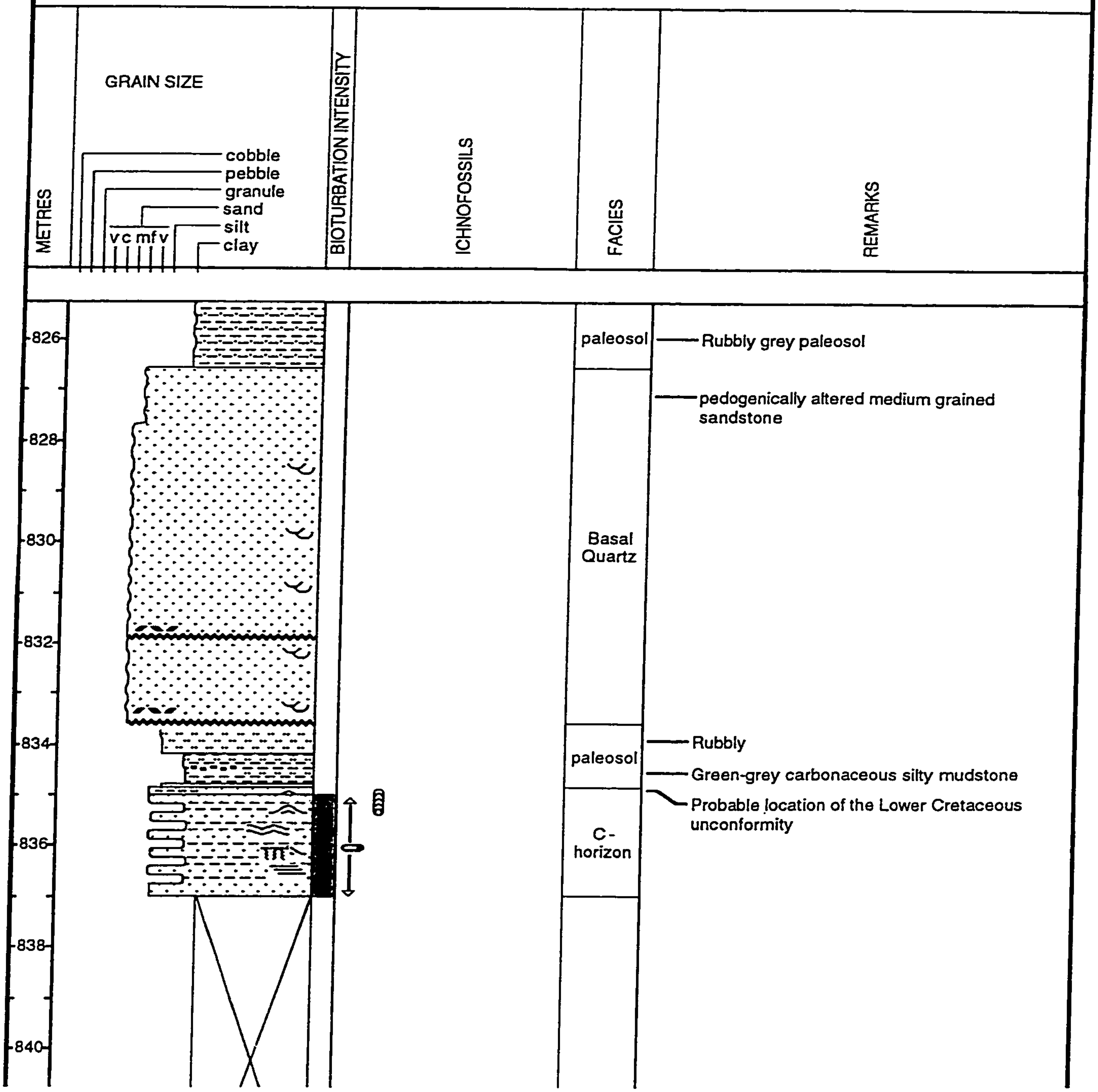

Mc Coll Front Union

11-6-2-8w4

Remarks: wireline core (1")
Rierdon Shale- dark ribbon sandstone - altered light ribbonsandstone - massive appearing strata - Basal Quartz sandstone
Cored interval: 2940 - 3220' ; only recovered 44'

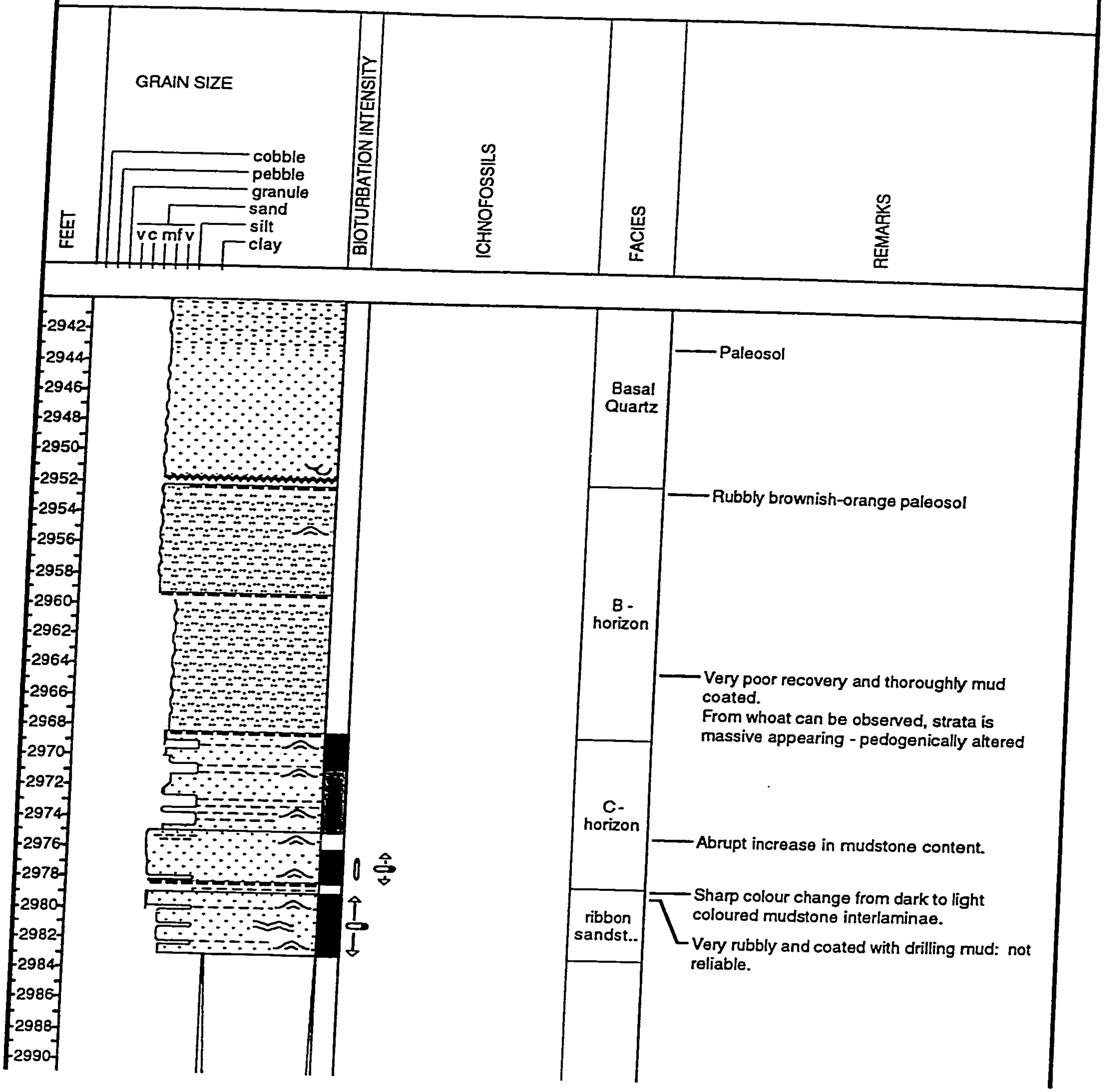

GMG Pan Am - Pendant d'Oreille

7-29-2-8w4

Remarks: dark and light ribbon sandstone - "A" sandstone
Cored interval 2818.5 - 2760 ft; recovered 58.5 ft

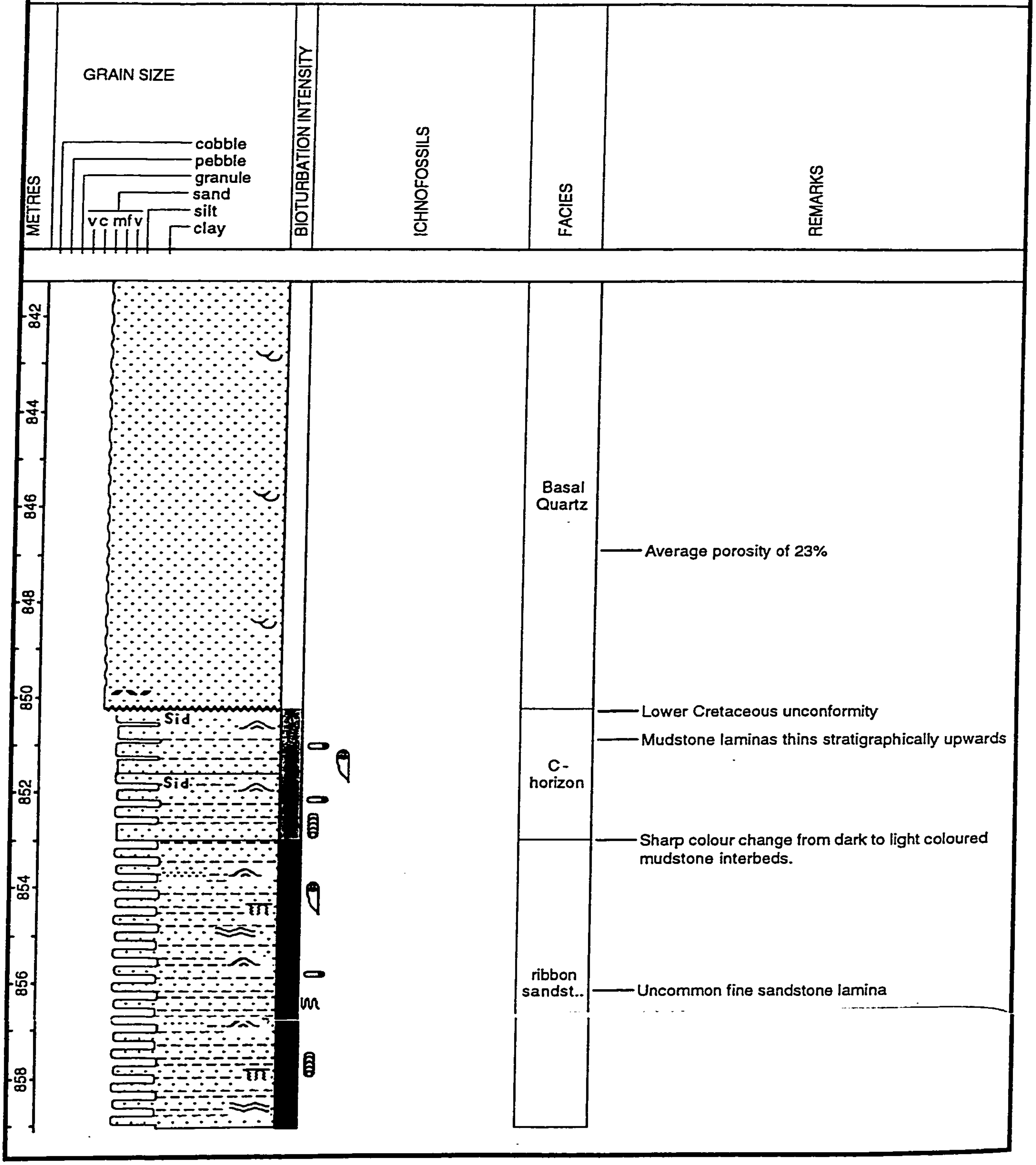

CMG Pan Am Pendor 6-31

6-31-2-8w4

Remarks: light (shoreface sandstone) - BQ
Core 1 2565 - 2582; recovered 17' - 4 boxes
Core 2 2582 - 2630; recovered 44' - 9 boxes

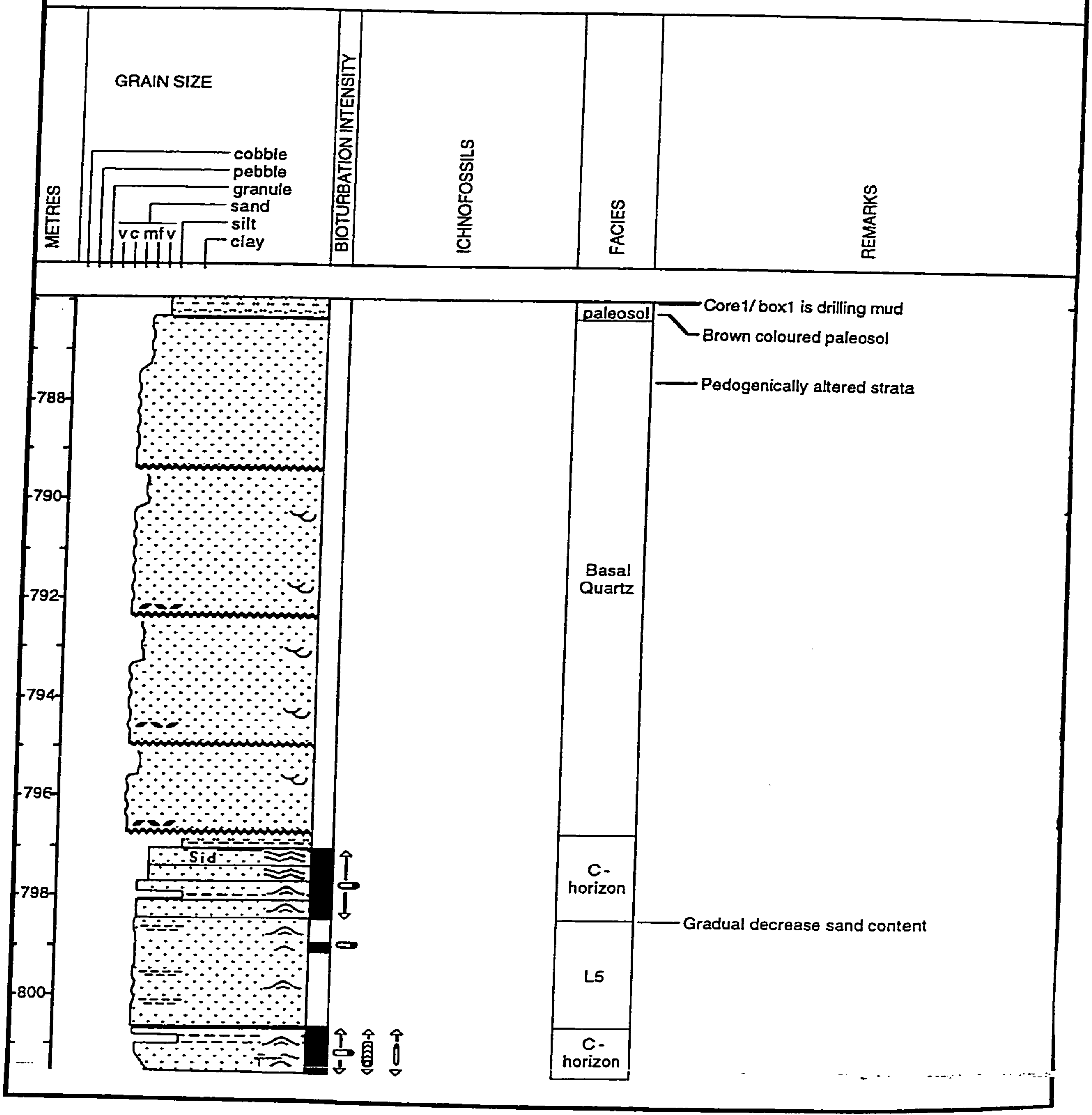

Gas Exploration Pinhorn #2

14-25-2-10w4

Remarks: Wireline core (1"). Cores # 62 - 80
Rierdon shale - chert pebble lag- dark ribbon sandstone - light ribbon sandstone
- Basal Quartz sandstone.

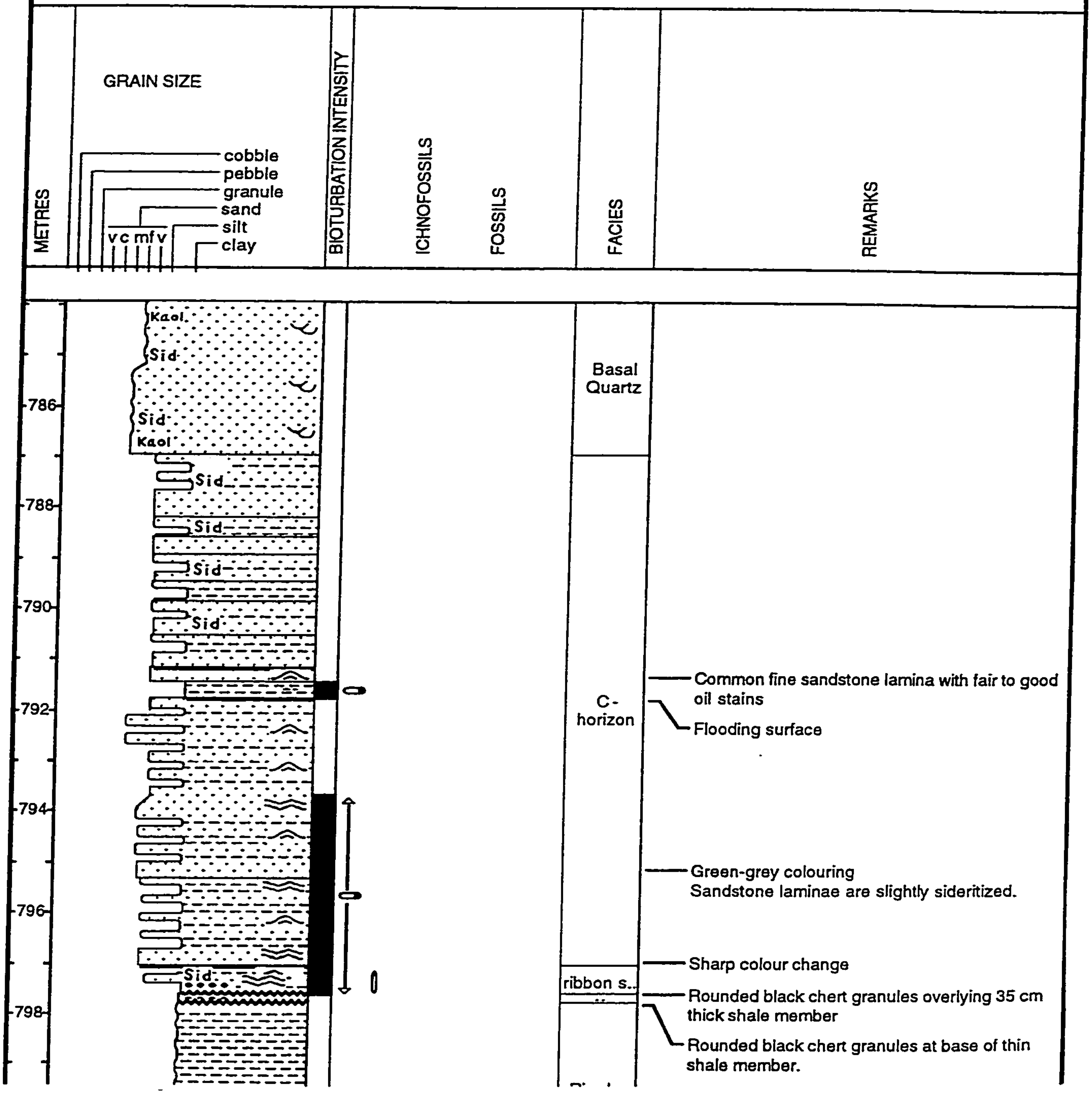

Common fine sandstone lamina with fair to good oil stains

Flooding surface

Green-grey colouring
Sandstone laminae are slightly sideritized.

Sharp colour change

Rounded black chert granules overlying 35 cm thick shale member

Rounded black chert granules at base of thin shale member.

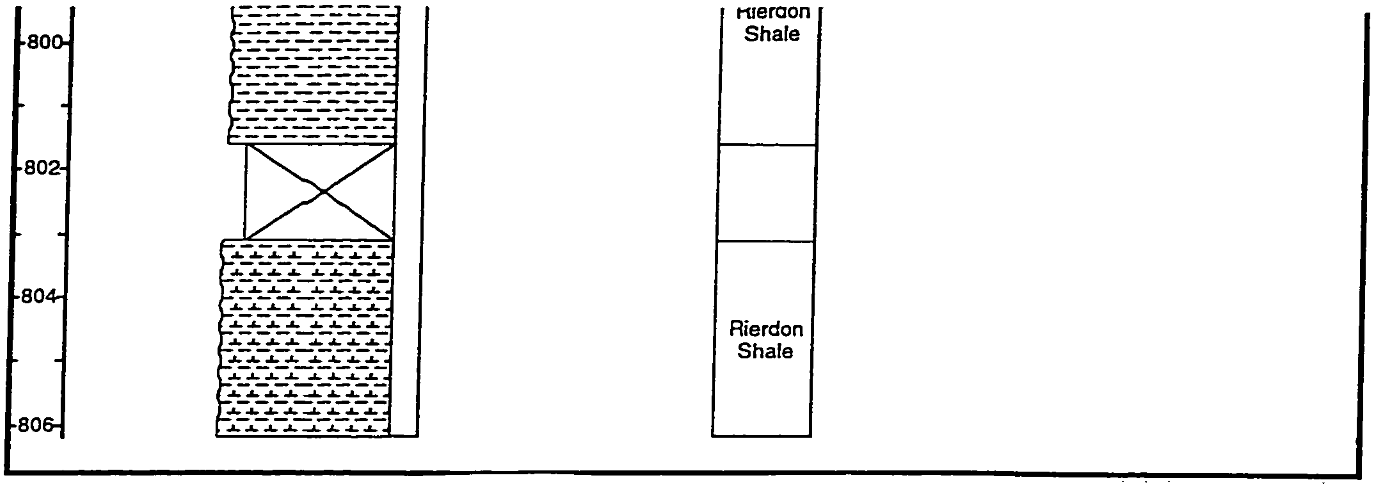
800
802
804
806
Rierdon Shale
Rierdon Shale

Shell Bain
12-14-3-5w4

Remarks: dark and light ribbon sandstone - green paleosol - Basal Quartz
Core 2: 1041.2 - 1052m recovered 9 m
7 boxes of slabbed core

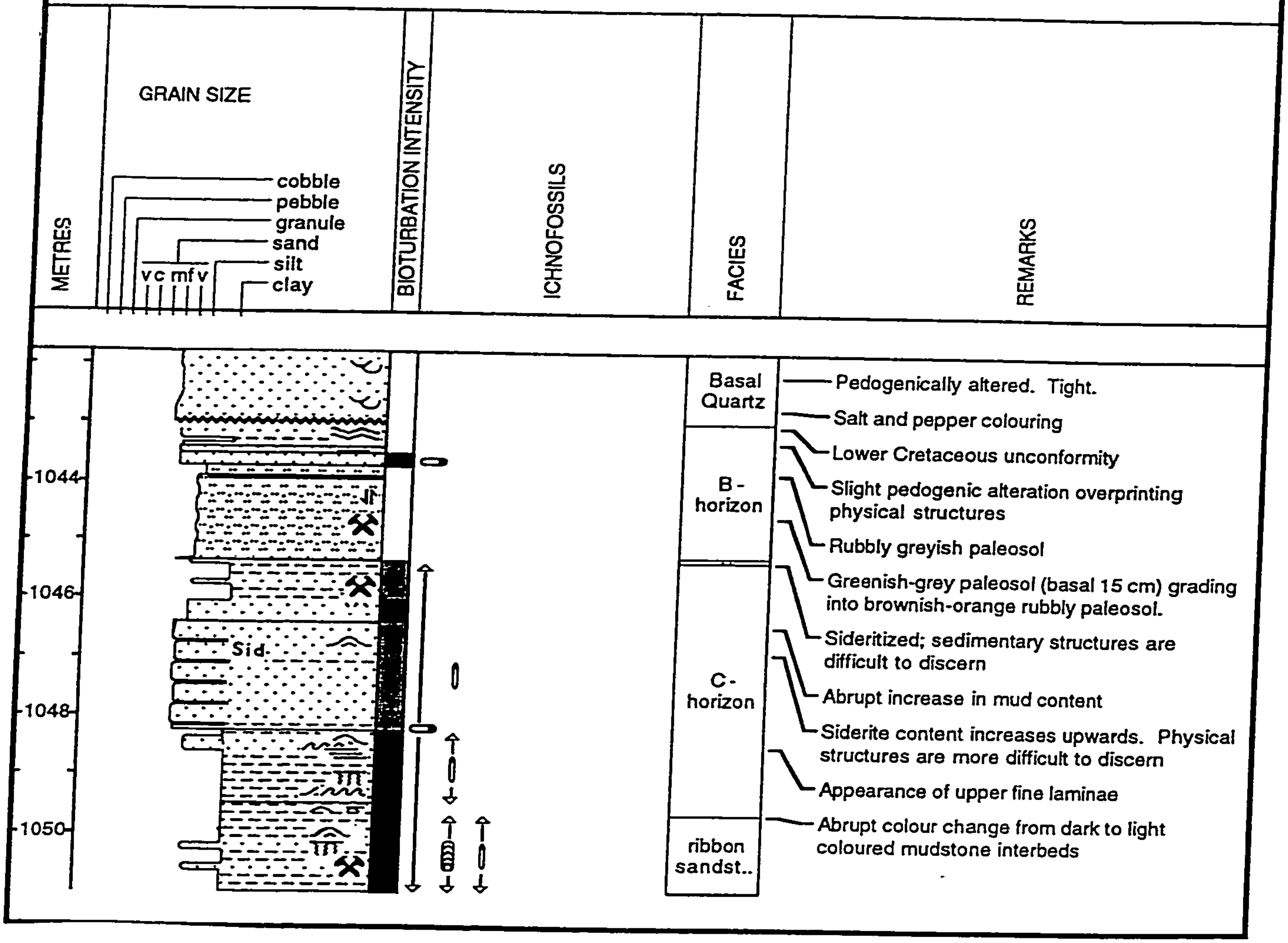

Cego Bumper Manyberries

14-31-3-5w4

Remarks: dark and light ribbon sandstone - Basal Quartz
Cored interval 981.3 - 999.3m; recovered 16.62m
16 boxes of 4" core
Logged boxes 13 - 16

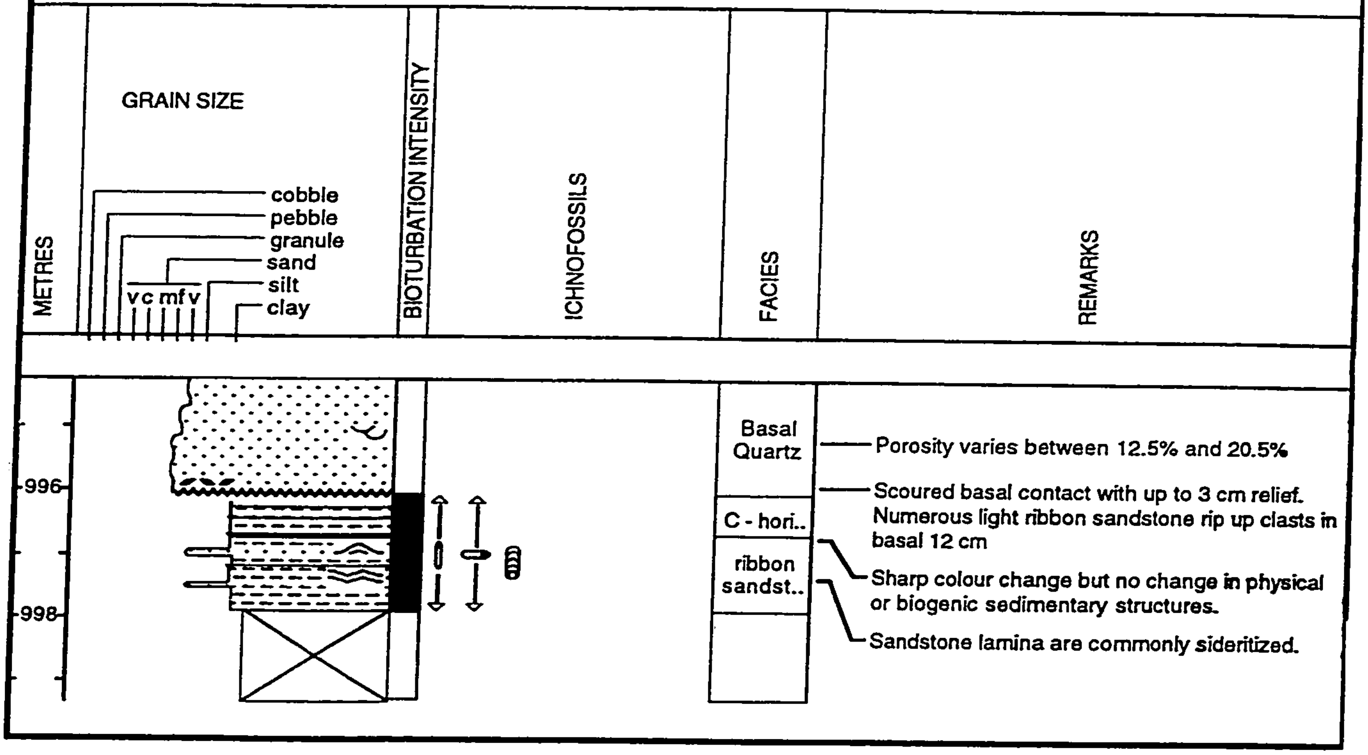

Porosity varies between 12.5% and 20.5%

Scoured basal contact with up to 3 cm relief. Numerous light ribbon sandstone rip up clasts in basal 12 cm

Sharp colour change but no change in physical or biogenic sedimentary structures.

Sandstone lamina are commonly sideritized.

Cego Bumper Manyberries

16-32-3-5w4

Remarks: dark ribbon sandstone - light ribon sandstone - Jurassic paleosol - Cretaceous paleosol
Cored interval 1004.5 - 1023.5m; recovered 16.84 m
15 boxes of 4" core

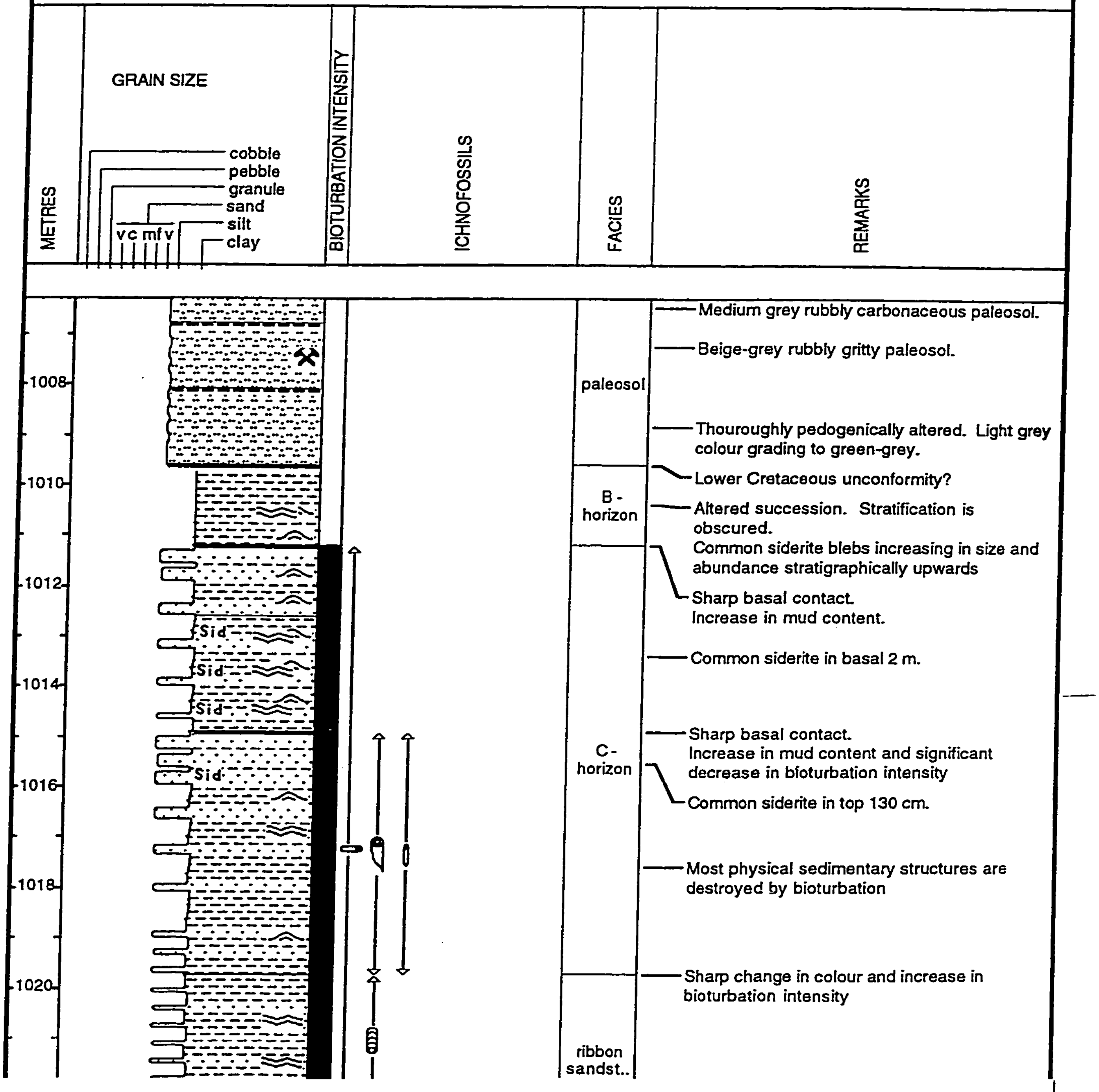

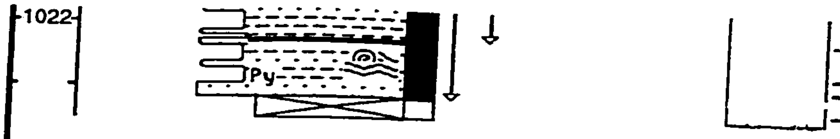

Sharp basal contact.
Increase in mud content upwards

Trace fossils are uncharacteristically larger scale.
Lamina thickness also thicker than usual (average 4 mm thick)

Common siderite and pyrite in basal 50 cm

Rubbly; can't log with confidence

Trident et Al.
7-34-3-5w4

Remarks: dark ribbon sandstone
Core 1 1045 - 1054 m ; recovered 9m - ? boxes
Core 2 1054 - 1063 m ; recovered 9m - ?boxes

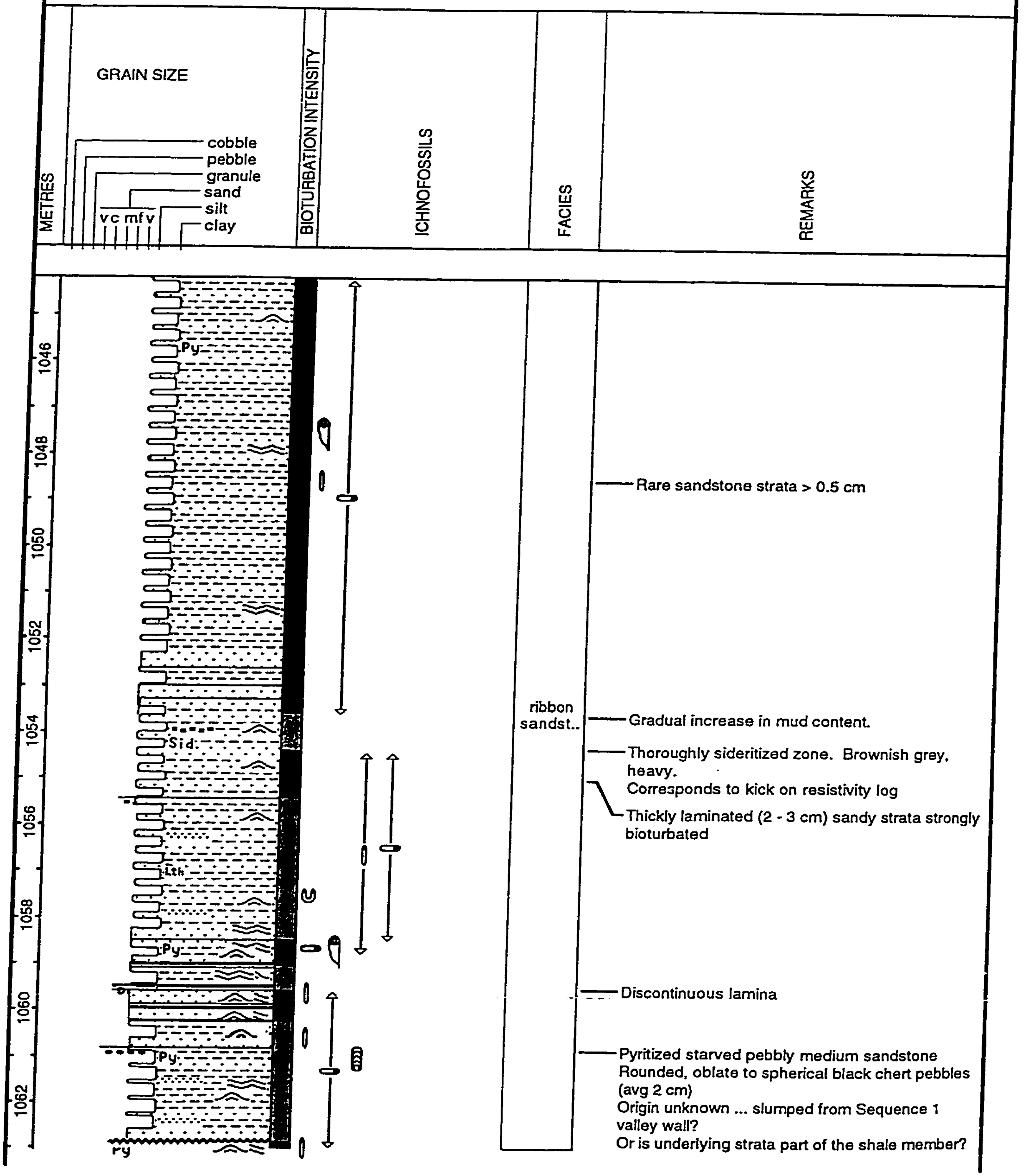

Rare sandstone strata > 0.5 cm

Gradual increase in mud content.

Thoroughly sideritized zone. Brownish grey, heavy.
Corresponds to kick on resistivity log

Thickly laminated (2 - 3 cm) sandy strata strongly bioturbated

Discontinuous lamina

Pyritized starved pebbly medium sandstone
Rounded, oblate to spherical black chert pebbles (avg 2 cm)
Origin unknown ... slumped from Sequence 1 valley wall?
Or is underlying strata part of the shale member?

Canadian Montana Gas Co. Pendor
10-20-3-7w4

Remarks: dark ribbon sandstone - BQ? or Jurassic fluvial sandstone?
Cored interval: 2875 - 2879' - 6 boxes
Slabbed
Difficult to match up core to log

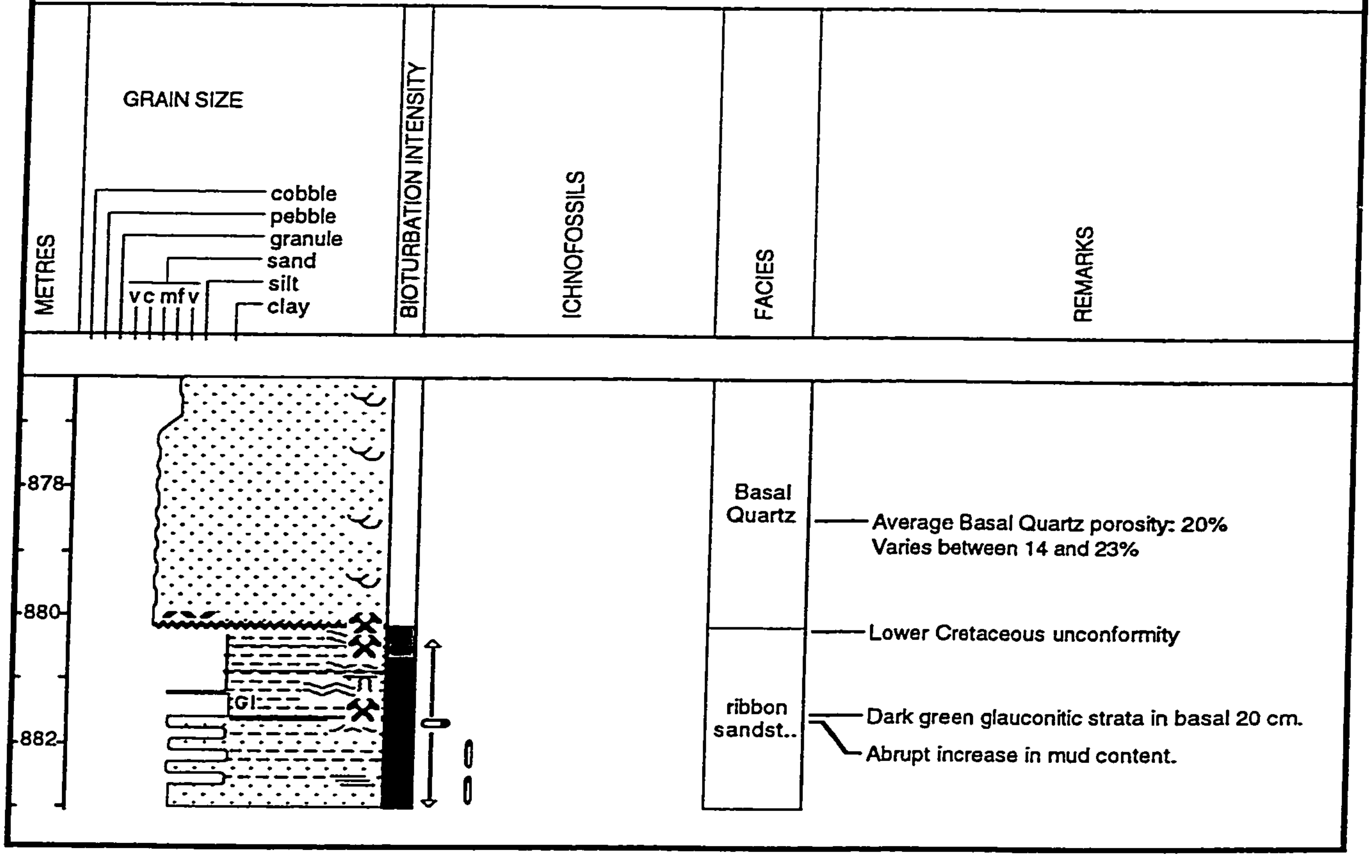

Average Basal Quartz porosity: 20%
Varies between 14 and 23%

Lower Cretaceous unconformity

Dark green glauconitic strata in basal 20 cm.

Abrupt increase in mud content.

Murphy et al. Pakowko

10-28-3-7w4

Remarks: dark ribbon sandstone - Cretaceous mudstone - paleosol - Basal Quartz
Cored interval: 2870 - 2930' - 12 boxes
Logged boxes 7-12; boxes 2-8 have Regional "A" sandstone

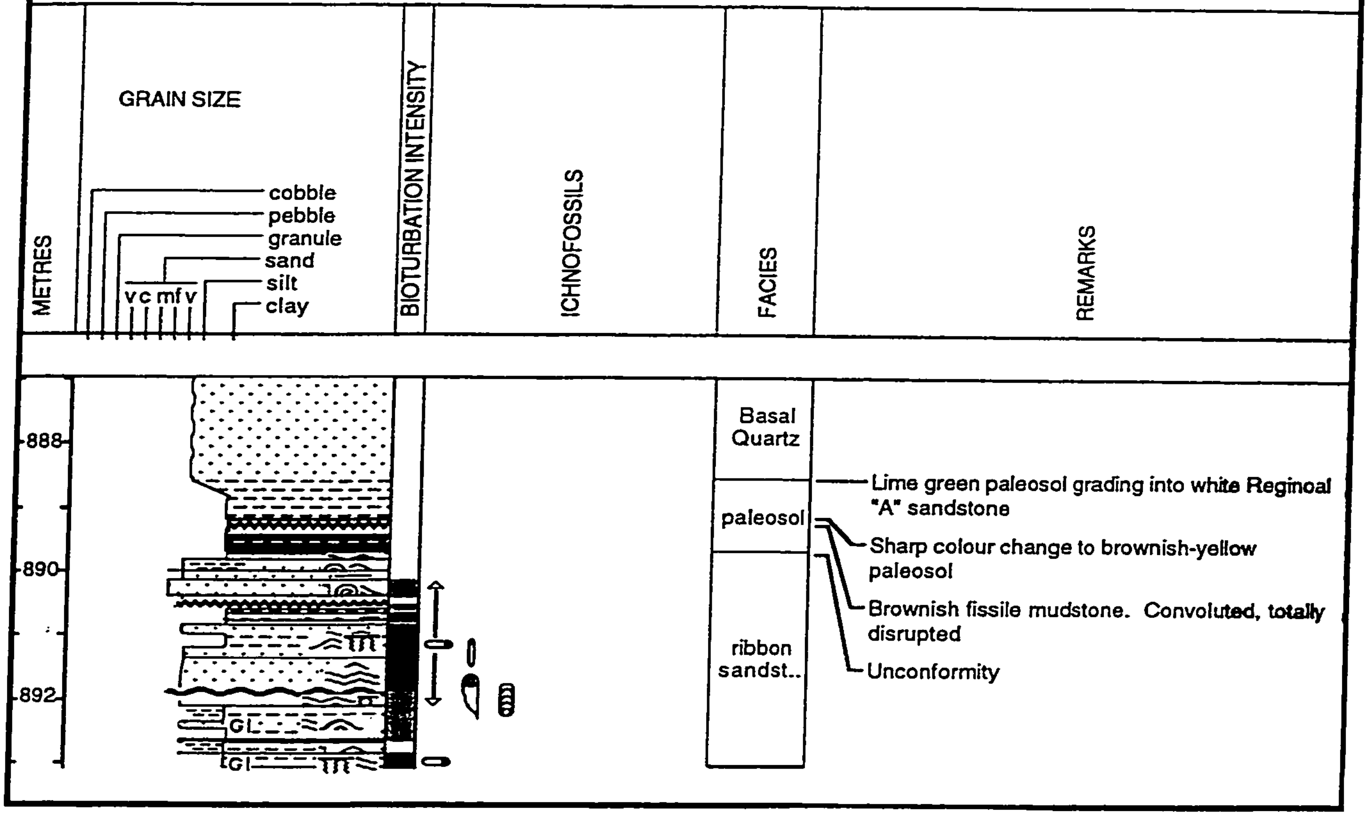

Lime green paleosol grading into white Reginoal "A" sandstone

Sharp colour change to brownish-yellow paleosol

Brownish fissile mudstone. Convoluted, totally disrupted

Unconformity

Home CMG Pendor

11-4-3-8w4

Remarks: dark ribbon sandstone - altered light ribbon sandstone - Basal Quartz sandstone
- rubbly paleosol
Cored interval 2775 - 2825 m; recovered 44 m - 10 boxes

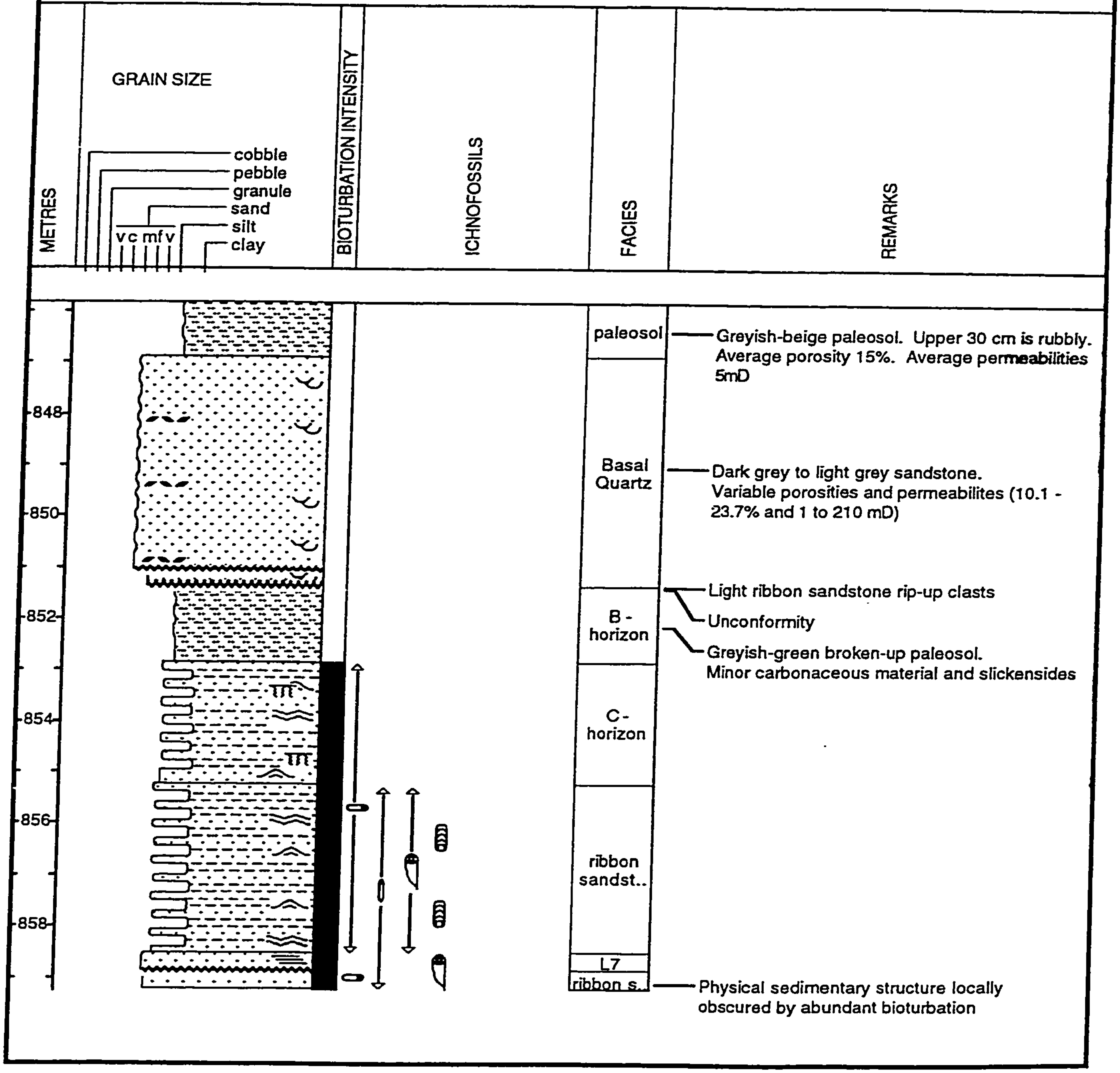

HB Pendant d'Oreille
10-8-3-8w4

Remarks: dark ribbon sandstone - altered light ribbon sandstone - paleosol - BQ
Core 2: 2800 - 2845' 10 boxes
Core 1: 2745 - 2800' 12 boxes

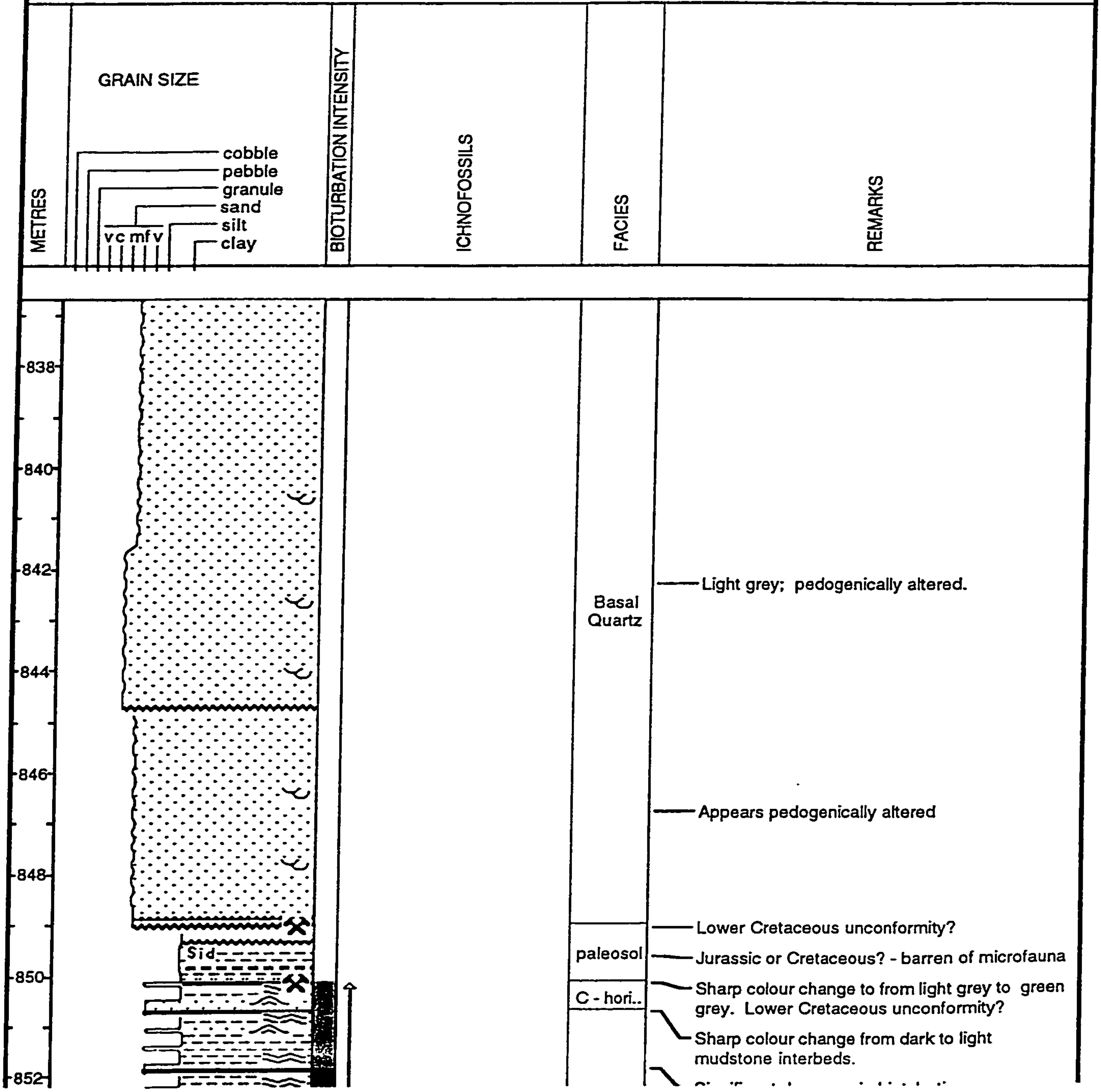

Light grey; pedogenically altered.

Appears pedogenically altered

Lower Cretaceous unconformity?

Jurassic or Cretaceous? - barren of microfauna

Sharp colour change to from light grey to green grey. Lower Cretaceous unconformity?

Sharp colour change from dark to light mudstone interbeds.

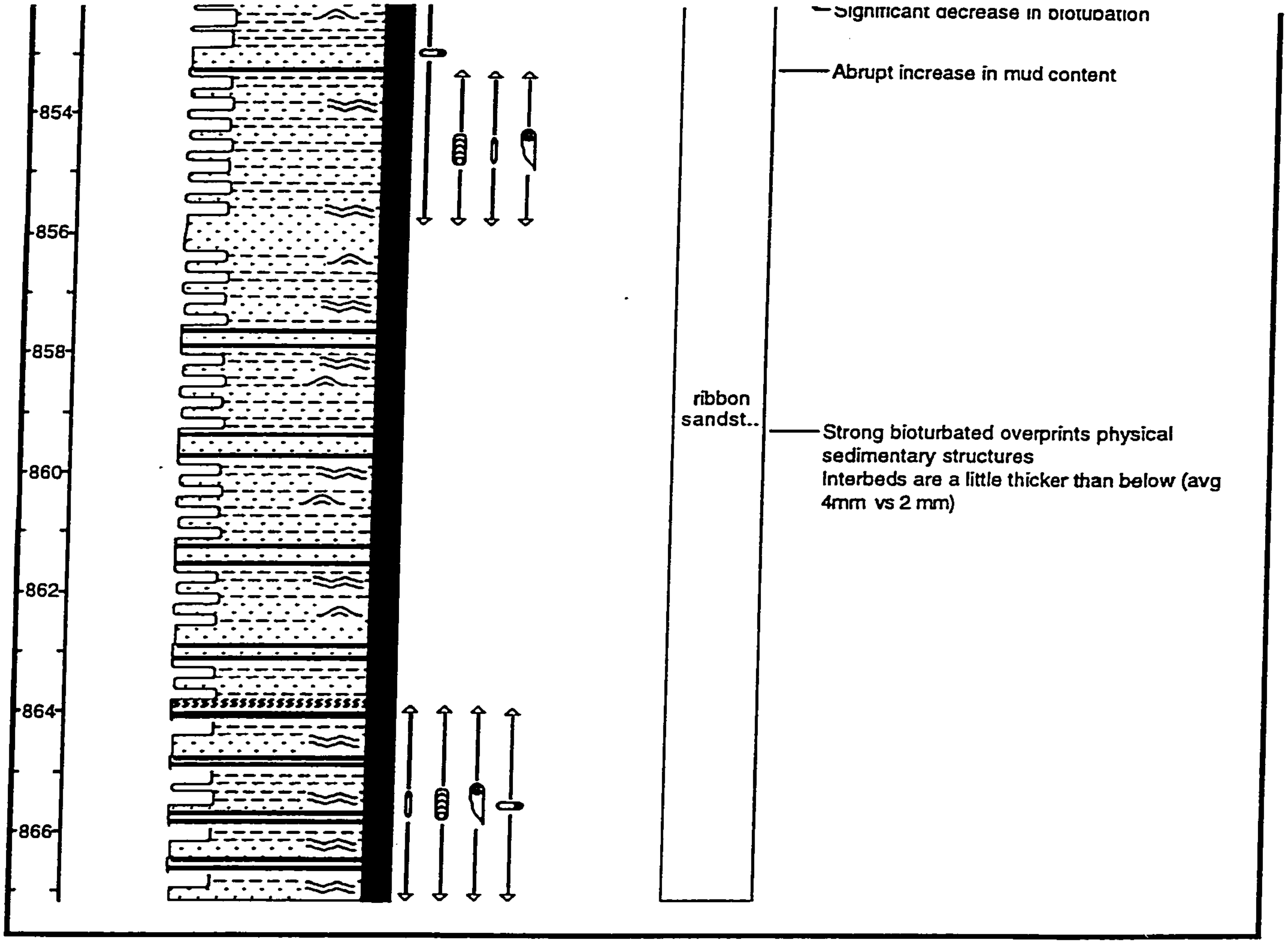
Significant decrease in bioturbation
Abrupt increase in mud content
854
856
858
860
862
864
866
ribbon sandst..
Strong bioturbated overprints physical sedimentary structures
Interbeds are a little thicker than below (avg 4mm vs 2 mm)

CMG Pan Am Pendor
6-11-3-9w4

Remarks: Is boxed like a Shell core - bottom's up
Light ribbon sandstone - Basal Quartz
Core 1: 2685 - 2706; 5 boxes - recovered 16'
Core 2: 2706 - 2732; 4 boxes - recovered 17'
2-1/2" core

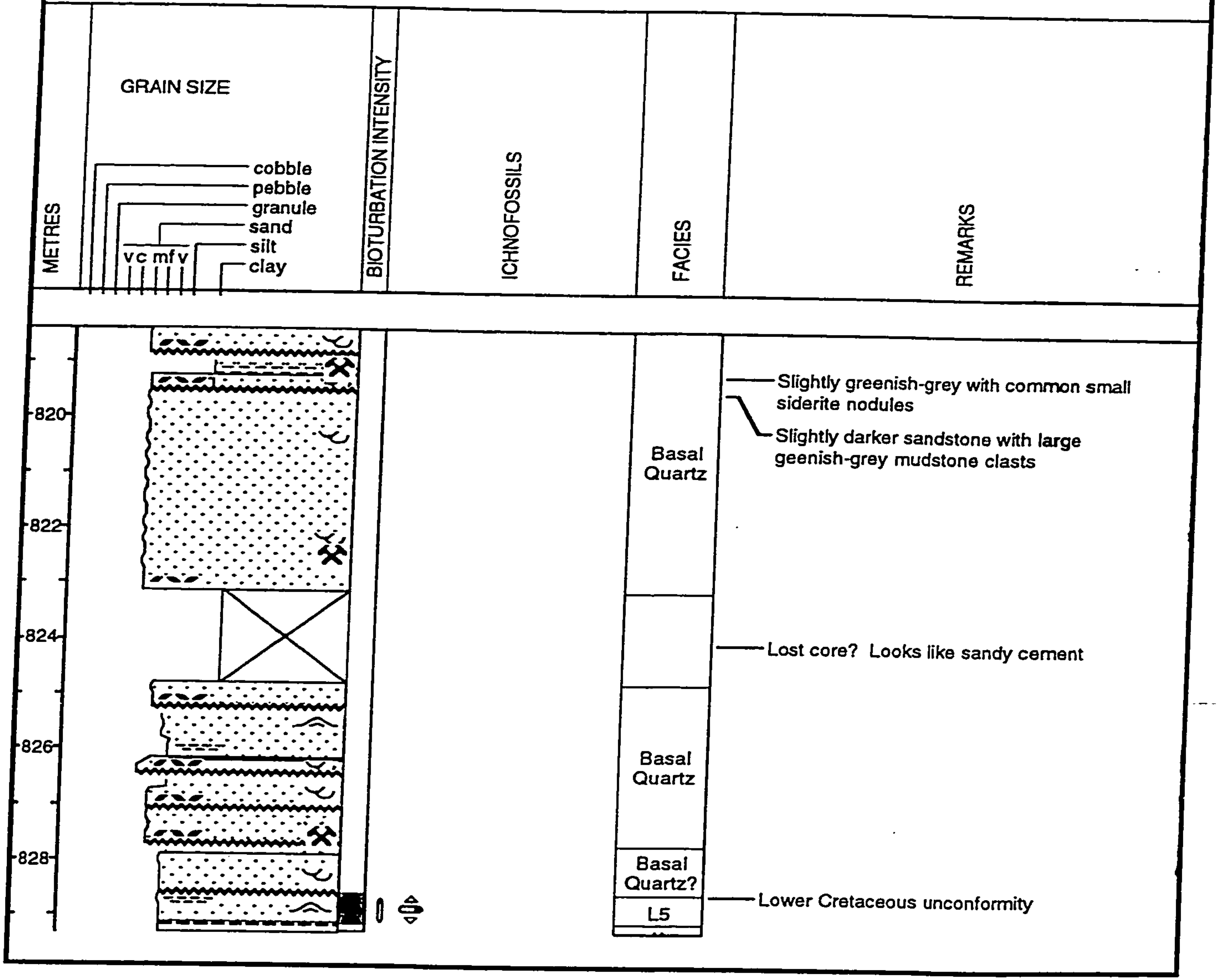

CMG Pan d'Or

6-19-3- 9w4

Remarks: Light Swift - BQ ("A" sandstone)
Cored interval 2772 - 2783'
3 boxes

Note: barren of bioturbation and dominated by sandstone

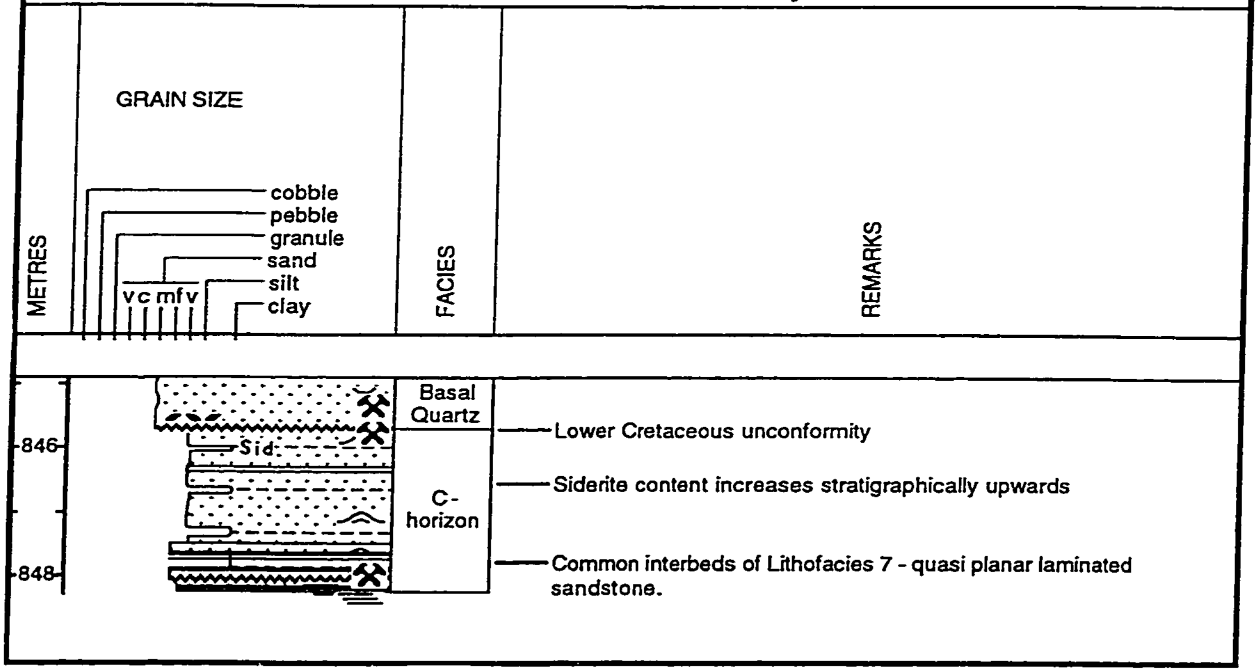

Ranchmen's et al. Manyberries

8-22-4-4w4

Remarks: dark and light ribbon sandstone - Basal Quartz - coal - paleosol
Core 2: 1053.6 - 1071.6m; recovered 16m
15 boxes

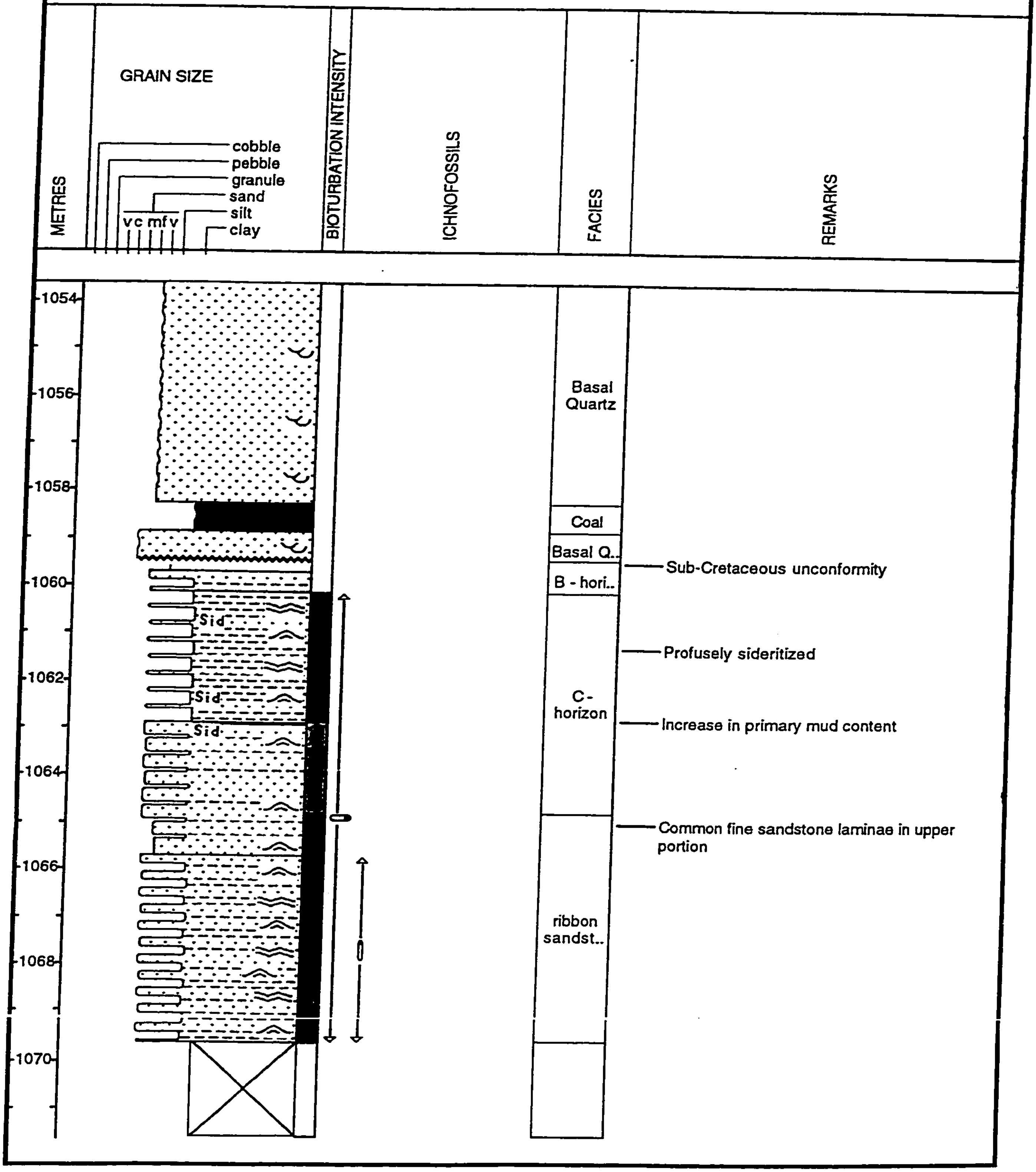

Sameddan AO & G Manyberries

6-30-4-4w4

Remarks: Dark Swift - Light Swift - BQ
Core 2: 1078.5 - 1088; recovered 9.5m - 6 boxes
Core 1: 1088.0 - 1094; recovered 6.0m - 4 boxes
Slabbed core

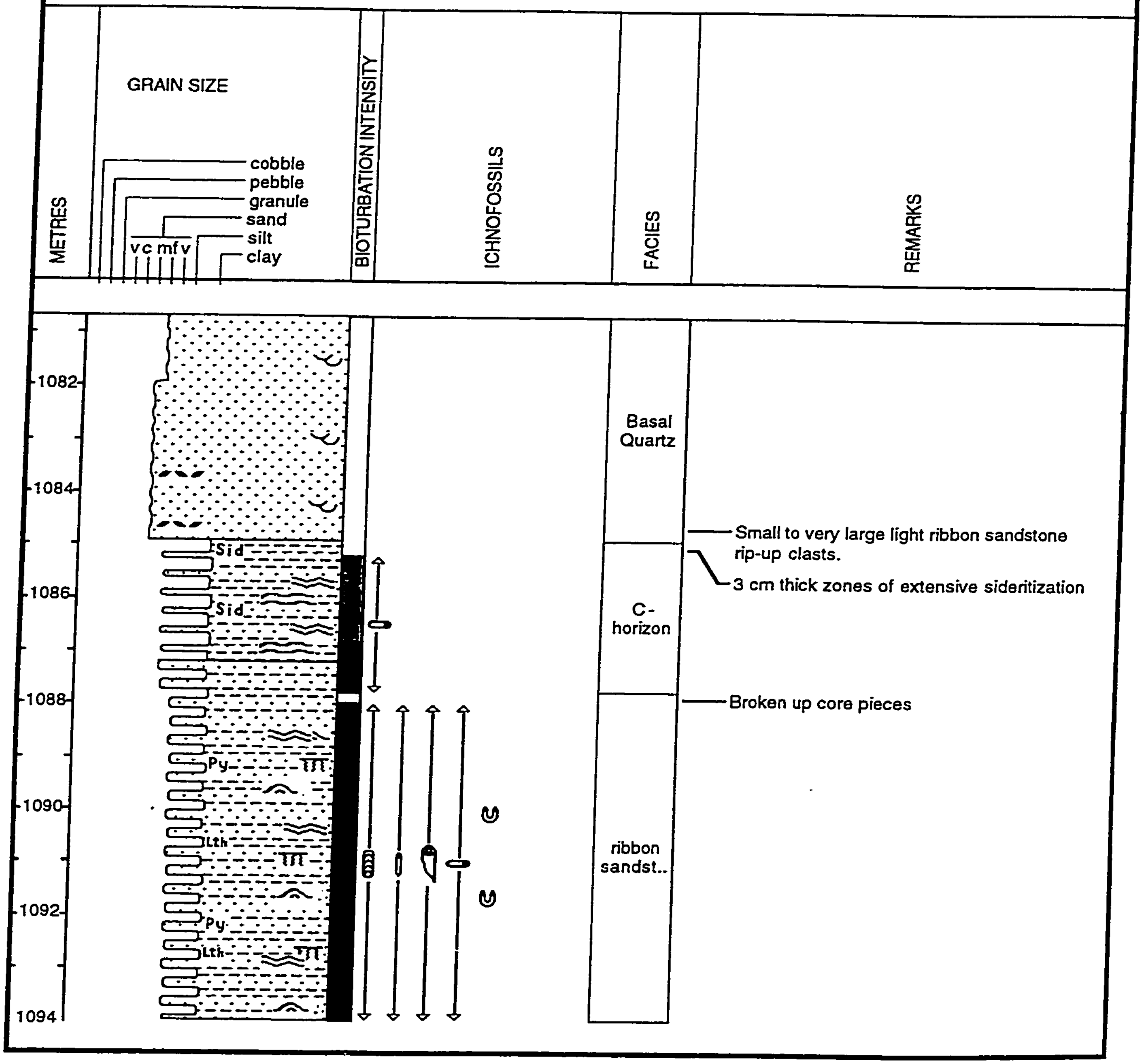

Home et al. Manyberries
8-4-4-5w4

Remarks: dark and light ribbon sandstone - Cretaceous paleosol
Cored interval 1032 - 1050 m; recovered 18 m
16 boxes of 4" core, slabbed and tested

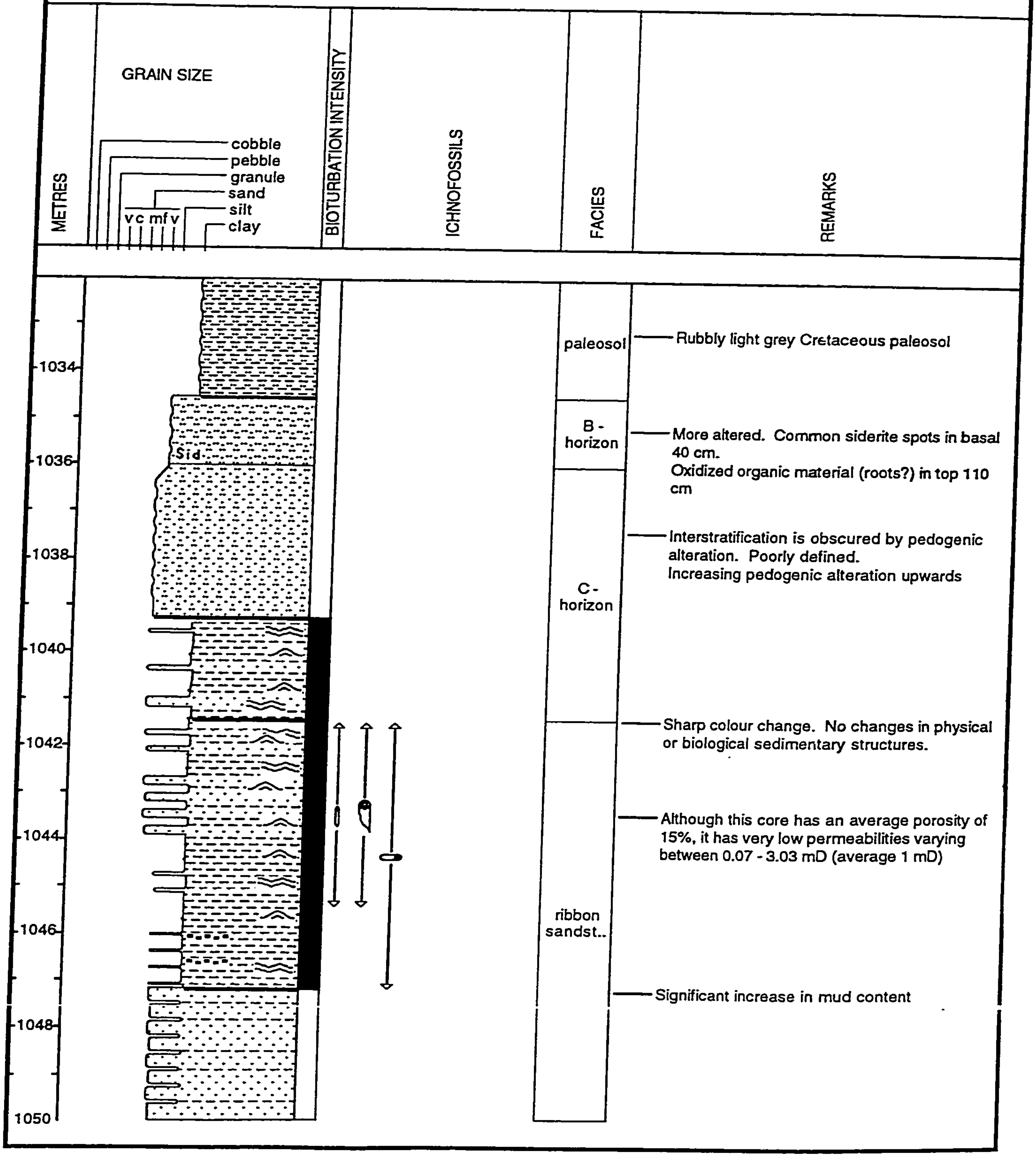

Rubbly light grey Cretaceous paleosol

More altered. Common siderite spots in basal 40 cm.
Oxidized organic material (roots?) in top 110 cm

Interstratification is obscured by pedogenic alteration. Poorly defined.
Increasing pedogenic alteration upwards

Sharp colour change. No changes in physical or biological sedimentary structures.

Although this core has an average porosity of 15%, it has very low permeabilities varying between 0.07 - 3.03 mD (average 1 mD)

Significant increase in mud content

Home Manyberries
14-14-4-5w4

Remarks: dark ribbon and light sandstone - Basal Quartz sandstone
Cored interval: 1073 - 1086m; recovered 11.3m
8 boxes of slabbed 3" core

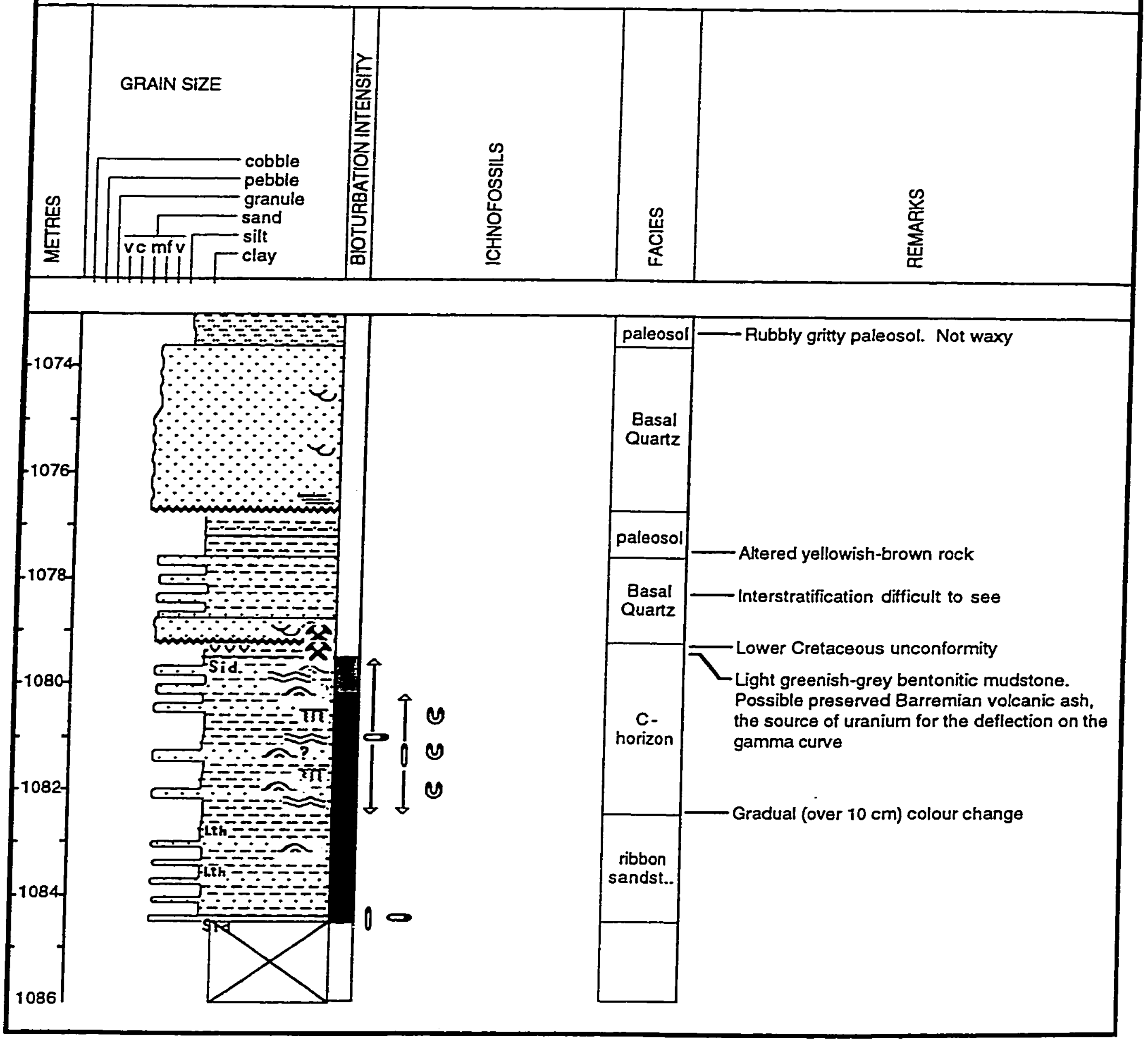

Rubbly gritty paleosol. Not waxy

Altered yellowish-brown rock

Interstratification difficult to see

Lower Cretaceous unconformity

Light greenish-grey bentonitic mudstone. Possible preserved Barremian volcanic ash, the source of uranium for the deflection on the gamma curve

Gradual (over 10 cm) colour change

Home Manyberries

8-23-4-5w4

Remarks: dark and light ribbon sandstone - Basal Quartz sandstone
Core interval 1123 - 1132m; recovered 7.7m
7 boxes of slabbed 4" core

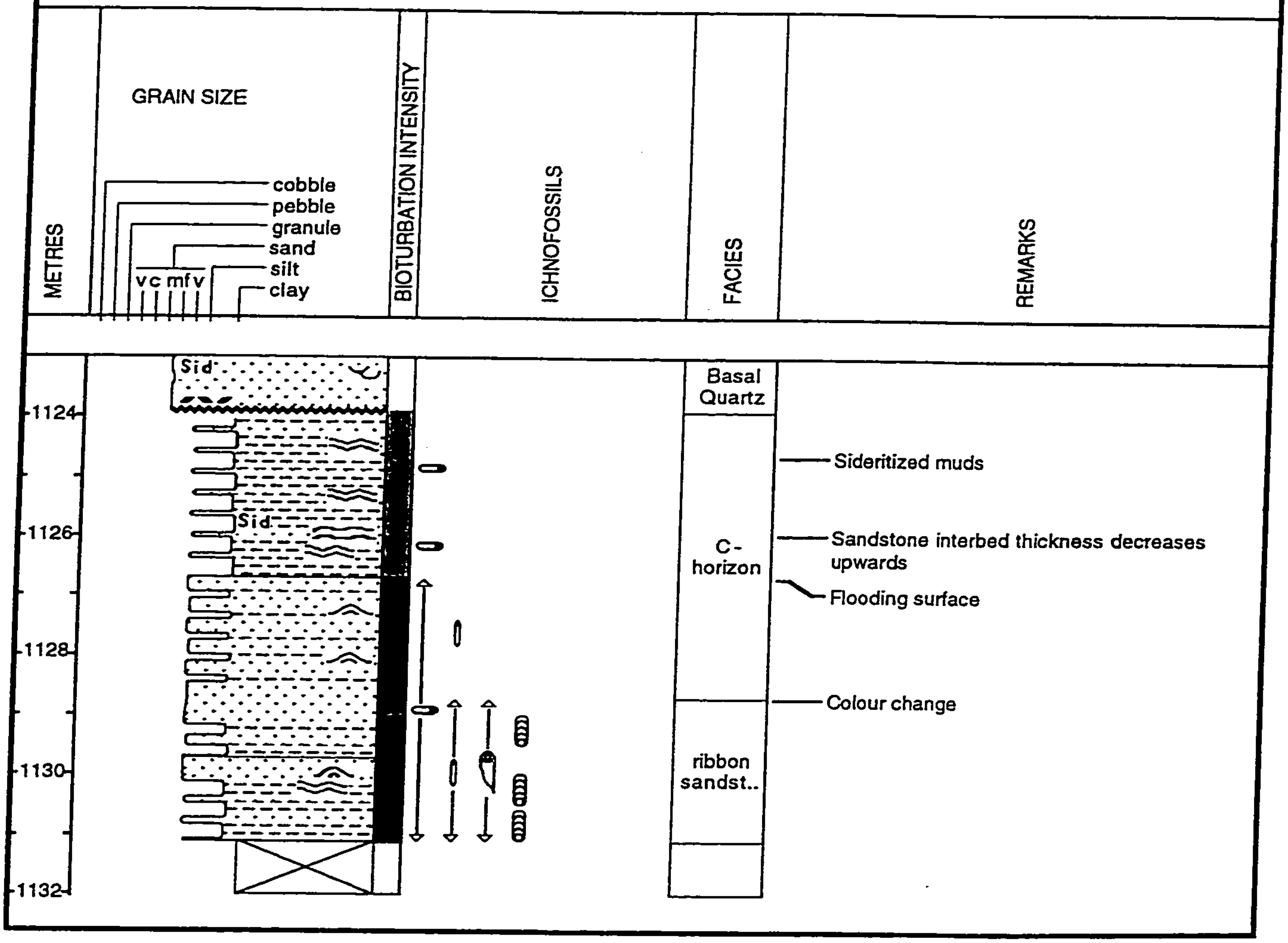

ANDERSON ET AL MANYBERRIES
8-35-4-5w4

Remarks: drak and light ribbon sandstone- massive appearing strata - rubbly paleosol

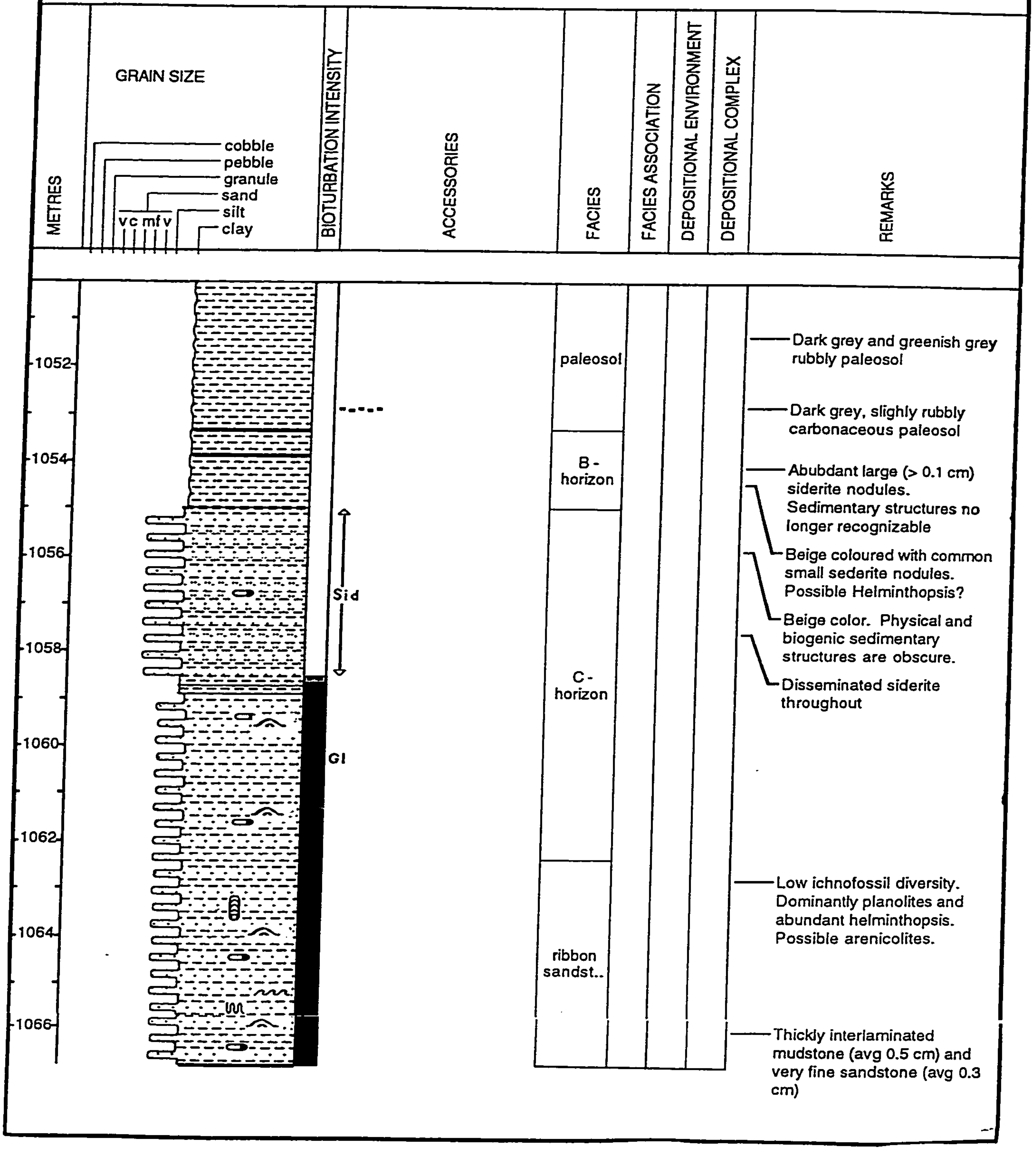

Dark grey and greenish grey rubbly paleosol

Dark grey, slighly rubbly carbonaceous paleosol

Abubdant large (> 0.1 cm) siderite nodules. Sedimentary structures no longer recognizable

Beige coloured with common small sederite nodules. Possible Helminthopsis?

Beige color. Physical and biogenic sedimentary structures are obscure.

Disseminated siderite throughout

Low ichnofossil diversity. Dominantly planolites and abundant helminthopsis. Possible arenicolites.

Thickly interlaminated mudstone (avg 0.5 cm) and very fine sandstone (avg 0.3 cm)

CEGO Bumper Manyberries
3-2-4-6w4

Remarks: Rierdon Shale - shale member - dark ribbon sandstone - altered light ribbon sandstone
Cored interval: 947 - 965m; recovered 18m - 15 boxes

Note: Boxes 2 and 3 are inversed

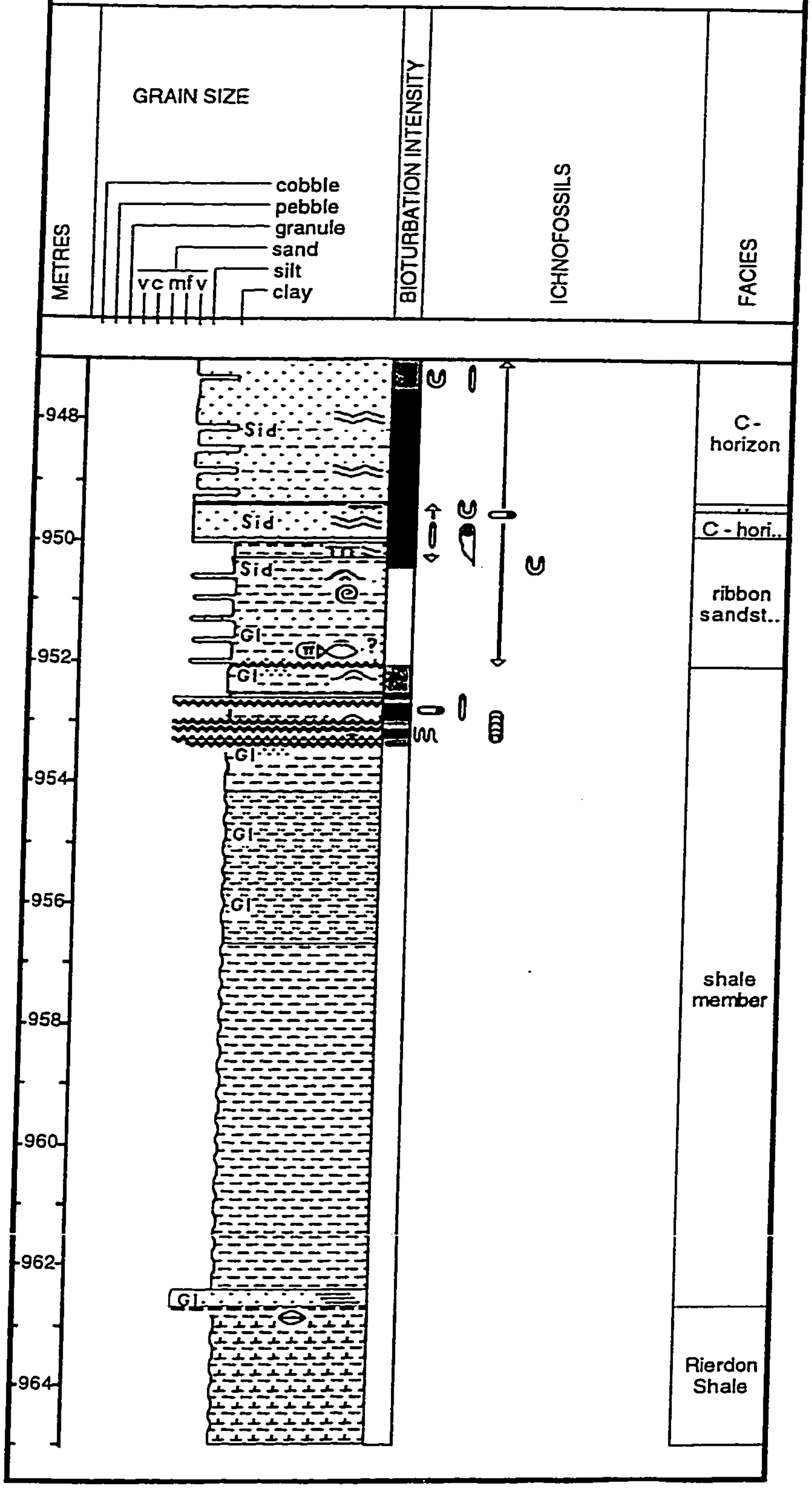

CMG Pakowki

6-2-4-7w4

Remarks: L5 - dark ribbon sandstone - L5 - light ribbon sandstone
Core 1: 2879 - 2885';   - 4 boxes
Core 2: 2885 - 2900'; recovered 14.5' - 4 boxes

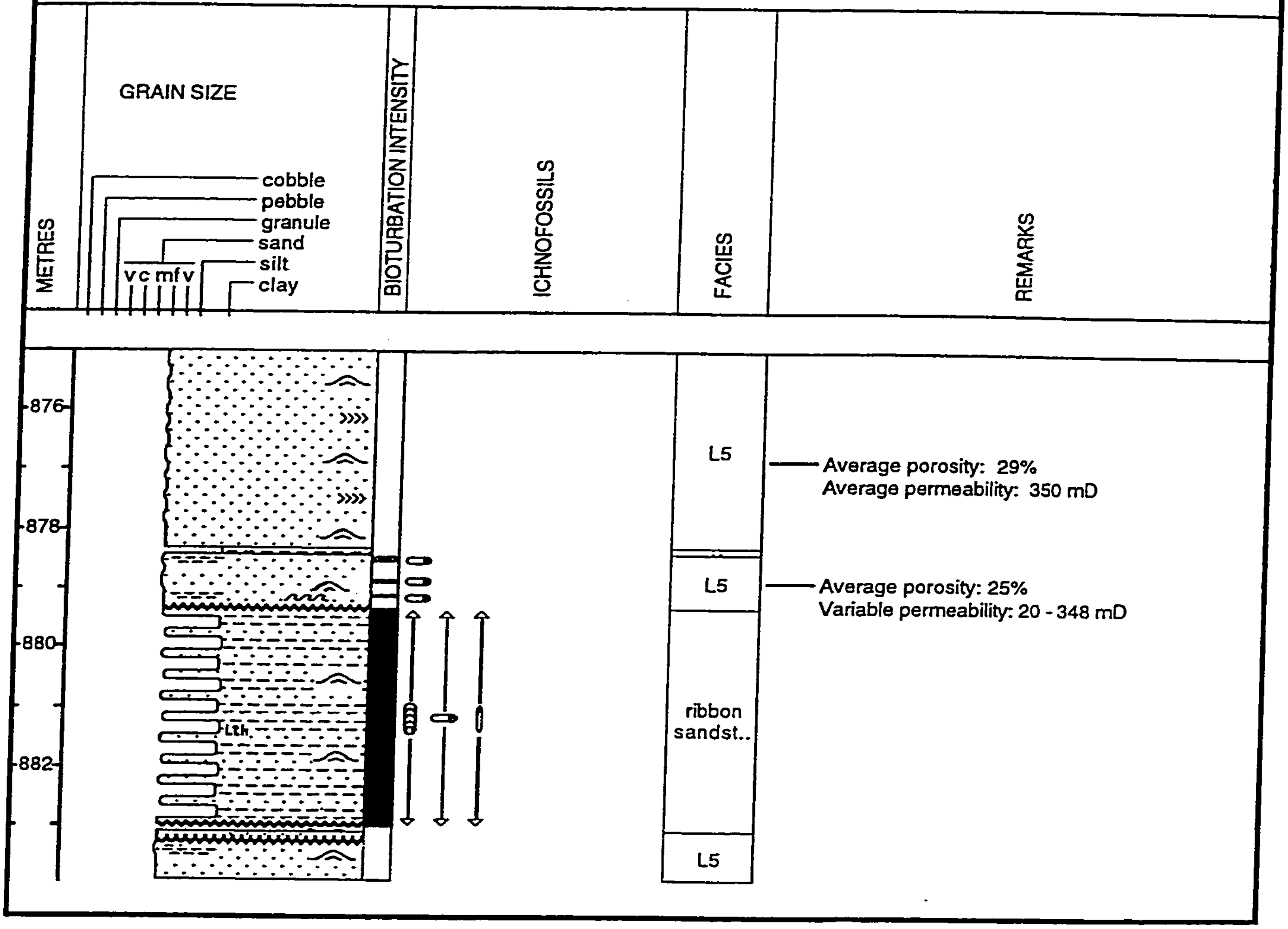

Average porosity: 29%
Average permeability: 350 mD

Average porosity: 25%
Variable permeability: 20 - 348 mD

Canadian Montana Pendor

7-6-4-7w4

Remarks: dark ribbon sandstone - Basal Quartz -lacustrine
Core 1: 2750 - 2778' - 7 boxes
Core 2: 2778 - 2808' - 4 boxes
Slabbed, plugs

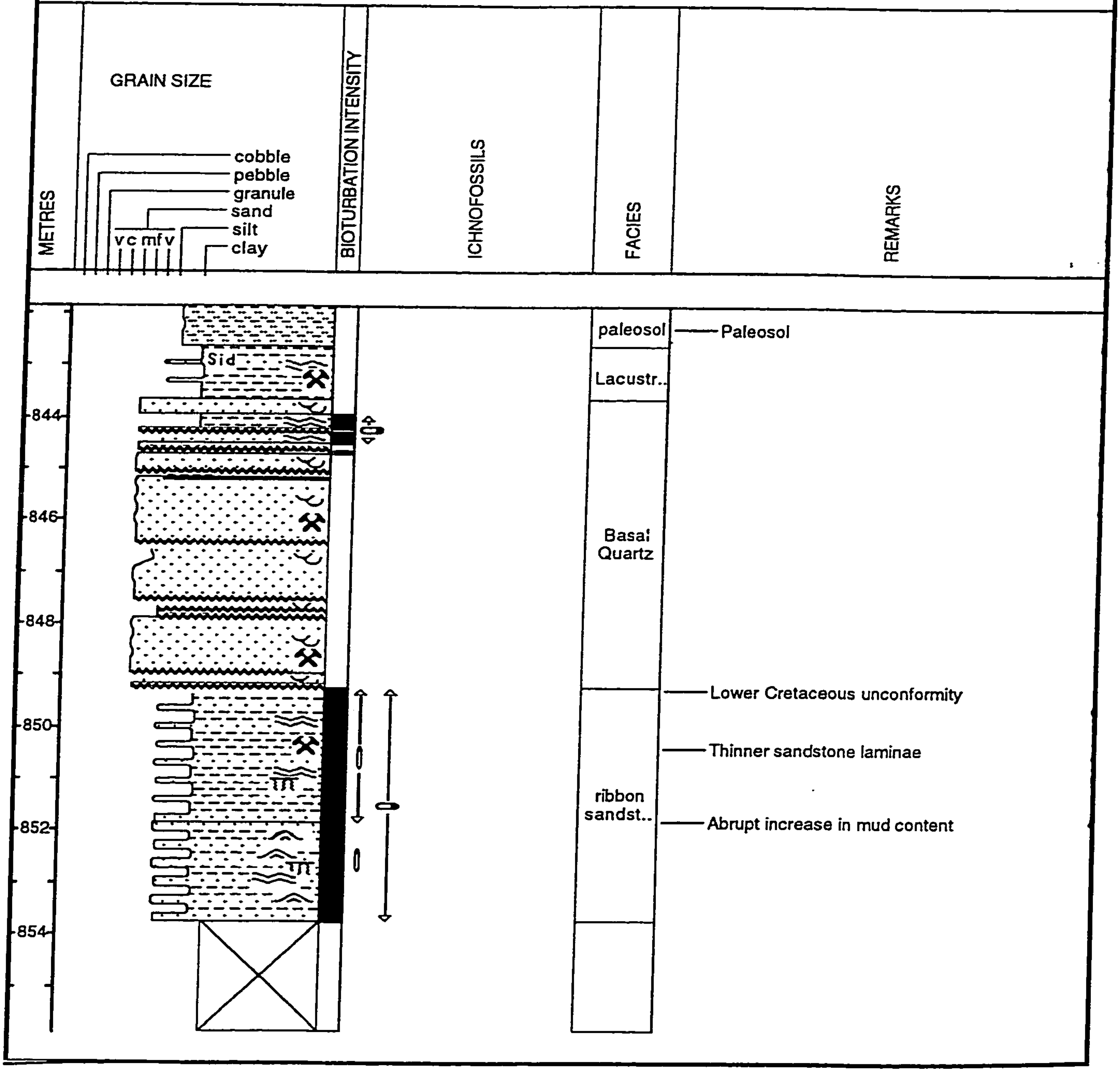

CMG Pendor
10-7-4-7w4

Remarks: dark ribbon sandstone - light ribbon sandstone - paleosol

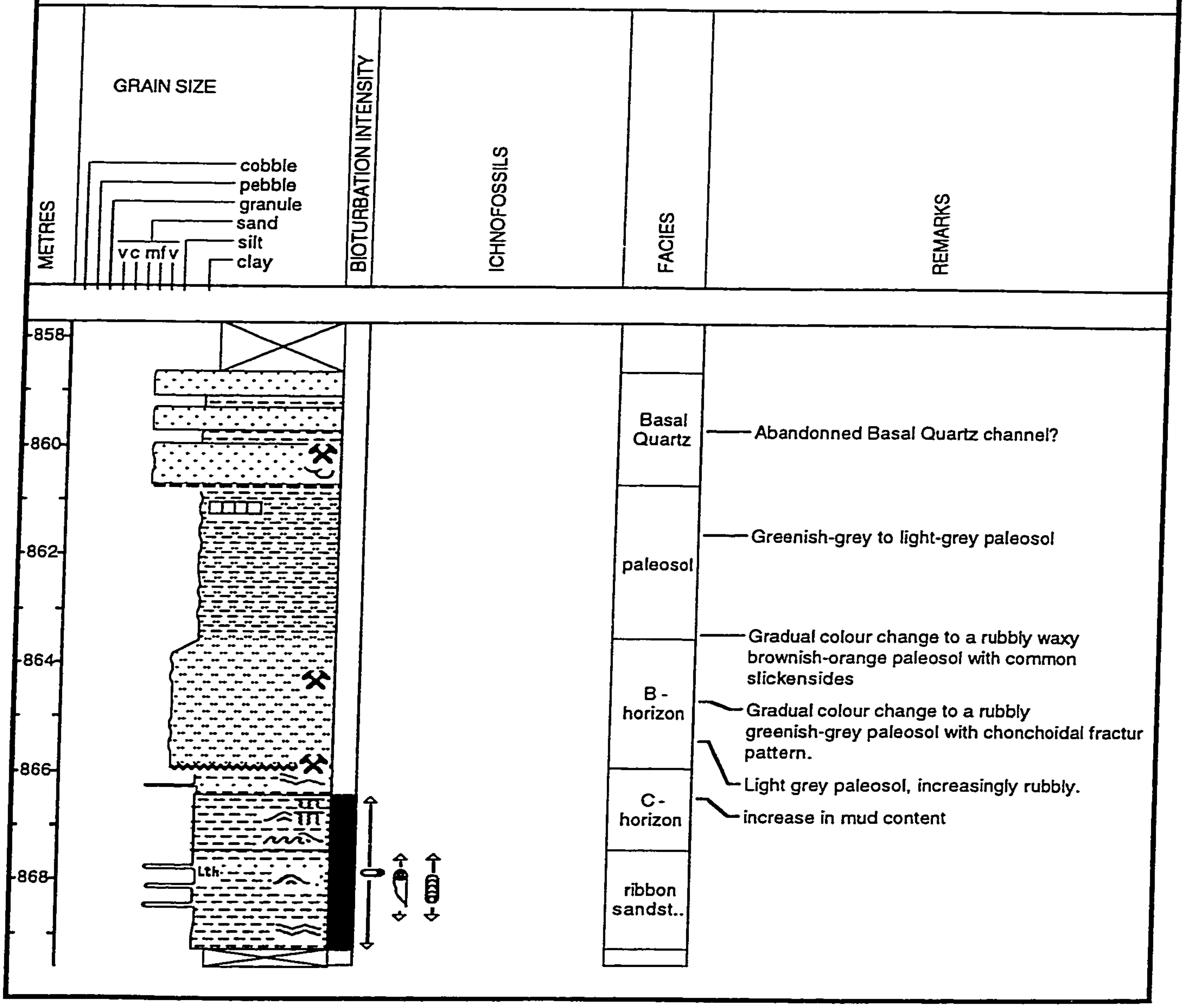

Canadian Montana

6-1-4-9w4

Remarks: dark and light ribbon sandstone - Basal Quartz
Cored interval 2853 - 2883'; recovered 30' - 8 boxes

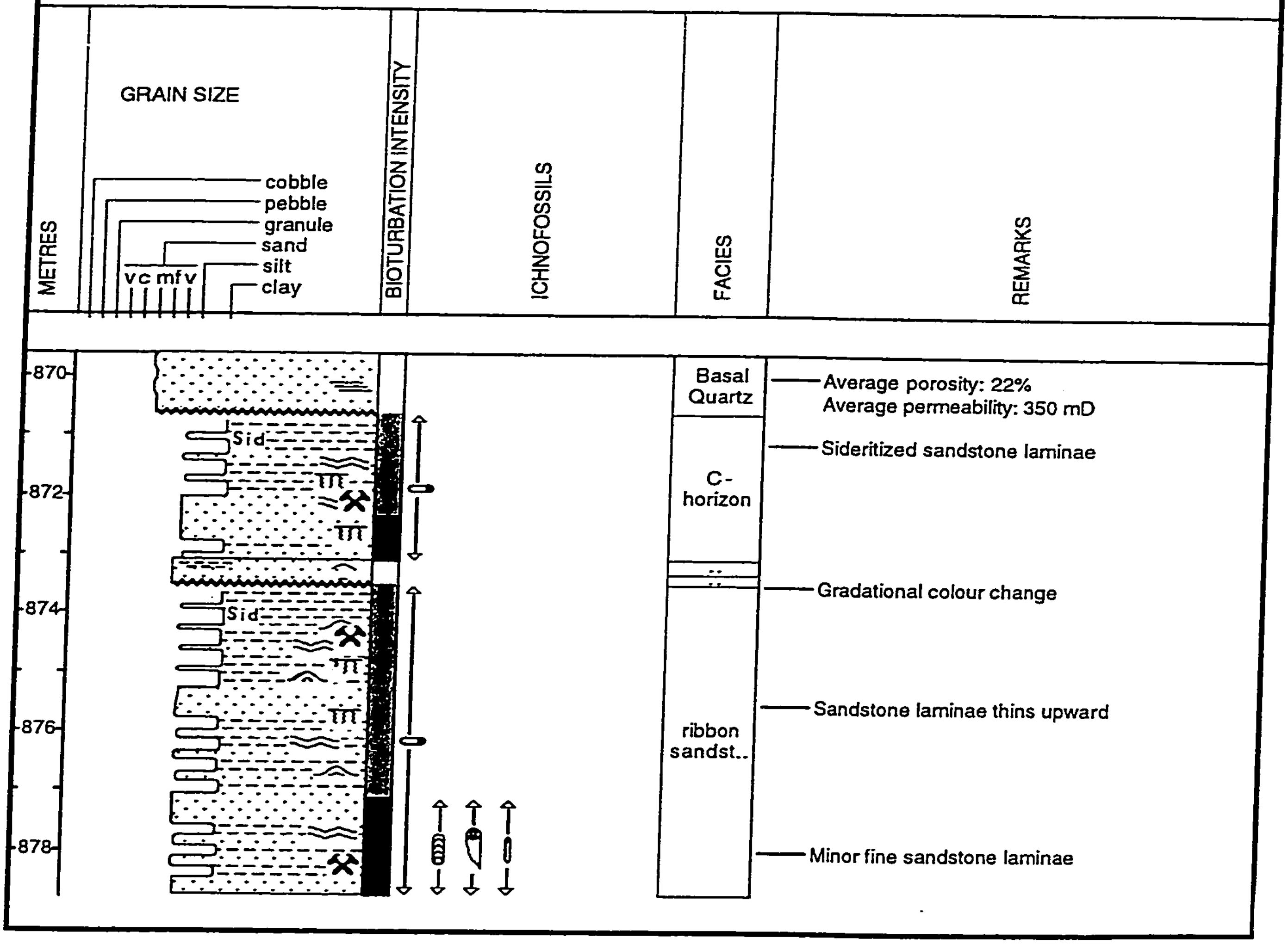

Cego Pex Manyberries

15-29-5-4w4

Remarks: Reirdon - Light Swift - Paleosol
Cored interval: 1214 - 1232.25m; Recovred 17.75m
15 boxes

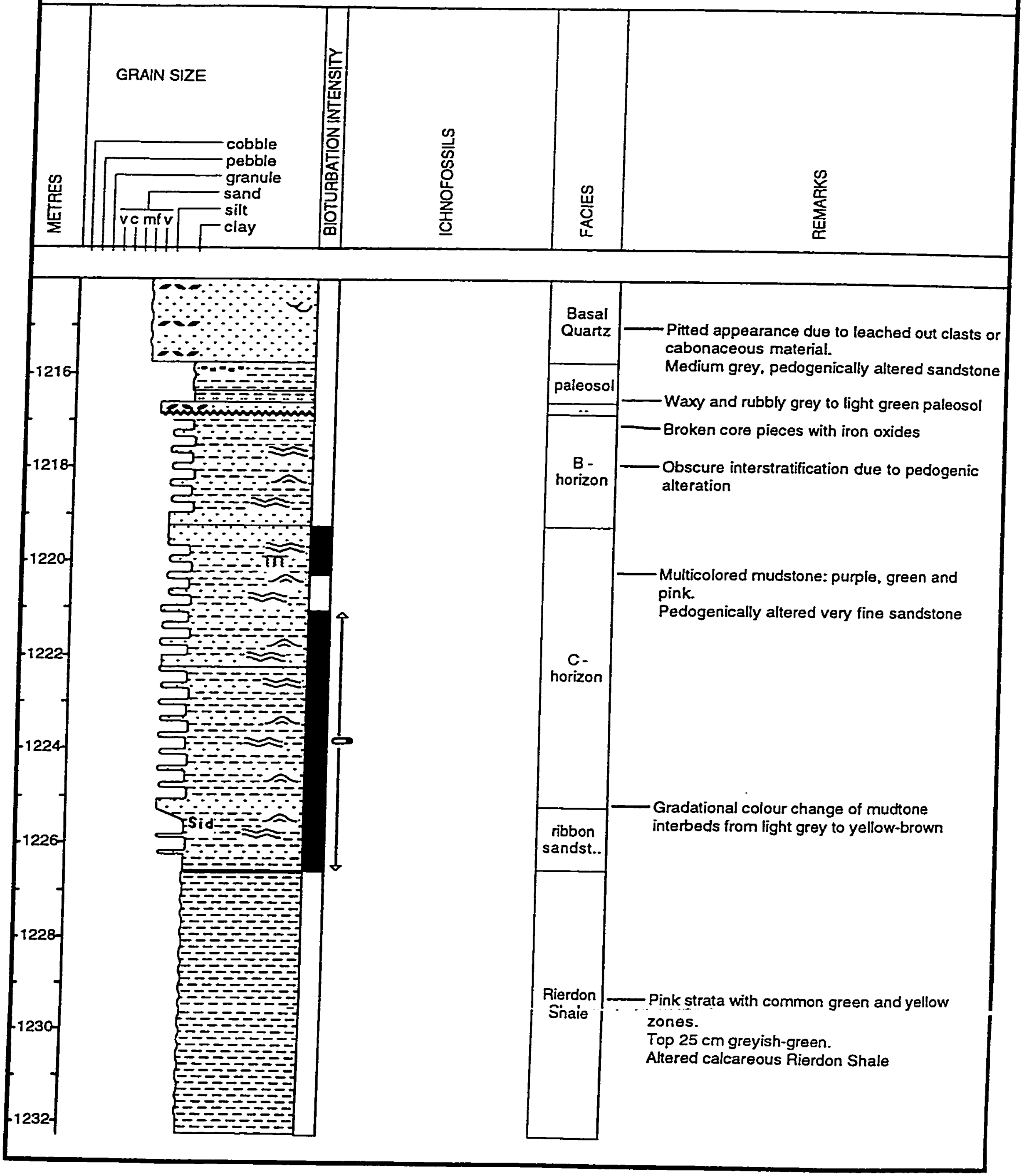

Pitted appearance due to leached out clasts or cabonaceous material.
Medium grey, pedogenically altered sandstone

Waxy and rubbly grey to light green paleosol

Broken core pieces with iron oxides

Obscure interstratification due to pedogenic alteration

Multicolored mudstone: purple, green and pink.
Pedogenically altered very fine sandstone

Gradational colour change of mudtone interbeds from light grey to yellow-brown

Pink strata with common green and yellow zones.
Top 25 cm greyish-green.
Altered calcareous Rierdon Shale

PLacer CeGoPex MAnyberries
10-31-5-4w4

Remarks: Rierdon Shale - dark and light ribbon sandstone - Basal Quartz
Cored interval 1212 - 1225m; recovered 12.4m
11 boxes of 4" core

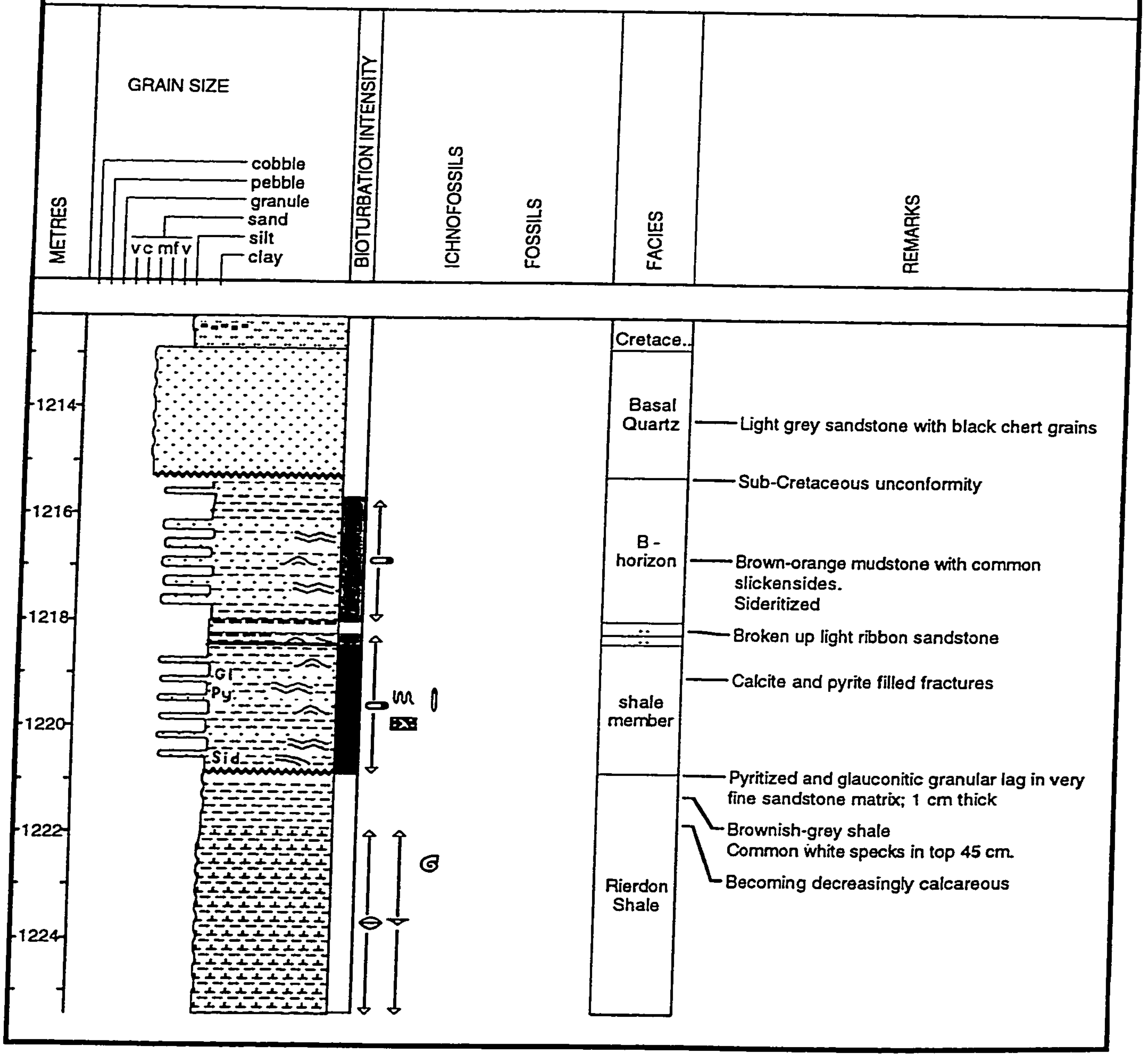

Ashland Murphy Manyberries

6-35-5-4w4

Remarks: light ribbon sandstone - Basal Quartz sandstone
Cored interval 4258-4300'; 8 boxes
3" core

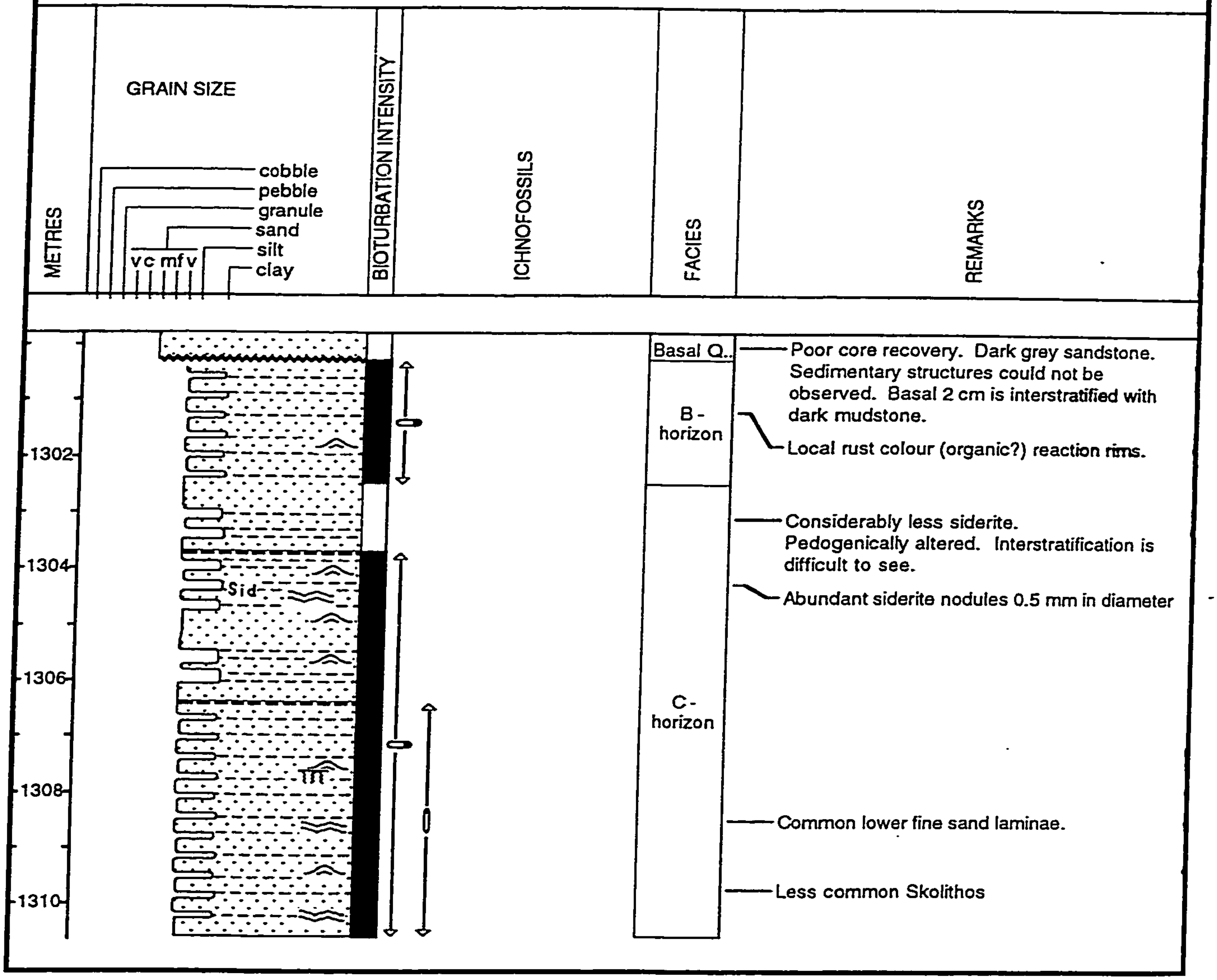

Poor core recovery. Dark grey sandstone. Sedimentary structures could not be observed. Basal 2 cm is interstratified with dark mudstone.

Local rust colour (organic?) reaction rims.

Considerably less siderite. Pedogenically altered. Interstratification is difficult to see.

Abundant siderite nodules 0.5 mm in diameter

Common lower fine sand laminae.

Less common Skolithos

Anderson et al Manyberries

16-1-5-5w4

Remarks: dark and light ribbon sandstone - Basal Quartz sandstone

Cored interval 1120 - 1134 m
Recovered 14 m
13 boxes

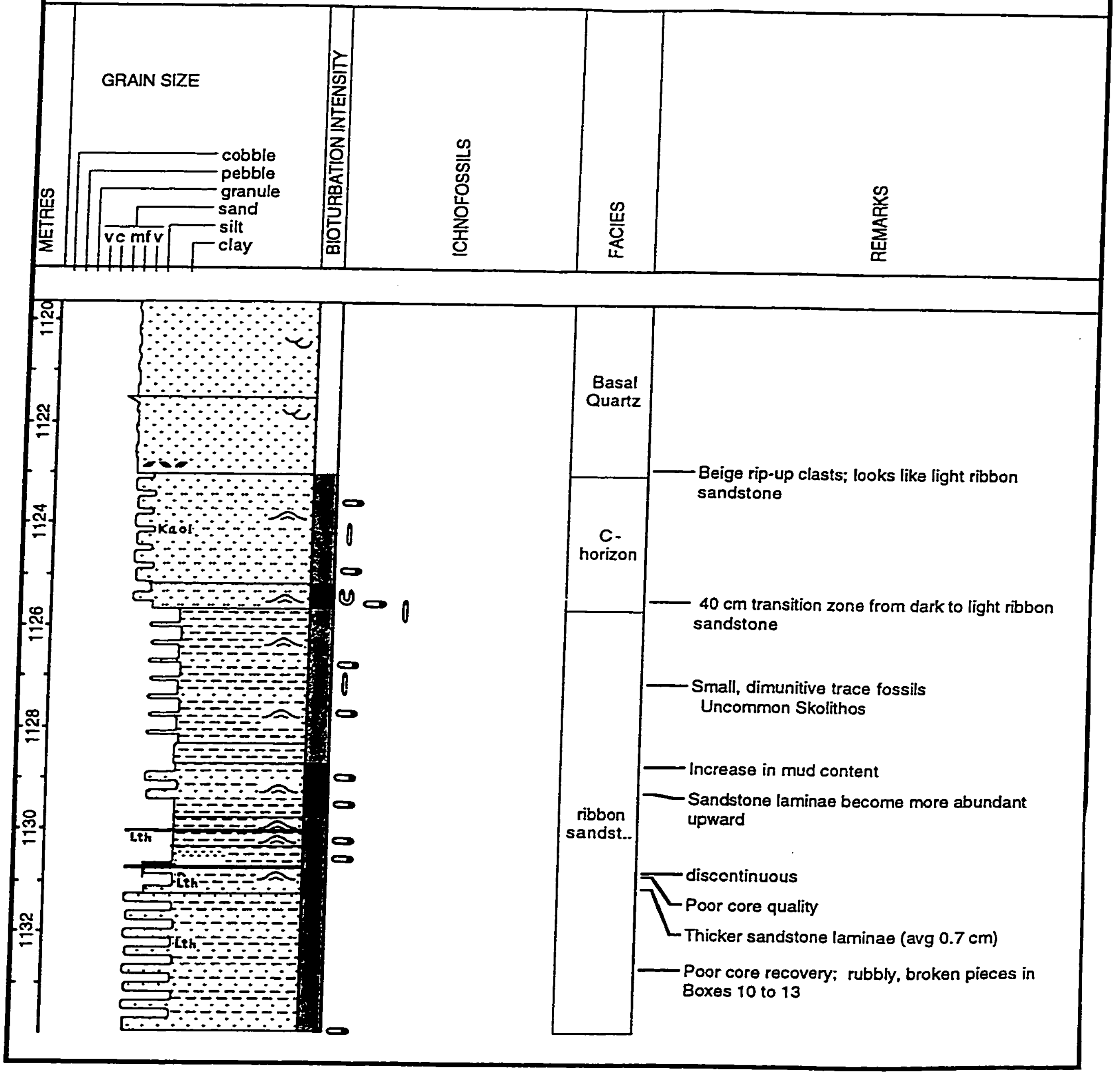

New Jordan et al Manyberries

10-36-5-5w4

Remarks: dark Sand light ribbon sandstone - Basal Quartz
Cored interval: 1168 - 1183m; Recovered 14.77m
11 boxes

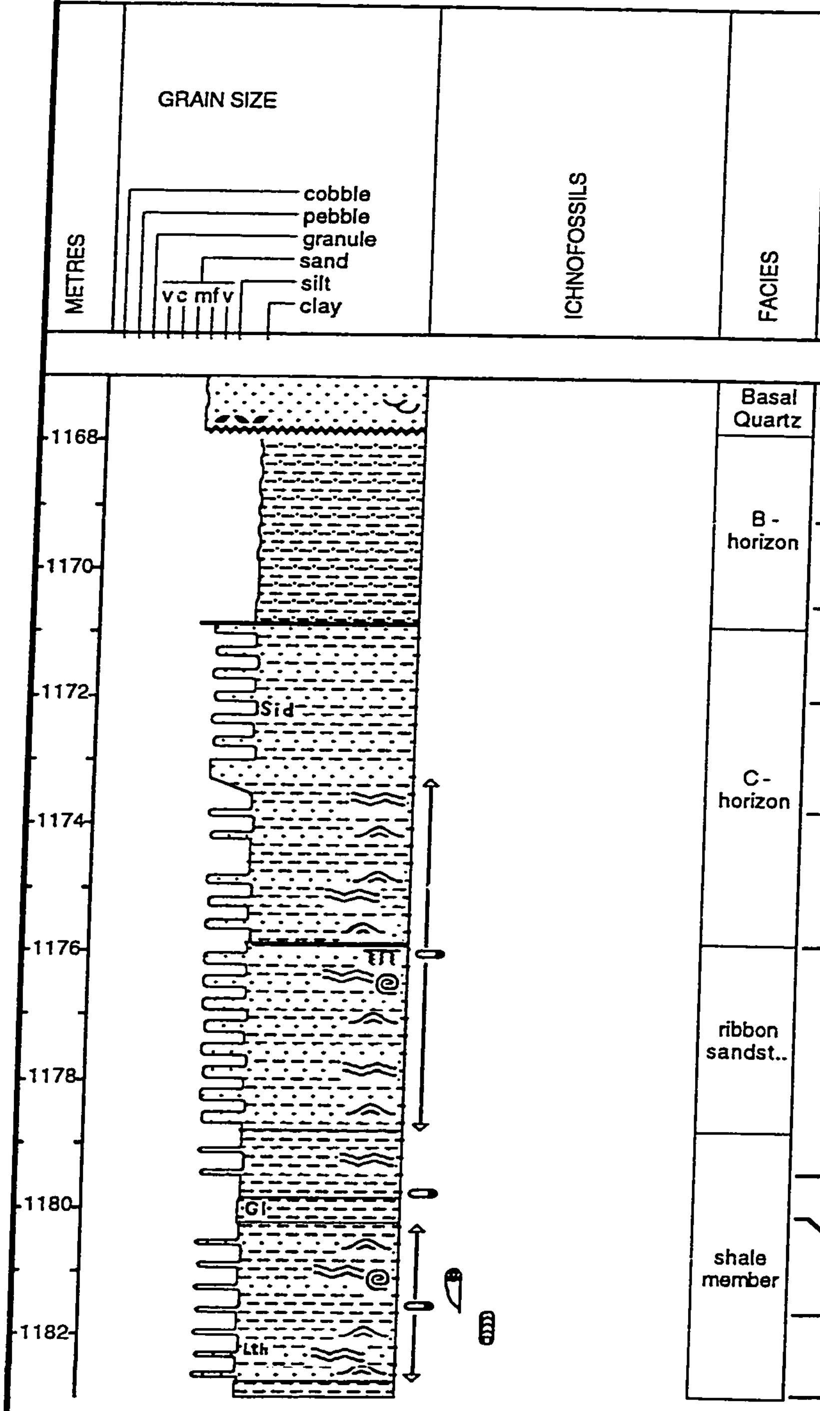

REMARKS

- Pinkish sandstone
- Beige coloured strata
- Few thin upper fine sand laminas.
- Pedogenically altered. Common siderite.
- Pedogenic alteration increases stratigraphically upward.
  Sandstone laminae thin upward.
- Sharp colour change
- Poorly cored section
  Minor fine sandstone laminae
- Lime green glauconitic shale grading into brown-grey shale
- Minor fine sandstone laminas
- Greenish-grey mudstone with chonchoidal fractures.

Shell Manyberries

9-29-5-6w4

Remarks: dark and light ribbon sandstone - Lithofacies 5 and 7 - Basal Quartz sandstone
Cored interval 940 - 958m; recovered 18m - 16 boxes
Slabbed Core with plugs

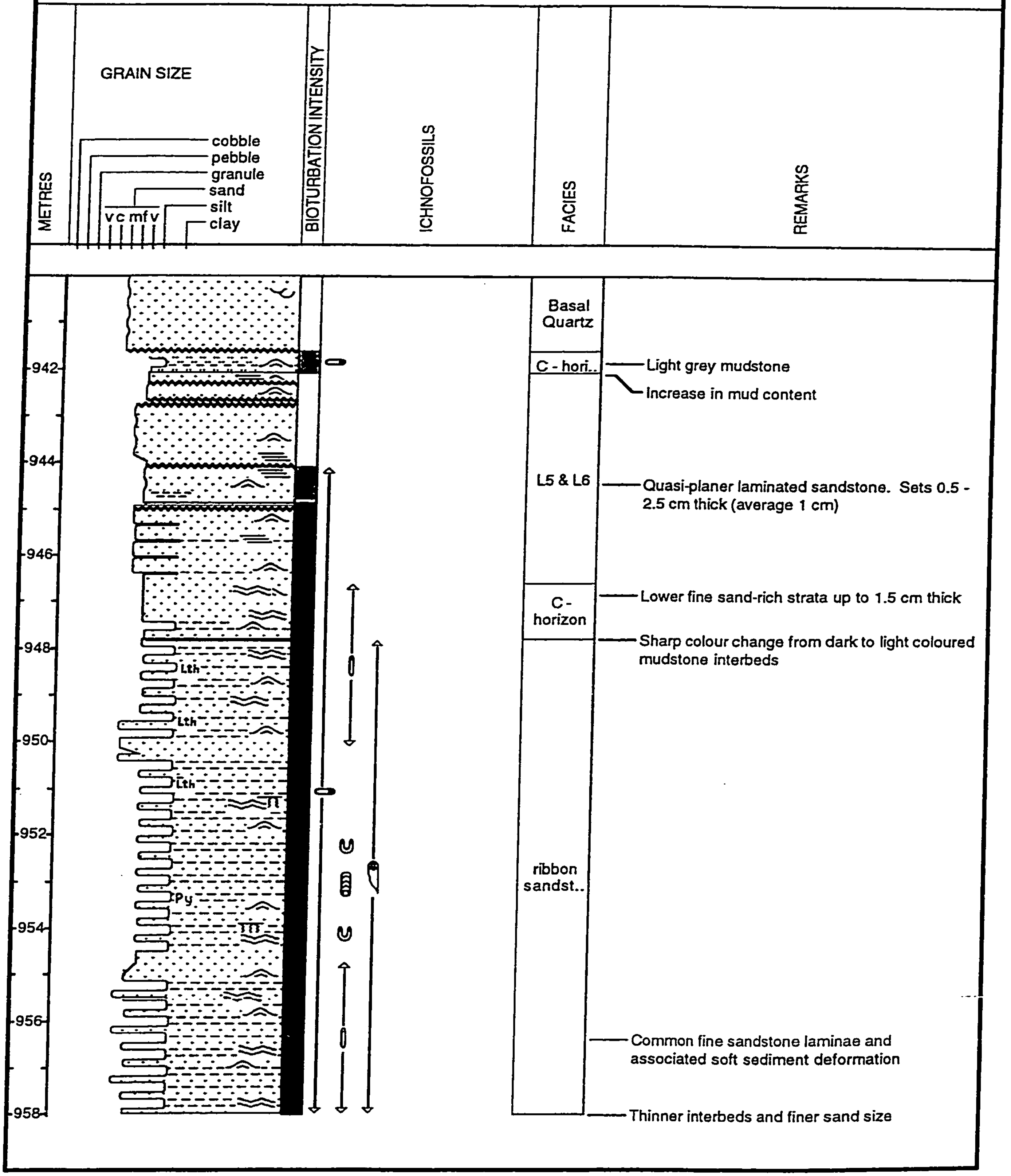

Con Res Manyberries

6-34-5-6w4

Remarks: Dark Swift - Light Swift - Shoreface sandstone? - Altered Light Swift
Core 1: 968 - 977m; recovered 8.5m - 6 boxes
Core 2: 977 - 986m; recovered 9.0m - 7 boxes

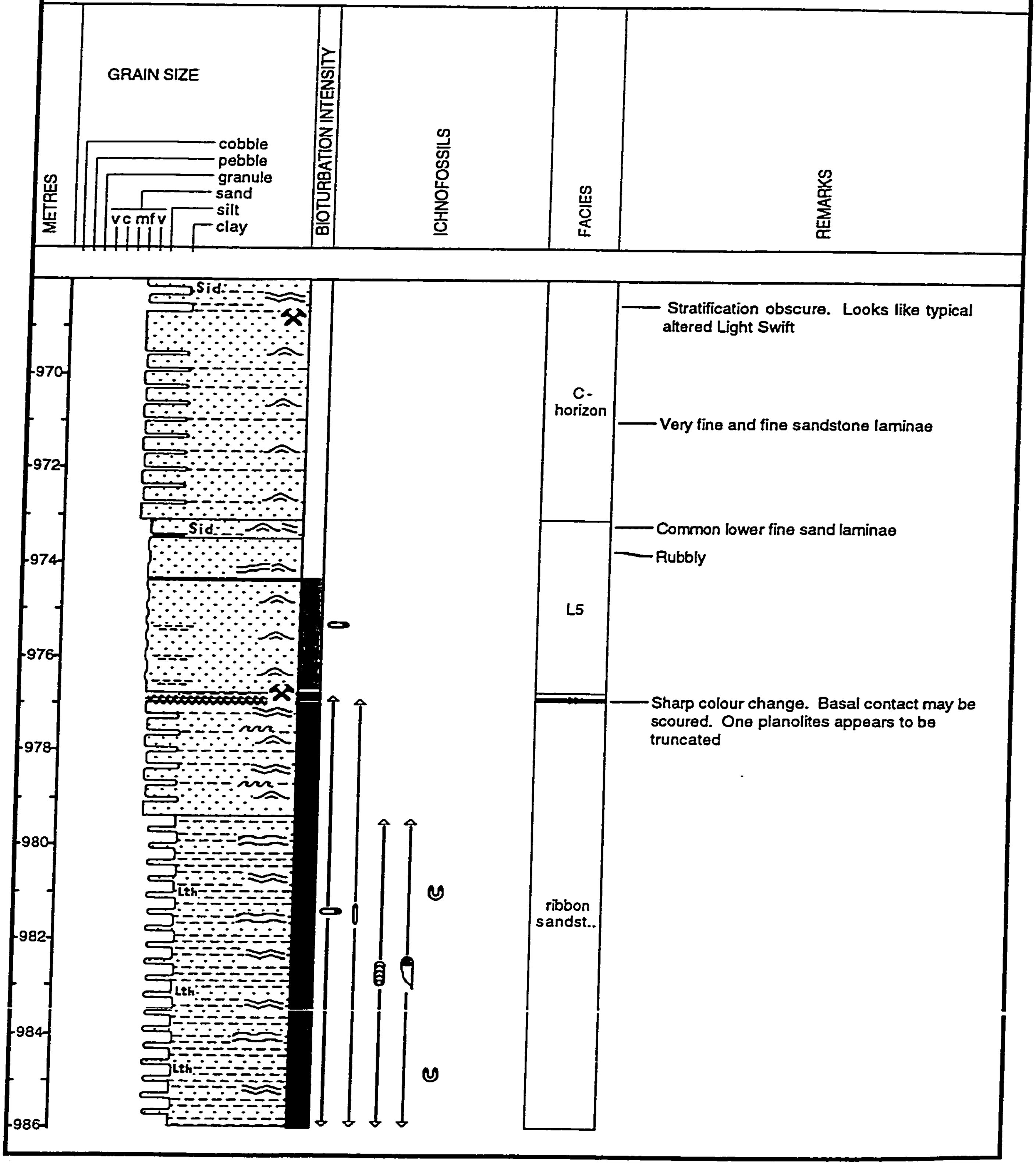

AGIP et Al. Manyberries

10-5-6-4w4

Remarks: Reirdon Shale - shale member - Basal Quartz
Core 1; 1290.0 - 1293.75 m; recovered 2.6 m; 2 boxes
Core 2; 1293.5 - 1311.80 m; recovered 16.2 m; 12 boxes

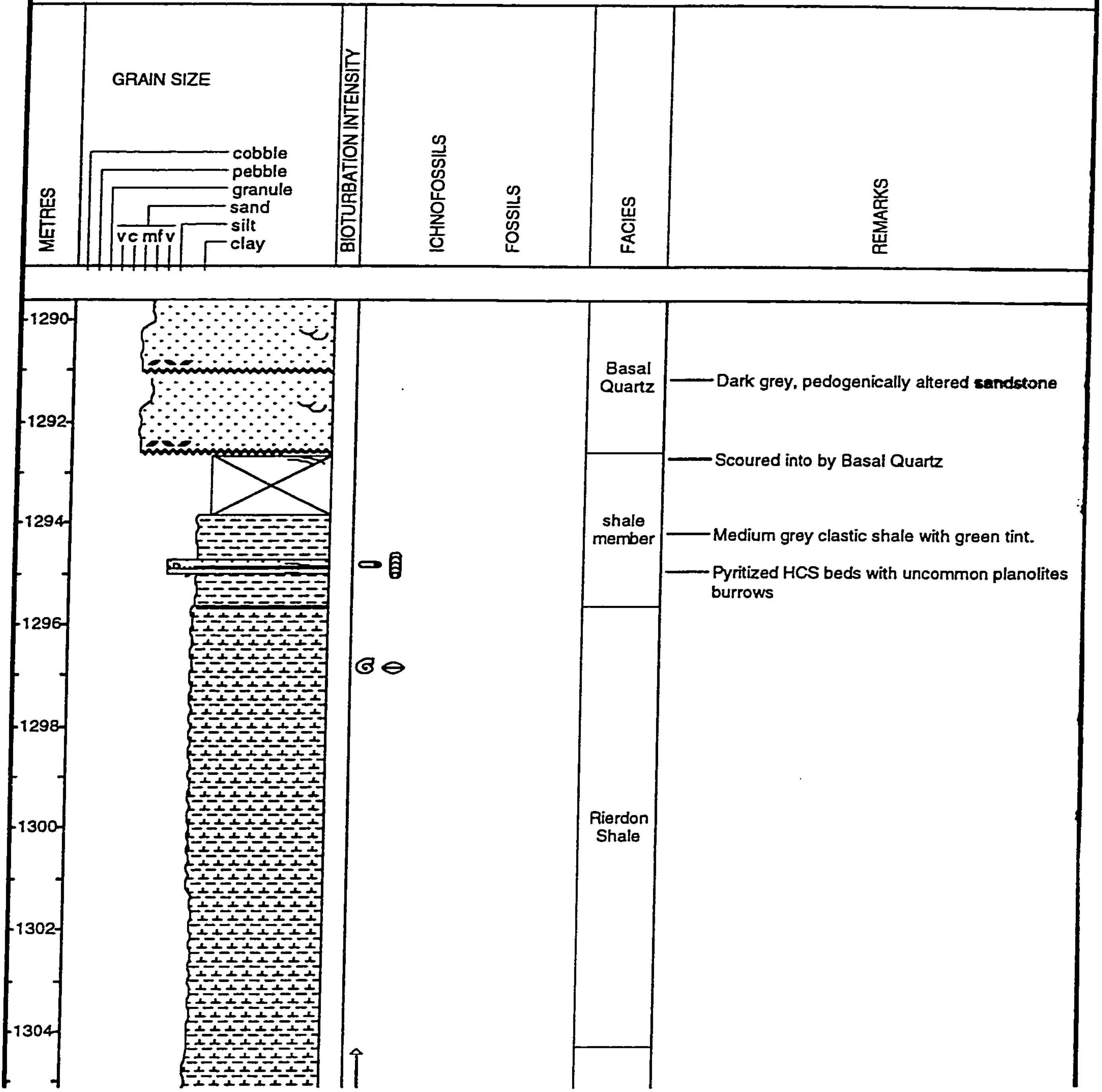

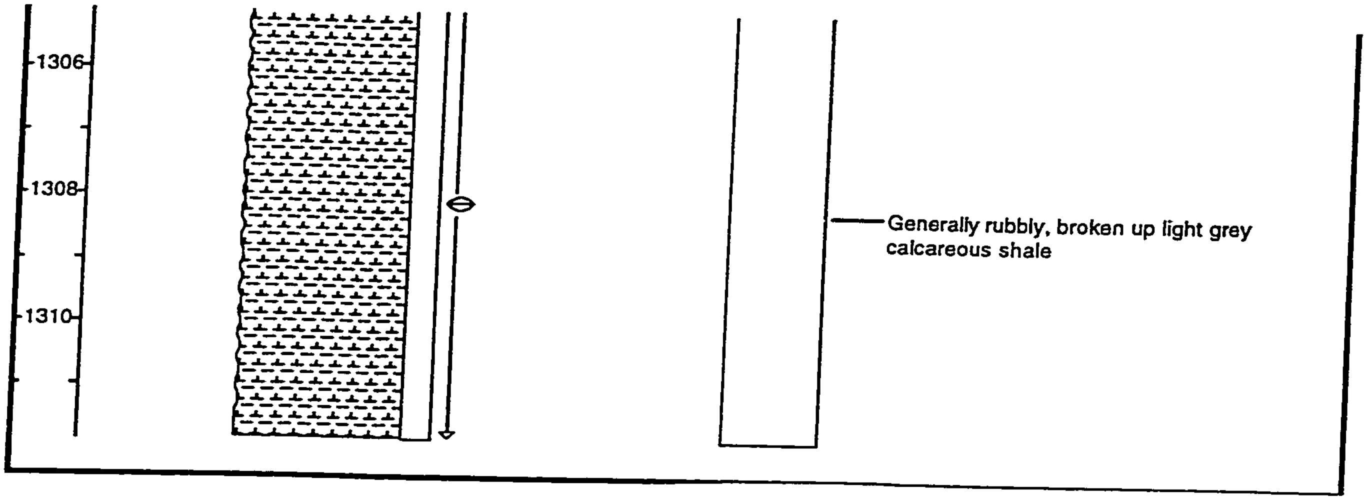
1306
1308
1310
Generally rubbly, broken up light grey calcareous shale

Shell Manyberries
16-4-6-5w4

Remarks: light ribbon sandstone, increasingly sideritized - Basal Qaurtz sandstone
3" core, slabbed, plugs
Core 1. 1074.5 - 1083.5 Recovered 9m; 7 boxes
Core 2. 1083.5 - 1092.5 Recovered 9m; 7 boxes

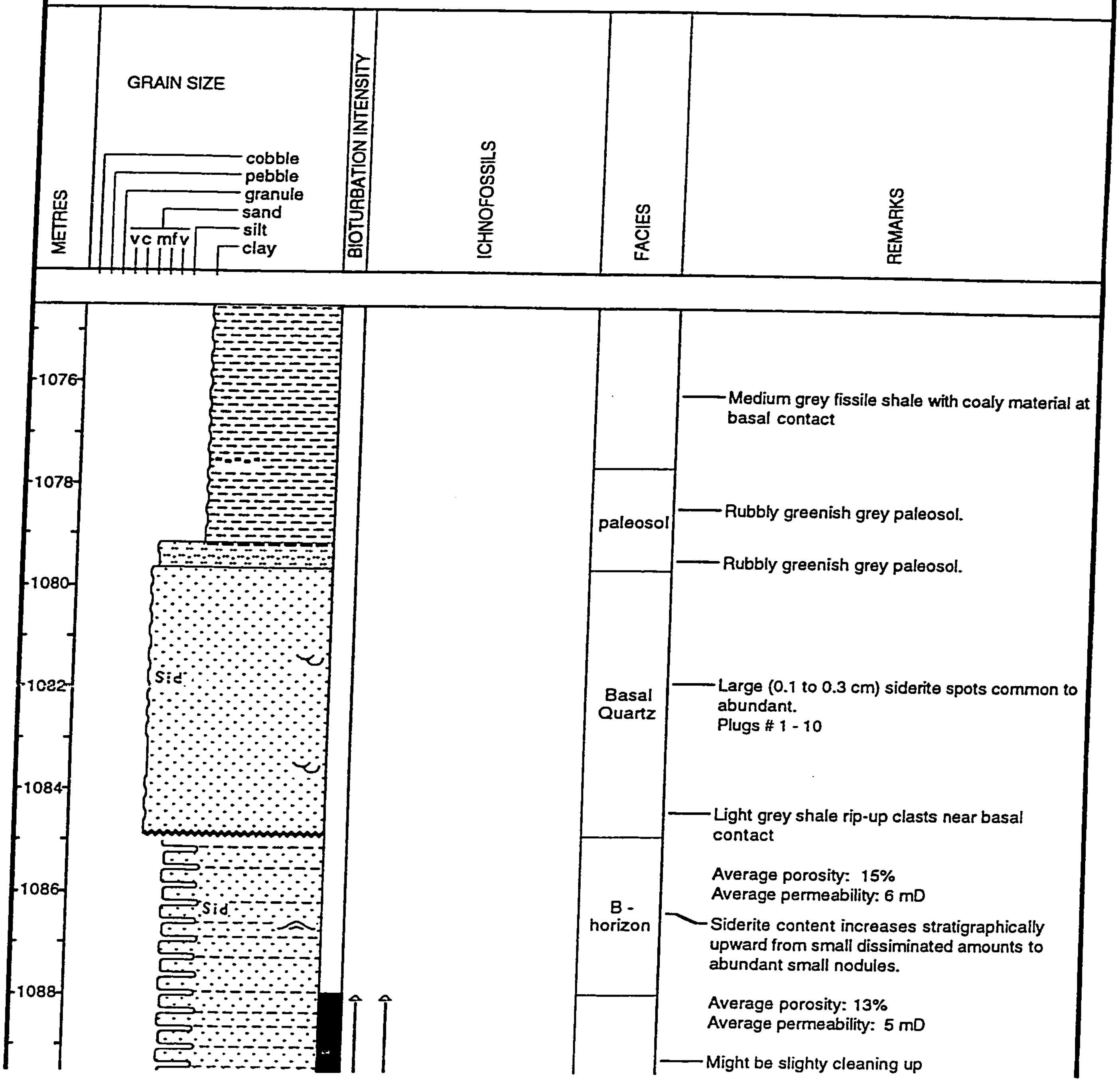

Medium grey fissile shale with coaly material at basal contact

Rubbly greenish grey paleosol.

Rubbly greenish grey paleosol.

Large (0.1 to 0.3 cm) siderite spots common to abundant.
Plugs # 1 - 10

Light grey shale rip-up clasts near basal contact

Average porosity: 15%
Average permeability: 6 mD

Siderite content increases stratigraphically upward from small disseminated amounts to abundant small nodules.

Average porosity: 13%
Average permeability: 5 mD

Might be slighty cleaning up

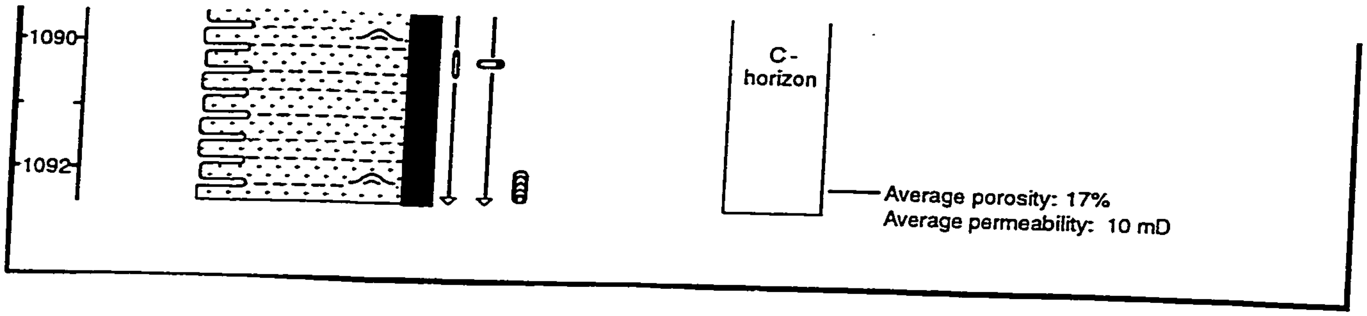
1090
1092
C-
horizon
Average porosity: 17%
Average permeability: 10 mD

Shell Manyberies 14 -5

14-5-6-5w4

Remarks: Rierdon Shale - dark ribbon sandstone - altered light ribbon sandstone
Core 4: 1082 - 1091m; recovered 7.75m - 7 boxes
Core 3: 1073 - 1082m; recovered 8.50m - 8 boxes
Core 2: 1064 - 1073m; recovered 8.70m - 8 boxes
Core 1: 1055 - 1064m; recovered 8.60m - 8boxes
Slabbed core

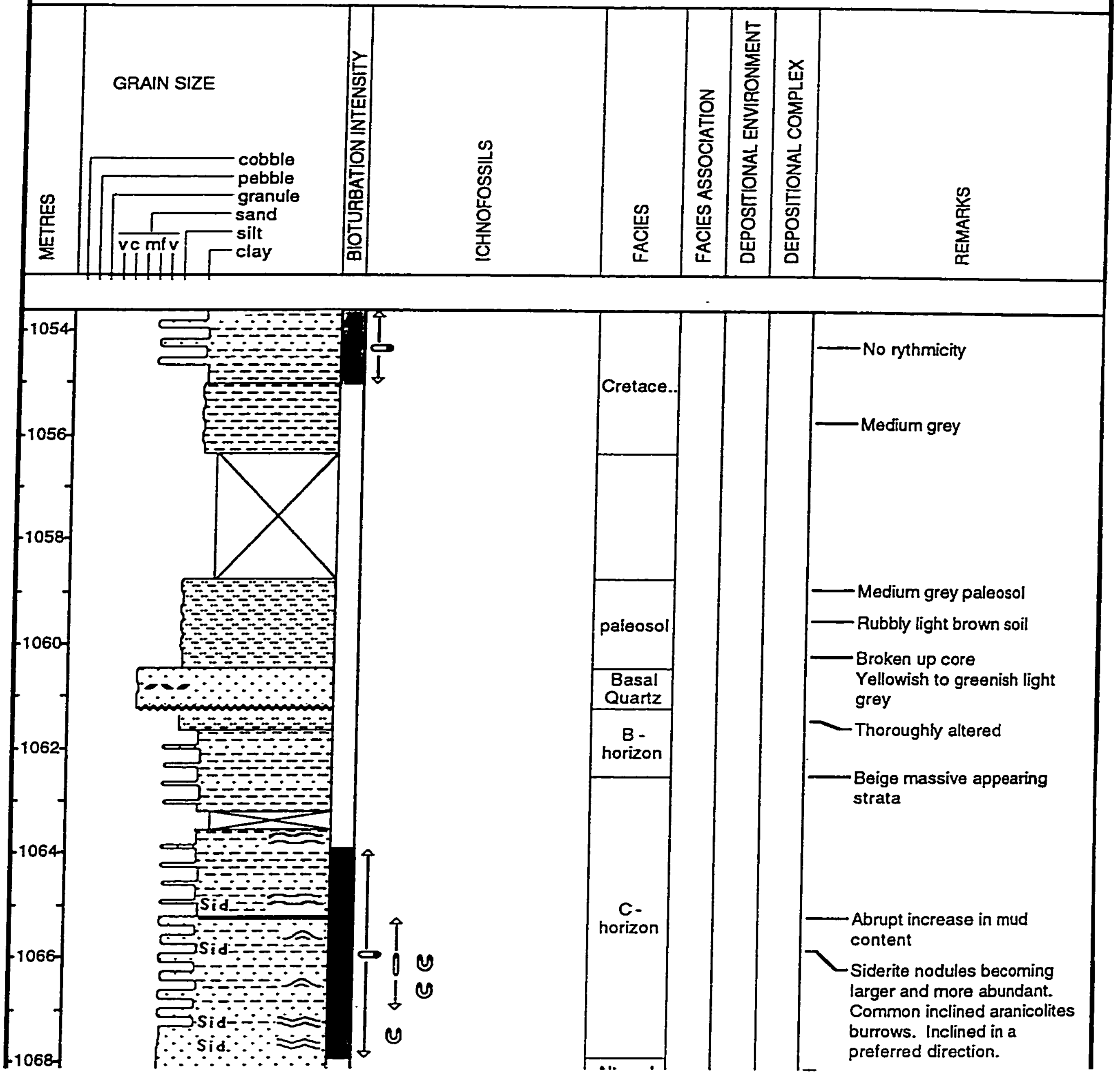

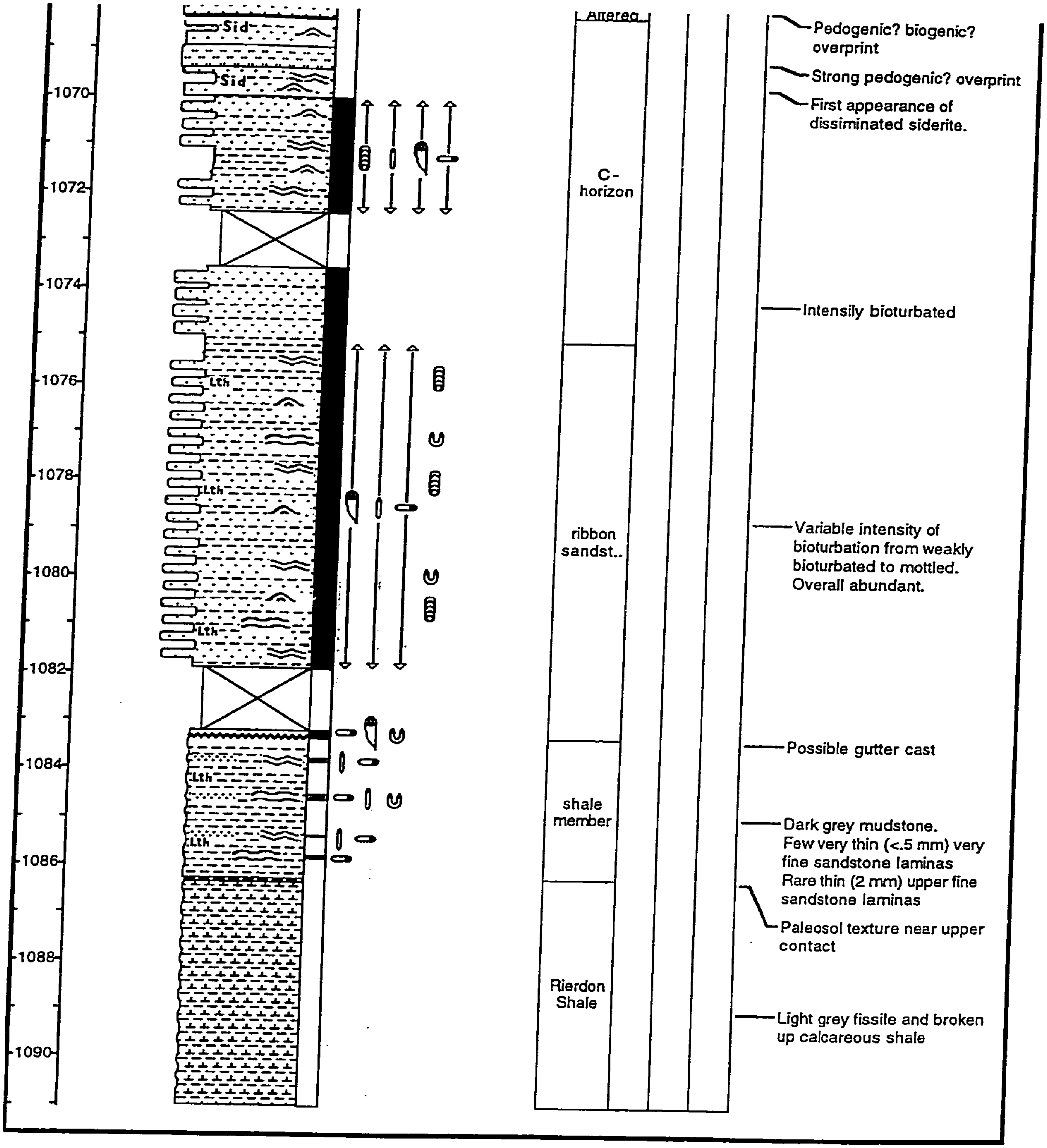
1070
1072
1074
1076
1078
1080
1082
1084
1086
1088
1090
Sid
Sid
Lth
Lth
Lth
Lth
Lth
Altered
C-horizon
ribbon sandst..
shale member
Rierdon Shale
Pedogenic? biogenic? overprint
Strong pedogenic? overprint
First appearance of dissiminated siderite.
Intensily bioturbated
Variable intensity of bioturbation from weakly bioturbated to mottled. Overall abundant.
Possible gutter cast
Dark grey mudstone. Few very thin (<.5 mm) very fine sandstone laminas Rare thin (2 mm) upper fine sandstone laminas
Paleosol texture near upper contact
Light grey fissile and broken up calcareous shale

Roan LL + E Manyberries

6-1-6-6w4

Remarks: shale member - dark ribbon sandstone
Cored interval: 1042 - 1051m; recovered 7.75m
7 boxes

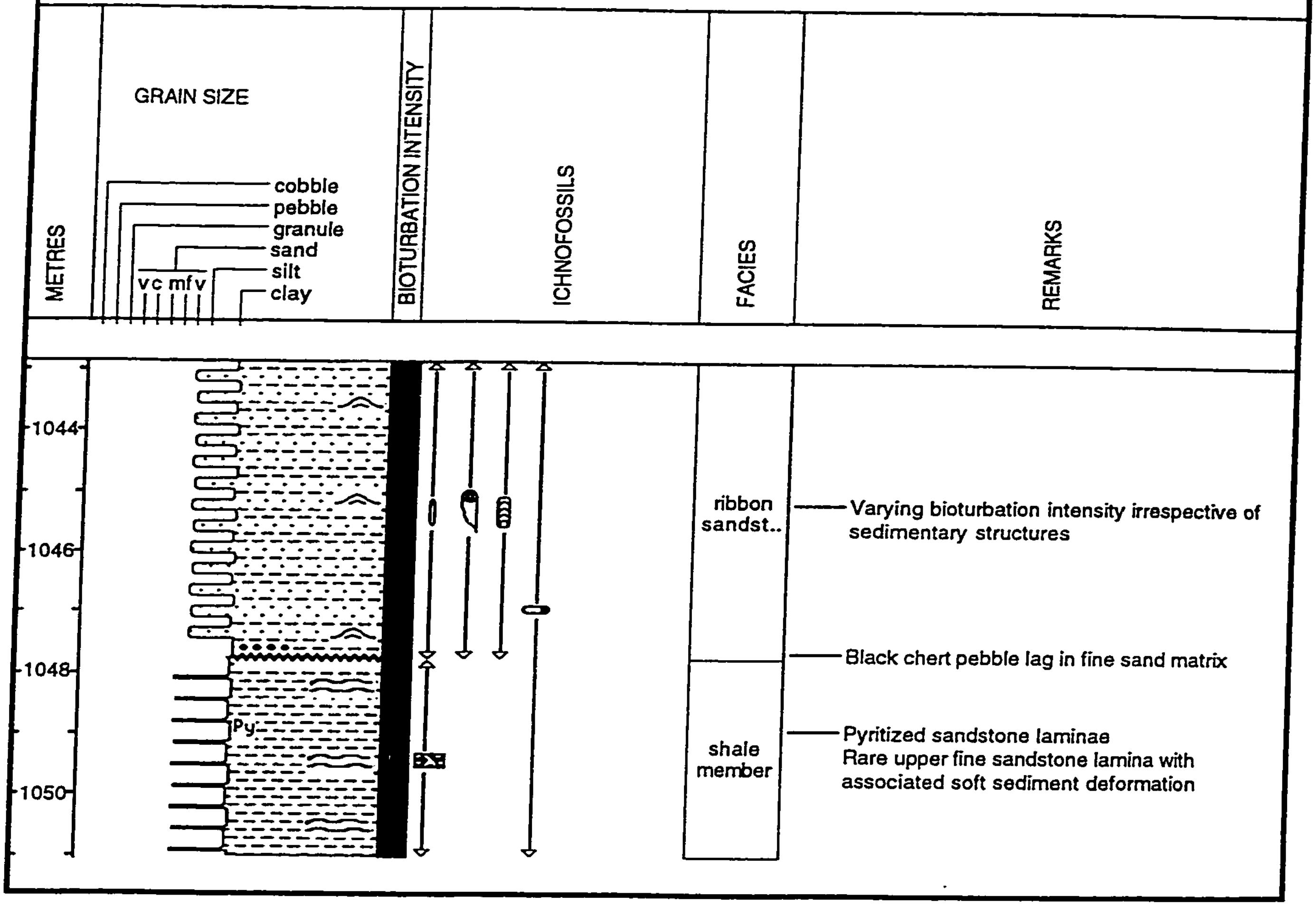

Varying bioturbation intensity irrespective of sedimentary structures

Black chert pebble lag in fine sand matrix

Pyritized sandstone laminae
Rare upper fine sandstone lamina with associated soft sediment deformation

Texaco CDN Reserves Manyberries

2/6-2-6-6w4

Remarks: dark and light ribbon sandstone - Basal Quartz
7 boxes

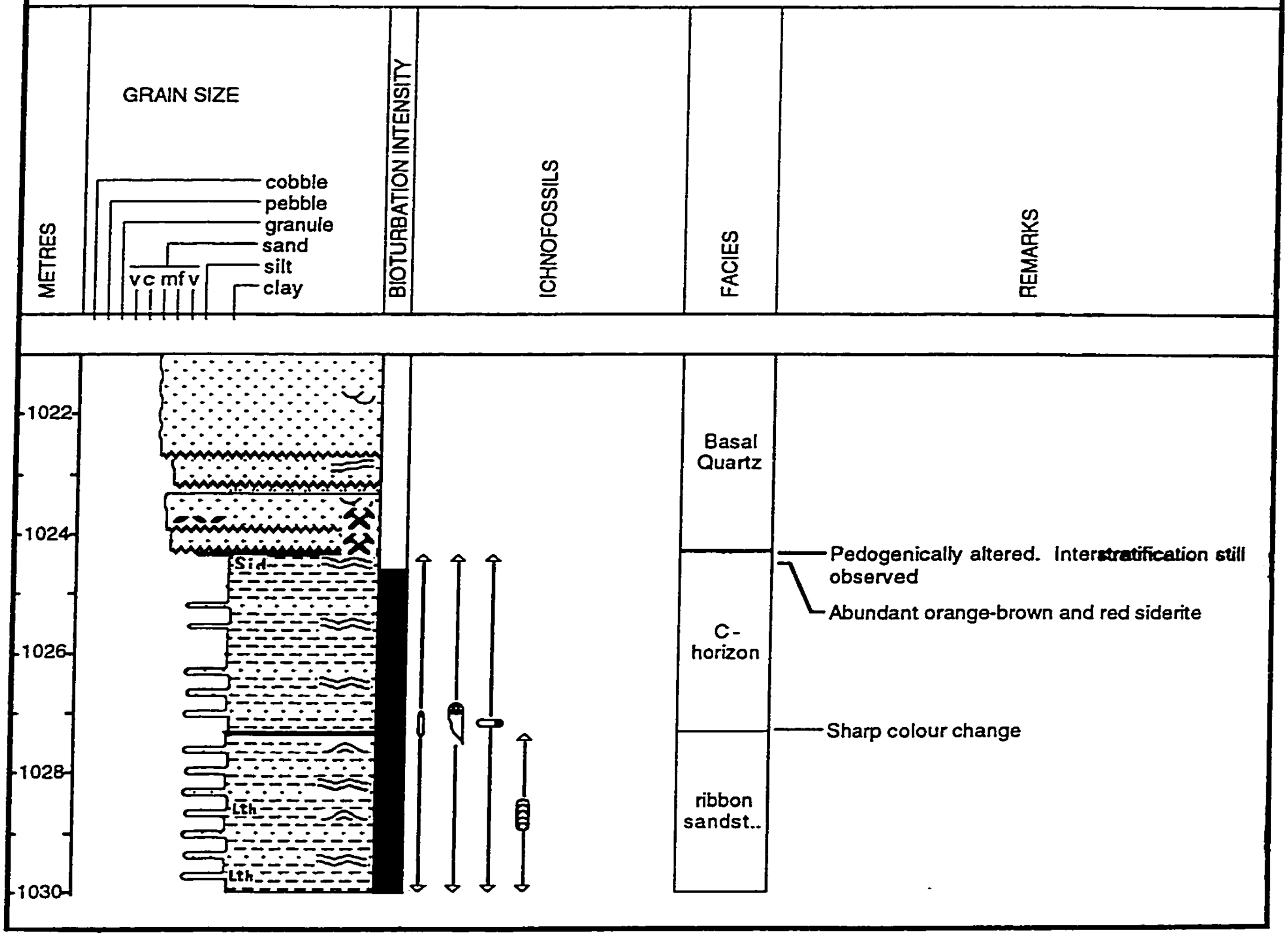

Home AGIP Manyberries
6-12-6-6w4

Remarks: dark and light ribbon sandstone - Basal Quartz sandstone
Cored interval: 1051-1069 m; recovered 10m
10 boxes

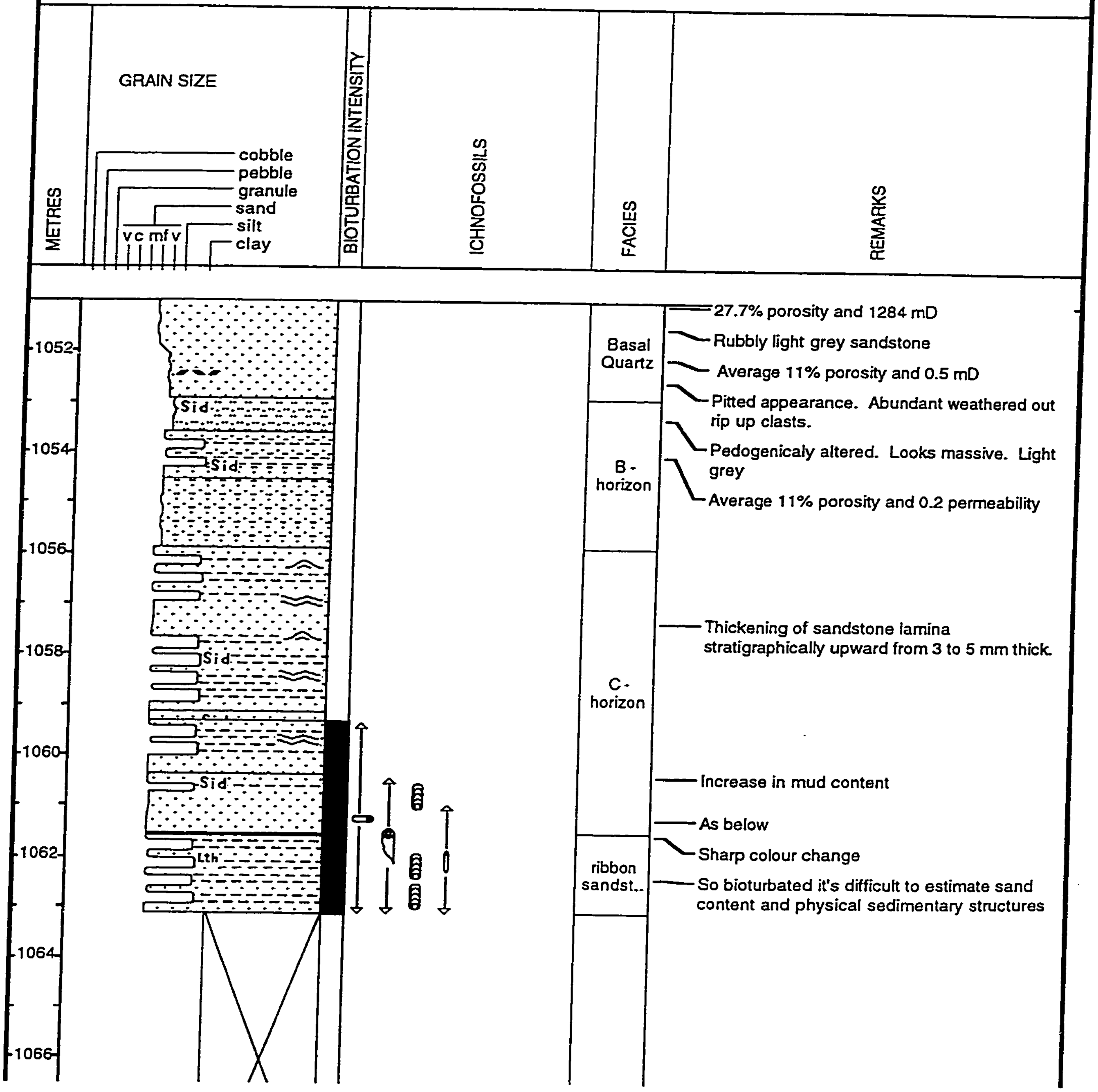

Carion et al Manyberies
8-34-6-6w4

Remarks: shale member - dark and light ribbon sandstone - Basal Quartz sandstone - coal
- paleosol
Cored interval: 1147 - 1163m - 11 boxes
Note: I'm not sure where Dark Swift/Light Swift contact is

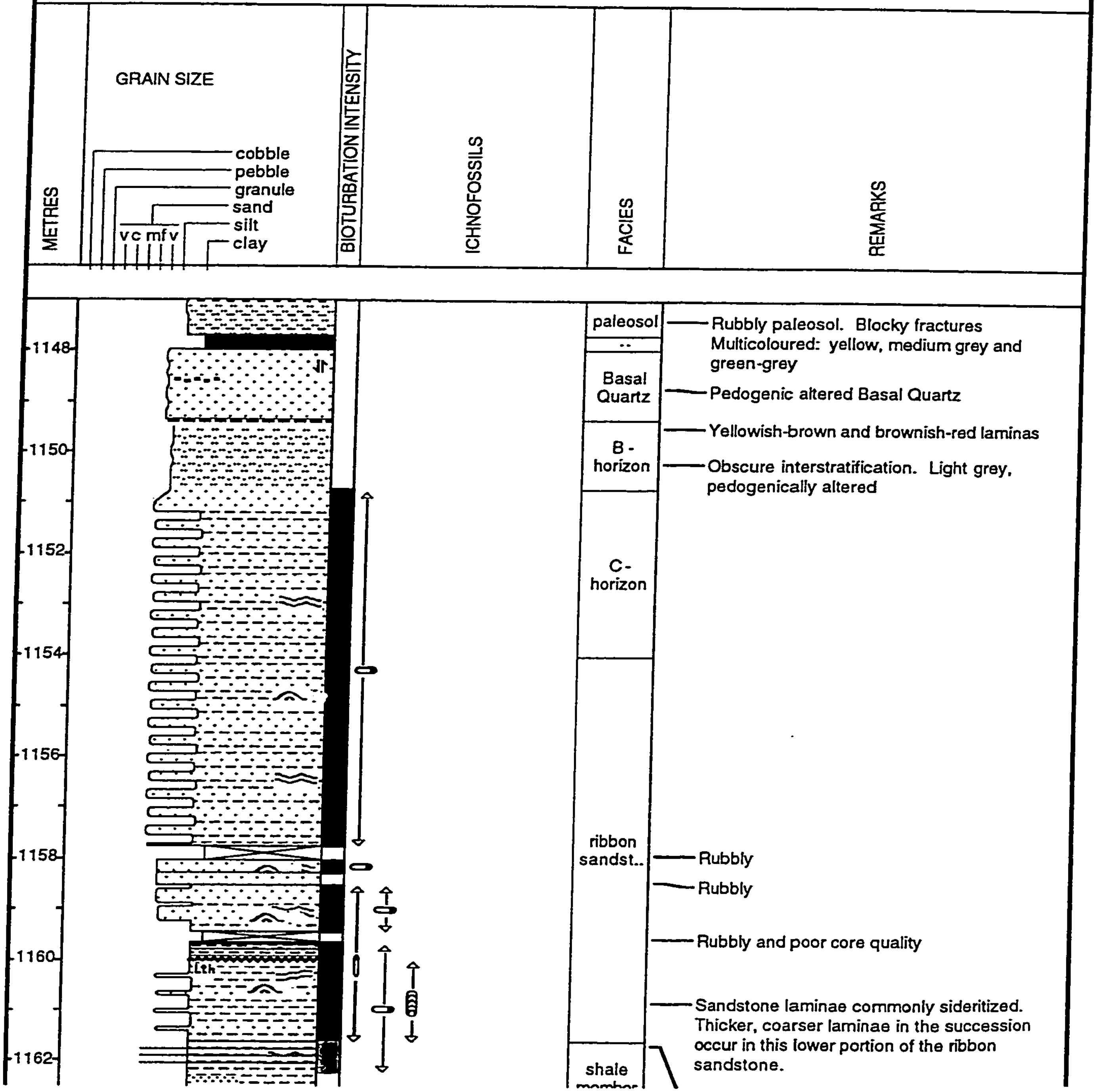

Rubbly paleosol. Blocky fractures Multicoloured: yellow, medium grey and green-grey

Pedogenic altered Basal Quartz

Yellowish-brown and brownish-red laminas

Obscure interstratification. Light grey, pedogenically altered

Rubbly

Rubbly

Rubbly and poor core quality

Sandstone laminae commonly sideritized. Thicker, coarser laminae in the succession occur in this lower portion of the ribbon sandstone.

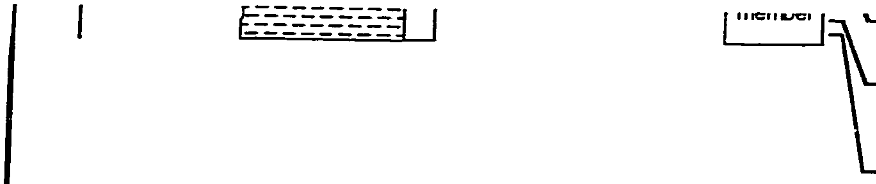

Top 5cm lighter in colour (greenish-grey). Oxidized?

Broken up small charcoal grey pieces. Abundant straight, cross-cutting and structured horizontal burrows at base of a bed.

Lag with rounded black chert granules up to 1 cm in diameter (avg 4 mm) in a glauconitic shale.
Abundant structured straight horizontal burrows at base of bed going in different directions and at different angles into bed.
Unknown where core piece truly fits stratigraphically.

McColl Union

13-5-6-7w4

Remarks: Sandstone-rich altered light ribbon sansdtone - Basal Quartz - paleosol
Wireline core (1")
2970 - 2995' 3 boxes

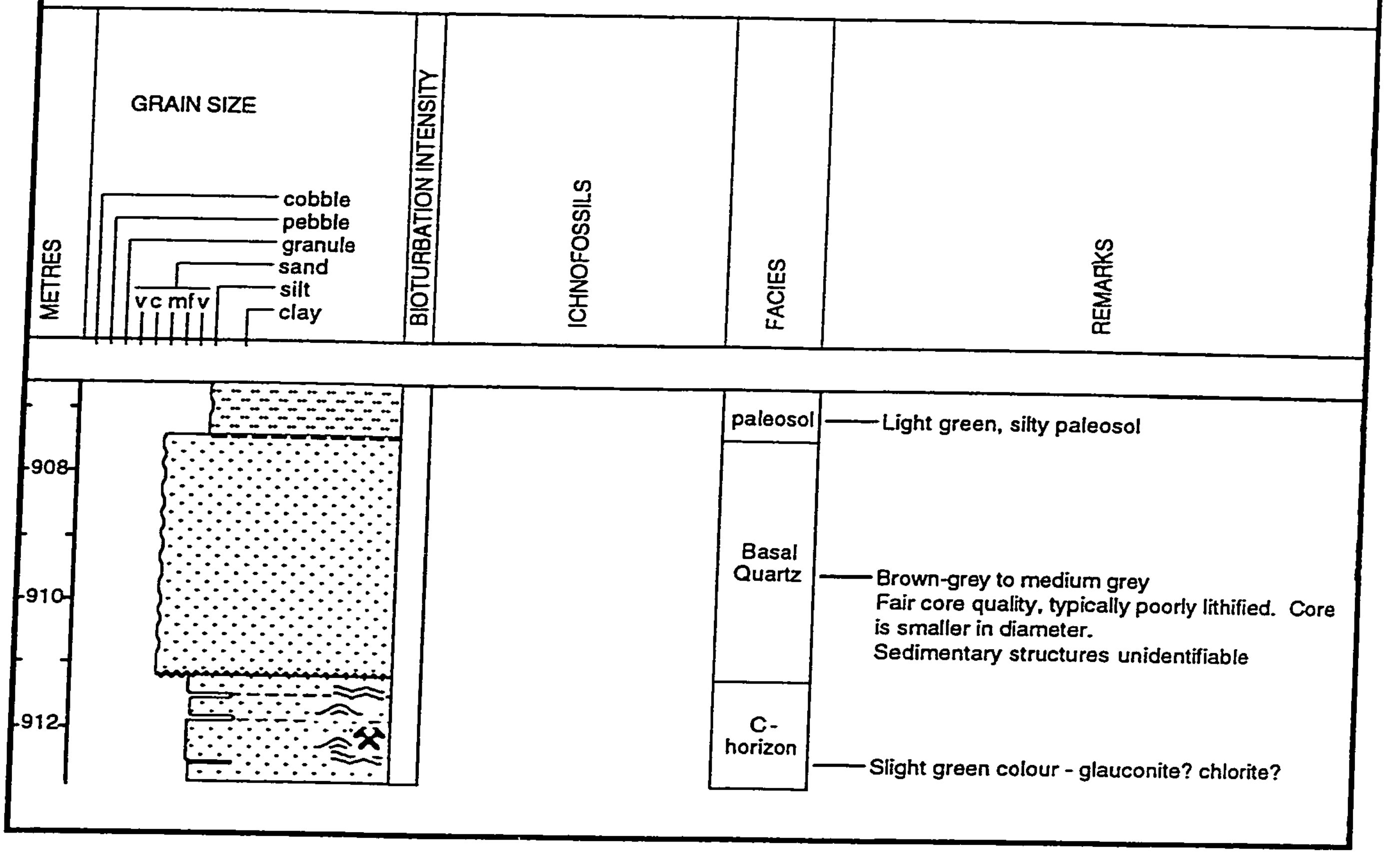

Light green, silty paleosol

Brown-grey to medium grey
Fair core quality, typically poorly lithified. Core is smaller in diameter.
Sedimentary structures unidentifiable

Slight green colour - glauconite? chlorite?

GMG Cypress

6-23-7-3w4

Remarks: dark and light ribbon sandstone
Cored interval: 4650 - 4700; recovered 50'
14 boxes

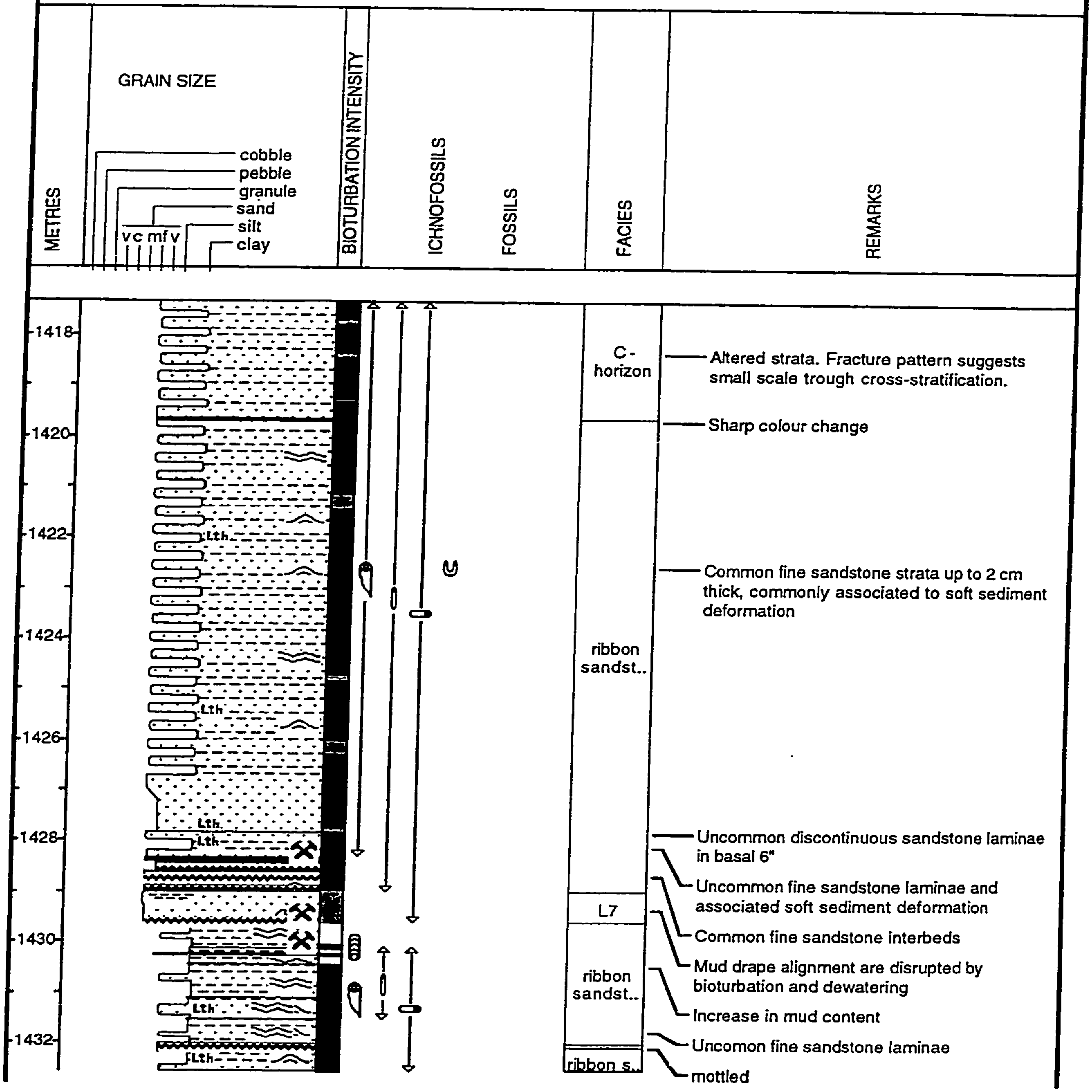

CMG Cypress
6-1-8-4w4

Remarks: dark and light Ribbon sandstone - Incised Valley (BQ)
Photographed core boxes

Core 1 4052 - 4069' 5 boxes
Core 2 4069 - 4101' 8 boxes

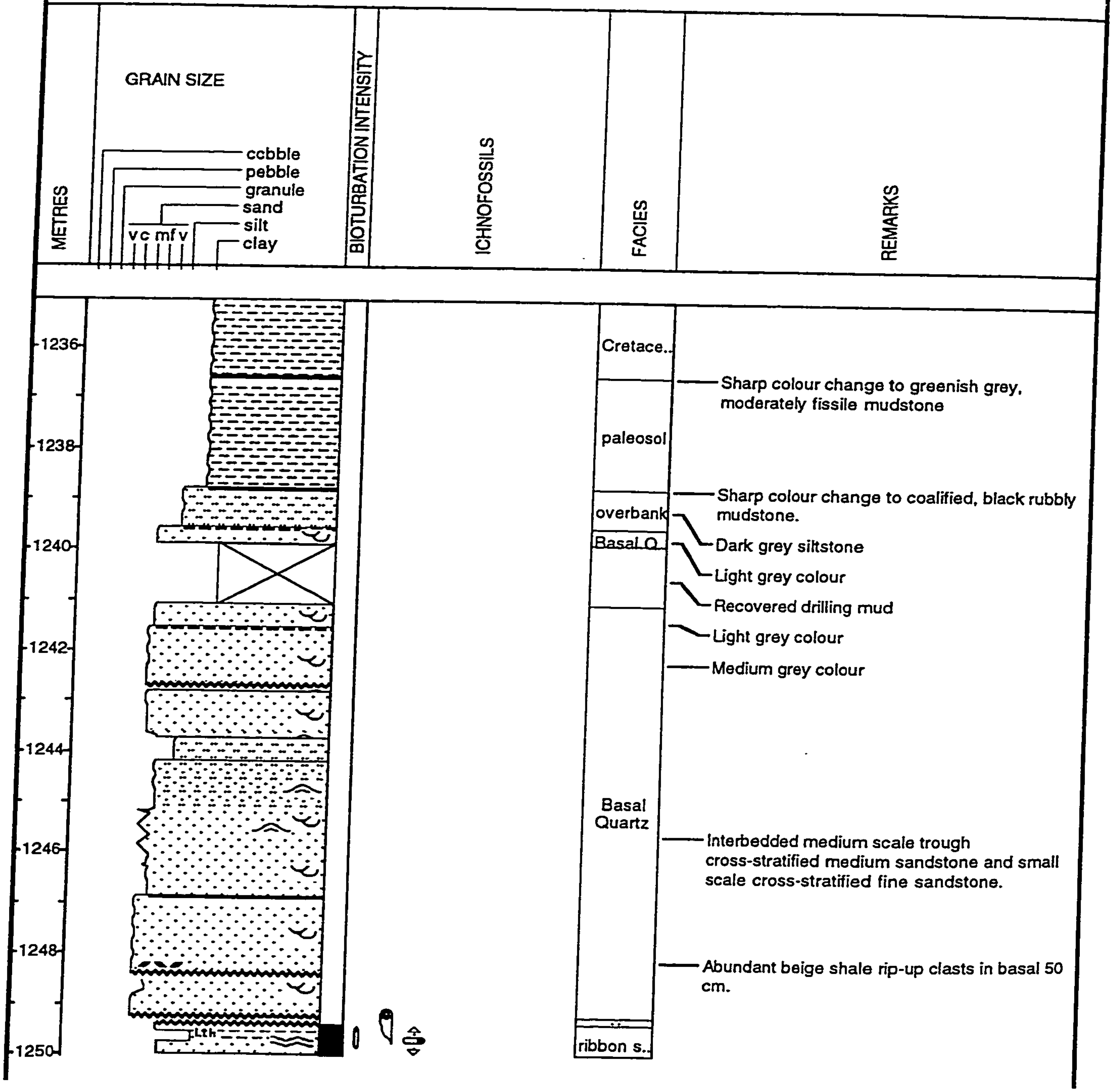

Appendix 2

Petrographical Analysis

Twenty-eight thin sections were analyzed from samples of ribbon sandstone strata collected from several different wells in southeastern Alberta (Fig. A-1.1). Thin sections were impregnated with blue-dyed epoxy that highlights void space (open pores). Estimated porosity ranges from 0 to 20% and measured permeability ranges from approximately 3 to 100 mD. Most thin sections were also stained with a cobaltinitrate solution that stains potassium feldspar bright yellow. This procedure helps differentiate quartz from potassium feldspar grains in the sandstone. Sandstones were classified according to Folk's classification (1970), and are plotted on a QFR ternary diagram (Fig. A-1.2). In this study the R-pole comprises unaltered and tripolitic (altered) chert, and other sedimentary rock fragments, principally compacted mudstone and siltstone clasts that commonly form a pseudomatrix. Results of petrographical analyses are summarized in Table A-1.1.

Ribbon sandstone are litharenites composed predominantly of moderately well sorted, rounded, very fine sandstone. Medium-grained litharenite are comparatively rare. Framework grain composition varies little and consists dominantly of monocrystalline quartz (average 55%), clean to muddy chert (25–40%), cherty mudstone, silty mudstone, and mudstone clasts (10-30%), and potassium feldspar (1-8%; average 3%) (Plates 1 and 2). Chert is present both as unaltered and tripolitic grains. Tripolitic chert is the term applied to partly dissolved (altered) chert grains (this dissolution creates ineffective secondary porosity, Plate 2). Outlines of silicified fossil fragments and silicified dolomite rhombohedral crystals were commonly observed in both altered and unaltered chert grains, suggesting that the chert was most probably derived from silicified limestone in nearby highland areas. Accessory minerals in the Swift sandstone consists of up 1% muscovite, and trace amounts of plagioclase, biotite, and heavy minerals, including tourmaline, zircon, and rutile.

The mudstone fraction in the Swift was not studied extensively. However, it is noteworthy that mica-rich mudstone interbeds in the dark ribbon sandstone are considerably darker than those of the light ribbon sandstone, which is the result of its significantly higher organic matter content (Plate 3).

Diagenetic grains are also present within strata of the Swift and include glauconite, pyrite and sphaerosiderite nodules. Generally, glauconite dark green (high maturity) and is characterized by rounded very fine grains or, compacted grains partly filling pores. Sphaerosiderite nodules are present only in altered (light) ribbon sandstone, and typically are <1 mm in diameter with a common radial internal fabric and uncommon discontinuous concentric layers of pyrite (Plate 5b). These compositional differences are interpreted to indicate fluctuating Eh conditions during iron mineral precipitation. Concentric, convex-downward laminated argillans are also abundant in the massive appearing facies of the light ribbon sandstone (Lithofacies 8), indicating elluvial deposition of silt and mud in the Bt horizon of an ancient soil profile (Plate 5a).

Sandstones of the ribbon sandstone are dominantly cemented by compacted mudstone and silty mudstone clasts that form a pervasive pseudomatrix (Plate 1). Locally, however, authigenic clay coatings, calcite cement, or pore-filling chlorite are present, and may make up to 30% of the mineralogy (Plate 4).

Although framework grain composition varies little in the Swift Formation, upward-changes in mineralogy do occur. It is important to note, however, that these changes are not primary, but developed during early diagenesis. For example, tripolitic chert is significantly more abundant upward. In the upper part of the altered ribbon sandstone, chert is consistently more altered, with poorly discernible grain boundaries. Because of heterogeneous and low vertical permeabilities, strata at higher stratigraphic levels were exposed for longer periods to aggressive meteoric fluids that partially dissolved chert grains. Similarly, feldspar and glauconite content appears to decrease stratigraphically upward. Samples with abundant tripolitic chert have few or no feldspars and glauconite was rare to absent in altered, light ribbon sandstone. This is interpreted to be related to extensive leaching that took place at the same time as chert alteration. In addition, compacted mudstone fragments (pseudomatrix) also become more altered stratigraphically upward from a dark brown, opaque, to a more greenish (caused by the underlying blue-dyed epoxy), translucent, milky character. Another upward change in mineralogy, as mentioned above, is the appearance of sphaerosiderite in the upper part of the Swift. Sphaerosiderite abundance and size generally increase upward in the altered ribbon sandstone because nodules occurring at higher stratigraphic levels would have nucleated earlier and have had more time for crystal growth.

A significant problem in southeastern Alberta is differentiating Upper Jurassic (Swift) from Lower Cretaceous (Basal Quartz) sandstones. This is especially problematic for interpreting geophysical and seismic logs. In addition, the Basal Quartz Formation is also commonly pedoturbated and exhibits pedogenic features similar to those observed in the light ribbon sandstone, such as sphaerosiderite and ubiquitous laminated argillans. In thin section, however, Swift sandstones are generally finer grained and characterized by high feldspar content; feldspar is generally absent in sandstone of the Basal Quartz (Dan Potocki, pers. communication, 1996).

Figure A-1.1. Location of samples collected for petrographical analysis

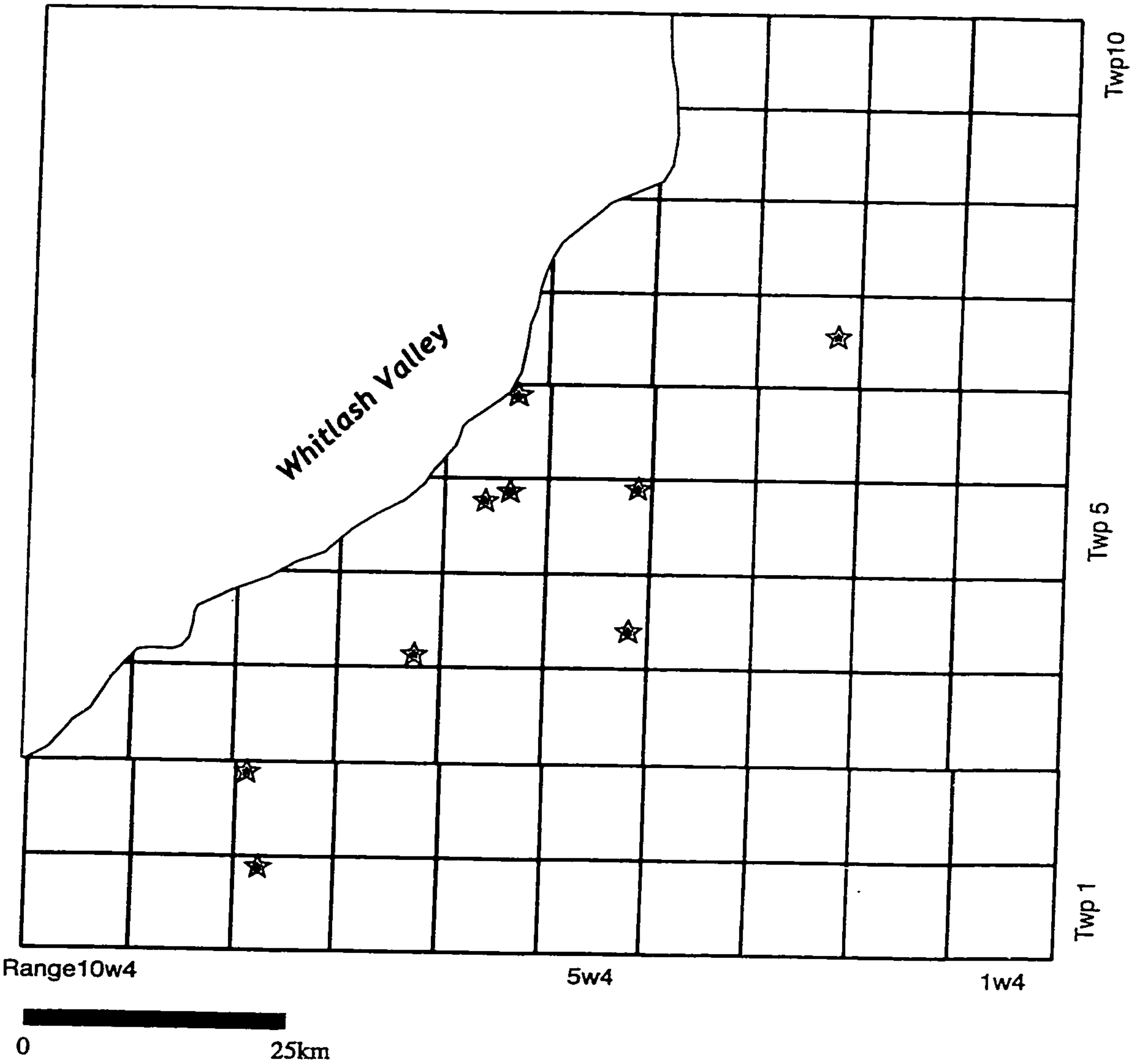
Whitlash Valley
Twp10
Twp 5
Twp 1
Range10w4
5w4
1w4
0
25km

Figure A-1.2. QFR ternary diagram. The Q pole comprises monocrystalline quartz, the F pole includes potassium feldspar and plagioclase, and the R pole comprises chert, tripolitic chert, cherty and silty mudstone fragments, and mudstone clasts.

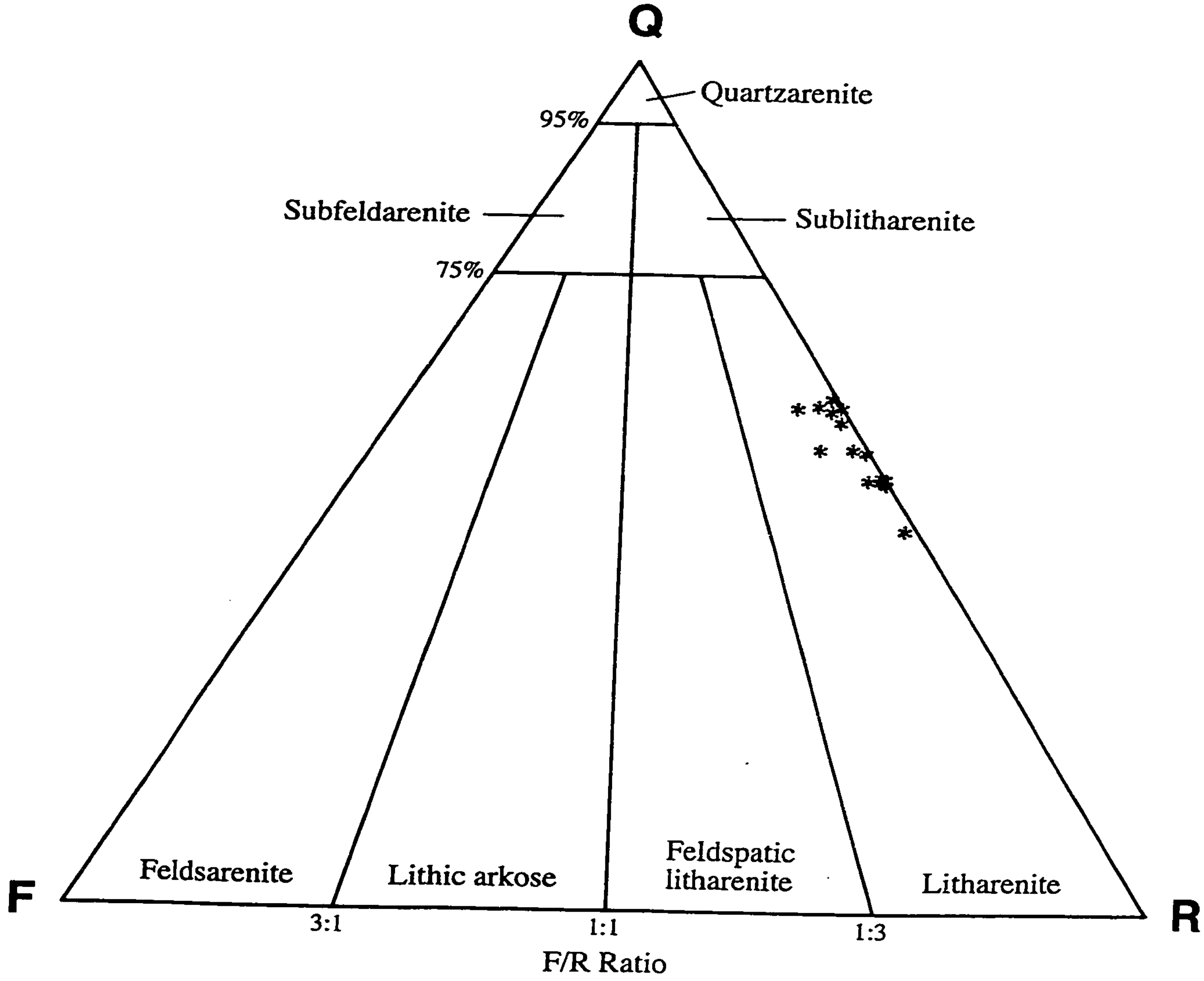
Q
Quartzarenite
95%
Subfeldarenite
Sublitharenite
75%
F
Feldsarenite
Lithic arkose
Feldspatic litharenite
Litharenite
R
3:1
1:1
1:3
F/R Ratio

Table A1-1. Summary of petrographical analysis

UWI	Depths (m)	Grain Size	Estimated ϕ (%)	Approximate % of framework grains										Post-depositional key features								Comments
				monocrystalline quartz	chert and tripolitic chert	mudstone clasts	k-feldspar	plagioclase	muscovite	biotite	glauconite	zircon	tourmaline	pyrite or opaques	pseudomatrix	tripolitic chert	argillans	sphaerosiderite	pore-filling chlorite	authigenic clay coatings	calcite cement	
6-32-1-8w4	926.8	very fine	10	60	15	20	5		tr				tr	5%	✓						tr	
6-32-1-8w4	926.55	very fine	2	50	20	30	3	tr	tr		tr	tr		tr	✓		tr					abundant pseudomatrix
6-32-1-8w4	800.3	very fine	unknown	65	25	10	?		tr				tr	tr	✓	✓						not stained; undyed epoxy
14-14-4-5w4	1078.9	very fine	5	50	20	30	tr				tr	1	tr	tr	✓	✓					tr	quartz overgrowths; burrowed
10-36-5-5w4	1176.25	coarse silt	3	55	5	35	>1	tr	1			1	1	1%	✓							dark L4; not stained
10-36-5-5w4	1176.2	very fine	3	60	25	15	>1	tr	tr			tr	tr	tr	✓				tr			dark L4; not stained
10-36-5-5w4	1176.05	c. silt - v. fine	5	60	5	35	?	tr	tr		tr	tr	tr	tr	✓							dark L4; burrowed; not stained
10-36-5-5w4	1175.9	very fine	2	60	20	20	?	tr	tr			tr		tr	✓	tr			1%			dark L4; burrowed; not stained
10-36-5-5w4	1175.8	coarse silt	3	60	5	35	?		tr		tr	1	tr	1%	✓							colour change; burrowed
10-36-5-5w4	1175.7	coarse silt	tr	60	5	35	?		tr		tr	1	tr	1%	✓	✓			tr			light L4; zircons at base of foresets
10-36-5-5w4	1175.5	silt	tr	55	35	10			1			1	tr	tr	✓	✓			tr			light L4; not stained
10-36-5-5w4	1174	silt	3	60	20	20			tr			tr	tr	tr	✓		✓	3%				laminated paleosol; not stained
10-36-5-5w4	1173	clay - c. silt	tr	80	10	10			tr			tr	tr	1%	✓	✓	✓	1%				discontinuously laminated paleosol
10-36-5-5w4	1172.25	clay - f. sand	0 - 2	70	10	20			tr			tr	tr	1%	✓	✓	✓	3%			5%	laminated paleosol; not stained
10-36-5-5w4	1170	clay - vf. sand	1	50	20	30			tr			tr	tr	tr	✓	✓	✓					unlaminated paleosol; abnt. argillans
8-29-5-6w4	944.5	very fine	10	55	20	30				tr		tr	tr	1%	✓	✓	tr				5%	low effective porosity
6-2-4-7w4	877	v fine - fine	20	55	25	15	2	tr		tr	tr	tr	tr	1%	✓	✓						qtz overgrowths; leached sed r. frag.
6-2-4-7w4	879	fine	unknown	50	30	20	?					tr	tr	tr								not stained; undyed epoxy
6-34-5-6w4	977	very fine	10	50	15	25	8			tr		tr	tr	tr		✓						quartz overgrowths
6-34-5-6w4	968.3	silt - m. sand	0	60	10	30			tr			tr	tr	1%	✓	✓		✓	20%			paleosol
13-5-6-7w4	912	very fine	5	55	25	15	3	tr	tr				tr	tr	✓			✓			2%	quartz overgrowths
13-5-6-7w4	911.3	very fine	unknown	60	30	10	?		tr			tr	tr	tr	✓				20%		3%	not stained; undyed epoxy
13-5-6-7w4	911.9	very fine	unknown	60	25	15	>1		tr				tr	tr	✓						1%	not stained; undyed epoxy
13-5-6-7w4	912.5	clayey silt	unknown											tr					tr		3%	not stained; undyed epoxy
8-34-6-6w4	1158	very fine	unknown	60	25	10	>1	tr	1		2	tr		1%	✓					tr		chlorite coated quartz grains
6-23-7-3w4	1429.4	fine - med	20	60	30	10	2	tr			1		tr	tr					tr	5		chert is partially glauconitic
6-23-7-3w4	1419.6	clay, silt & vf	0 -10	60	15	25	?	tr	1		tr	tr	tr	1%								not stained; interstratified; burrowed

Plate 1 Typical mineralogy of the sandstone-rich lithofacies of the ribbon sandstone.

A) Fine grained sandstone composed dominantly of monocrystalline quartz (M) and clean to muddy chert (CC and MC, respectively). Potassium feldspar (K) is commonly present but generally constitutes less than 5% of framework grains. Note the partially dissolved, light green sedimentary rock fragments compacted and squeezed between quartz and chert grains forming a pseudomatrix. Blue background is coloured epoxy within pores. Scale bar is 0.25 mm. Well 6-2-4-7w4, 877 metres.

B) In Figure A, chert and quartz can be easily differentiated under cross-polarized light.


A
M
B

Plate 2 Close-up view of tripolitic chert in sandstone-rich lithofacies of the ribbon sandstone (large arrow). Chert was altered by aggressive fluids, which locally has completely (small arrow) or partially dissolved grains forming secondary intragranular porosity (large arrow). This additional porosity, however, is ineffective, and can lead to the overestimation of effective porosity in the interpretation of density or neutron logs. Note quartz overgrowths around monocrystalline quartz grains. Also, note rhombic pores within the tripolitic chert grain (large arrow), which likely represents preferential dissolution of silicified carbonate crystals. Scale bar is 0.25 mm. Well 6-23-7-3w4, 1429.4 metres.

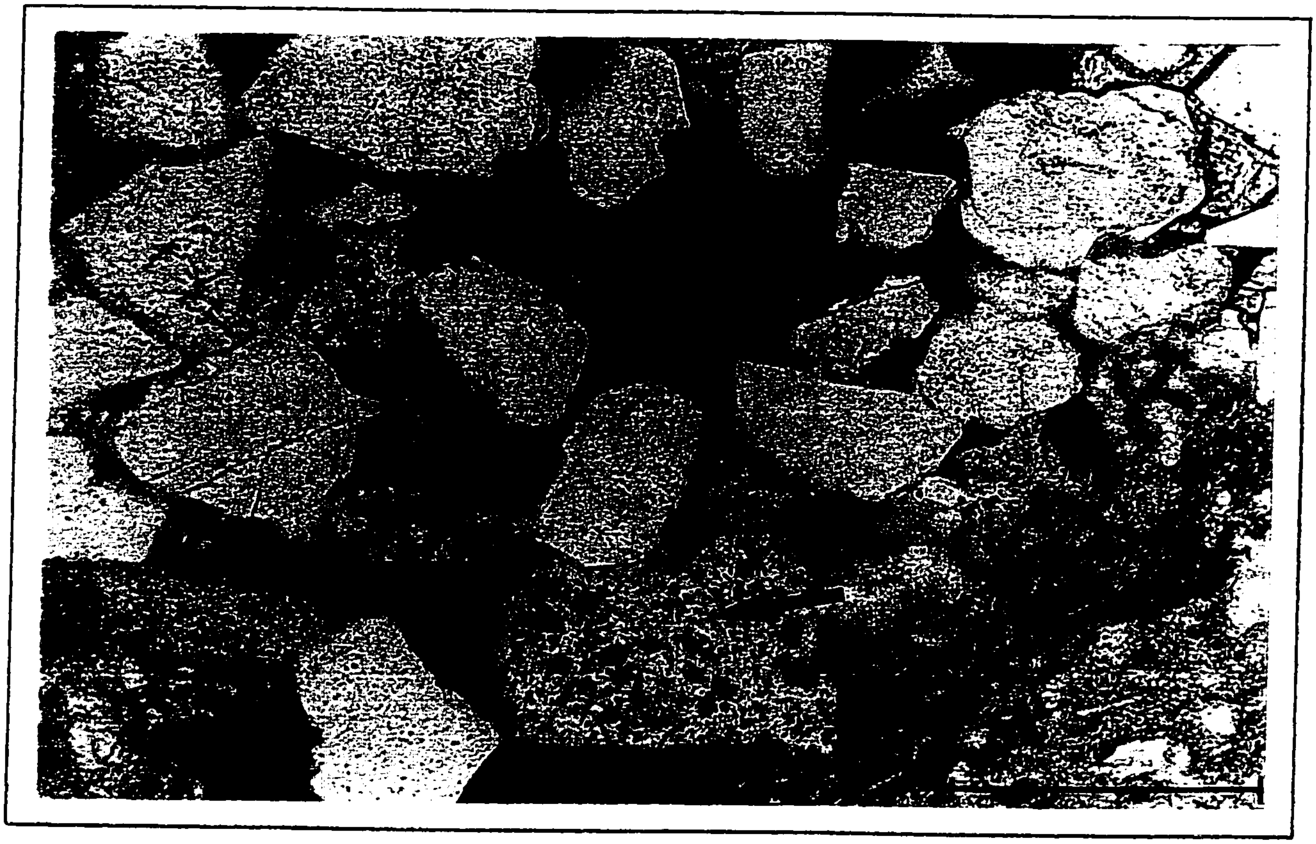

Plate 3 Light (A) and dark (B) ribbon sandstone. Note the abundant dark coloured, organic rich detrital sediment in the dark ribbon sandstone (B), and its general absence in the light ribbon sandstone (A). Organic matter was decomposed in light ribbon sandstone during pedogenesis. In (A) note the contact between the soil ped (left arrow) in which primary stratification has been preserved, and an ancient soil crack (right arrow) where layering has been destroyed and illuvial argillans accumulated. Well 6-23-7-3w4, (1419.6 m) (A) and 10-36-5-5w4, (1170 m) (B). Scale bars are 0.5 mm.


A
B

Plate 4 Cements of the sandstone-rich lithofacies of the ribbon sandstone. Sandstone is generally cemented by compacted sedimentary rock fragments and mudstone. In addition, local pore-filling green chlorite (A; narrow arrow) and highly birefringent patchy calcite cement (B; wide arrow) occur. Note the abundant yellow-stained feldpar in (A). Scale bar is 0.25 mm in (A) and 0.5 mm in (B). Wells 13-5-6-7w4, 912 m (A), and 10-8-3-8w4, 868.7 m (B).


A
B

Plate 5 Evidence for pedogenic alteration and changes in chemical conditions in light ribbon sandstone:

A) Radial concave-downward, laminated argillans emplaced by elluviation of fine-grained sediment into cracks between soil peds within the Bt-horizon of the ribbon sandstone paleosol. Scale bar is 0.25 mm. Well 10-36-5-5w4, 1170 m.

B) Radial sphaerosiderite in the Bt-horizon of the Swift paleosol. Note discontinuous concentric pyrite layer within the nodule. Pyrite was precipitated under lower Eh conditions that developed because of lower pCO_2, which is likely related to reduced activity of respiring microbes. Well 10-36-5-5w4, 1170.6 m. Scale bar is 0.25 mm.


A
B

Appendix 3

Geochemical Analysis

10-36-5-5w4

sample	run	depth (m)	SiO2 %	TiO2 %	Al2O3 %	Fe2O3 %	MnO %	MgO %	CaO %	Na2O %	K2O %	P2O5 %	V ppm	Cr ppm	Co ppm	Ni ppm	Zn ppm	Rb ppm
6b	1	1177.1	77.01	0.879	15.60	1.742	0.0084	0.599	0.115	0.27	2.071	0.065	133	95	22	32	22	80
5b	1	1176.9	75.87	0.858	17.04	1.626	0.0078	0.606	0.123	0.30	1.943	0.074	141	94	33	40	18	79
4b	1	1176.7	74.40	0.927	18.22	1.547	0.0068	0.572	0.112	0.26	1.920	0.088	139	96	31	62	14	80
3b	1	1176.5	73.51	0.899	20.33	1.379	0.0070	0.516	0.102	0.14	1.687	0.090	144	88	51	72	20	72
2b	1	1176.3	73.47	0.904	20.00	1.241	0.0069	0.482	0.095	0.21	1.570	0.067	129	93	28	24	19	70
1b	1	1176.1	74.87	0.944	19.40	1.051	0.0078	0.451	0.088	0.17	1.488	0.060	122	96	3	17	21	66
3	2	1176.05	78.06	0.842	16.79	1.066	0.0066	0.383	0.087	0.26	1.327	0.053	106	87	29	24	12	63
4	2	1175.95	75.54	0.874	18.31	1.018	0.0067	0.407	0.087	0.21	1.375	0.054	114	91	3	8	29	67
5	2	1175.9	76.62	0.824	17.49	1.187	0.0062	0.397	0.081	0.23	1.333	0.048	110	79	7	9	14	65
6	2	1175.8	79.33	0.750	14.75	1.405	0.0061	0.355	0.075	0.16	1.259	0.037	119	81	3	13	10	59
8	2	1175.5	75.28	0.913	18.53	1.419	0.0071	0.475	0.069	0.18	1.437	0.039	148	89	0	3	11	76
9	2	1175.75	77.32	1.172	17.33	1.684	0.0110	0.295	0.077	0.02	0.892	0.126	125	85	<1	9	8	50
10	2	1173.5	76.20	0.955	17.61	2.848	0.0242	0.418	0.127	0.04	0.982	0.192	128	87	2	23	24	55
11	2	1172.25	75.21	1.322	16.58	3.962	0.0651	0.285	0.585	0.01	0.757	0.069	89	92	5	14	8	42
12	2	1170	79.75	1.009	15.28	0.692	0.0036	0.135	0.043	0.00	0.407	0.030	49	84	<1	2	4	20
3	1	1176.05	?	?	?	?	?	0.380	0.090	0.09	1.329	0.052	101	87	28	23	12	56
4	1	1175.95	?	?	?	?	?	0.400	0.090	0.10	1.385	0.052	121	91	2	6	29	51
5	1	1175.9	?	?	?	?	?	0.390	0.080	0.09	1.343	0.049	111	90	10	10	13	59
6	1	1175.8	?	?	?	?	?	0.350	0.070	0.06	1.261	0.037	115	87	3	10	9	53

10-36-5-5w4 (continued)

sample	run	depth (m)	Sr ppm	Y ppm	Zr ppm	Nb ppm	Ba ppm	La ppm	Ce ppm	Nd ppm	Pb ppm	Th ppm	U ppm	Ga ppm	Total %
6b	1	1177.1	138	135	495	33	330	85	180	125	12	10.68	<1	17.4	98.608
5b	1	1176.9	147	141	416	33	301	128	203	171	17	10.69	2.27	18.6	98.711
4b	1	1176.7	139	151	323	34	303	162	304	246	22	11.01	1.15	20.0	98.325
3b	1	1176.5	133	142	414	33	275	153	342	256	19	11.33	6.20	19.2	98.950
2b	1	1176.3	131	81	367	34	265	102	245	150	10	10.25	10.32	19.3	98.287
1b	1	1176.1	126	72	396	39	279	95	207	143	6	8.85	14.45	19.9	98.756
3	2	1176.05	116	65	639	36	258	83	174	99	15	15.32	30.50	16.0	99.119
4	2	1175.95	117	58	484	34	255	76	144	94	10	14.06	23.14	16.8	98.095
5	2	1175.9	113	51	442	33	275	55	137	78	6	11.79	4.81	15.7	98.415
6	2	1175.8	101	40	488	29	255	44	72	32	11	9.80	0.00	14.3	98.305
8	2	1175.5	117	38	427	33	255	43	63	25	0	11.53	0.00	18.7	98.524
9	2	1175.75	322	29	458	56	422	194	302	99	47	14.35	<1	24.7	99.215
10	2	1173.5	528	32	463	37	555	182	323	130	10	9.10	0.00	19.0	99.728
11	2	1172.25	154	31	483	72	274	62	105	25	38	20.78	1.38	24.6	99.046
12	2	1170	81	30	519	51	314	40	60	11	5	11.76	<1	18.7	97.516
3	1	1176.05	116	66	593	35	261	60	163	95	16	12.73	29.09	15.4	97.996
4	1	1175.95	120	62	454	38	267	76	152	102	9	11.95	24.45	17.8	97.548
5	1	1175.9	111	53	414	36	282	57	127	69	7	10.66	5.38	16.4	98.171
6	1	1175.8	102	41	457	31	285	37	62	16	11	8.43	<1	14.6	97.758

10-36-5-5w4

Sample #	depth (m)	weight loss on combustion (%)	% organic carbon (%)
6b	1177.1	6.9	1.74
5b	1176.9	7.6	1.89
4b	1176.7	7.8	2.47
3b	1176.5	7.6	2.18
2b	1176.3	6.6	1.92
1b	1176.1	7.8	1.59
3a	1176.05	5.4	1.91
4a	1175.95	5.6	3.95
5a	1175.9	3.6	0.51
6a	1175.8	3.3	0.34
7a	1175.7	not analysed	0.40
8a	1175.5	4.9	0.29
9a	1174.75	5.1	0.23
10a	1173.5	5.4	0.19
11a	1172.25	5.6	0.29
12a	1170	4.5	0.21

Appendix 4

Stratigraphic Cross Sections

Figure A4-1. Map illustrating location of stratigraphic cross sections in Appendix 4

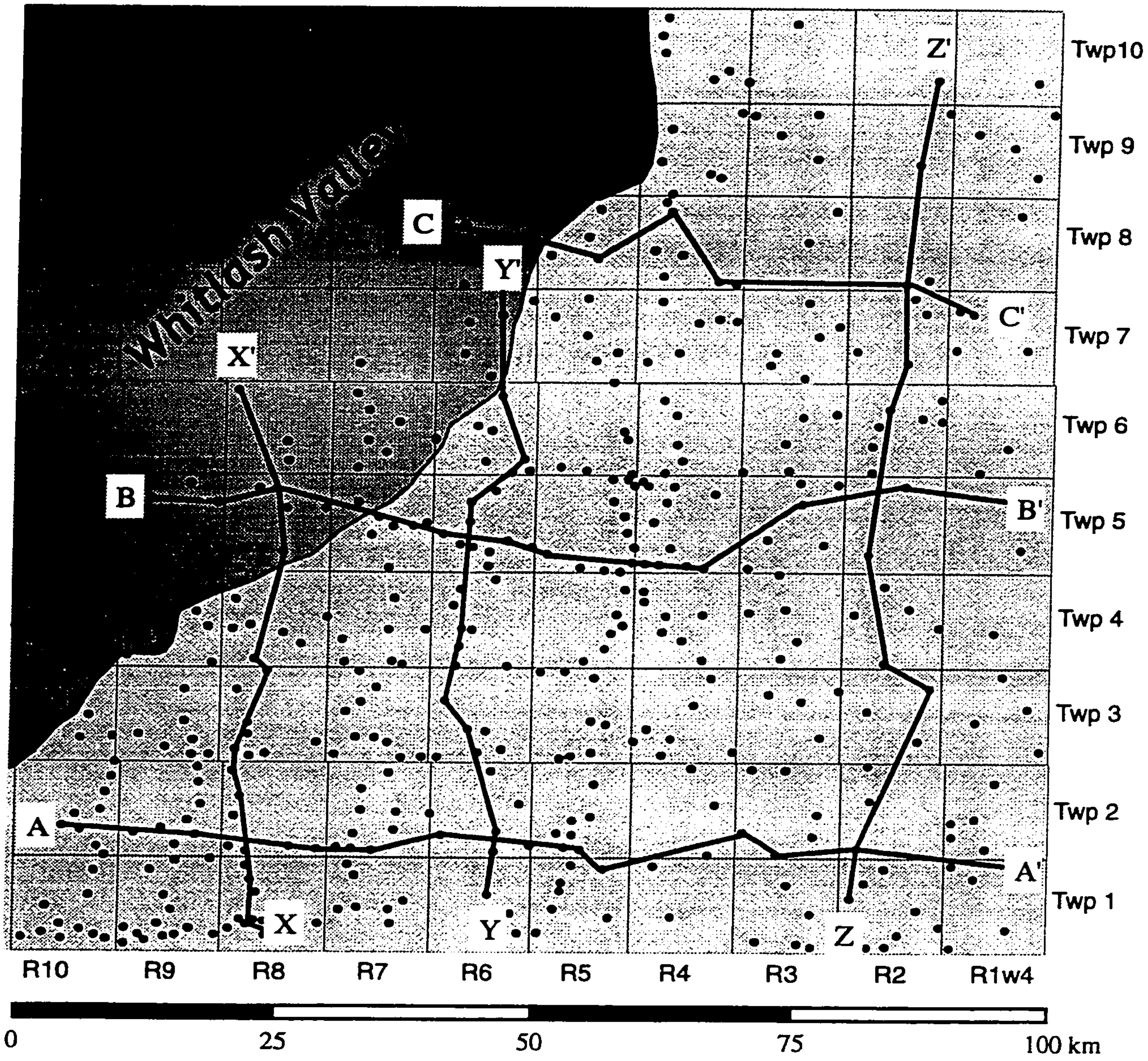
Whitlash Valley
C
Y'
X'
B
Z'
C'
B'
A
A'
X
Y
Z
Twp10
Twp 9
Twp 8
Twp 7
Twp 6
Twp 5
Twp 4
Twp 3
Twp 2
Twp 1
R10
R9
R8
R7
R6
R5
R4
R3
R2
R1w4
0
25
50
75
100 km

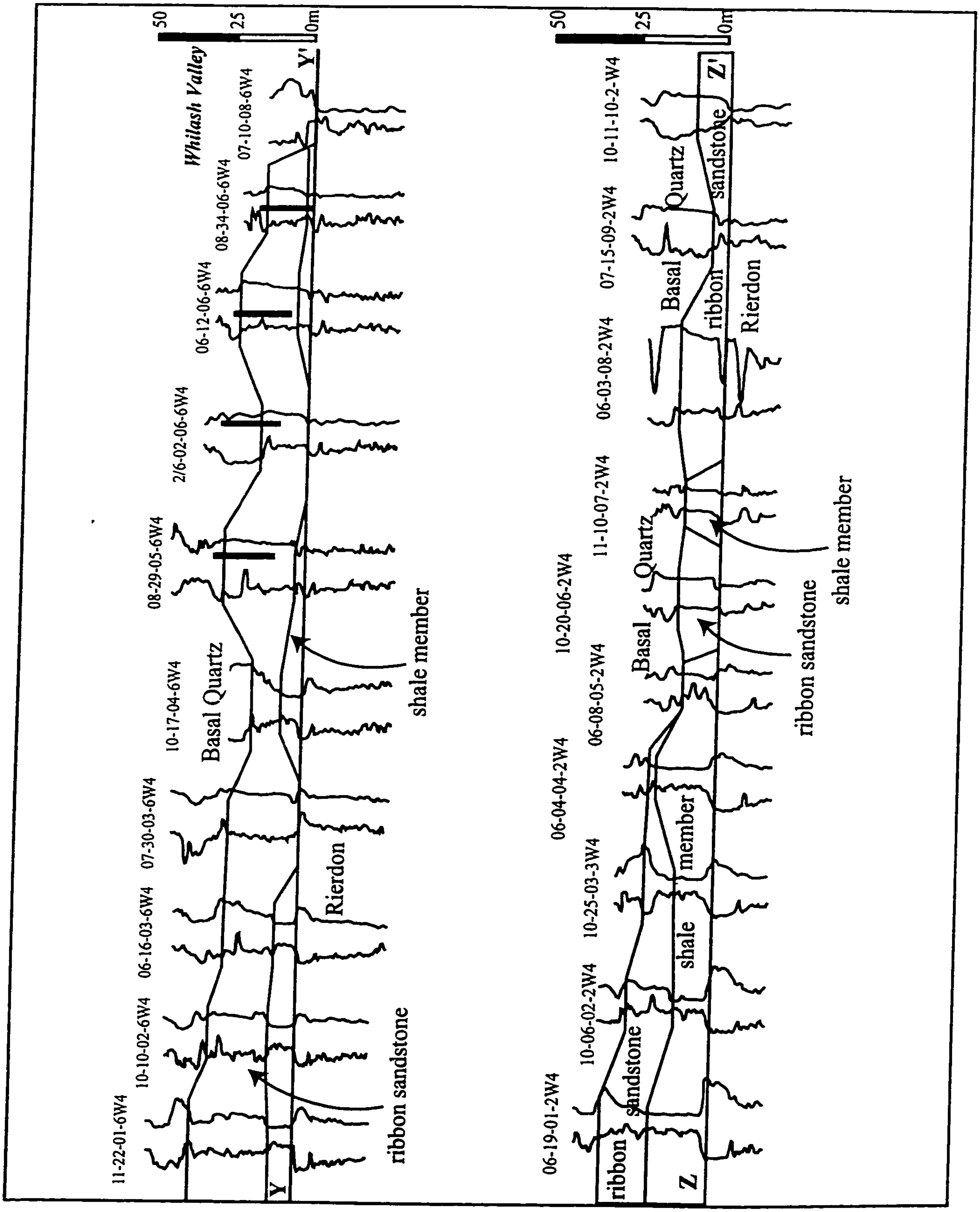
Whilash Valley
50
25
0m
Y'
Y
11-22-01-6W4
10-10-02-6W4
06-16-03-6W4
07-30-03-6W4
10-17-04-6W4
08-29-05-6W4
2/6-02-06-6W4
06-12-06-6W4
08-34-06-6W4
07-10-08-6W4
Basal Quartz
Rierdon
shale member
ribbon sandstone
50
25
0m
Z'
Z
06-19-01-2W4
10-06-02-2W4
10-25-03-3W4
06-04-04-2W4
06-08-05-2W4
10-20-06-2W4
11-10-07-2W4
06-03-08-2W4
07-15-09-2W4
10-11-10-2-W4
Basal Quartz
Basal Quartz
sandstone
ribbon
Rierdon
shale member
ribbon sandstone
ribbon
sandstone
shale
member

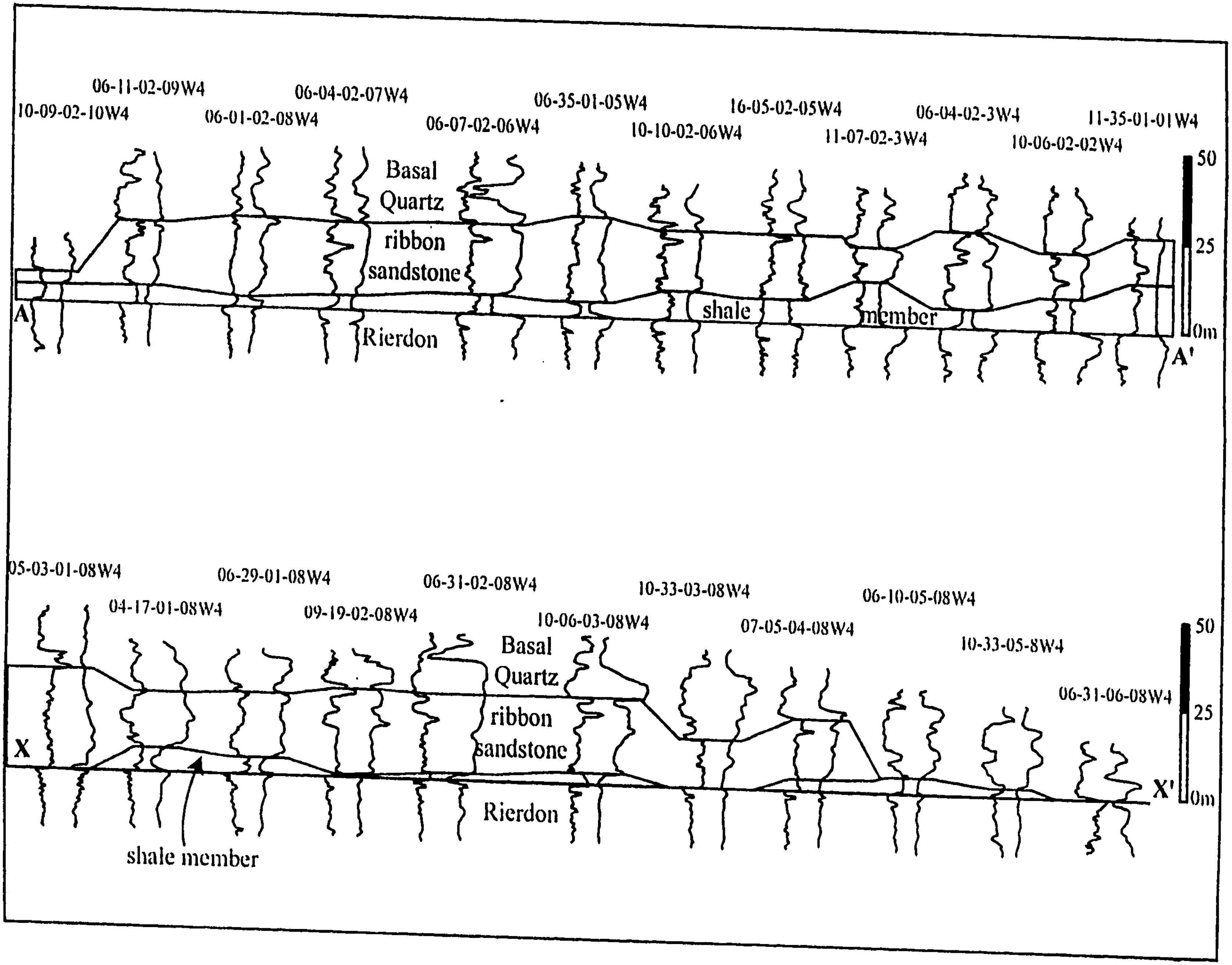
10-09-02-10W4
06-11-02-09W4
06-01-02-08W4
06-04-02-07W4
06-07-02-06W4
06-35-01-05W4
10-10-02-06W4
16-05-02-05W4
11-07-02-3W4
06-04-02-3W4
10-06-02-02W4
11-35-01-01W4
Basal
Quartz
ribbon
sandstone
shale
member
Rierdon
A
A'
50
25
0m
05-03-01-08W4
04-17-01-08W4
06-29-01-08W4
09-19-02-08W4
06-31-02-08W4
10-06-03-08W4
10-33-03-08W4
07-05-04-08W4
06-10-05-08W4
10-33-05-8W4
06-31-06-08W4
Basal
Quartz
ribbon
sandstone
Rierdon
shale member
X
X'
50
25
0m

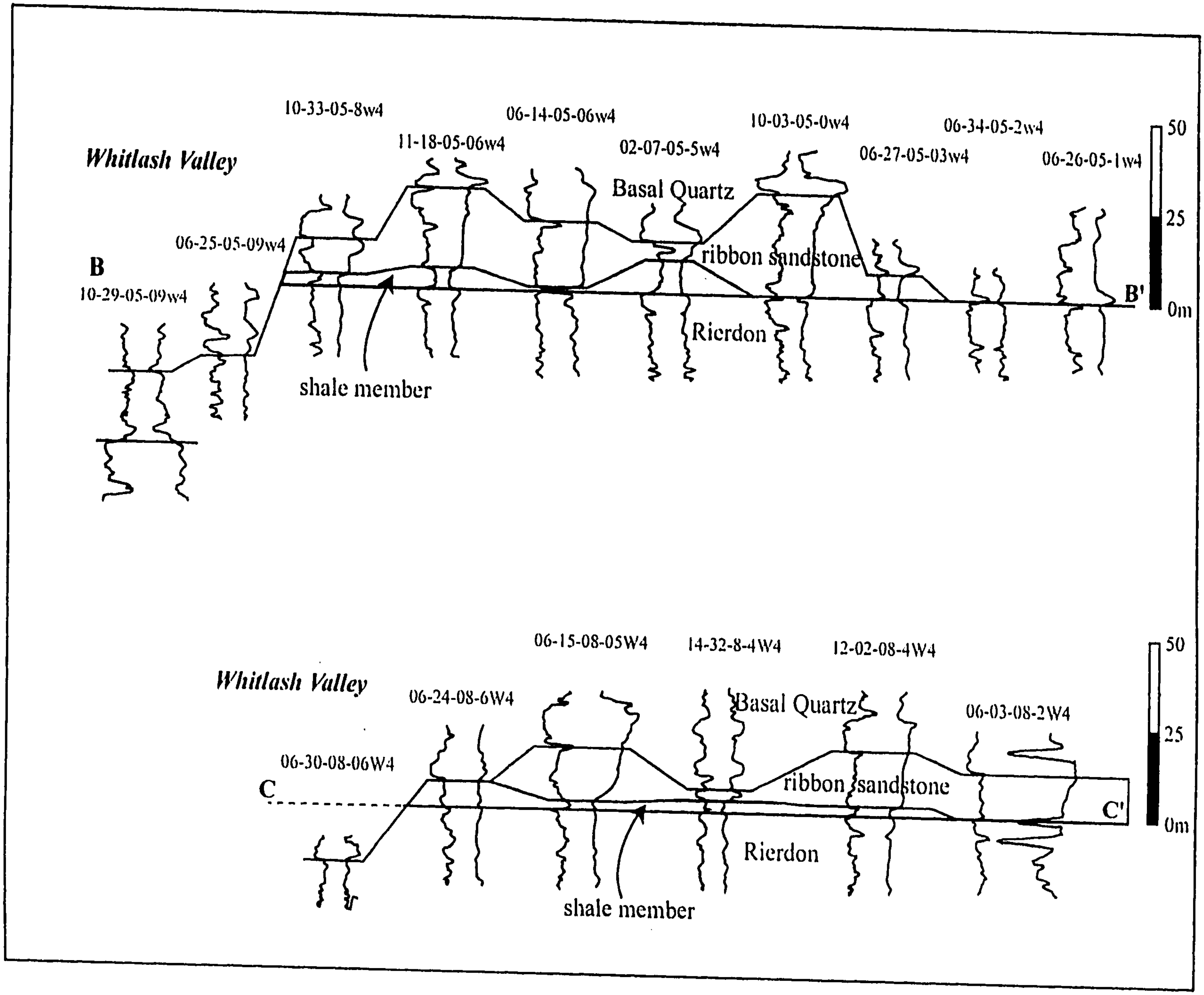
Whitlash Valley
B
10-29-05-09w4
06-25-05-09w4
10-33-05-8w4
11-18-05-06w4
06-14-05-06w4
02-07-05-5w4
10-03-05-0w4
06-27-05-03w4
06-34-05-2w4
06-26-05-1w4
B'
Basal Quartz
ribbon sandstone
Rierdon
shale member
50
25
0m
Whitlash Valley
C
06-30-08-06W4
06-24-08-6W4
06-15-08-05W4
14-32-8-4W4
12-02-08-4W4
06-03-08-2W4
C'
Basal Quartz
ribbon sandstone
Rierdon
shale member
50
25
0m

Appendix 5

Slice Maps

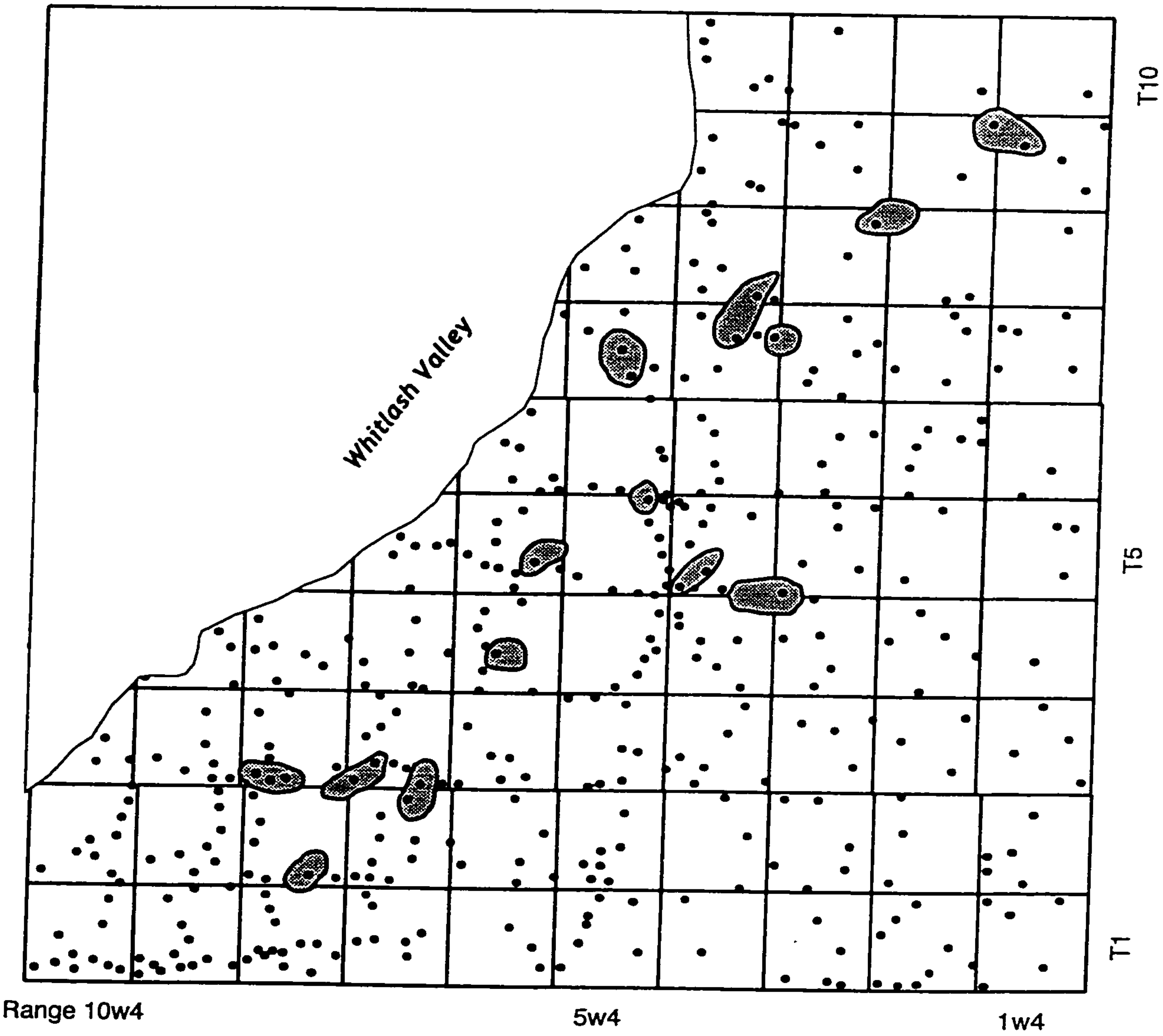

0 - 5 metre interval

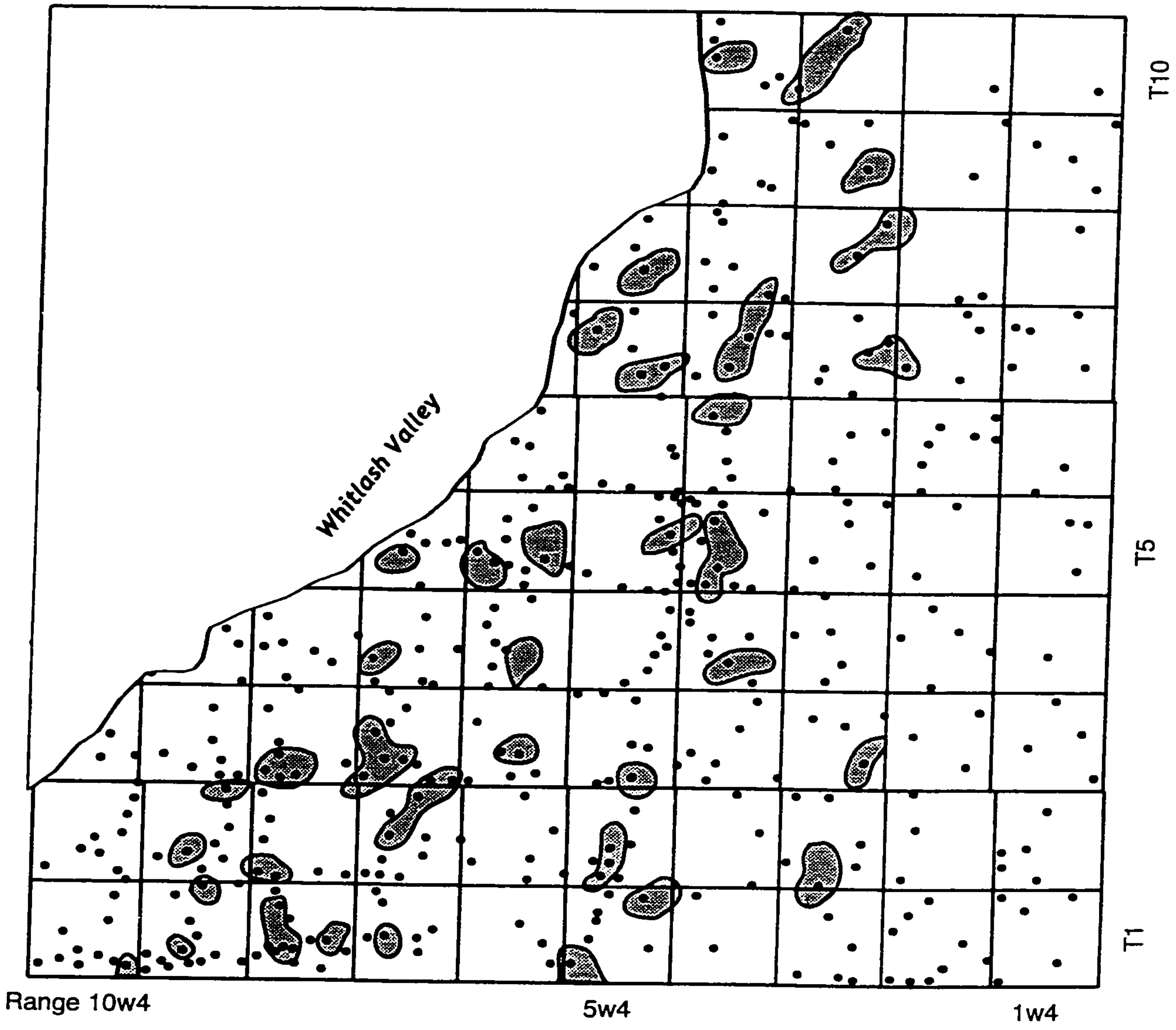

5-10 metre interval

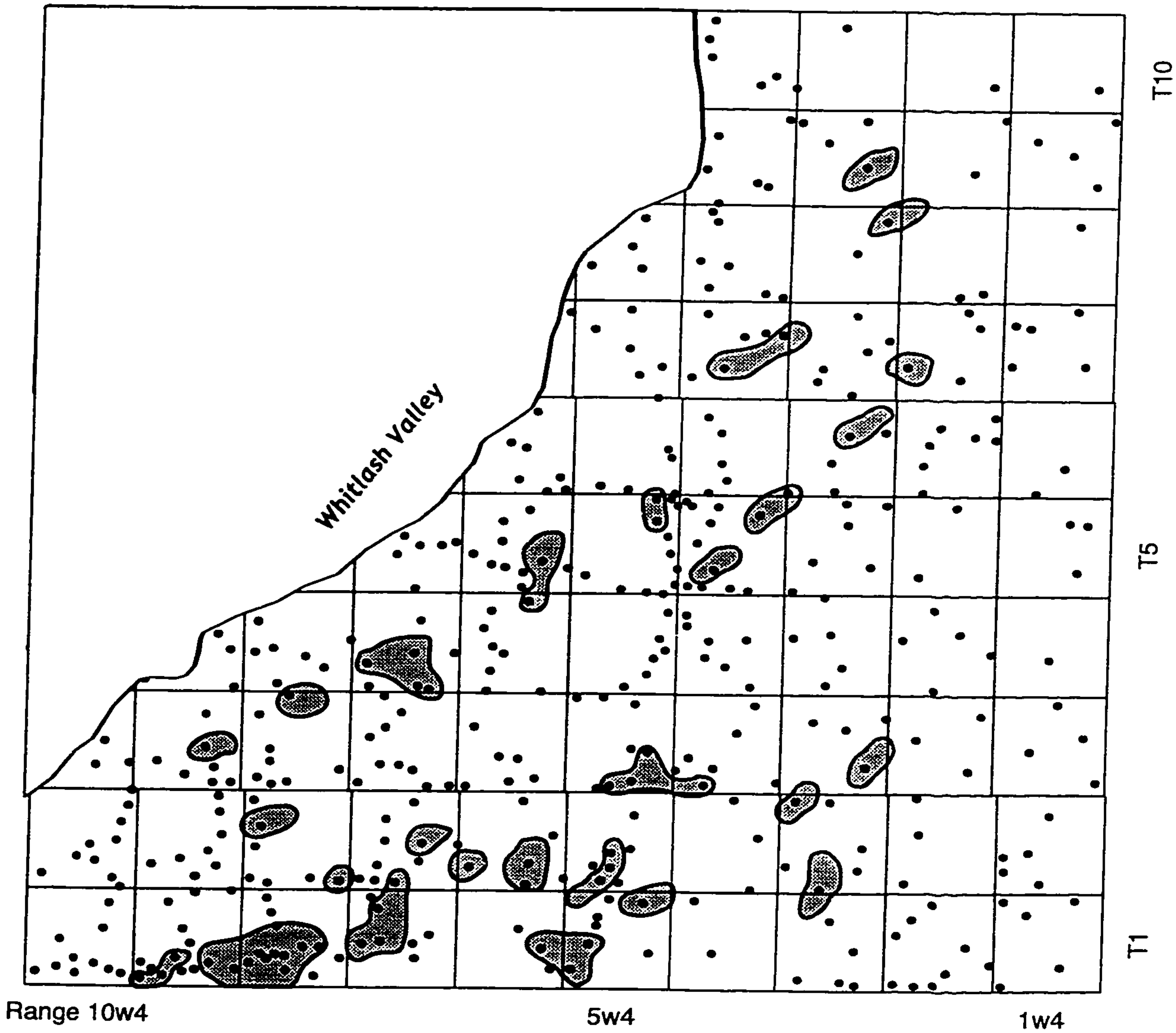

10 - 15 metre interval

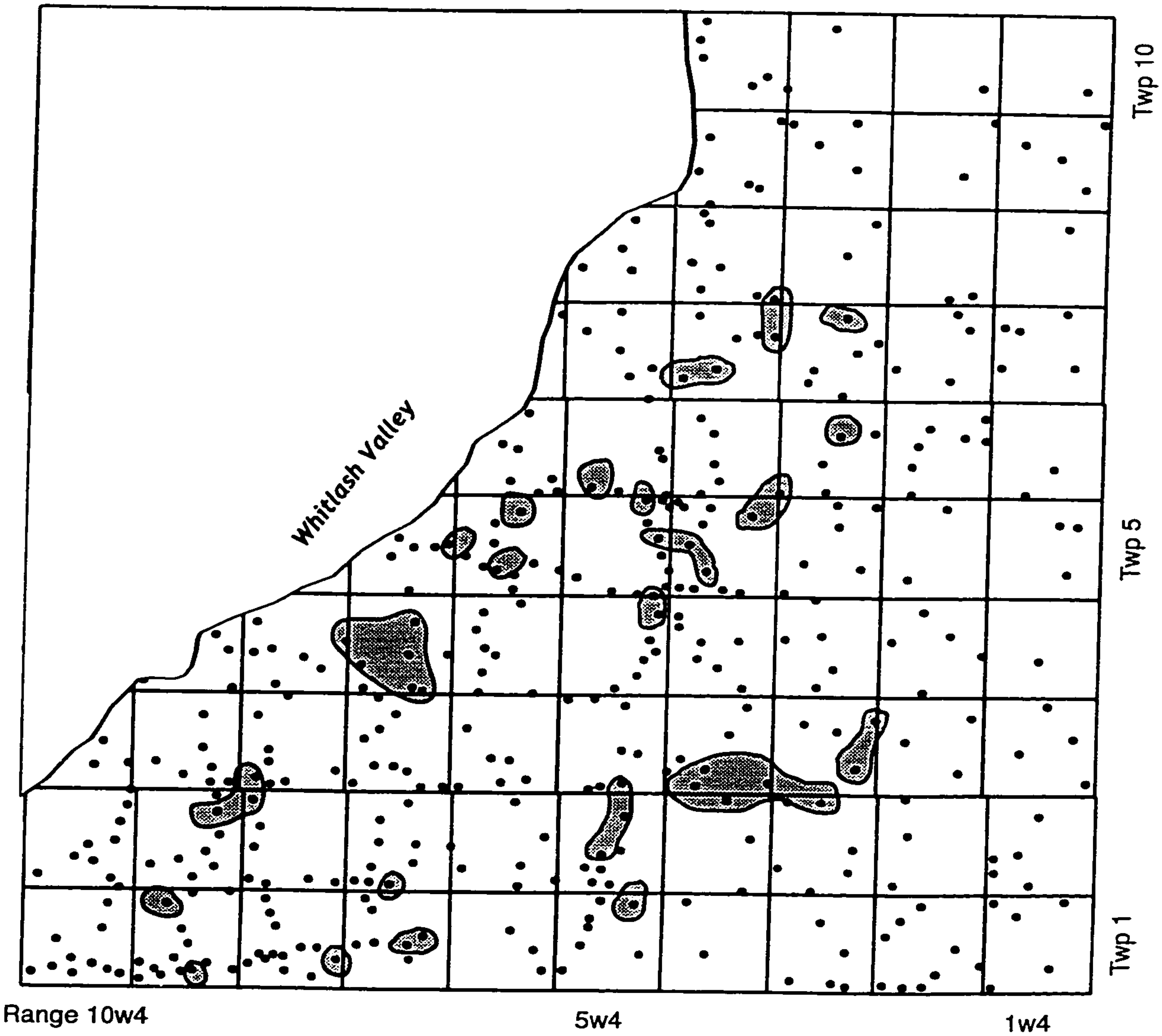

15 - 20 metre interval

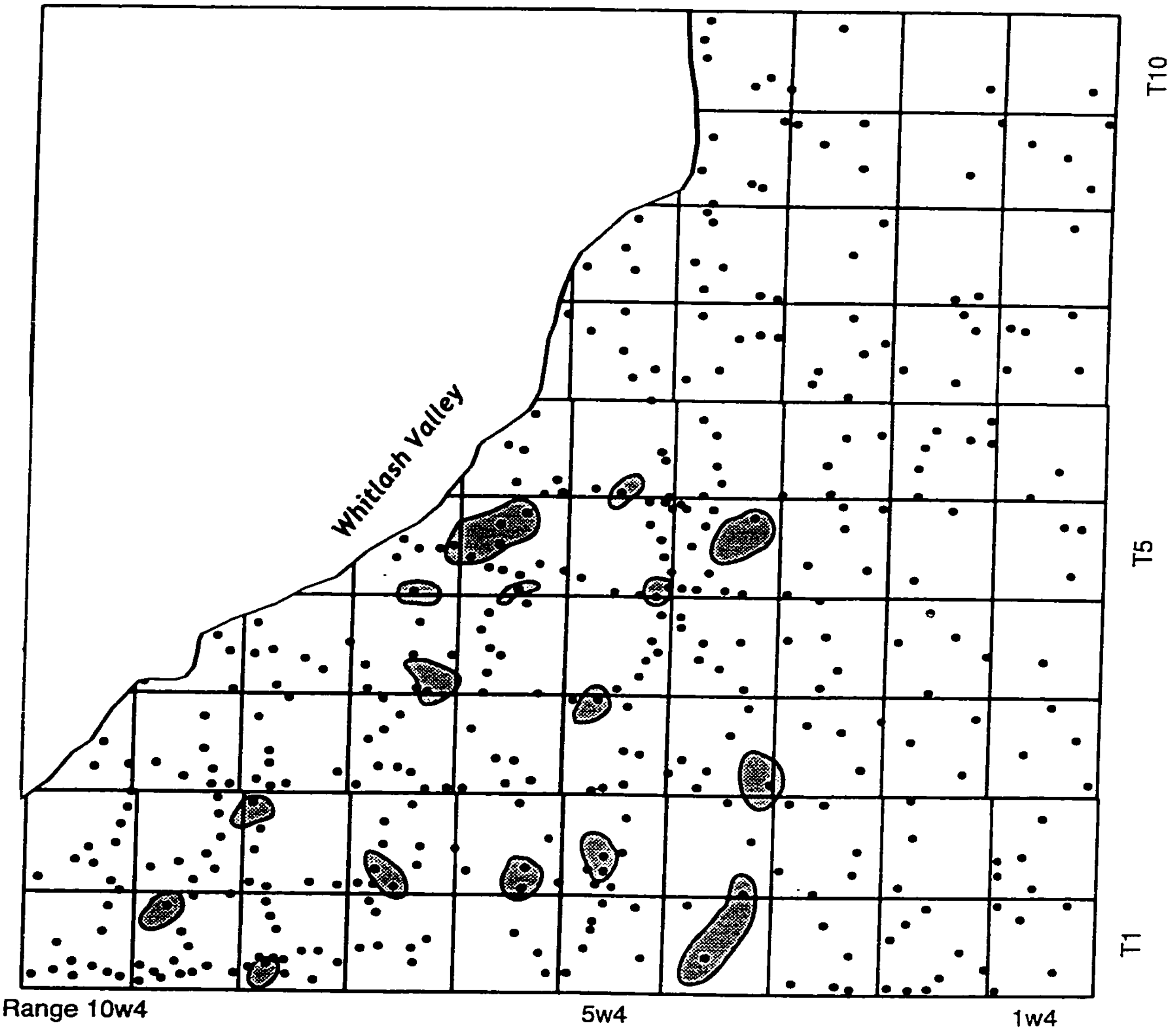

20 - 25 metre interval

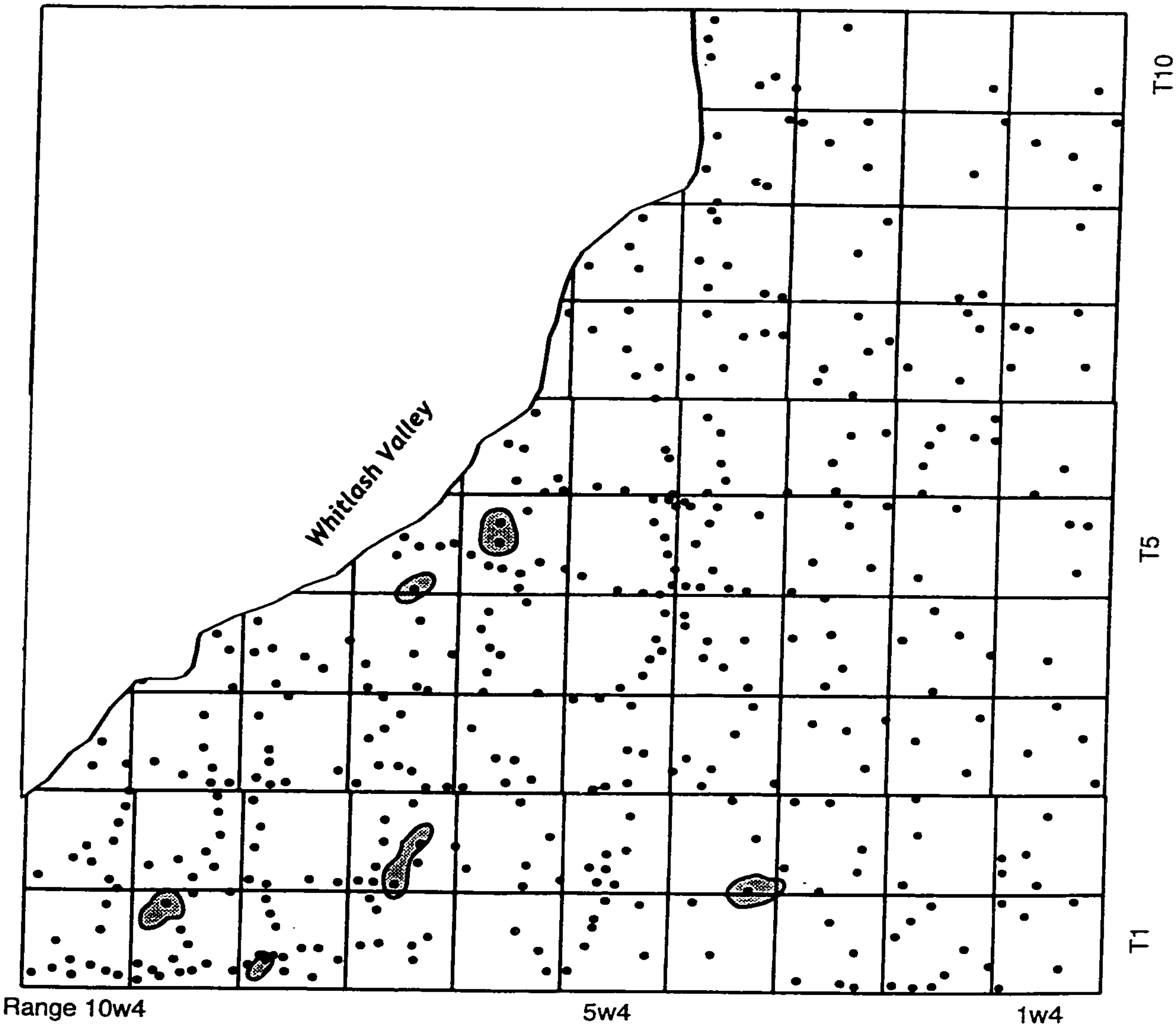

25 - 30 metres interval

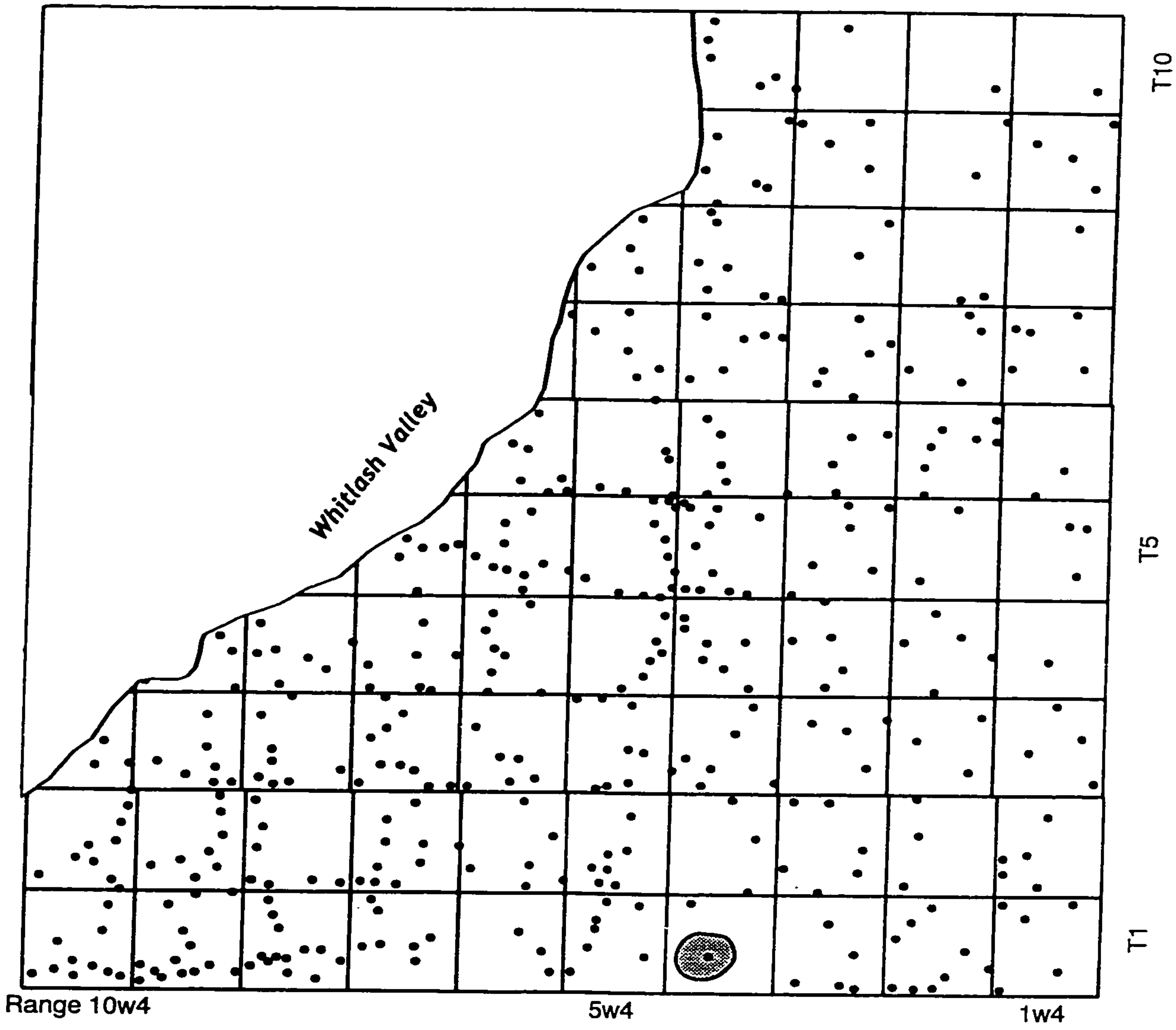

30 - 35 metre interval